

# **Identification of potential disease-driving proteins in mouse models of ALS caused by mutant TDP-43**

**Dissertation**

zur Erlangung des Doktorgrades der Naturwissenschaften an der Fakultät für  
Mathematik, Informatik und Naturwissenschaften der Universität Hamburg

von

**Rita Francisco Marques**  
**aus Lissabon, Portugal**

**Hamburg, 2018**

Examiners of the dissertation:

Dr. Kent Duncan

Prof. Dr. Christian Lohr

Date of the disputation:

1<sup>st</sup> of March, 2019

## Table of contents

	Page
Abbreviations .....	xiii
Acknowledgements .....	xix
Abstract.....	xxi
Zusammenfassung.....	xxii
1. Introduction.....	3
1.1. Amyotrophic lateral sclerosis (ALS) is a devastating neurological disorder.....	3
1.2. Different mutated genes have been identified to be the cause of ALS .....	4
1.2.1. Similarities and differences between genetics of sALS and fALS .....	6
1.3. Disease models to study ALS: an overview of their advantages and disadvantages .....	8
1.4. TDP-43 protein: a close look into its properties.....	10
1.4.1. Structure of the TDP-43 protein.....	10
1.4.2. Characterization of the physiological function of TDP-43.....	11
1.4.3. Mechanisms of pathogenicity of TDP-43 in ALS.....	12
1.4.4. Role of TDP-43 in SGs .....	12
1.4.5. Role of TDP-43 in RNA metabolism .....	13
1.4.6. TDP-43 proteinopathies .....	14
1.5. Translation is a crucial step to define protein levels in a cell.....	15
1.5.1. Available genome-wide methods cannot study translation in specific cell types <i>in vivo</i> .....	18
2. Aims of the thesis .....	23
3. Results .....	27
3.1. Behavioral characterization of the mouse lines .....	27
3.1.1. Disease onset determination .....	27
3.1.1.1. Neurological score.....	28
3.1.1.2. Peak body weight .....	30
3.1.1.3. Muscle coordination and strength .....	31
3.1.1.3.1. Accelerating rotarod test.....	32
3.1.1.3.2. Forelimb grip strength test.....	33
3.2. Analysis of total TDP-43 expression levels in spinal cord of hTDP-43 and A315T mouse lines .....	35
3.3. Mild muscular denervation pathology correlates with disease .....	39

3.4. Successful purification of the motor neuronal translome via TRAP .....	40
3.4.1. One spinal cord can be used with TRAP .....	41
3.4.2. Optimized TRAP protocol is compatible with high-throughput sequencing.....	43
3.4.3. All A315T female animals were carefully checked for symptoms prior TRAP .....	45
3.5. Genotype is the major driver of changes in female MN translome.....	45
3.6. Deregulated mRNAs were identified in diseased MNs .....	49
3.7. Potential disease drivers were validated in an independent cohort of animals.....	51
3.7.1. Validation at the RNA level.....	51
3.7.1.1. <i>Tex26</i> validated as an upregulated candidate at the RNA level.....	52
3.7.1.2. <i>Plekhb1</i> validated as a downregulated candidate at the RNA level.....	52
3.7.1.3. <i>Syng4</i> shows a trend as an upregulated candidate at the RNA level .....	54
3.7.1.4. <i>Tia1</i> shows a trend towards different isoform regulation at the RNA level .....	54
3.7.2. Validation at the protein level.....	56
3.7.2.1. PLEKHB1 protein levels are decreased in spinal MNs of TDP-43 mutants.....	58
3.7.2.2. SYNGR4 protein levels are increased in MNs of TDP-43 mutants.....	60
3.7.3. SYNGR4 protein does not colocalize with SVs.....	62
3.8. Comparison of neurodegenerative mechanisms in SOD1 and TDP-43 mouse models of ALS .....	63
3.9. Preliminary experiments to establish a new method to monitor translation: Gradient-TRAP.....	64
3.9.1. Establishment of conditions for Gradient-TRAP <i>in vitro</i> .....	65
3.9.2. NaAsO <sub>2</sub> massively down regulates translation and alters ribosome density on most mRNAs.....	67
3.9.3. Altered ribosome density is silent in TRAP.....	70
3.9.4. Gradient-TRAP <i>in vivo</i> from mouse spinal cord.....	72
4. Discussion and future perspectives.....	77
4.1. Correct establishment of disease onset is necessary to identify potential disease drivers.....	77
4.2. Both up and downregulated mRNAs and proteins were identified in diseased MNs.....	80
4.2.1. Purification of the motor neuronal translome from ALS models via TRAP .....	80
4.2.2. Genotype rather than age is the major driver of mutant TDP-43's effect on the MN translome .	81
4.2.3. A short list of deregulated genes was generated.....	82
4.3. Validation of altered regulation of mRNAs and/or proteins.....	83
4.3.1. Validation of altered mRNA levels in an independent TRAP cohort .....	83
4.3.1.1. <i>Tex26</i> mRNA is upregulated in MNs at disease onset in an independent TRAP cohort .....	83
4.3.1.2. <i>Plekhb1</i> mRNA is downregulated in MNs at disease onset in an independent TRAP cohort .....	83

---

4.3.1.3. <i>Syngn4</i> mRNA might be upregulated in MNs at disease onset in an independent TRAP cohort...	84
4.3.1.4 <i>Tia1</i> mRNA 3' end processing might be altered in MNs by hTDP-43 <sup>A315T</sup> expression .....	84
4.4. No common potential disease drivers were identified in SOD1 and TDP-43 dataset.....	88
4.5. Potential role of validated targets in ALS pathology .....	89
4.5.1. PLEKHB1 is involved in the recruitment of membrane proteins.....	89
4.5.2. SYNGR4 might be involved in protein transport .....	91
4.5.3. TEX26's function is unknown .....	92
4.5.4. TIA1 down regulation caused by TDP-43 could altered SG dynamics and ultimately lead to ALS....	93
4.6. Novelty of this study.....	95
4.7. Gradient-TRAP enables the measurement of ribosome density in specific cell types <i>in vivo</i> .....	96
4.7.1. NaAsO <sub>2</sub> massively down regulates translation and alters ribosome density.....	96
4.7.2. Altered ribosome density is silent in TRAP.....	98
4.7.3. <i>In vivo</i> Gradient-TRAP can be used to monitor translation from specific cell types.....	99
5. Conclusions.....	103
6. Materials used in the experimental procedures of the thesis .....	107
6.1. Buffers and media .....	107
6.1.1. Genotyping .....	107
6.1.2. WB.....	107
6.1.3. TRAP Buffers.....	108
6.1.4. MN1 cell line.....	109
6.1.5. Polysome profiling.....	109
6.2. Primers .....	109
6.4. Technical equipment .....	111
6.5. Software .....	112
7. Methods .....	115
7.1. Experimental animals .....	115
7.2. Genotyping .....	115
7.2.1. PCR.....	116
7.3. WB.....	116
7.4. Behavioral experiments.....	117
7.4.1. Neurological score .....	118
7.4.2. Peak body weight .....	119

7.4.3. Grip strength .....	119
7.4.4. Rotarod.....	119
7.5. Muscle dissection and NMJ IHC .....	120
7.6. RNA isolation via TRAP .....	120
7.6.1. Affinity matrix preparation.....	121
7.6.2. Tissue lysate preparation .....	121
7.6.3. RNA clean up and purification protocol .....	122
7.7. RNA concentration determination .....	122
7.8. cDNA synthesis .....	122
7.9. Real-time PCR.....	123
7. 10. Sequencing .....	123
7.11. Bioinformatics .....	124
7.12. IHC .....	124
7.13. MN1 cell culture .....	125
7.13.1. Maintenance of the MN1 cell culture .....	125
7.13.2. Preservation and usage of the MN1 cell line .....	126
7.13.3. Transfection of MN1 cells.....	126
7.14. Oxidative stress induction in MN1 cells .....	127
7.15. Polysome profiling from MN1 cells .....	127
7.15.1. Strategy to pool the fractions.....	128
7.16. Polysome profiling from spinal cord .....	129
7.17. Monosome to polysome calculation .....	129
7.18. Gradient-TRAP .....	130
7.18.1. Gradient-TRAP from MN1 cells .....	130
7.18.2. Gradient-TRAP from spinal cord.....	130
8. Bibliography.....	133
9. Appendix.....	147
9.1. GO biological processes (David tool).....	147
9.2. List of up and downregulated genes: Chat-BacTrap; A315T 9 weeks vs Chat-BacTrap; A315T 14 weeks.....	148
9.3. List of up- and downregulated genes.....	149
9.5. Spinal cord (IC) - High-throughput sequencing data .....	157

9.6. MN TRAP (IP) – qRT-PCR from 9 weeks..... 158

9.7. *Tia1* mouse gene product isoforms..... 159

9.8. Venn diagram comparison of the candidates: this study vs the study from MacNair L. et al.; 2016 160





## Figures

	Page
Figure 1. MNs affected in ALS. ....	3
Figure 2. Timeline of gene discovery for genetic mutations linked to ALS (1990 to 2017). ....	5
Figure 3. Known genetic causes of sALS and fALS. ....	7
Figure 4. Schematic representation of the domain structure of TDP-43 and location of mutations that cause ALS. ....	11
Figure 5. Translation initiation. ....	16
Figure 6. Translation elongation. ....	17
Figure 7. Translation termination. ....	18
Figure 8. Behavioral analysis was used to define disease onset and progression. ....	28
Figure 9. Both sexes show deficits in hindlimb extension according to the neurological score at 16 weeks of age. ....	29
Figure 10. Female A315T mice develop stronger neurological deficits later than males. ....	30
Figure 11. The A315T female and male mice have different timings of peak of body weight. ....	31
Figure 12. The A315T mice show clear deficits in motor coordination and muscle weakness. ....	33
Figure 13. A315T female and male cohorts show different strength patterns throughout time in the forelimbs. ....	34
Figure 14. Time of ALS disease onset in the A315T mice. ....	35
Figure 15. Relative TDP-43 protein levels at 9 and 17 weeks in spinal cord of hTDP-43 and A315T mouse lines. ....	37
Figure 16. hTDP-43 <sup>A315T</sup> protein expression levels in spinal cord. ....	38
Figure 17. Mutant males show higher levels of hTDP-43 <sup>A315T</sup> protein with aging relative to mutant female mice. ....	39
Figure 18. Mild denervation of the NMJ concomitant with early symptomatic phase. ....	40
Figure 19. Female mice were selected through behavioral and denervation analysis to be studied by TRAP. ....	41
Figure 20. TRAP from one single spinal cord gives good enrichment. ....	42
Figure 21. Optimized TRAP protocol gives reliable high-throughput sequencing data in a pilot experiment. ....	44
Figure 22. The Chat-BT; A315T animals used in TRAP were early-symptomatic at 14 weeks of age. ....	45
Figure 23. TRAP methodology efficiently purifies MN mRNAs from spinal cord of female ALS model and controls. ....	46
Figure 24. Major differences between samples are driven by genotype. ....	48
Figure 25. Strategy applied to identify candidates for mRNAs exclusively deregulated in Chat-BT; A315T mice. ....	49
Figure 26. Identification of deregulated mRNAs in diseased MNs. ....	50
Figure 27. Samples for validation by qRT-PCR were efficiently immunoprecipitated via TRAP. ....	51
Figure 28. <i>Tex26</i> is upregulated at the RNA level during early symptomatic phase of the disease. ....	52
Figure 29. <i>Plekhb1</i> is downregulated at the RNA level during early symptomatic phase of the disease. ...	53
Figure 30. <i>Syngr4</i> shows a strong tendency as an upregulated candidate at the RNA level. ....	54

Figure 31. *Tia1* shows no significant differences between genotypes at the coding sequencing part of the gene. .... 55

Figure 32. *Tia1-202* RNA isoform shows a trend towards being downregulated. .... 56

Figure 33. Q331K mutant mice show ALS-like symptoms at 21 weeks of age according to the neurological score. .... 57

Figure 34. IHC from spinal cord MNs. .... 58

Figure 35. PLEKHB1 protein is downregulated in diseased spinal cord MNs of mice expressing hTDP-43<sup>A315T</sup>. .... 59

Figure 36. PLEKHB1 protein is downregulated in diseased spinal cord MNs of mice expressing hTDP-43<sup>Q331K</sup>. .... 60

Figure 37. SYNGR4 protein is upregulated in diseased spinal cord MNs of mice expressing hTDP-43<sup>A315T</sup>. 61

Figure 38. SYNGR4 protein is also upregulated in diseased spinal cord MNs of mice expressing hTDP-43<sup>Q331K</sup>. .... 62

Figure 39. SYNGR4 protein does not colocalize with SVs. .... 63

Figure 40. Comparison of deregulated genes in MNs of ALS models expressing hSOD1<sup>G37R</sup> versus hTDP-43<sup>A315T</sup>. .... 64

Figure 41. Gradient-TRAP as a new method to measure translational control from specific cell types. ... 65

Figure 42. Model to establish Gradient-TRAP: NaAsO<sub>2</sub> induced oxidative stress in MN1 cells. .... 67

Figure 43. NaAsO<sub>2</sub> has a dramatic impact on translation and ribosome density in MN1 cells. .... 69

Figure 44. Evidence that TRAP fails to detect major changes in the number of ribosomes per mRNA. .... 71

Figure 45. Adapting Gradient-TRAP to *in vivo* material. .... 73

Figure 46. Identified changes in MNs when hTDP-43<sup>A315T</sup> and hTDP-43<sup>Q331K</sup> proteins are present. .... 87

Figure 47. Representative images of the tests applied to the mice to evaluate disease onset and progression. .... 119

Figure 48. MN1 cells in culture medium. .... 125

Figure 49. Gradient former from BioComp. .... 127

Figure 50. Piston Gradient Fractionator. .... 128

Figure 51. Scheme of the pooled RNA fractions. .... 128

Figure 52. A representative profile where the monosome (M) and polysome (P) areas are highlighted. 129

## Tables

	Page
Table 1. Genes associated with dominant mutations showing principal neuropathological protein aggregates. Adapted from [22, 42].	6
Table 2. Disease models of ALS pathology: advantages and disadvantages. Adapted from [51, 52].	9
Table 3. Methods to study translation. Adapted from [156, 162].	19
Table 4. Overview of the validation stage of the candidates by qRT-PCR and IHC.	87
Table 5. Lysis buffer for tail biopsies.	107
Table 6. RIPA buffer.	107
Table 7. Running buffer.	107
Table 8. Transfer buffer.	107
Table 9. TBST-Tween buffer.	108
Table 10. 0.15M KCl washing buffer.	108
Table 11. Dissection buffer.	108
Table 12. Lysis buffer.	108
Table 13. 0.35M KCl washing buffer.	109
Table 14. MN1 cell line medium composition.	109
Table 15. Lysis/Gradient buffer.	109
Table 16. Primer sequences used in genotyping PCR reactions.	109
Table 17. Mouse primer sequences (Invitrogen) used for qRT-PCR.	110
Table 18. List of primary antibodies used in WB and IHC.	110
Table 19. List of secondary antibodies used in WB and IHC.	111
Table 20. Equipment used in the ZMNH.	111
Table 21. Mouse lines used in the experimental procedure for the development of this thesis.	115
Table 22. PCR reaction mix per each sample.	116
Table 23. PCR protocol.	116
Table 24. Genotypes tested in behavioral analyses.	118
Table 25. ALS neurological score. Adapted from Jackson laboratory guidelines [167].	118
Table 26. Number of animals used in the TRAP experiment.	121
Table 27. Real-time PCR protocol.	123



## Abbreviations

In order of appearance:

<b>ALS</b>	Amyotrophic lateral sclerosis
<b>MND</b>	Motor neuron disease
<b>UMNs</b>	Upper motor neurons
<b>LMNs</b>	Lower motor neurons
<b>MNs</b>	Motor neurons
<b>fALS</b>	Familial ALS
<b>sALS</b>	Sporadic ALS
<b>SOD1</b>	Superoxide dismutase 1
<b>CNS</b>	Central nervous system
<b>TDP-43</b>	TAR DNA-binding protein-43
<b>TARDBP</b>	TAR DNA-binding protein gene
<b>FUS</b>	Fused in sarcoma
<b>UBQLN2</b>	Ubiquilin2
<b>P62</b>	Sequestosome-1
<b>VAPB</b>	Vesicle-associated membrane protein associated protein B/C
<b>ANG</b>	Angiogenin
<b>OPTN</b>	Optineurin
<b>RNA</b>	Ribonucleic acid
<b>VCP</b>	Valosin-containing protein
<b>SETX</b>	Senataxin
<b>PFN1</b>	Profilin1
<b>HnRNPA1/A2</b>	Heterogeneous nuclear ribonucleoprotein A1/A2
<b>CHMP2B</b>	Charged multivesicular body protein 2B

<b>ATXN2</b>	Ataxin2
<b>DCTN1</b>	Dynactin subunit 1
<b>NEFH</b>	Neurofilament heavy
<b>ALS2</b>	Alsin
<b>iPSCs</b>	Induced pluripotent stem cells
<b>UBIs</b>	Ubiquitinated protein inclusions
<b>WT</b>	Wild type
<b>NTD</b>	N-terminal domain
<b>NLS</b>	Nuclear localization signal
<b>RRM1</b>	RNA recognition motif 1
<b>RRM2</b>	RNA recognition motif 2
<b>NES</b>	Nuclear export signal
<b>CTD</b>	C-terminal domain
<b>PrLD</b>	C-terminal domain
<b>hnRNPA1</b>	Heterogeneous nuclear ribonucleoprotein A1
<b>hnRNPA2B1</b>	Heterogeneous nuclear ribonucleoprotein A2/B1
<b>mRNA</b>	Messenger RNA
<b>DNA</b>	Deoxyribonucleic acid
<b>RBP</b>	RNA-binding protein
<b>LTR</b>	Long terminal repeat
<b>HIV1</b>	Immunodeficiency virus type 1
<b>lncRNA</b>	Long noncoding RNA
<b>ncRNA</b>	Noncoding RNA
<b>NMD</b>	Nonsense-mediated decay
<b>SGs</b>	Stress granules
<b>mRNP</b>	Messenger ribonucleoprotein
<b>KO</b>	Knockout

---

<b>snRNPs</b>	Small nuclear ribonucleo proteins
<b>KD</b>	Knockdown
<b>TIA1</b>	T-cell-restricted intracellular antigen-1
<b>DRiPs</b>	Defective ribosomal products
<b>AD</b>	Alzheimer's disease
<b>FTLD</b>	Frontotemporal lobar degeneration
<b>FLD</b>	Frontotemporal lobar degeneration
<b>LBD</b>	Lewy-body disease
<b>HpScl</b>	Hippocampal sclerosis
<b>U</b>	Uracil
<b>T</b>	Thymine
<b>PTR</b>	posttranscriptional regulation
<b>ER</b>	Endoplasmatic reticulum
<b>PIC</b>	Pre-initiation complex
<b>eIFs</b>	Eukaryotic initiation factors
<b>tRNAs</b>	Transfer ribonucleic acid
<b>AUG</b>	Initiation codon
<b>GTP</b>	Guanosine-5'-triphosphate
<b>GDP</b>	Guanosine-5'-diphosphate
<b>eEFs</b>	Elongation factors
<b>aa-tRNAs</b>	Aminoacyl-tRNAs
<b>RFs</b>	Release factors
<b>ABCE1</b>	ABC family ATPase E1
<b>TRAP</b>	Translating ribosome affinity purification
<b>EGFP</b>	Enhanced green fluorescent protein
<b>HA</b>	Hemagglutinin
<b>IP</b>	Immunoprecipitation

<b>A315T</b>	hTARDBP <sup>A315T</sup>
<b>hTDP-43</b>	Human TDP-43
<b>SEM</b>	Standard error of the mean
<b>2-way RM ANOVA</b>	Two-way repeated measurement ANOVA
<b>NS</b>	Not significant
<b>WB</b>	Western blot
<b>NMJs</b>	Neuromuscular junctions
<b>SV</b>	Synaptic vesicle
<b>Deep-sequencing</b>	High-throughput sequencing
<b>IC</b>	Input control
<b>qRT-PCR</b>	Quantitative Real-time-Polymerase chain reaction
<b>PCA</b>	Principal component analysis
<b>PC</b>	Principal component
<b>TAL</b>	Transcriptome and Genome Analysis Laboratory
<b>UMG</b>	University Medical Center Göttingen
<b>INIMS</b>	Institute of Neuroimmunology and Multiple Sclerosis
<b>ZMNH</b>	Center for Molecular Neurobiology Hamburg
<b>BT</b>	BacTrap
<b>TEX26</b>	Testis expressed 26
<b>SYNGR4</b>	Synaptogyrin 4
<b>NHLH1</b>	Helix-loop-helix 1
<b>MXD3</b>	MAX Dimerization Protein 3
<b>PLEKHB1</b>	Pleckstrin Homology Domain Containing B1
<b>AD</b>	Average deviation
<b>IHC</b>	Immunohistochemistry
<b>Q331K</b>	TDP-43 <sup>Q331K</sup>
<b>SA/NaAsO<sub>2</sub></b>	Sodium arsenite



---

<b>UV</b>	Ultra-violet
<b>80S</b>	Monosome
<b>FS</b>	Free subunits
<b>ISH-IHC</b>	In situ hybridization-IHC
<b>PHD</b>	Pleckstrin homology domain
<b>CVB3</b>	Coxsackievirus B3
<b>TGN</b>	Trans-Golgi network
<b>KI</b>	Knock-in
<b>SLMVs</b>	Microvesicles
<b>siRNA</b>	Small interfering
<b>bZIP</b>	Basic leucine zipper
<b>SDS</b>	Sodium dodecyl sulfate
<b>DTT</b>	Dithiothreitol
<b>CHX</b>	Cycloheximide
<b>HBSS</b>	Hanks' Balanced salt solution
<b>FBS</b>	Fetal Bovine Serum
<b>PBS</b>	Phosphate buffered saline
<b>TRIC-<math>\alpha</math>BTX</b>	Tetramethylrhodamine- $\alpha$ bungarotoxin
<b>EtOH</b>	Ethanol
<b>RT</b>	Room temperature
<b>BSA</b>	Bovine serum albumin
<b>DHPC</b>	Dihexanoylphosphatidylcholine
<b>H<sub>2</sub>O</b>	Water
<b>PFA</b>	Paraformaldehyde
<b>FDR</b>	Discovery rate values
<b>ChAT</b>	Choline acetyltransferase
<b>DMSO</b>	Dimethyl sulfoxide

## Abbreviations

---

<b>M/P</b>	Monosome to polysome
<b>M</b>	Monosome

## Acknowledgements

I would like to thank first Dr. Kent Duncan for trusting me with this challenging project and for all his guidance and helpful discussions throughout my PhD. I would also like to thank Prof. Dr. Manuel Friebe and Dr. Jan Broder Engler for all their insight and input on my project.

A sincere thank you to Dr. Sabine Hoffmeister-Ullerich for her incredible patience and scientific suggestions and to Dr. Fabio Morellini for helping me to set up all the behavioral experiments. I would like to express my sincere gratitude to Katrin Kuchler for all her help and support provided with the maintenance of the mouse lines, genotyping and IHC and to Eva Kronberg for animal care. I would also like to express my gratitude to all the external collaborators of this project: Dr. Ross A. Jones, Prof. Dr. Thomas Lingner, Dr. Gabriela Salinas-Riester and Dr. Thomas H. Gillingwater for believing in this project.

Many thanks to all the member of the Neuronal Translational Control group: Florian Stelzner, Jolena Böge, Nagammal Neelagandan, Aida Cardona, Kawssar Harb, Katrin Kuchler and Christoph Janiesch for their fruitful discussions. A special thank you to Florian Stelzner and Jolena Böge, for working closely with me. It was a pleasure to do science with you two. Also, to all the community at ZMNH for their support and great scientific discussions. A very special thank you to Dr. med. Sergio Castro Gómez and Federico Tenedini for all the support and true friendship. You made this process a lot more fun!

To all my close friends in Hamburg, Lisbon and where else in the world, who made this experience more enjoyable: Anna Dammann, Christin Schwarzer, Carolina Pinto, Joana Godinho dos Santos, Célia Fernandes, Rubina Marques, Cátia Pereira, Sara Silva, Tania Santos, Joana Fernandes, Pavlos Zeleznov, Sergey Dyshlovoy, Alicia Ramírez and Katarina Horvathová.

This experience would have been tougher without the support and affection of my entire family, especially of my brother Miguel Marques, my mother Maria Joaquina Francisco, my father Carlos Marques, my grandmother Ivone Marques, and my grandfathers Manuel Avelino and Orlando Marques. A very special thank you to my grandmother Maria da Luz, to whom I dedicate this thesis.



## Abstract

Amyotrophic lateral sclerosis (ALS) is a devastating neurological disease that leads to progressive loss of motor neuron (MN) function. It is almost always fatal and there is currently no curative treatment. The RNA-binding protein TDP-43 is frequently mislocalized in ALS patient MNs and is the major component of ubiquitinated aggregates that characterize ALS pathology. Moreover, a subset of ALS patients have mutations in *TARDBP*, the gene, encoding TDP-43. Numerous studies analyzing patient samples, as well as animal and cell-based disease models, strongly support altered RNA regulation by TDP-43 within MNs as a major cause of disease. Nevertheless, the specific molecular changes that actually trigger disease onset remain unclear.

Here, I investigate molecular changes in MNs during the transition from the pre-symptomatic phase to disease onset in TDP-43-driven ALS. For this purpose, I applied Translating Ribosome Affinity Purification (TRAP) to established mouse models of ALS caused by mutant TDP-43. After a time-course with behavioral characterization, I collected spinal cords from mutant TDP-43 mice and matched controls at time points corresponding to pre-symptomatic and early symptomatic phases. Ribosome-associated mRNA from MNs was isolated via TRAP, followed by genome-wide high-throughput sequencing (RNA-Seq). Bioinformatic analysis of these samples revealed a number of mRNAs that are up- or downregulated in MNs of ALS models specifically at disease-onset. I confirmed altered regulation of *TEX26* and *PLEKHB1* via qRT-PCR in an independent TRAP experiment. Moreover, using quantitative immunostaining, I also detected corresponding changes at the protein level for *PLEKHB1* and *SYNGR4* in spinal MNs of two different hTDP-43 mutant mouse ALS models at disease onset. Thus, I have identified proteins that have the potential to be disease drivers, since they show altered regulation in MNs of ALS mouse models at the time when disease develops.

TRAP enables access to ribosome-associated mRNAs from specific cells in a complex mixture. However, TRAP presumably cannot monitor ribosome density, since an mRNA should be immunoprecipitated regardless of the number of ribosomes bound. To overcome these limitations, I started to develop a new method, Gradient-TRAP. This method combines sucrose density gradient separation of mRNAs according to the number of bound ribosomes, with immunoprecipitation of tagged ribosomes and associated mRNAs from specific gradient fractions. I first performed *in vitro* proof-of-concept experiments with a motor neuronal cell line transfected with GFP-L10a for TRAP. An established paradigm for translational control was used: induction of oxidative stress with sodium arsenite. This led to a strong inhibition of translation and polysome collapse, as expected. Using qRT-PCR to monitor mRNA levels across the gradients, it was found that most mRNAs showed dramatically reduced ribosome density after treatment. Remarkably, TRAP directly from lysates did not reveal any changes in ribosome co-immunoprecipitation. Thus, dramatic changes in ribosome density escape detection by conventional TRAP assays, as predicted. I also obtained evidence that Gradient-TRAP can work with *in vivo* material from adult mouse spinal cord.

## Zusammenfassung

Amyotrophe Lateralsklerose (ALS) ist eine verheerende neurologische Erkrankung, die zu einem fortschreitenden Verlust der Funktion von Motoneuronen (MN) führt. Die Krankheit endet fast immer tödlich und es gibt derzeit keine Heilungschancen. Das RNA-bindende Protein TDP-43 ist häufig in MN von ALS-Patienten fehllokalisiert und gilt als Hauptbestandteil ubiquitiniertes Aggregate, welche die ALS-Pathologie kennzeichnen. Darüber hinaus hat eine Untergruppe von ALS-Patienten Mutationen in *TARDBP*, dem Gen, das TDP-43 kodiert. Zahlreiche Studien, die Patientenproben sowie Tier und zellbasierte Krankheitsmodelle analysieren, legen nahe, dass die veränderte RNA-Regulation durch TDP-43 in MN Hauptauslöser für die Erkrankung ist. Dennoch bleiben die spezifischen molekularen Veränderungen, die den Ausbruch der Krankheit auslösen, noch unklar.

In dieser Arbeit untersuche ich molekulare Veränderungen in MN während des Übergangs von der präsymptomatischen Phase zum Ausbruch der Krankheit bei TDP-43-induziertem ALS. Zu diesem Zweck habe ich die *Translating Ribosom Affinity Purification* (TRAP) auf etablierte Mausmodelle von ALS angewendet, die durch mutiertes TDP-43 verursacht wurden. Nach einem Zeitverlauf, bei dem eine Verhaltenscharakterisierung erfolgte, sammelte ich Rückenmarkstränge von Mutanten TDP-43-Mäusen in präsymptomatischen und frühen symptomatischen Phasen. Die Ribosom-assoziierte *mRNA* aus MN wurde über TRAP isoliert. Im Anschluss wurde eine genomweite Hochdurchsatz-Sequenzierung (RNA-Seq) durchgeführt. Die bioinformatische Analyse dieser Proben ergab, dass - vor allem bei Krankheitsbeginn - eine Reihe von *mRNAs* in den MNs von ALS-Modellen hoch- oder herunterreguliert sind. Des Weiteren konnte ich eine veränderte Regulation von *TEX26* und *PLEKHB1* über *qRT-PCR* in einem unabhängigen TRAP-Experiment bestätigen. Durch die Verwendung quantitativer Immunfärbung entdeckte ich zu Krankheitsbeginn entsprechende Veränderungen auf der Proteinebene für *PLEKHB1* und *SYNGR4* in MNs des Rückenmarks von zwei verschiedenen hTDP-43-mutierten Maus-ALS-Modellen. Vor diesem Hintergrund habe ich Proteine identifiziert, die als Krankheitstreiber in Frage kommen könnten, da sie - zum Zeitpunkt der Krankheitsentwicklung - eine veränderte Regulation in MNs von ALS-Mausmodellen zeigen.

TRAP ermöglicht den Zugang zu Ribosom-assoziierten *mRNAs* aus spezifischen Zellen in einer komplexen Zusammensetzung. TRAP kann die Ribosomendichte vermutlich jedoch nicht bestimmen, da eine *mRNA* unabhängig von der Anzahl der gebundenen Ribosomen immunpräzipitiert würde. Um diese Einschränkungen zu überwinden, habe ich begonnen, eine neue Methode, die *Gradient-TRAP*, zu entwickeln. Diese Methode kombiniert Saccharose-Dichtegradiententrennung von *mRNAs*, getreu der Anzahl von gebundenen Ribosomen, mit Immunpräzipitation von markierten Ribosomen und assoziierten *mRNAs* aus spezifischen Gradientenfraktionen. Ich führte zuerst *In-vitro-Proof-of-Concept*-Experimente mit einer motorischen neuronalen Zelllinie durch, die mit GFP-L10a für TRAP transfiziert war. Ein in der Literatur beschriebenes Paradigma für die Translationskontrolle wurde verwendet: Induktion von oxidativem Stress mit Natriumarsenit. Dies führte wie erwartet zu einer starken Hemmung der Translation und zum Polysomenkollaps. Mit *qRT-PCR* zur Bestimmung der *mRNA*-Konzentrationen über die Gradienten wurde festgestellt, dass die meisten *mRNAs* nach der Behandlung eine drastisch verringerte Ribosomendichte aufwiesen. Bemerkenswerterweise zeigte TRAP direkt aus Lysaten keine

Veränderungen in der Ribosomen-Co-Immunpräzipitation. Daher können dramatische Änderungen der Ribosomendichte durch herkömmliche TRAP-Assays, wie vorhergesagt, nicht aufgedeckt werden. Ausserdem konnte Ich zeigen, dass es möglich ist Gradienten-TRAP mit *in vivo* Material aus dem Rückenmark erwachsener Mäuse durchzuführen.





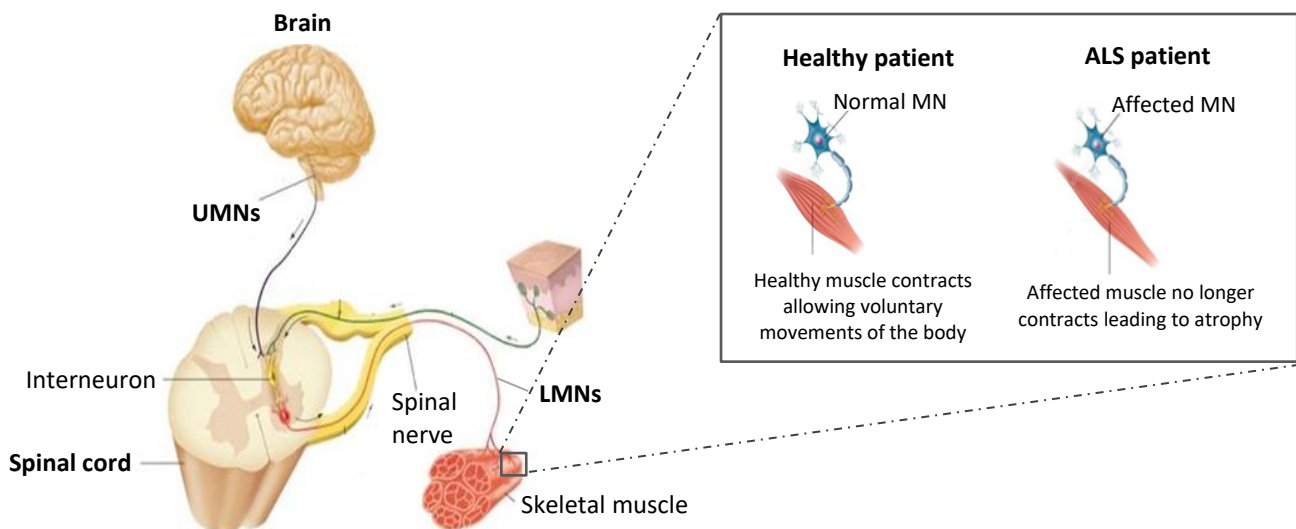
# **1. Introduction**



# 1. Introduction

## 1.1. Amyotrophic lateral sclerosis (ALS) is a devastating neurological disorder

Amyotrophic lateral sclerosis (ALS), also known as motor neuron disease (MND) or Lou Gehrig's disease, was first described by the neurologist Jean-Martin Charcot in 1874 and is characterized as a progressive neurodegenerative disorder that affects both upper motor neurons (UMNs), located in the motor cortex area of the brain, and lower motor neurons (LMNs), located in the brainstem and the ventral segmental horns of the spinal cord [1-3]. The disease usually begins with a focal onset weakness of a muscle, followed by a gradual spread to other muscles, leading to atrophy, paralysis and death. Most of patients die within 3 to 5 years after disease onset. These physical manifestations (phenotypes) of the disease are consequence of UMN and LMN degeneration. UMN degeneration results in muscle stiffness and spasticity, whereas, LMN degeneration leads to spontaneous muscle twitching (fasciculations) due to excessive electrical activity and loss of synaptic connectivity with target muscles, which then atrophy (Figure 1). The principal feature of the degeneration of motor neurons (MNs) is the presence of pathologic inclusions also known as aggregates within the cytoplasm of both upper and lower MNs. The presence of these aggregates is a major pathological hallmark of MN degeneration caused by ALS [3-6].



**Figure 1. MNs affected in ALS.**

The upper motor neurons (UMNs) originate in the brain and travel downward to connect with interneurons or directly to lower motor neurons (LMNs). Interneurons are intermediate neuronal cells that ultimately connect with LMNs, which localize in the brainstem and the spinal cord [7]. The LMNs innervate the striated muscles of the axial skeleton (neck and trunk) and the muscles of the upper and lower limbs. Degeneration of MNs in the brain stem and spinal cord causes muscle weakness, fasciculation and ultimately atrophy. Adapted from: <https://www.researchgate.net>.

## 1. Introduction

---

Currently, ALS has an incidence and prevalence of 1-2 and 3-5 per 100,000 individuals worldwide each year, respectively, which makes it an orphan disease. About 10% of ALS cases are familial (fALS), usually inherited as dominant traits, while the remaining 90% of ALS cases are sporadic (sALS), occurring without any family history. In fALS the ratio of the disease between women and men is 1:1. Curiously, in sALS there are fewer women diagnosed with ALS than men during the age range of 55 to 70 years old (ratio of 2:3), whereas, afterwards the ratio becomes more equal with increasing age. ALS has a median age of onset of 60 years, but in some cases may begin as early as the first or second decade of life [8-10]. However, recent studies showed an increasing incidence in older people [11-13].

Presently, there is no primary therapy available for ALS that treats the underlying cause effectively. Nevertheless, two drugs are currently approved for treating ALS. Riluzole (chemical name: 6-trifluoromethoxy-2-benzothiazolamine), was the first approved drug available on the market and has been commercially accessible in dozens of countries worldwide since the late 1990s. It can extend the patient's life for 2-3 months more, on average. Its mechanism of action is not yet fully understood, but it has been shown to: 1) have an inhibitory effect on glutamate release, 2) inactivate voltage-dependent sodium channels, and 3) interfere with intracellular events that follow transmitter binding at excitatory amino acid receptors [14, 15]. Edaravone (chemical name: 3-methyl-1-phenyl-2-pyrazolin-5-one), was the latest drug to be approved for the treatment of ALS worldwide (2017) [16]. Like Riluzole, its mechanism of action is also not known, but it slows the rate of decline in ALS patients. Its therapeutic effect could be due to its antioxidant properties. Both *in vitro* and *in vivo* studies have shown that, Edaravone confers protection against oxidative stress, by acting as a free radical scavenger [16-19].

To date, it is still unclear what causes ALS. Nonetheless, numerous perturbations of cellular functions in diseased MNs such as protein misfolding, excessive excitatory tone, impaired energy production, abnormal calcium metabolism, altered axonal transport and activation of proteases and nucleases have been identified [20, 21]. Several factors have been proposed to be the source of these perturbations. In the next section, some of these factors will be addressed in more detail.

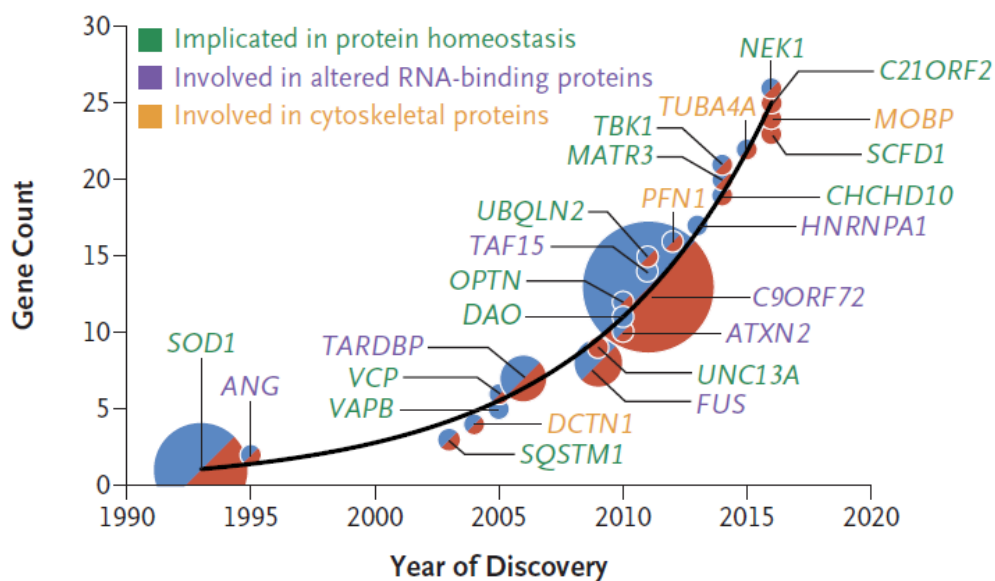
### 1.2. Different mutated genes have been identified to be the cause of ALS

In fALS, ALS can be inherited in an autosomal dominant, autosomal recessive or X-linked manner [22, 23]. On the other hand, sALS refers to disease that presents without a family history, although this term is sometimes mistakenly thought to refer to ALS that occurs without a genetic basis [6].

Even though only 10% of ALS cases have a family history component, it was the fALS forms of the disease that allowed the identification of several ALS genes [24, 25]. The first ALS gene identified, superoxide dismutase 1 (*SOD1*), was reported in 1993 [26]. *SOD1* protein is ubiquitously expressed, makes up 1-2% of the total soluble protein in the central nervous system (CNS) and is predominantly expressed in the cytosol [27]. It functions as a cytosolic and mitochondrial antioxidant enzyme, converting superoxide to molecular oxygen and hydrogen peroxide [27, 28]. So far more than 170 mutations in this gene have been identified to cause disease [8, 29].

Mutations in this gene result in the deposition of SOD1 into insoluble aggregates in MNs, probably as a consequence of structural destabilization and/or oxidative damage which in turn contributes to the misfolding and aggregation of SOD1 into neurotoxic species. Evidence of these aggregates was first reported in 1994 in post mortem spinal cord samples from sALS patients [30, 31]. The formation of these aggregates is considered a hallmark of SOD1-associated ALS [32, 33]. Thus far, SOD1 aggregates have only been observed in sALS and fALS cases containing *SOD1* mutations.

Since the discovery of mutations in the *SOD1* gene, at least 25 genes have been confirmed in several studies to be implicated in fALS, sALS or in both (Figure 2) [25, 34]. Most of these potential ALS genes were identified due to the evolving technologies for gene mapping [4, 6].



**Figure 2. Timeline of gene discovery for genetic mutations linked to ALS (1990 to 2017).**

Currently, more than 25 genes have been associated to ALS. Blue depicts genes that are associated with fALS, while red depicts genes associated with sALS. The presence of both colors indicates that mutations in that gene are present in both forms of the disease. Further, the size of each circle reflects the proportion of all familial and sporadic cases of ALS associated with that gene. Adapted from Brown R. H. et al.; 2017, [4].

It was not until 2006 that TAR DNA-binding protein-43 (TDP-43) protein was found to be the major component of protein aggregates frequently observed in post mortem brain and spinal cord of ALS patients [35, 36]. Candidate gene studies later identified mutations in the TAR DNA-binding protein (*TARDBP*) gene, which encodes the TDP-43 protein, in fALS and sALS cases [25, 36-38].

TDP-43 aggregates are found in both sALS and fALS and are characterized as complex structures since they recruit a large number of other proteins. One interesting fact about these inclusions is that different mutated genes show different proteins in these aggregates, leading to speculation about whether ALS might be a heterogeneous disease. For example, in a patient carrying the TDP-43<sup>G298S</sup> mutation, inclusions of fused in sarcoma (FUS) and TDP-43 proteins were detected [39]. Moreover, a patient with

## 1. Introduction

the UBQLN2<sup>P506T</sup> mutation showed on the cytoplasm of spinal cord MNs the presence of positive inclusions of ubiquilin2 (UBQLN2), sequestosome-1 (p62), TDP-43 and FUS [40]. Nevertheless, TDP-43 seems to be a common protein found in most of these inclusions present in most types of ALS (Table 1). Thus, TDP-43 is not only causing disease when mutated, but is also implicated in the vast majority of ALS cases due to aggregation in affected neuronal populations. This makes it a particularly interesting protein to study in the context of ALS [22, 25, 41].

**Table 1. Genes associated with dominant mutations showing principal neuropathological protein aggregates.**  
Adapted from [22, 42].

Gene	Neuropathological protein aggregates	External references
<b>SOD1</b>	SOD1 aggregates, or neurofilaments (e.g, I113T); generally, no TDP-43 aggregates, UBQLN2 aggregates	[40, 43]
<b>VAPB</b>	VAPB aggregates; probable TDP-43 aggregates	[44, 45]
<b>ANG</b>	TDP-43 aggregates	
<b>TARDBP</b>	TDP-43 aggregates, FUS and UBQLN2 aggregates (TDP-43 <sup>G298S</sup> )	[39, 43]
<b>FUS</b>	FUS aggregates, UBQLN2 aggregates	[39]
<b>OPTN</b>	TDP-43 aggregates	
<b>C9orf72</b>	TDP-43 aggregates, UBQLN2 aggregates	
<b>UBQLN2</b>	UBQLN2 aggregates, TDP-43 aggregates, FUS aggregates, p62 aggregates, OPTN aggregates	[40, 43]

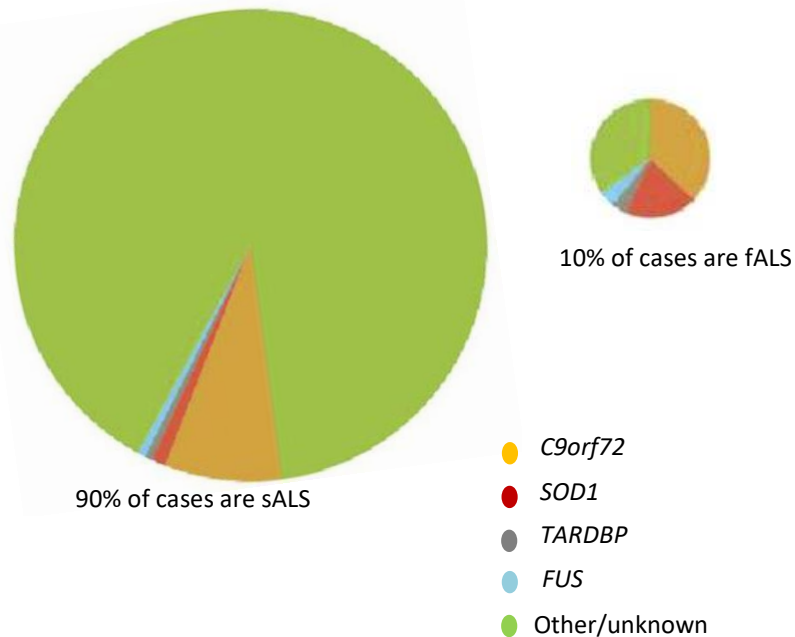
Legend: *VAPB*: Vesicle-associated membrane protein-associated protein B/C; *ANG*: Angiogenin; *OPTN*: Optineurin.

### 1.2.1. Similarities and differences between genetics of sALS and fALS

At least two-thirds of fALS cases can now be linked to the hexanucleotide repeat sequence in *C9orf72*, one of the four major genes linked to ALS, including *SOD1*, *TARDBP* and *FUS*. Mutations in the *SOD1* gene account for 20% of fALS and *TDP-43* and *FUS* around 5% each (Figure 3).

In sALS the vast majority of the causes of disease are still unknown. Many factors have been proposed to be the genetic cause of this form of the disease including low-penetrance mutations in genes responsible for hereditary disease, *de novo* mutations, variations in disease-susceptibility genes, and epigenetic events. From the current studies available, it seems that all of these processes are connected to sALS [46]. The expansions of the hexanucleotide repeat sequence in *C9orf72* and mutations of other genes, such as *SOD1*, *TARDBP* and *FUS* are also detectable in a small but significant proportion of sALS cases reporting no family history. *C9orf72* is causing approximately 10% of sALS, *SOD1* 3% and *TDP-43* 2% [47, 48]. Thus, some patients with sALS seem to carry an ALS-causing gene variant found in fALS (Figure 3)

[22, 23, 48]. Accordingly, it has become increasingly evident that there is thin barrier between fALS and sALS. In addition, misclassification of fALS to sALS in patients can happen, especially in situations where the family size is small. Specifically, as the penetrance of the causative variant reduces, there is an increasing probability that it will manifest as sALS, especially in smaller families [49].



**Figure 3. Known genetic causes of sALS and fALS.**

The vast majority of sALS causes remain unknown. The hexanucleotide repeat expansions in *C9orf72* are causing approximately 10% of sALS, with mutations in *SOD1* 3% and *TARDBP* 2%. Like in sALS, the hexanucleotide repeat expansions in *C9orf72* are currently the most common genetic cause in fALS accounting for almost 40%, followed by mutations in *SOD1* with 20%, and the genes encoding TDP-43 and *FUS* with ~5% each. Several other genes have been identified as genetic causes of ALS and collectively today over 60% of fALS can be explained by known mutations. Adapted from Tuner M. R. et al.; 2017 [47, 48].

With all the current discovered ALS genes, it appears that the mutant proteins they encode are involved in a variety of critical processes like mitochondrial function, ribonucleic acid (RNA) processing, nuclear import/export and protein aggregation, which allows these genes to be grouped into (1) those that alter protein homeostasis and quality control; (2) those that disturb aspects of RNA stability, function and metabolism; and (3) those that disturb cytoskeletal dynamics within the MN axon and distal terminal [6].

Clinically, ALS is depicted as a disease that results from UMN and LMN degeneration. Conversely, from the molecular point of view both sALS and fALS are caused by several distinct genes, whose mutations impair different biochemical pathways, resulting in overlapping clinical and pathological phenotypes, leading to the general idea that ALS is a final common pathway for processes initiated in different ways. A great deal of new knowledge has been collected on ALS, especially in terms of its underlying genetics and potential mechanisms. In contrast, identification of risk factors, especially non-genetic factors, for ALS has proven difficult, and likely reflects the complexity of the disease. A recent idea describes that

each individual has a determined prenatal genetic load and during life accumulates a number of risky environmental exposures and progressive age-related cell damage. In sum, ALS would be the final result of a complex interplay between genetics, environment, aging and perhaps other unidentified factors. Regardless of the unknown contribution of each of these factors, the malady would start to develop when their sum reaches a certain threshold. Once established, several auto-perpetuating mechanisms would occur, leading to disease progression. While in fALS, the genetic aspect has a high relevance, in sALS the environmental exposures may be the crucial aspect to reach the threshold [50].

### 1.3. Disease models to study ALS: an overview of their advantages and disadvantages

A full understanding of the mechanism that leads to MN degeneration is still necessary. Presently, the model systems vary from *in vitro* biochemical systems to cell culture systems, invertebrates and non-mammalian vertebrates, rodent models and to human patient-derived stem cell models (Table 2). The aim of these models is to mimic the neuropathological or genetic aspects of the disease to reveal the molecular players involved in the pathology that might be potential targets for therapeutic intervention. Even though, these models opened up new avenues for ALS research and provided a good balance between throughput and relevance for human disease, none of the available models fully reproduce all of the pathological and behavioral features of ALS [51, 52]. Furthermore, examples of successful translation from these disease models to patients are still lacking [52, 53].



**Table 2. Disease models of ALS pathology: advantages and disadvantages.** Adapted from [51, 52].

Model	Gene mutation linked to ALS	Advantages	Disadvantages
Yeast ( <i>Saccharomyces cerevisiae</i> )	<i>C9orf72, SOD1, TARDBP, FUS, VAPB, VCP, OPTN, SETX, PFN1, hnRNPA1/A2</i>	Readily available, low maintenance; homologous basic cellular structures to humans; non-animal; rapid turnover; high throughput	Cellular toxicity arising simply from overexpression of human proteins; facultative anaerobe unlike human cells
Worm ( <i>Caenorhabditis elegans</i> )	<i>C9orf72, SOD1, TARDBP, FUS, VAPB, ALS2, CHMP2B, ANG, VCP</i>	Readily available, low maintenance; homologous basic neuromuscular structures to humans	Limited human clinical similarity
Fruit fly ( <i>Drosophila melanogaster</i> )	<i>C9orf72, SOD1, TARDBP, FUS, VAPB, ALS2, CHMP2B, VCP, SETX, ATXN2, SQSTM1, hnRNPA1/A2</i>	Readily available, low maintenance; homologous basic neuromuscular structures to humans; short life cycle	Limited human clinical similarity
Zebrafish ( <i>Danio rerio</i> )	<i>C9orf72, SOD1, TARDBP, FUS, VAPB, ALS2, OPTN, ATXN2, SQSTM1</i>	Rapid breathing, low maintenance; homologous basic neuromuscular structures to humans; short life cycle	Limited human clinical similarity
Rodent ( <i>Mus musculus, Rattus norvegicus</i> )	<i>Mus musculus: C9orf72, SOD1, TARDBP, FUS, DCTN1, NEFH, VAPB, ALS2, CHMP2B, VCP, ATXN2, UBQLN2, SQSTM1, hnRNPA1/A2</i> <i>Rattus norvegicus: SOD1, TARDBP, FUS, DCTN1, NEFH, UBQLN2</i>	Consistent motor phenotype; readily available, low maintenance; homologous basic neuromuscular structures to humans; short life cycle	Costly infrastructure; ethical concerns; poor translation of therapeutic response in SOD1 mouse to human studies so far; TDP-43 models show limited motor phenotype
Dog (Pembroke Welsh corgi, Boxer)	<i>SOD1</i>	Similar to human SOD1-related ALS in being a delayed adult-onset disorder	Ethical concerns, availability and infrastructure issues; long latency to symptoms; limited relevance to non-SOD1-related ALS
Monkey ( <i>Macaca fascicularis</i> )	<i>TARDBP</i>	Closest species to humans physically and behaviorally	Major ethical concerns and infrastructure issues; limited relevance to slowly developing human ALS
Cells/primary cultures	<i>C9orf72, SOD1, TARDBP, FUS, VAPB, ALS2, CHMP2B, ANG, VCP, OPTN, SETX, ATXN2, UBQLN2, SQSTM1, PFN1, hnRNPA1/A2</i>	Easy to understand the principles of protein aggregation and gene mutation; identification of disease-modifying genes	Do not recapitulate the complexity of human disease, only remotely mimic the disease
Induced pluripotent stem cells (iPSCs)	<i>C9orf72, SOD1, TARDBP, FUS, VAPB, CHMP2B, ANG, VCP, SETX, ATXN2</i>	Capacity to differentiate into spinal MNs; carries endogenous gene mutations; possible to correct disease-causing mutations	Generation of UMN remains a challenge; lack of aging and complex interactions with surrounding non-neuronal cells

## 1. Introduction

---

Legend: *VCP*: valosin-containing protein; *SETX*: senataxin; *PFN1*: profilin1, *hnRNPA1/A2*: heterogeneous nuclear ribonucleoprotein A1/A2; *CHMP2B*: charged multivesicular body protein 2B; *ATXN2*: Ataxin2; *DCTN1*: dynactin subunit 1; *NEFH*: neurofilament heavy; *ALS2*: alsin.

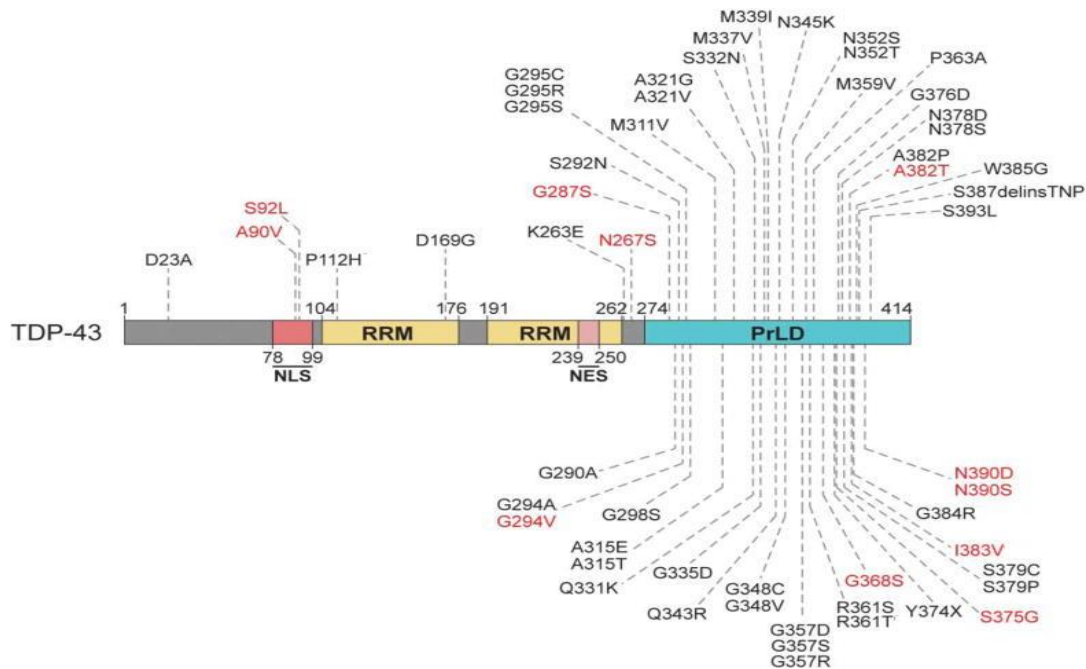
The presence of TDP-43 aggregates in ubiquitinated protein inclusions (UBIs) in the cytoplasm of MNs in both sALS and fALS makes studying TDP-43 of particular interest for understanding ALS pathology [35]. Collectively, disease models based on altered TDP-43 protein expression have shown that: 1) overexpression of TDP-43 in MNs causes toxic effects on their morphology and function [54]; 2) because overexpressing wild type (WT) TDP-43 already causes phenotypes it is hard to determine whether effects of overexpressing ALS mutations are actually due to the mutation; 3) TDP-43's RNA-binding activity is essential for toxicity [55] and 4) formation of aggregates is not necessary for disease development [56]; 5) several cell types are involved in ALS pathology, including neighboring non-neuronal supporting cells, which are crucial to neuronal dysfunction [57] and 6) expression of mutant TDP-43 only in MNs is sufficient to promote disease onset and progression [54]. Overall, these studies support a model in which altered RNA regulation by TDP-43 causes disease in MNs [58].

### 1.4. TDP-43 protein: a close look into its properties

Studies have revealed that 60% of patients with mutations in *TARDBP*-linked ALS initially demonstrate primarily upper extremity impairment and the mean age of onset is around 50 years in four of the five most common mutations in *TARDBP* gene (G298S, A315T, M337V, G34BC, A382T). Like ALS in general, most patients die within 5 years of developing the symptoms [49, 59].

#### 1.4.1. Structure of the TDP-43 protein

TDP-43 is 414 amino acids long and has a molecular weight of 43kDa. The domain structure of TDP-43 is comprised of an N-terminal domain (NTD, residues 1–104) that contains a nuclear localization signal (NLS, residues 78–99), two RNA recognition motifs, RRM1 (residues 104–176) and RRM2 (191–262), a nuclear export signal (NES) (residues 239–250) and a C-terminal domain (CTD, residues 274–414) (Figure 4). This C-terminal domain, because of its low complexity is also referred to as a prion-like domain (PrLD). This name is based on similarity in amino acid composition to yeast prion domains (Figure 4) [60–63]. The vast majority of the identified mutations in TDP-43 are found in its C-terminal domain, which is critical for normal protein function [64, 65]. The C-terminal domain facilitates miRNA biogenesis by mediating interactions with both the nuclear Drosha and cytoplasmic Dicer complex [66]. The C-terminus is also involved in mediating protein-protein interactions with other splicing factors, including heterogeneous nuclear ribonucleoprotein A1 (hnRNPA1), heterogeneous nuclear ribonucleoprotein A2/B1 (hnRNPA2B1) and FUS, and is essential for the regulation of splicing of certain messenger RNA (mRNA) transcripts [65, 67, 68]. Studies in cell culture and from mouse brains propose that TDP-43 is a dimeric protein and that dimer formation is mediated by several regions in the protein, including the NTD, RRM2, and/or the PrLD [69–72].



**Figure 4. Schematic representation of the domain structure of TDP-43 and location of mutations that cause ALS.** TDP-43 comprises a nuclear localization signal (NLS) and nuclear export signal (NES), two RNA recognition motifs (RRMs) and a C-terminal glycine-rich region, the PrLD, where the majority of the mutations that have been identified in patients with ALS are located. Mutations in red have also been observed in healthy control individuals suggesting something else is necessary in these cases to cause ALS. Adapted from Harrison A. F. et al.; 2017 [73].

#### 1.4.2. Characterization of the physiological function of TDP-43

TDP-43 is a deoxyribonucleic acid (DNA)- and RNA-binding protein (RBP) that was first discovered as a ubiquitously expressed cellular factor that binds the TAR element in the long terminal repeat (LTR) region of the human immunodeficiency virus type 1 (HIV1), which is fundamental for the control of viral gene expression [74].

This protein is primarily a nuclear protein, although it shuttles between the nucleus and the cytoplasm. TDP-43 plays a role in regulating mRNA splicing, stability, transport and translation as well as gene transcription [75]. Further, TDP-43 is also implicated in microRNA processing and regulation, control and stabilization of long intron-containing RNA, long noncoding RNA (lncRNA) and noncoding RNA (ncRNA) expression [58, 76]. TDP-43 binds preferentially to long UG repeats or UG-enriched RNA sequences [77-79]. A minimum number of six UG single-stranded dinucleotide stretches is necessary and the binding affinity increases with the number of repeats [80]. TDP-43 levels are tightly regulated through a negative feedback loop by binding to its own mRNA in the 3'-UTR region. A nonsense-mediated decay (NMD) independent mechanism seems to play a major role in TDP-43 mRNA degradation. The exosome system, a multiprotein complex able to degrade different classes of RNAs is responsible for degrading TDP-43 mRNA. However, an additional NMD-dependent mechanism was observed to take place in a minor variant of TDP-43 mRNA, the V2 [78, 81, 82]. Recent studies suggest that TDP-43 solubility can be

## 1. Introduction

---

modulated by RNA or DNA binding [69, 83]. In normal physiological conditions, TDP-43 resides mainly in the nucleus, whereas during stress, this protein shifts to the cytoplasm to become part of small ( $\leq 5\mu\text{m}$ ) non-membrane-bound cytoplasmic domains called stress granules (SGs), where it modulates their assembly and dynamics [84-86]. SGs are conserved cytoplasmic messenger ribonucleoprotein (mRNP) granules that form from pools of untranslating mRNA (mRNAs stalled in translation initiation) [87] and contain various translation initiation factors, a variety of RBPs and many non-RBPs [88]. Alterations in SGs formation were suggested to play a role in TDP-43 aggregation and pathology [89-91]. Due to the important role of TDP-43 in RNA-related functions, Knockout (KO) mouse models of TDP-43 are embryonically lethal, while heterozygous mice are not affected, possibly because of the tight control TDP-43 has over its own expression levels [92, 93]. The *TARDBP* gene is also highly conserved in humans, mice, *Drosophila melanogaster*, and *Caenorhabditis elegans* [62].

### 1.4.3. Mechanisms of pathogenicity of TDP-43 in ALS

Several studies have tried to shed light on how mutations in *TARDBP* cause MN death. In disease, TDP-43 is aberrantly ubiquitinated, phosphorylated, acetylated, sumoylated, and cleaved into C-terminal fragments accumulating in the cytoplasm of MNs in the form of aggregates. The formation of aggregates is usually accompanied by depletion of TDP-43 from the nucleus, as well as sequestration of other RNA binding proteins into these aggregates [94-96]. Mislocalization of TDP-43 to the cytoplasm is a well-established feature of ALS but not an absolute requirement for cell toxicity. While, some studies have shown that mutations in TDP-43 promote mislocalization to various subcellular locations in the cytoplasm [97, 98], one study showed that TDP-43 mutants are retained in the nucleus [56]. Clearance of TDP-43 from the nucleus leads to a loss of TDP-43 nuclear function and gain of a cytoplasmic one, which can cause numerous downstream effects that lead to neurotoxicity [99, 100]. For example TDP-43 was shown to localize in mitochondria and repress the expression of mitochondrial mRNAs. Interestingly, mutant forms of TDP-43 had increased mislocalization to the mitochondria, suggesting that mutant TDP-43 can cause greater mitochondria dysfunction [101]. In rat hippocampal neurons, cytoplasmic TDP-43 resides within RNA granules that travel to dendritic arbors upon depolarization [102], however, ALS-associated mutant forms of TDP-43 (A315T and Q343R) severely reduced the movement of the granules to dendrites, preventing the transport and therefore local translation of mRNAs encoding proteins that are required for proper synaptic function [103, 104]. Whether TDP-43 drives disease due to gain of function or loss of function or a combination of both remains an important question that still needs to be resolved.

### 1.4.4. Role of TDP-43 in SGs

When cells undergo stress, this leads to phosphorylation of eIF2 $\alpha$  by stress-induced kinases and translation arrest of most proteins which are not essential to a stress response. During this process, mRNAs that are not required in response to stress and respective RNA-binding proteins accumulate in SGs [105]. Likewise, upon stress induction, TDP-43 is often found in SGs in the cytoplasm where it is thought to modulate SG assembly and dynamics [69, 106, 107]. Alterations to these SG processes have

been suggested to play a key role in TDP-43 aggregation and pathology. Specifically, reduced levels of TDP-43 in primary cultures of cortical neurons and astrocytes resulted in an acceleration of SG disassembly in cortical neurons and astrocytes. Interestingly, SG assembly was impaired by TDP-43 depletion in both cortical neurons and astrocytes reaffirming the important role of TDP-43 in regulating this essential cell stress response mechanism [108]. A study showed that when TDP-43 is knocked down (KD), SGs form more slowly, take longer to reach their average normal size, and dissipate more quickly [85]. Nonetheless, light still needs to be shed on whether SGs are direct precursors to TDP-43 aggregates or whether TDP-43 aggregates are formed independently and recruited later to SGs [91].

The association of proteins involved in ALS to SGs, such as TDP-43, FUS and T-cell-restricted intracellular antigen-1 (TIA1), favors the hypothesis in which the disease might be the consequence of disturbed SG regulation in both unstressed and stressed conditions. In unstressed conditions, mutant ALS factors might induce an uncontrolled and sustained activation of SG-mediated translational repression, whereas under stress conditions, such response might escape this regulation. Several studies have allowed formulating three points favoring this hypothesis:

- 1 - Genes involved in the regulation of SGs are known to be modifiers of the toxicity of mutant ALS genes, including *TARDBP*, *Profilin 1* and *C9orf72*, in yeast and *Drosophila* [109-111];
- 2 - Several ALS-linked genes have a physiological role in SG formation and dynamics. Loss of these functions might be involved in ALS [106, 112];
- 3 - Mutant ALS proteins might interfere with chaperone-mediated clearance from SGs of defective ribosomal products (DRiPs) constituted by terminated polypeptides that are released by disassembling polysomes prior to SG formation [112].

There is evidence suggesting that the cytoplasmic aggregates are toxic to cells and lead to cell death through a toxic gain-of-function, although alternative theories of TDP-43 aggregates as cytoprotective structures do exist in *Drosophila* models [97, 113-116]. Indeed, in cellular and animal models, toxicity induced by mutant TDP-43 does not appear to require its aggregation [98, 117-119].

#### 1.4.5. Role of TDP-43 in RNA metabolism

TDP-43 is known for its role in RNA metabolism, the process by which RNA is generated, transported, regulated, stored and translated. Crosslinking and immunoprecipitation followed by sequencing experiments identified the global RNA targets of TDP-43. These experiments showed that TDP-43 binds to thousands of RNAs [78, 79, 120, 121]. TDP-43 was showed to have a strong preference for UG-repeat motifs, but also binds to non-UG sequences. One function of TDP-43 is controlling alternative splicing. The nuclear loss of TDP-43 and subsequent formation of aggregates can lead to altered splicing events causing altered gene regulation. In this context, experimental depletion of TDP-43 in mice altered hundreds of splicing events in the brain and resulted in depletion of several RNAs encoding synaptic proteins [78]. Further, the loss of this protein in the nucleus may lower the levels of correctly spliced

protein-encoding mRNAs [122]. Moreover, loss of TDP-43 also alters miRNA biogenesis by increasing pri-miRNA and reducing the pre-miRNA levels. Reduction in expression of microRNAs was seen in model systems, including *Drosophila* and iPS-derived from patients with TDP-43 mutations, suggesting a possible role for altered RNA silencing in ALS [123]. A role in RNA transport, translation, and stability by TDP-43 was reported [79, 124]. A large percentage of the proteins that co-purify with TDP-43 are involved in RNA transport, splicing and translation [125]. In neurons, the pathways that control RNA trafficking and translation are intimately linked [126], with localized mRNAs being translationally repressed while in transit, and only being actively translated upon reaching their synaptic destinations [127]. Translation is also tightly regulated when the cell is under stress. TDP-43 was shown to associate with mRNAs that are bound to stalled ribosomes during non-lethal stress events and to contribute to cell survival [128]. TDP-43 was shown to control RNA stability through several mechanisms. Moreover, TDP-43 negatively regulates its own transcript by binding to the 3'UTR of its own mRNA [81, 129].

The contribution of altered RNA metabolism to neurodegeneration is becoming increasingly clear. Since several disease-associated pathways are perturbed in neurodegenerative diseases, it is unlikely that targeting only one of these events will lead to a complete cure. Nonetheless, reversing some of these RNA aberrations could prove to be effective in modifying the course of the diseases where they are prominent [130].

### 1.4.6. TDP-43 proteinopathies

Neurodegenerative diseases are increasingly viewed as “proteinopathies”, where a specific protein or peptide is involved in the pathogenesis of the disease by misfolding, polymerization, reduced degradation and final accumulation in the form of insoluble inclusions leading to neurodegeneration by various interacting mechanisms [131, 132]. In Alzheimer’s disease (AD) extracellular beta amyloid peptides and intracellular hyperphosphorylated tau proteins accumulate in the brain. In parkinsonian syndromes, alpha synuclein ( $\alpha$ -Syn) or 4R tau isoforms are found in various cytoplasmic inclusions.

The cytoplasmic mislocalization, fragmentation, aggregation, and post-translational modification of TDP-43, is not restricted to ALS. This type of pathology is also found in about 50% of patients with frontotemporal lobar degeneration (FTLD) [33, 132]. The two clinical conditions may coexist in the same patient or in the same family with TDP-43 being the major culprit in the ALS-FTLD spectrum [76]. However, TDP-43 inclusions were also observed in neurodegenerative disorders, such as AD, Lewy-body disease (LBD) and hippocampal sclerosis (HpScl) suggesting that these inclusions might be part of a broad disease spectrum [133, 134]. This common pathological feature of TDP-43 has attracted a lot of interest in trying to understand the pathomechanisms underlying TDP-43 proteinopathy. However, a still unanswered question is whether TDP-43 proteinopathy is required for the development of disease and could be used as a therapeutic target.

### 1.5. Translation is a crucial step to define protein levels in a cell

Control of mRNA translation seems to play an important role in ALS pathology [135]. However, further studies are necessary to determine how is the regulation of mRNAs affected by mutations in ALS-linked genes and whether targeting mRNA translation could be an effective treatment against ALS.

Translation is one crucial part of gene expression, which is responsible for driving complexity in a living organism. For genes that encode proteins, expression converts information stored in DNA, into a product called protein and this process is under tight regulation. Two major phases of gene expression are transcription and translation [136, 137]. Since in the focus of my thesis are mammalian models of ALS, a human disease, this section will concentrate on the details of mammalian gene expression. Moreover, since transcription is beyond the scope of this thesis, it will be only briefly described.

Transcription is the first step of gene expression and it involves unwinding of the DNA double strand to serve as a template to create a single-stranded RNA copy of the gene, a mRNA for protein coding genes. This process takes place in the nucleus of the cell and encompasses three phases: initiation, elongation, and termination.

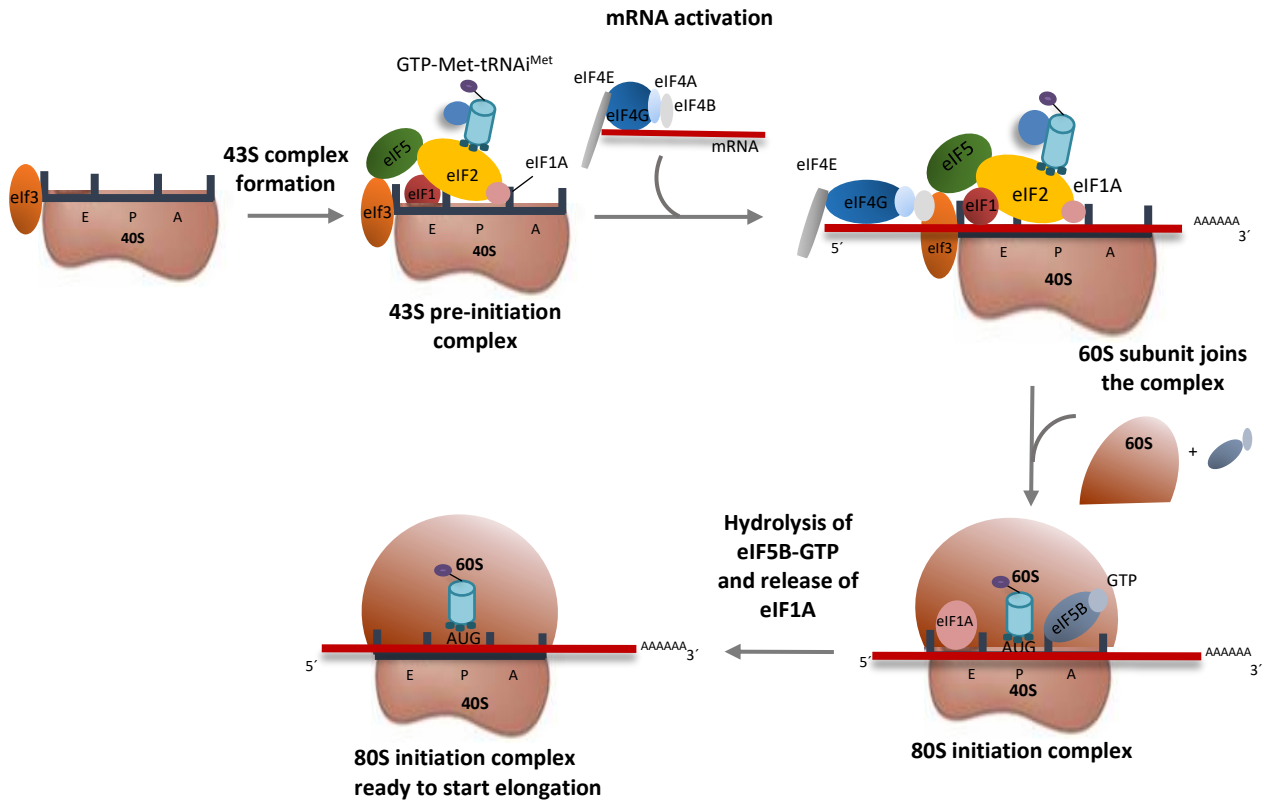
During initiation the RNA polymerase binds to the promoter separating the DNA strands, which provides a single-stranded template for transcription. During elongation the RNA polymerase is responsible for linking nucleotides in a specific manner, from the 5' to 3' direction, to form a single RNA strand [138]. The new RNA transcript carries the same information as the non-template strand of DNA, but it contains the base uracil (U) instead of thymine (T). In the last step of translation, a termination sequence signals that the RNA transcription is finished, and the RNA polymerase disassembles from the newly formed strand. An example of a termination mechanism involves the formation of a hairpin in the RNA. In eukaryotes, RNA molecules must be processed after transcription: they are spliced and have a 5' cap and poly-A tail put on their 5' and 3' ends, respectively [139]. Regulatory steps following transcription are denominated posttranscriptional regulation (PTR) steps and are directly involved in the assembly of the structure and abundance of the final protein. These PTR steps are in chronologic order of events: splicing, polyadenylation, translation and RNA decay [140]. It is the step of translation that controls cellular protein expression and it is therefore the focus of this section. All descriptions given regarding translation will be referent to mammalian systems, since ALS is a mammalian disease.

Translation is comprised of three major phases: initiation, elongation and termination where ribosomes play an important role. Ribosomes are the specialized structures within a cell, responsible for the translation. In eukaryotic organisms, mature mRNA needs to leave the nucleus in order to be translated, whereas in prokaryotic organisms, translation by ribosomes begins while DNA is still being transcribed. In eukaryotes these structures localize in two pools of the cytoplasm of eukaryotic cells: 1) in the endoplasmic reticulum (ER) for synthesis of membrane proteins, and 2) in a cytosolic pool, in which cytosolic proteins are synthesized [141, 142].

Translation initiation is believed to be the most tightly regulated stage of this process. Here the 43S pre-initiation complex<sup>2</sup> (PIC) associates with the mRNA 5' terminal m<sup>7</sup>G cap in coordination with the

## 1. Introduction

eukaryotic initiation factors (eIFs) of the eIF4F complex: eIF4A, eIF4G, and eIF4E. This allows the 40S ribosomal subunit to scan for the initiation AUG codon and for the 60S subunit to join. The assembly of the 40S (small ribosomal subunit) together with the 60S (large ribosomal subunit) forms the 80S monosome which pairs with a methionyl-charged transfer ribonucleic acid (Met-tRNA) at the initiation codon (Figure 5) [143-145].



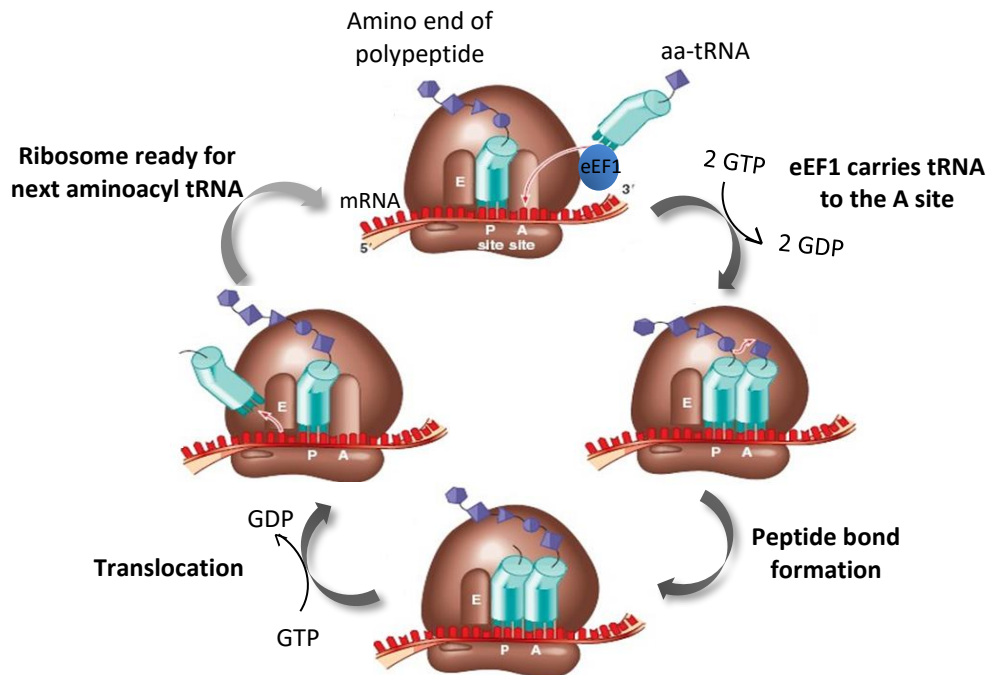
**Figure 5. Translation initiation.**

Translation initiation starts with the formation of the 43S pre-initiation complex (PIC). The 43S PIC consists of 40S (small subunit), eIF2.GTP-Met-tRNA<sup>iMet</sup>, eIF1, eIF1A, eIF3, and eIF5. The 43S PIC assembles with the activated mRNA, near the 5'-cap. The mRNA is scanned from 5' to 3' direction until the initiation codon (AUG) is found. The 60S joins the PIC and detachment of eIF2-GDP and other translation factors mediated by eIF5B takes place. Hydrolysis of eIF5B-guanosine-5'-triphosphate (GTP) and release of guanosine-5'-diphosphate (GDP)-bound eIF5B and eIF1A, allows the newly 80S assembled complex to start elongation. Adapted from [138, 143, 145, 146].

Subsequently, elongation is defined as the step where amino acids are transported by tRNAs to the ribosomes and are linked together to form a chain (figure 6). Specifically, each group of three bases in mRNA constitutes a codon and each codon specifies a particular amino acid (triplet code). Thus, the mRNA sequence is used as a template to assemble the chain of amino acids, with the help of ribosomes to form the protein. Translation elongation factors (eEFs) are recruited to promote polypeptide chain extension until the ribosome reaches the sequence of the stop codon. At the beginning of elongation, the Met-tRNA assembles to the P site of the ribosome, leaving both the E and A site free. eEF1A binds to the Aminoacyl-tRNAs (aa-tRNAs) and allows them to bind to the A site. After this event, a peptide bond is



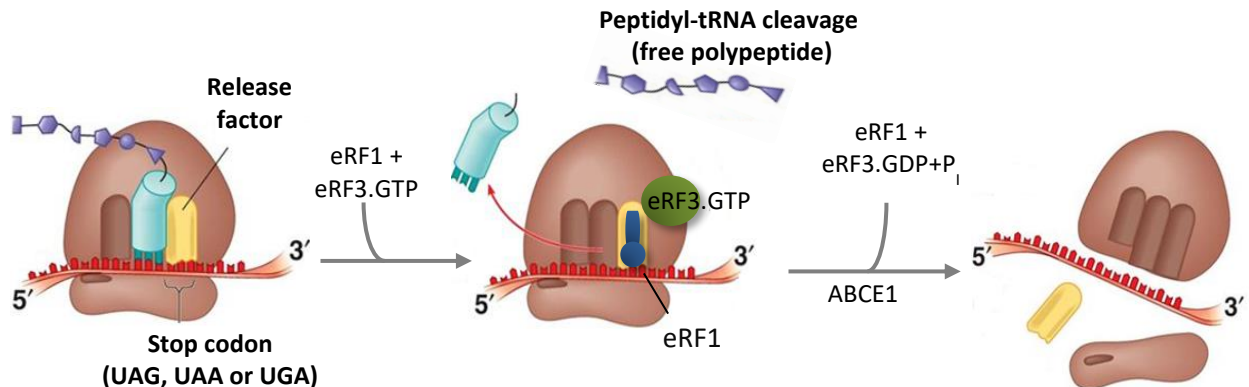
established and a transfer of the peptidyl tRNA occurs followed by a process called translocation [147]. In this process, the first tRNA shifts from the P to the E site and the tRNA from the A site moves to the P site, leaving the A site free again [148]. The tRNA that is in the E site is released, leaving just the tRNA in the P site connected with the nascent peptide chain. This process is repeated until the stop codon is reached.



**Figure 6. Translation elongation.**

The Met-tRNA is situated at the P site and the aminoacyl-tRNA (aa-tRNA), which is bound to eEF1 comes and binds to the A site. Next, the amino acid in the P site binds to the amino acid from the tRNA on the A site and a new peptide bond is formed. At the same time, the empty tRNA is moved to the E site (translocation due to GTP hydrolysis) and the peptidyl tRNA is moved to the P site, while the ribosome moves on the mRNA by three bases. The process restarts again until the stop codon is reached. Adapted from [http://www.pinsdaddy.com/codon-subunit\\_6IZ4iixWqMkIVdcEhJ9eUUdJzfrQYHH8fL\\*BNKYWZ4/](http://www.pinsdaddy.com/codon-subunit_6IZ4iixWqMkIVdcEhJ9eUUdJzfrQYHH8fL*BNKYWZ4/) [143].

At this step, termination starts once the stop codon is reached. Termination requires two release factors (RFs), eRF1 and eRF3, which bind to the A-site of the ribosome forming a complex with guanosine-5'-triphosphate (GTP) (Figure 7). The action of this complex leads to the release of the completed protein product. The ribosomal subunits are then recycled for further rounds of translation [144, 149].



**Figure 7. Translation termination.**

Translation termination occurs when the translating ribosome reaches one of the stop codons. Two release factors (eRFs) are involved in termination: eRF1 and eRF3. eRF1 is involved in stop codon recognition, while eRF3 binds to eRF1 and facilitates release of the polypeptide chain through GTP hydrolysis. Here, the peptidyl tRNA moves to the P site and the link between the polypeptide chain and the tRNA is hydrolyzed by the enzymatic activity of rRNA which releases the completed protein and subsequently tRNA and mRNA. With the addition of the ABC family ATPase E1 (ABCE1), the ribosomal subunits are separated, terminating translation. The ribosome is disassembled, and its subunits recycled. Adapted from [143, 150, 151] and from [http://www.pinsdaddy.com/codon-subunit\\_6Iz4iixWqMkIVdcEhJ9eUUdJzfrQYHH8fL\\*BNKYWZ4/](http://www.pinsdaddy.com/codon-subunit_6Iz4iixWqMkIVdcEhJ9eUUdJzfrQYHH8fL*BNKYWZ4/).

It is fundamental for cellular and organismal health that fidelity in mRNA translation is kept under strong regulation, while errors in this step often lead to proteins with reduced or aberrant function. Such proteins can sometimes be subjected to abnormal folding followed by protein aggregation and cytotoxicity to the cell [152, 153].

#### 1.5.1. Available genome-wide methods cannot study translation in specific cell types *in vivo*

Advances in genome-wide methods have improved the current way to study translation. Techniques such as microarrays and high-throughput sequencing (deep sequencing) have emerged as techniques that allow gene discovery by offering unbiased approaches and by the fact that they can be modified to investigate specific aspects of RNA regulation.

The original idea that mRNA expression correlates closely with the encoded protein is long proved wrong [154, 155]. Since multiple mechanisms are in place to control mRNA translation, it is in fact expected a lack of correlation. In addition, it is also known that gene expression patterns vary greatly from one cell type to another, therefore requiring genome-wide studies to be done from specific cell populations. Four techniques, polysome profiling, ribosome profiling, translating ribosome affinity purification (TRAP) and RiboTag, are currently available to study translation (Table 3) [156]. Polysome profiling is used to study ribosome-associated mRNAs (ribosome density) by separating polysomes (more than 2 ribosomes per

mRNA), monosome and other mRNP complexes by centrifugation through a sucrose gradient [157]. Ribosome profiling allows mapping the exact position of ribosomes in the transcriptome, and can also be used to measure translation efficiency, by comparing the ratio of ribosome footprint density to total mRNA [158, 159]. Both techniques give information about the translational status of specific mRNAs. On the other hand, TRAP uses bacterial artificial chromosome transgenic mice, bacTrap mice, which express an enhanced green fluorescent protein (EGFP)-tagged ribosomal protein, L10a, under defined promoters that are activated in specific cell types [160]. Similarly, RiboTag uses a mouse line that contains three hemagglutinin (HA) tags inserted into the locus of *Rlp22*, a gene encoding another ribosomal protein. The expression of this protein is dependent on Cre recombination. In its absence only endogenous (WT) *Rlp22* is expressed [161]. Both methods take advantage of immunoprecipitation techniques to have access to ribosome-bound mRNAs from specific cell types within a mixed population of cells.

**Table 3. Methods to study translation.** Adapted from [156, 162].

Methods	RNA isolation methodology	Advantages	Limitations
<b>Polysome profiling</b>	Purification of ribosome-associated mRNAs by centrifugation through a sucrose gradient	Original method to examine translation status of transcriptome	Labor intensive; scaling issues; does not confer access to specific cell types <i>in vivo</i>
<b>TRAP</b>	Immunoprecipitation (IP) of EGFP-L10a-associated mRNAs from mouse brain or other tissue	Examines ribosome-associated mRNAs within a specific cell type <i>in vivo</i>	Each BacTrap mouse line is limited to one cell type; EGFP antibodies are costly relative to anti-HA antibody; many cell types lack specific gene markers
<b>RiboTag</b>	IP of Rlp22-HA-associated mRNAs from mouse tissue	Examines polysome-associated mRNAs within a specific cell type <i>in vivo</i> ; takes advantage of Cre recombinase-expressing mouse lines to expand the range of cell types that can be investigated; commercial anti-HA antibody is less costly than in-house EGFP	Cre transgenic lines for each cell type need to be created; many cell types lack specific gene markers
<b>Ribosome profiling</b>	Nuclease digestion of polysome complexes, followed by centrifugation through a sucrose gradient or cushion to purify ribosome-mRNA complexes; ribosome-protected fragments are deep sequenced	Determines ribosome position and translation efficiency for individual mRNAs; reveals novel translational regulatory features (start and termination sites, ribosome stall position)	Only possible in genome-wide configuration; requires extensive bioinformatics; cannot resolve impact of mRNA isoform-specific translational control

Genome-wide methods are emerging as powerful tools to gain mechanistic insight into translation. Although progress has been made, most of these methods show several limitations and a disconnection between the amount of data generated and the available techniques (molecular and computational) to deal with this type of data [156]. Thus, improvement of the available readout methods is necessary. One interesting fact about these currently available methods to study translation is that none of them can measure changes in ribosome density on mRNAs from specific cell types *in vivo*.



## **2. Aims**



## 2. Aims of the thesis

ALS is a devastating neurological disease involving progressive loss of MN function. The current lack of therapeutic options would be improved by a better understanding of the underlying disease-causing mechanisms. Significant attention has centered on the RNA-binding protein TDP-43, since it is the major component of MN aggregates that characterize ALS pathology. Further, dozens of dominant mutations in the TDP-43 gene have been found to cause ALS. This extensive link between TDP-43 and ALS pathology, strengthens the idea that RNA metabolism might play an important role in disease. A major hypothesis is that altered TDP-43 function affects the expression of specific genes in MNs to cause ALS. However, the identity of these genes and how their misregulation leads to disease remain unclear.

The development of methods like TRAP, which allow purification and analysis of ribosome-associated mRNAs from specific cell types, have changed the way RNA metabolism is studied, especially in disease. In this thesis I sought to take advantage of such methods to further understand the role of mutant TDP-43 in controlling gene expression in MNs in ALS.

The major goal of my thesis was to identify molecules whose altered expression in MNs lead to degeneration in ALS: i.e. “disease drivers”. To address this goal, I pursued four specific aims:

- 1) To carefully determine the timing of disease onset in mouse models of ALS caused by mutant TDP-43
- 2) To identify differentially regulated molecules in MNs from healthy vs diseased mice
- 3) To validate in independent cohorts these molecules as potential disease drivers
- 4) To develop a new method to measure ribosome density *in vivo*: Gradient-TRAP.





## **3. Results**



### 3. Results

#### 3.1. Behavioral characterization of the mouse lines

To determine which proteins show altered expression in MNs as disease develops, I worked mainly with a specific mouse model of ALS: the *hTARDBP*<sup>A315T</sup> (A315T) transgenic mice, expressing the hTDP-43<sup>A315T</sup> protein, from the Baloh group [118]. This line was obtained from Jackson Laboratory and expresses a transgene coding for human TDP-43 bearing the patient mutant allele that substitutes a threonine residue for alanine at position 315 in the TDP-43 amino acid sequence. I also used two control lines: the Chat-BacTrap mouse line [160] and the hTDP-43 mouse line that reported to over express human TDP-43 protein (hTDP-43) at level insufficient to cause disease [163]. The Chat-BacTrap mouse line was chosen because the line expresses a tagged ribosomal protein (EGFP-L10a) under the *Chat* promoter and associated upstream control sequences. Since MNs are known to be highly cholinergic cells, it is expected to produce the EGFP-L10a protein in higher levels than the other surrounding cells in spinal cord. The presence of the EGFP-L10a protein confers access to mRNAs that are bound and presumably being actively translated by ribosomes (often referred to as the “translatome”).

The hTDP-43 line was chosen as a control line because, even though it overexpresses the hTDP-43 protein compared to the endogenous mouse TDP-43 protein, the expression levels are not sufficient to cause disease. Thus, the usage of this line helps to identify molecular changes in the A315T animals that correlate with disease. I crossed both the A315T and the hTDP-43 lines with the Chat-BacTrap line to have access to the ribosome-bound mRNAs of MNs as disease develops.

The A315T line was previously described in the literature to have a different disease progression in males and females. It was reported that the males develop disease phenotypes earlier than the females [164]. This effect was also seen in other animal models of ALS, such as the SOD1 with the G93A mutation [165]. Intriguingly, the same tendency was also reported in ALS patients. Indeed, several studies demonstrated that men develop symptoms earlier than women [9]. In line with all this evidence, I decided to separately study the disease progression in male and female mice.

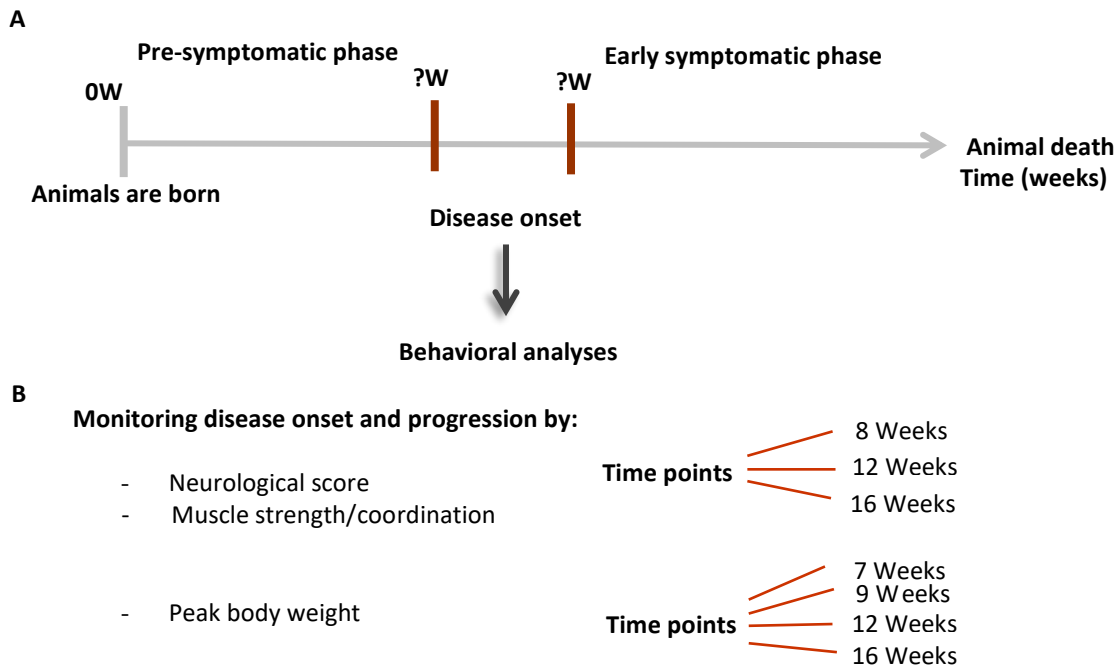
To simplify nomenclature, in point 3.1 and 3.2., “hTDP-43” refers to both hTDP-43 and Chat-BacTrap; hTDP-43 groups and “A315T” refers to both A315T and Chat-BacTrap; A315T groups.

##### 3.1.1. Disease onset determination

In order to determine disease onset, I performed behavioral analysis. The establishment of the beginning of the disease is important, since I am interested in identifying disease drivers, proteins that are altered at the very early stage of the disease (early symptomatic phase) when comparing to the non-symptomatic phase (pre-symptomatic phase). I monitored disease onset and progression by assessing the neurological score, peak body weight, muscle weakness and coordination. The animals were tested

### 3. Results

at different time points (7, 8, 9, 12 and 16 weeks of age), depending on the assay and only until phenotypes concomitant with the early symptomatic phase were observed (Figure 8). Based on what was observed earlier in the literature, I separately studied the disease progression in male and female mice. Moreover, I tested both animals with and without the *Chat::L10a-GFP* transgene, in order to determine whether this transgene would show phenotypes on its own or would modify the phenotypes observed with the other lines.

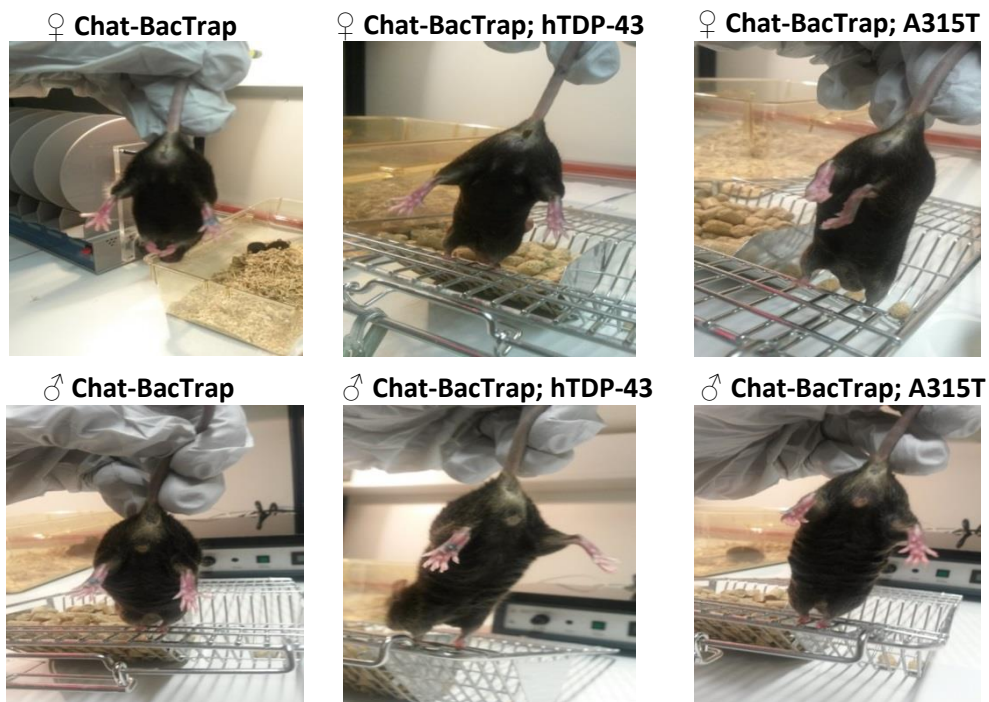


**Figure 8. Behavioral analysis was used to define disease onset and progression.**

(A) Schematic of the experiment used to characterize disease onset and progression in both female and male cohorts. The major aim was to define the timing of the transition from pre-symptomatic to early symptomatic phases of the disease. (B) Behavioral tests used to monitor disease onset and progression. This included evaluation of the neurological score and muscle strength/coordination at 8, 12 and 16 weeks of age and peak body weight at 7, 9, 12 and 16 weeks of age.

#### 3.1.1.1. Neurological score

The neurological score is based on extension of the hindlimbs after tail lift and ranges from 0 (no ALS symptomology) to 4 (end stage) [166]. A full description of the scoring system is provided in methods section 7.4.1 and representative images of neurological score phenotyping for 16 week-old mice are shown in Figure 9.

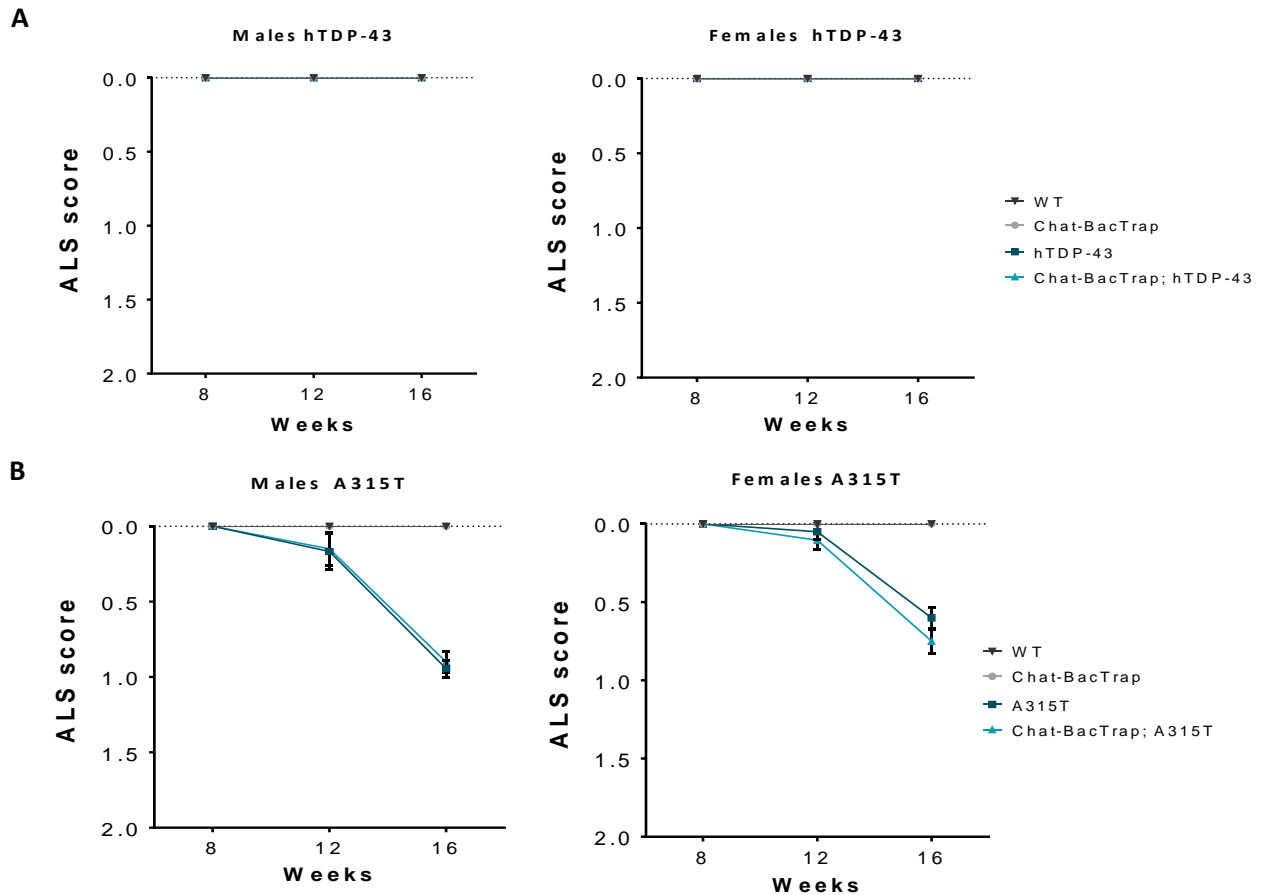


**Figure 9. Both sexes show deficits in hindlimb extension according to the neurological score at 16 weeks of age.**

The animals were tail-lifted and the capacity of leg extension was scored according to the neurological scoring system described in the laboratory guidelines from the Jackson Laboratory [167]. At 16 weeks of age hTDP-43 animals show no phenotypes while the A315T animals, both males and females curl the hindlimb toes, a sign of early disease. These images are representative for all animals tested.

Quantification of neurological scores for the entire mouse cohorts are shown in Figure 10. Both hindlimbs were assessed and the mean value was taken as the mouse's score. As expected, neither the hTDP-43 control mouse line nor their non-transgenic littermates (WT) showed a neurological score phenotype at any age (Figure 10 A). Conversely, all A315T males at 12 weeks of age already showed clear difficulty in full extension of the hindlimbs, while A315T females started to show partial collapse of the hindlimbs (Figure 10 B). To sum up, in the A315T line, both sexes show progression over time, with males showing a more pronounced phenotype. Importantly, when assessing the neurological score, the presence of *Chat::L10a-GFP* transgene had no influence on the development of ALS-like phenotypes.

### 3. Results



**Figure 10. Female A315T mice develop stronger neurological deficits later than males.**

(A) The hTDP-43 line shows no phenotypes throughout the time points tested, for both males and females. (B) The A315T line shows phenotypes concomitant with ALS symptomology in mice which progresses over time. Males show stronger phenotypes earlier than the females and a faster progression of those. Both hindlimbs were evaluated and the average per animal, group and time point was calculated.  $n=8-12$ ; error bars:  $\pm$  standard error of the mean (SEM).

#### 3.1.1.2. Peak body weight

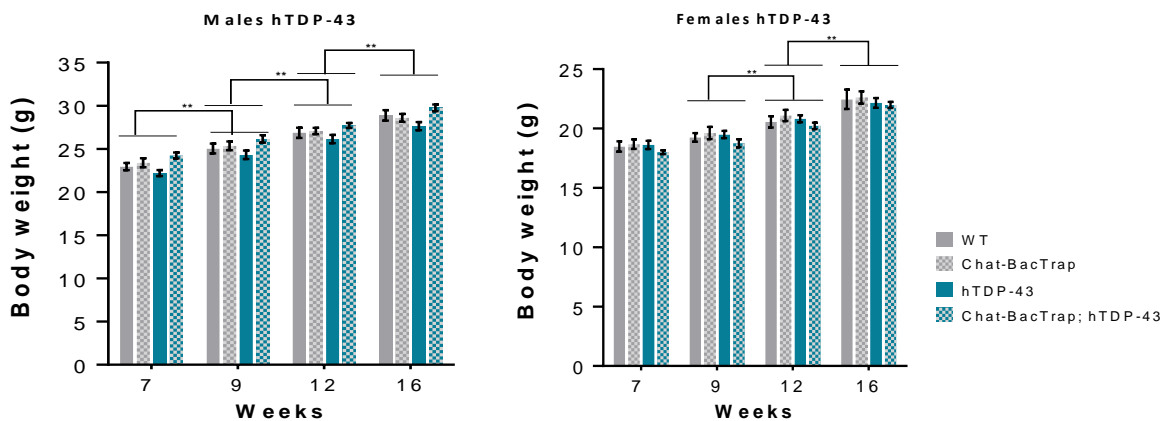
The peak body weight test has been suggested to be a good parameter to determine disease onset [166]. Since the mice are being tested between their juvenile and adulthood phases, it is expected that their weight would change from week to week, thus, I tested the animals at the following time points: 7, 9, 12 and 16 weeks of age. In this test, the weight was assessed, and the mean of each group considered for graphical representation.

As expected, the hTDP-43 control mice showed an increase in body weight over time and there was no difference relative to control littermates at any specific time point (Figure 11 A). Male A315T mice

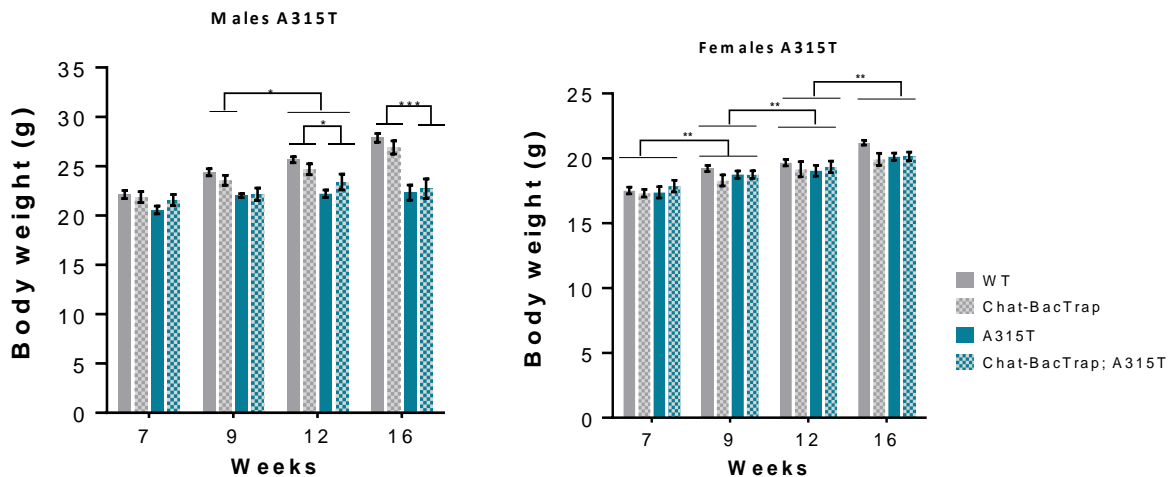
reached peak body weight at 9 weeks of age, whereas the littermate control animals lacking this transgene showed the expected increase in body weight over time (Figure 11 B).

Female A315T mice, showed increased body weight among all genotypes throughout time. This result indicates that male and female A315T mice show very different timing with respect to peak body weight. As for neurological score, the presence of *Chat::L10a-GFP* transgene did not affect body weight on its own and did not modify the phenotypes of either hTDP-43 or A315T mice (Figure 11).

A



B



**Figure 11. The A315T female and male mice have different timings of peak of body weight.**

(A) Body weight measurements throughout time for the hTDP-43 mice and littermate controls. (B) Body weight measurements throughout time for the A315T mice and littermate controls. The average weight of each group per time point was calculated.  $n = 8-12$ ; error bars:  $\pm$ SEM; two-way repeated measurement (2-way RM) ANOVA with Bonferroni's post hoc test; significance: \* $p < 0.05$  and \*\* $p < 0.01$ .

### 3.1.1.3. Muscle coordination and strength

I used two tests, the accelerating rotarod and grip strength, to assess muscle coordination and strength. The accelerating rotarod test was used to determine both motor coordination and strength [168]. This

### 3. Results

---

test focuses on the hindlimbs and measures the latency to fall of an animal. The animals were left to run on a rotarod for 300sec at an increasing speed. The longer an animal can run on the rotarod, the better its motor coordination capacity is and stronger its hindlimbs are. The average of three replicates per animal was calculated, followed by calculation of the average of each group, per time point.

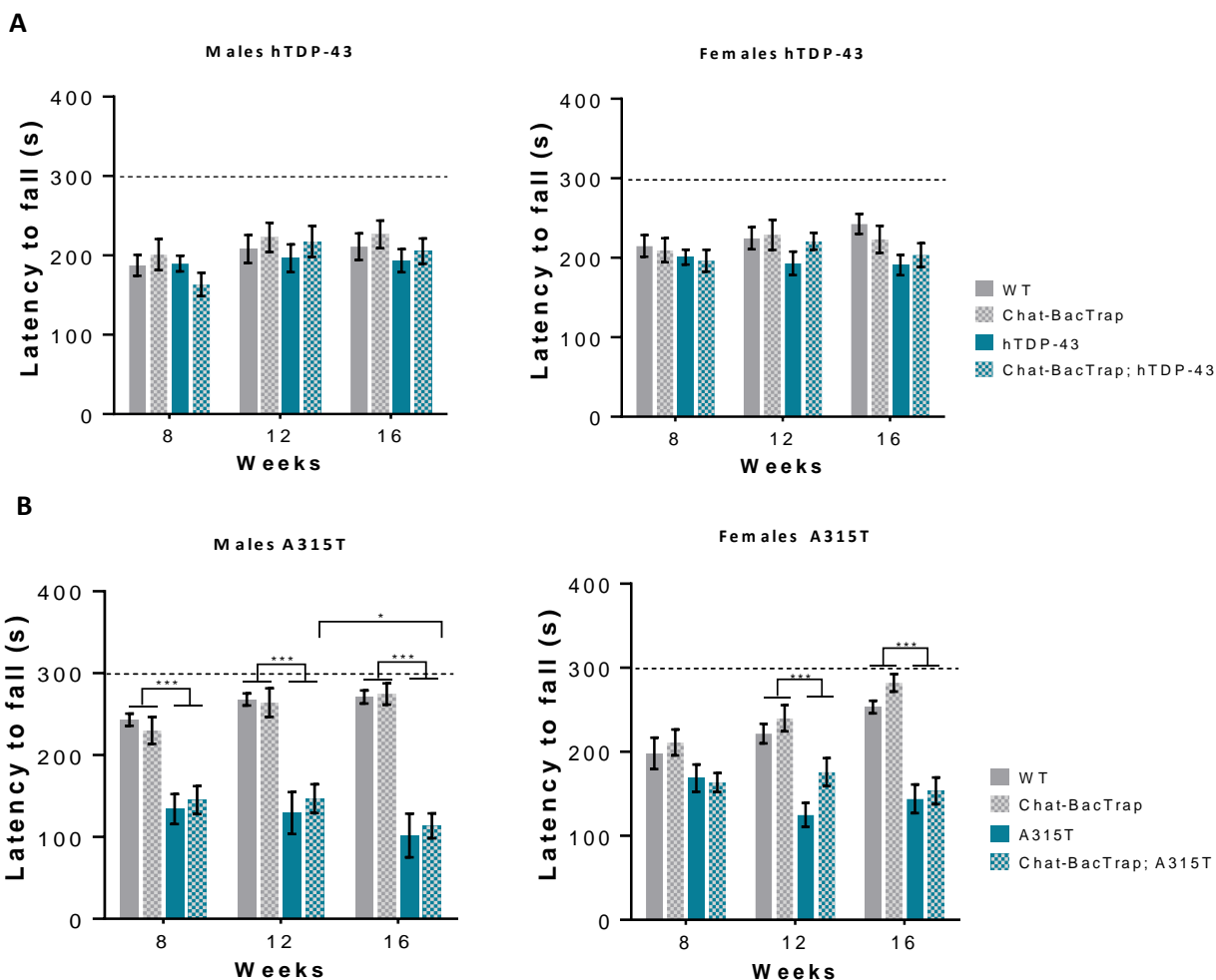
The forelimb grip strength test aims to determine the strength on the forelimbs of the mice. The strength is measured upon release of the forelimbs from a metal detector bar when the mice are gently pulled by the tail. It has been previously demonstrated that in rodent models of ALS, the animals develop a focal disease onset that starts in the hindlimbs and only in later stages of the disease spreads to the forelimbs [169]. I performed this test to determine if and when there is a spread of muscle weakness to the forelimbs. Here, the average of three replicates per animal was calculated, followed by calculation of the average of each group, per time point.

#### 3.1.1.3.1. Accelerating rotarod test

hTDP-43 control mice showed WT behavior on the rotarod (Figure 12 A). For both sexes and in all genotypes, the animals could not stay longer than 200sec on average, on the rotarod. For this mouse cohort no differences between genotypes were observed between or within each time point, as expected.

In contrast, A315T males showed clear deficits in rotarod performance relative to control littermates already at 8 weeks of age and their performance worsened with time (Figure 12 B). In comparison to control littermates, female mice carrying the A315T mutation performed equally well at 8 weeks and started to show significantly reduced performance at 12 weeks of age. Moreover, relative performance of the A315T female mice did not decline from 12 weeks to 16 weeks (Figure 12 B). As for neurological score and body weight, the presence of the *Chat::L10a-GFP* transgene had no influence on rotarod phenotypes.





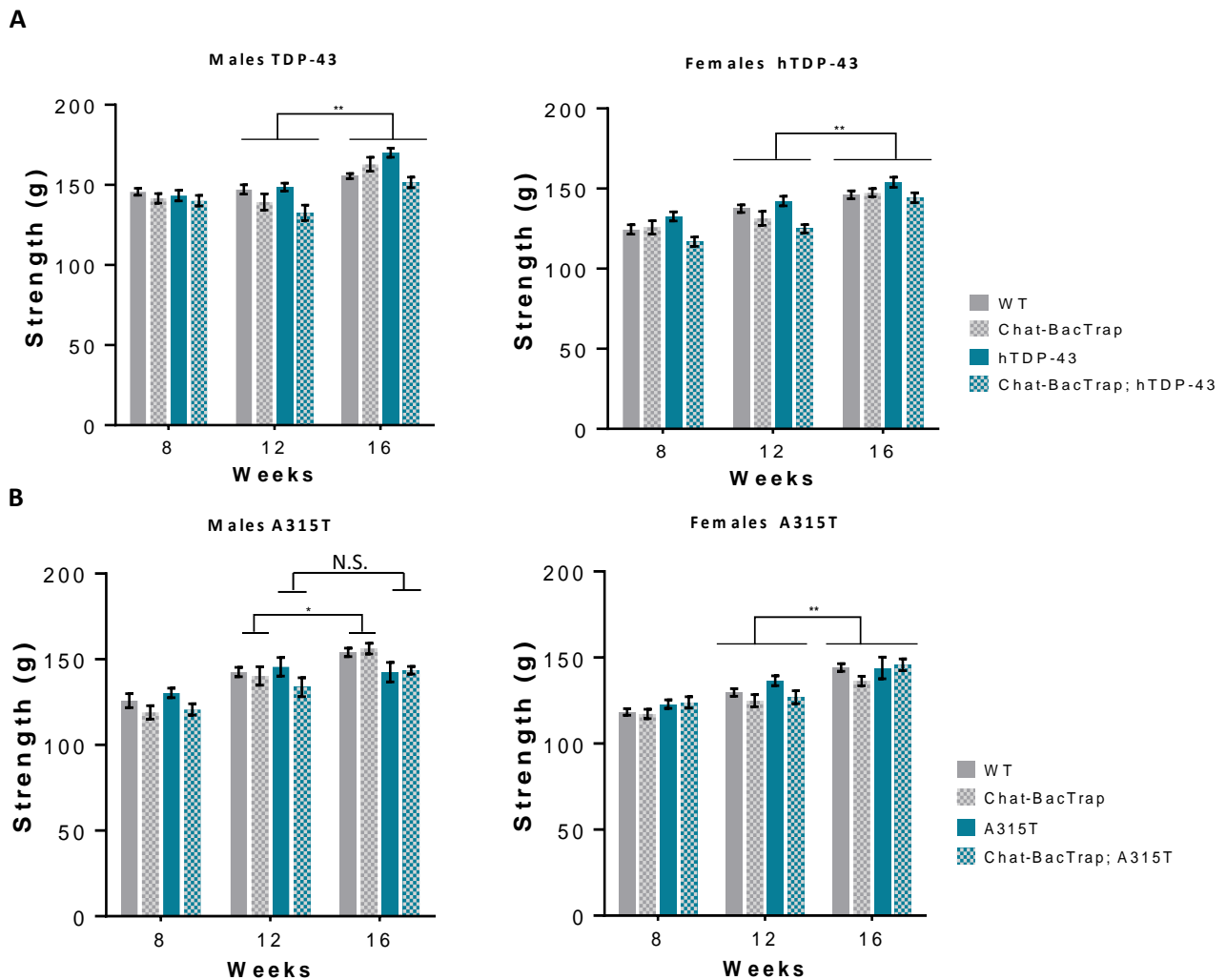
**Figure 12. The A315T mice show clear deficits in motor coordination and muscle weakness.**

(A) Latency to fall of the hTDP-43 mice and littermate controls throughout time for both male and female cohorts. (B) Latency to fall of the A315T mice and littermate controls throughout time for both male and female cohorts. Male cohorts show ALS-like phenotypes earlier than female cohorts. The average of three replicates per animal was calculated, followed by calculation of the average of each group, per time point.  $n = 8-12$ ; dash line (---): represents the maximum time the animals can run on the rotarod; error bars:  $\pm$  SEM; 2-way RM ANOVA with Bonferroni's post hoc test; significance: \* $p < 0.05$ ; \*\* $p < 0.01$  and \*\*\* $p < 0.001$ .

### 3.1.1.3.2. Forelimb grip strength test

In the case of the hTDP-43 mouse cohorts it was observed that both sexes gained significant strength throughout time with no differences between genotypes (Figure 13 A).

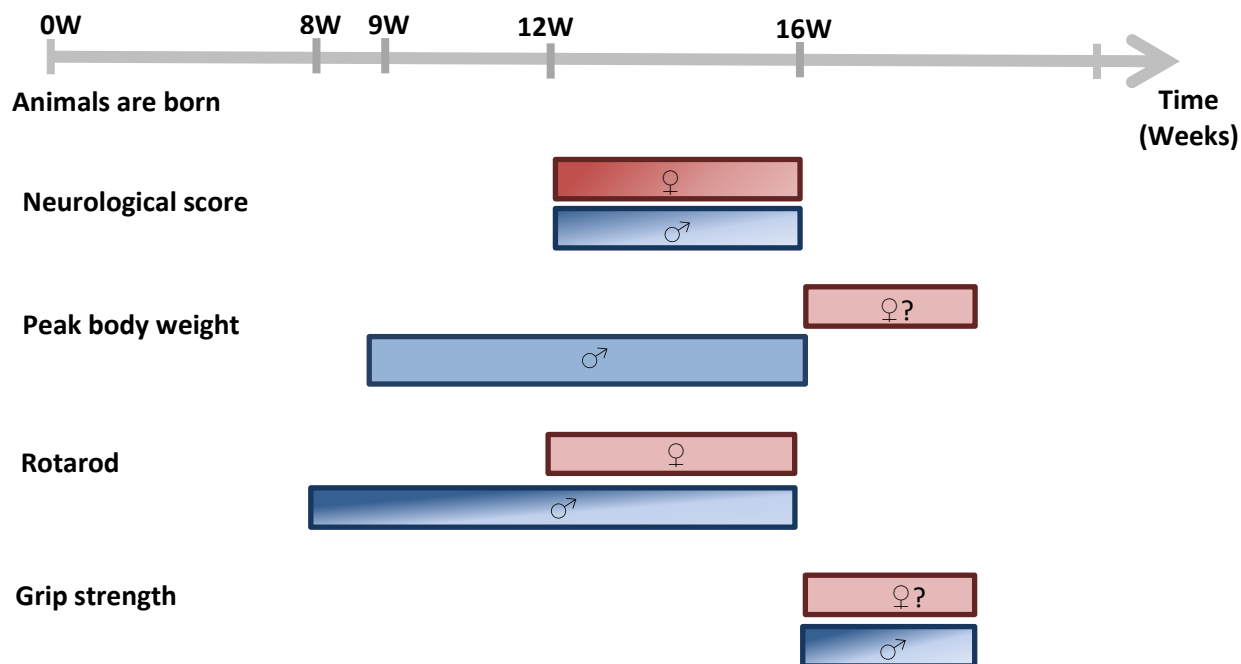
Male A315T mice showed no increase in strength at 16 weeks of age, when comparing with the control littermates (Figure 13 B). For female A315T mice, no differences between genotypes within each time point were observed. All groups showed a similar increase in forelimb strength from 12 to 16 weeks. The presence of *Chat::L10a-GFP* transgene also had no significant influence on this test.



**Figure 13. A315T female and male cohorts show different strength patterns throughout time in the forelimbs.**

Forelimb strength was measured at the indicated timepoints for littermate controls vs. hTDP-43 (A) or A315T (B) cohorts. The average of three replicates per animal was calculated, followed by calculation of the average of each group, per time point. N.S.: not significant. n= 8-12; error bars:  $\pm$ SEM; 2-way RM ANOVA with Bonferroni's post hoc test; Significance: \* $p < 0.05$  and \*\* $p < 0.01$ .

Figure 14 summarizes the results from all behavioral tests and the information that they provide with respect to establishing timing of disease onset for A315T mice. Males had visible rotarod deficits and their peak body weight was already at 9 weeks of age. This means that their pre-symptomatic phase is presumably earlier and remains undefined. In contrast, females showed no phenotypes in any assays at 8 weeks, but clear motor phenotypes in both rotarod and neurological score at 12 weeks of age. Neither body weight nor grip strength differed from controls, even at 16 weeks, suggesting that these tests do not reveal disease onset in females. Thus, females, but not males, carrying the A315T mutation show a clear transition between pre-symptomatic to early symptomatic phases of the disease in the 8-12 week time window.



**Figure 14. Time of ALS disease onset in the A315T mice.**

Schematic representation of the behavioral results obtained and described above. Four independent tests were applied to determine disease onset: neurological score, peak body weight, accelerating rotarod and grip strength. Bars indicate the first point where phenotypes are manifest. Solid coloring reflects a constant phenotype. Gradient shading reflects a progressively stronger phenotype. Results for male and female cohorts are represented in blue and red, respectively. While males already show a rotarod phenotype at 8 weeks of age, females show a clear transition between pre-symptomatic to early symptomatic phases of the disease for the two most important behavioral tests in the 8-12 week period.

The behavioral tests revealed that the A315T male mice develop ALS-like phenotypes earlier than female mice. Because of this difference could be driven by different expression levels of mutant TDP-43 protein, I next examined this explicitly.

### 3.2. Analysis of total TDP-43 expression levels in spinal cord of hTDP-43 and A315T mouse lines

I checked by western blot (WB) whether the expression levels of TDP-43 protein in the A315T mutant mice and in the hTDP-43 mice are similar (Figure 15) and whether the *Chat::L10α-GFP* transgene would alter TDP-43 protein expression levels. Two different time points were tested, 9 weeks and 17 weeks.

With the aim of determining the total levels of TDP-43 protein in mouse spinal cord, I used a TDP-43 antibody that recognizes both the human and the mouse forms of the protein. The results are displayed in Figure 15. In the case of the hTDP-43 male mice, it is observed that the total levels of TDP-43 are

### 3. Results

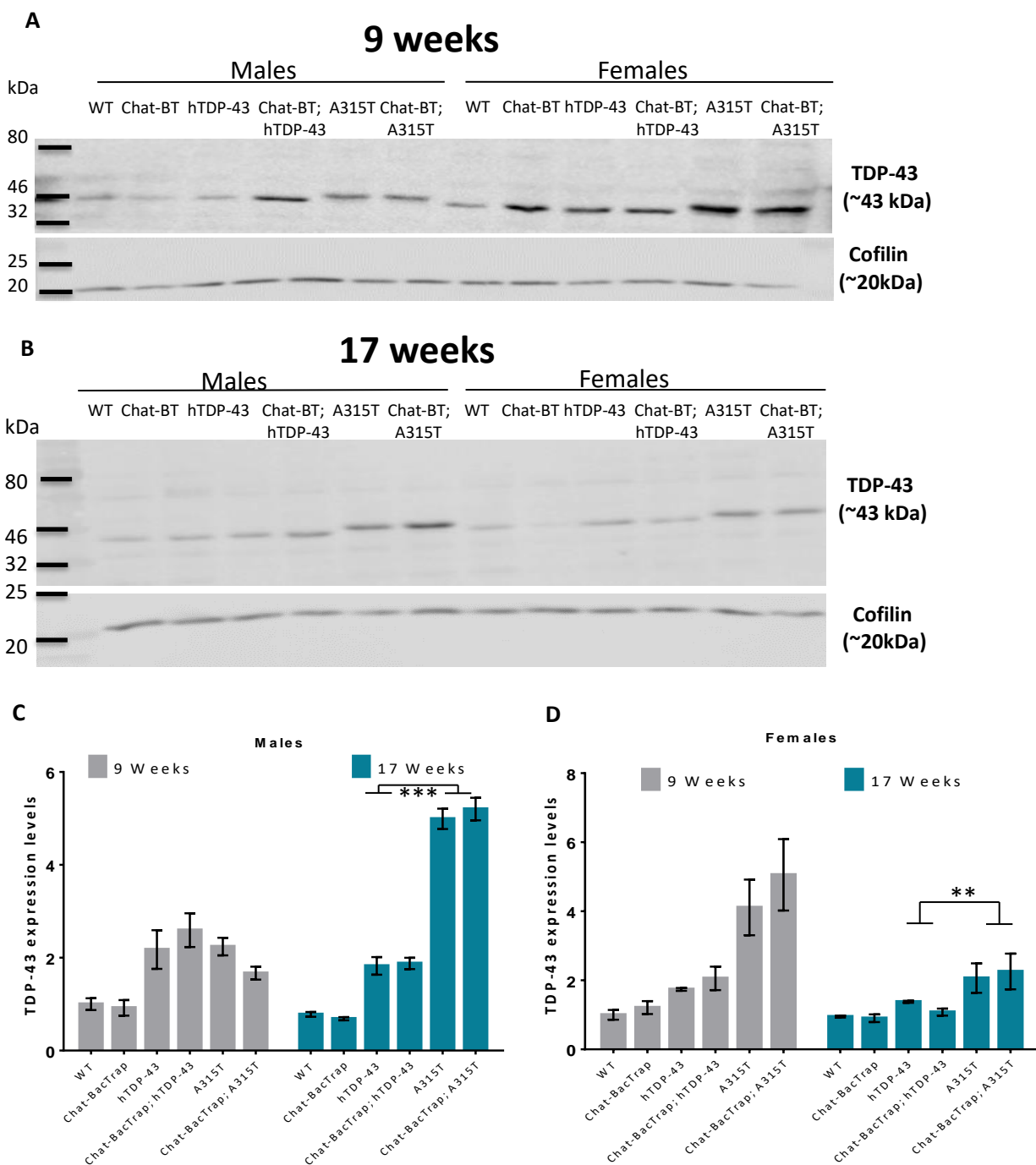
---

increased (~2x) at both 9 and 17 weeks when comparing to the control group (male WT) (Figure 15 C). On the other hand, the hTDP-43 females show less than 2x increase in expression levels of TDP-43 in comparison to the control group (female WT) at both time points (Figure 15 D).

With respect to the total levels of TDP-43 in the A315T groups, the A315T males show an increase at 9 weeks of ~2x, whereas, at 17 weeks an increase of ~5.5x more protein than the corresponding male WT groups. The A315T female mice show at 9 weeks an ~4.5x increase in the total protein levels of TDP-43 when comparing to the female WT group. Nevertheless, at 17 weeks only an increase of ~2x, when comparing with the control group, is observed (Figure 15 D).

The quantification of TDP-43 protein levels is important to determine what is driving the development of the symptoms. Specifically, if it is because of an increase in protein levels, presence of mutated protein or combination of both. A direct way to check for this is to compare the levels of TDP-43 protein in the hTDP-43 mice with the levels in the A315T mutant mice. The overall levels of TDP-43 protein between the hTDP-43 mouse line and the A315T mutated mouse line are different in both male and female cohorts, thus, it is not possible for both sexes, to infer if the animals get sick due to an increase in the protein level, mutation or combination of both.

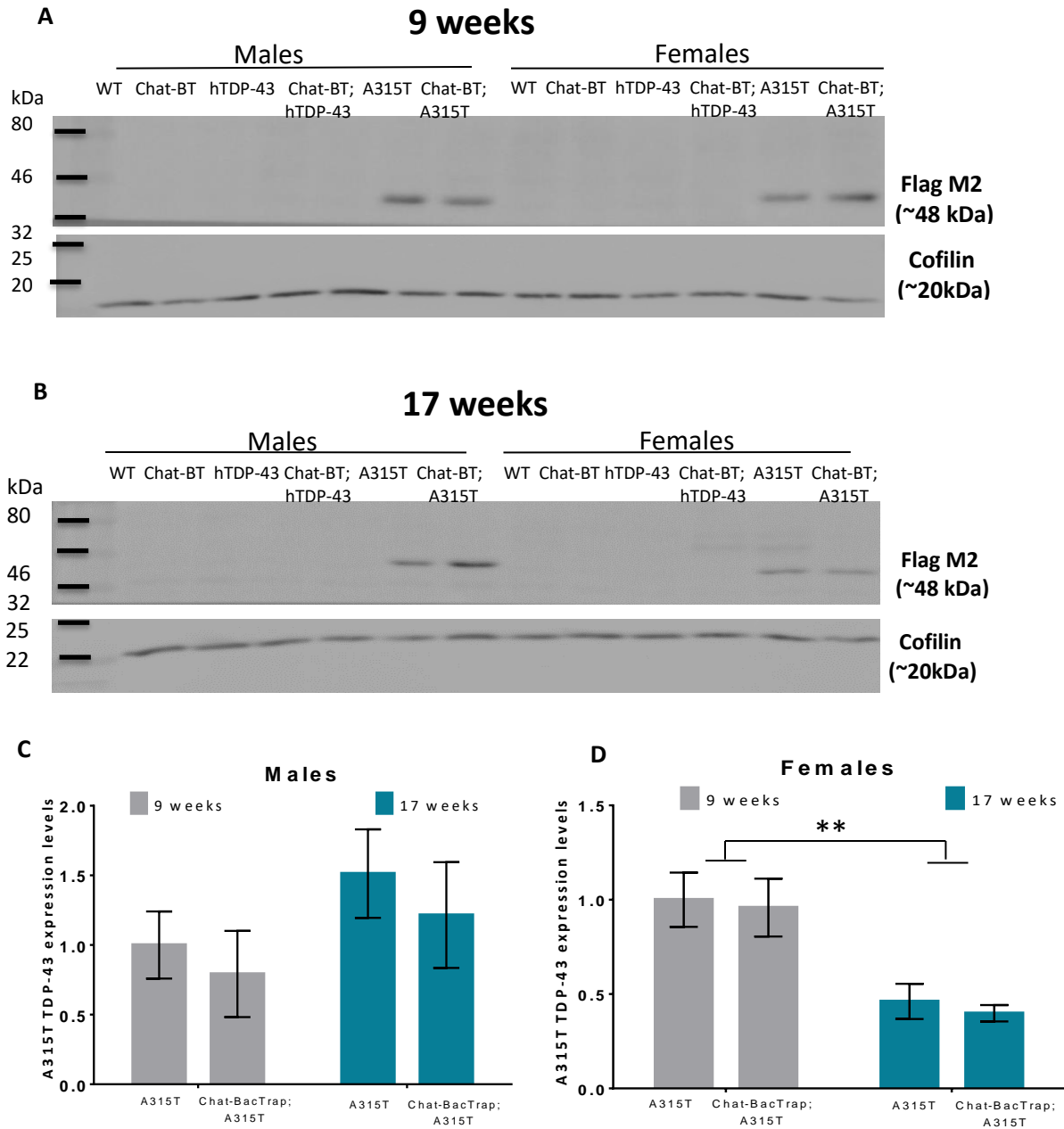
Importantly, the presence of the *Chat::L10a-GFP* transgene had no effect on the total TDP-43 protein levels when comparing with the respective control groups (e.g. WT vs Chat-BacTrap) (Figure 15).



**Figure 15. Relative TDP-43 protein levels at 9 and 17 weeks in spinal cord of hTDP-43 and A315T mouse lines.** TDP-43 protein levels from spinal cord material at 9 weeks (A) and 17 weeks (B) of age were determined via WB. (C) Quantification of the WB data for each time point and genotype for males. (D) Quantification of the WB data for each time point and genotype for females. For each time point and sex, the data was normalized to Cofilin protein levels and the 9 weeks male or female A315T sample, respectively. n=3; Error bars:  $\pm$ SEM. 2 tail t-test; significance: \*\* $p < 0.01$ ; \*\*\*  $p < 0.001$ .

### 3. Results

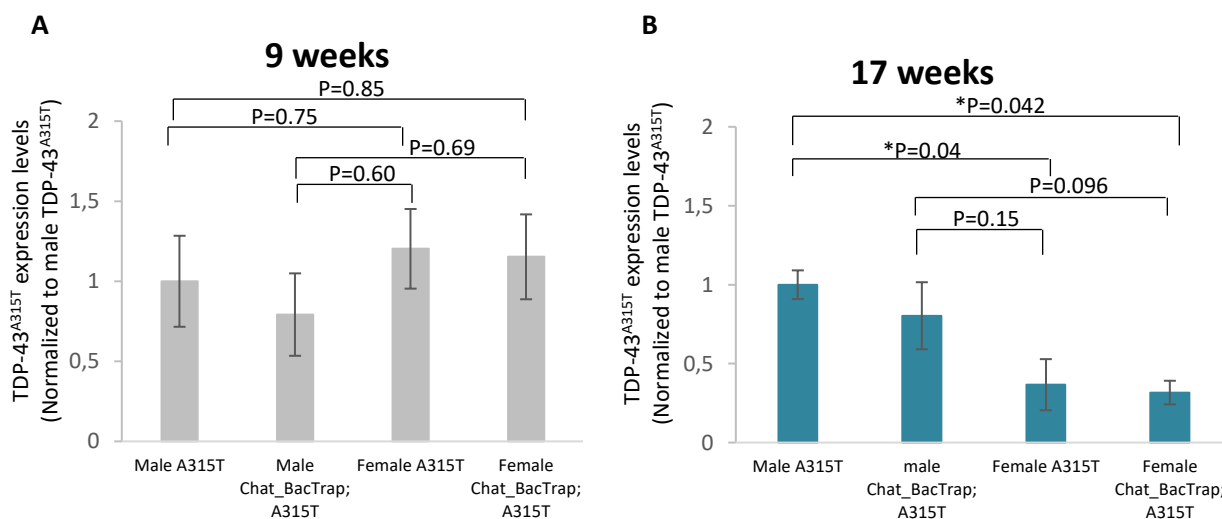
The FLAG tag (DYKDDDDK) on the hTDP-43<sup>A315T</sup> protein was also used to compare expression levels (Figure 16). The anti-FLAG WBs showed that from 9 to 17 weeks, the hTDP-43<sup>A315T</sup> protein increased in males, decreased in females, and this was not affected by the *Chat::L10a-GFP* transgene.



**Figure 16. hTDP-43<sup>A315T</sup> protein expression levels in spinal cord.**

TDP-43 protein levels from spinal cord material at 9 weeks (A) and 17 weeks (B) of age were determined via WB. (C) Graphical representation of the quantification of the WB for males based on genotype and time points. (D) Graphical representation of the quantification of the WB for females based on genotype and time points. For each time point and sex, the data was normalized to Cofilin protein levels and to 9 weeks male and female A315T, respectively. n=3; Error bars:  $\pm$ SEM. ; 2 tail t-test; significance: \*\*p<0.01.

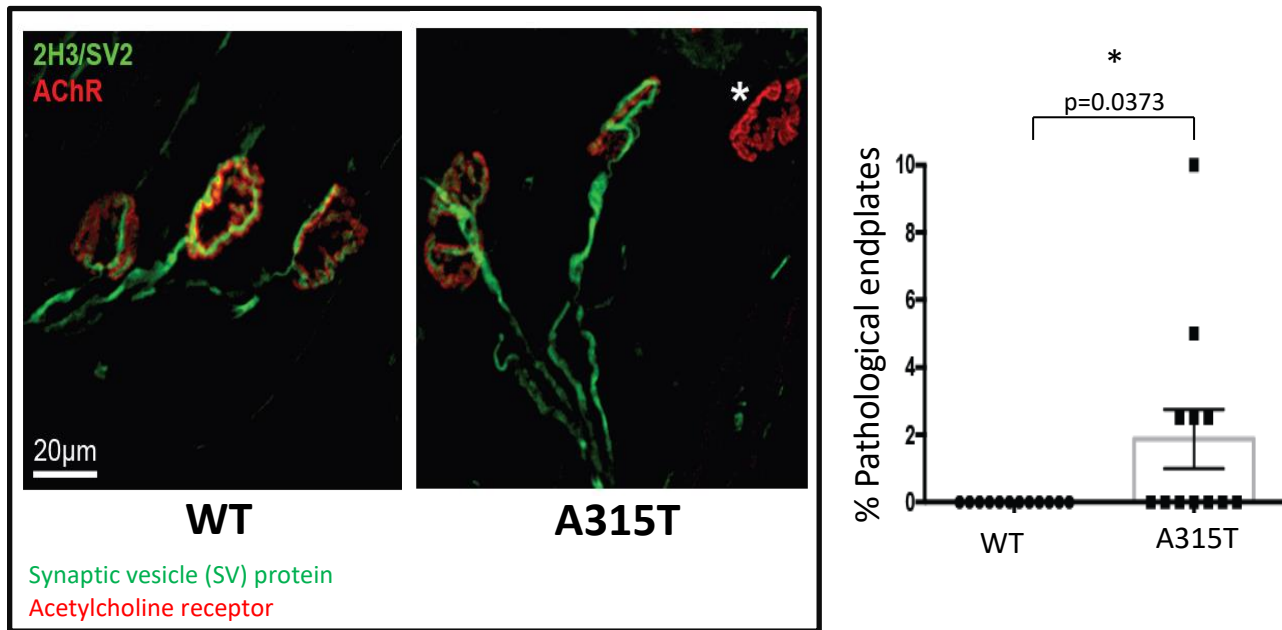
Higher levels of hTDP-43<sup>A315T</sup> protein in male vs. female mice could potentially explain why males develop symptoms earlier than females. As observed in Figure 17 B, male mice show higher expression levels of mutant TDP-43 protein than females at 17 weeks, which correlates with a stronger phenotype at this time point in males. However, at 9 weeks, when male mice are already symptomatic, but females are still pre-symptomatic, there is no significant difference in mutant protein levels between males and females (Figure 17 A). Thus, differences in transgene expression do not appear to be the reason that male mice develop symptoms earlier than females. Even though there are no hTDP-43<sup>A315T</sup> protein level differences at 9 weeks, still an analysis of the total protein levels in a similar way to Figure 17 (data where male and female mice are directly compared) could help to explain why males develop symptoms earlier.



**Figure 17. Mutant males show higher levels of hTDP-43<sup>A315T</sup> protein with aging relative to mutant female mice.** Calculation of hTDP-43<sup>A315T</sup> protein expression levels between sexes. (A) Expression levels of hTDP-43<sup>A315T</sup> protein at 9 weeks in both male and female mutant mice. (B) Expression levels of hTDP-43<sup>A315T</sup> protein at 17 weeks in both male and female mutant mice. Data was normalized against Cofilin and male A315T. n=3; Error bars:  $\pm$ SEM; 2 tail t-test; significance: \*p<0.05.

### 3.3. Mild muscular denervation pathology correlates with disease

To confirm disease onset in an independent approach, neuromuscular junction (NMJ) morphology was examined. Denervation of this synapse correlates with the level of the impairment of signal transmission from pre-synaptic MNs to post-synaptic muscles [170]. NMJs from symptomatic animals at 14 weeks of age, were stained and the percentage of pathological endplates quantified (Figure 18). A mild denervation of the NMJ, 2%, was detected by calculating the percentage of pathological endplates. This result confirms that 14 weeks is an early symptomatic phase of the disease according to this pathological readout.



**Figure 18. Mild denervation of the NMJ concomitant with early symptomatic phase.**

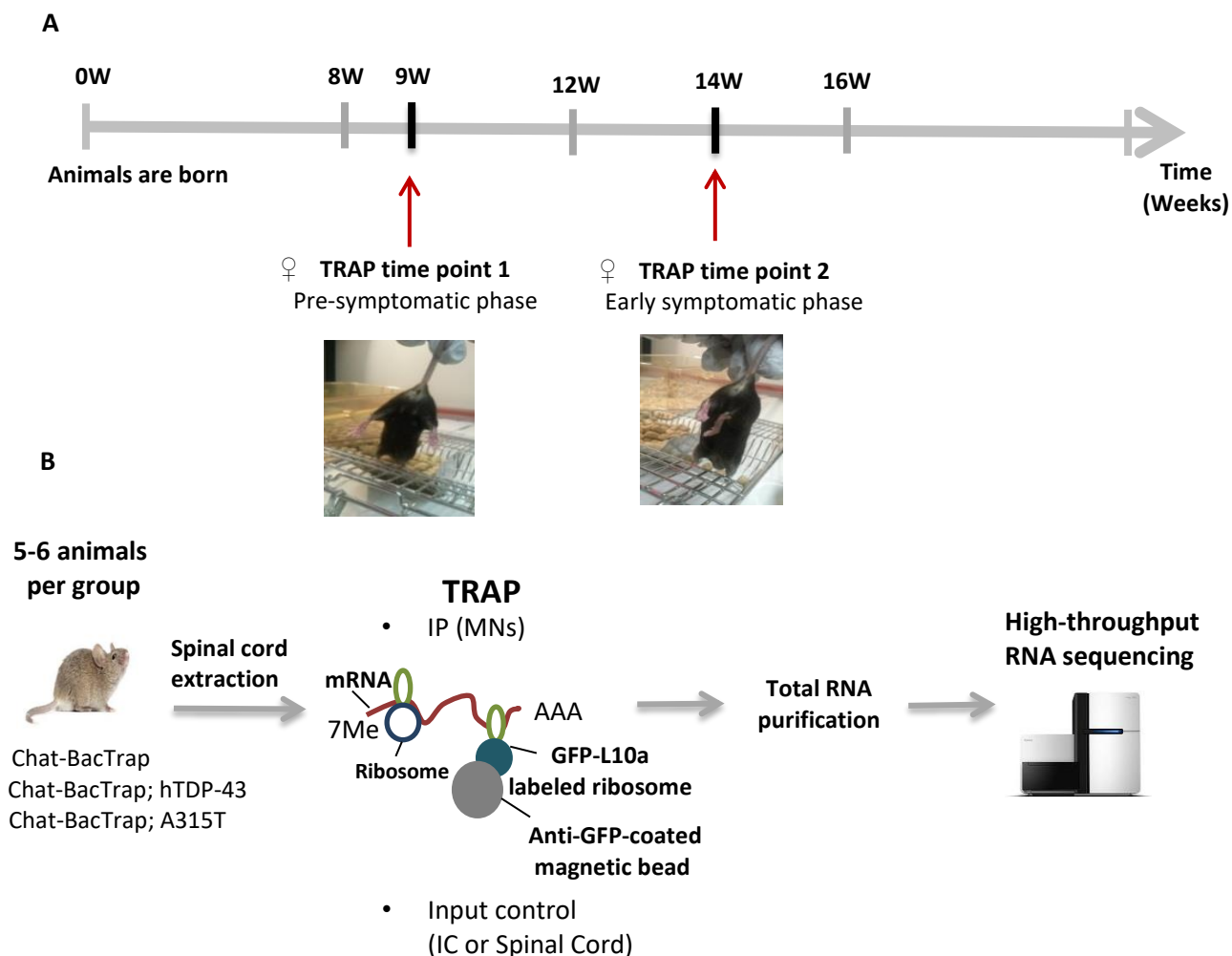
The NMJs of a mixed cohort of female and male mice, at 14 weeks of age were stained to investigate the denervation level of the muscle in the hindlimbs. 2H3/SV2 antibodies stain the pre-synaptic side and the acetylcholine receptor staining marks the post-synaptic side of the NMJ. Quantification was done based on the percentage of pathological endplates. White asterisk represents an example of a denervated NMJ.  $n=6$  animals per group, 3 males and 3 females;  $*p<0.05$ ; statistical test: Mann-Whitney. \*\* These unpublished data were obtained by Dr. Ross A. Jones in collaboration with Prof. Dr. Thomas H. Gillingwater's lab, from the University of Edinburgh, Edinburgh, UK.

#### 3.4. Successful purification of the motor neuronal transcriptome via TRAP

The structure of the experiment for purification of the motor neuronal transcriptome by TRAP was chosen based on the results presented above. From the behavioral analysis it is clear that only the female mice carrying the *hTARDBP-43<sup>A315T</sup>* mutation show a transition in the 8-12 week window from a pre-symptomatic to early-symptomatic phase of the disease. Consequently, all the follow up experiments were done with female mice to enable identification of molecular changes in MNs that correlate tightly with disease onset. Because the phenotypes were progressive and 14 weeks was still an early time point according to both behavior and NMJ denervation analyses, 9 weeks and 14 weeks were chosen as time points for pre-symptomatic and early symptomatic phases of the disease, respectively, to which the TRAP methodology was applied (Figure 19 A).

TRAP is an immunoprecipitation method for purification of ribosome bounded mRNA from specific cells within a tissue of interest. In the context of this thesis, TRAP enables purification of motor neuronal mRNA from adult mouse spinal cord (Figure 19 B). With this method, I was able to isolate and purify RNA which was later sent for high-throughput sequencing (deep-sequencing). By applying a genome-wide method I can find deregulated molecules to be further validated as potential disease drivers.





**Figure 19. Female mice were selected through behavioral and denervation analysis to be studied by TRAP.**

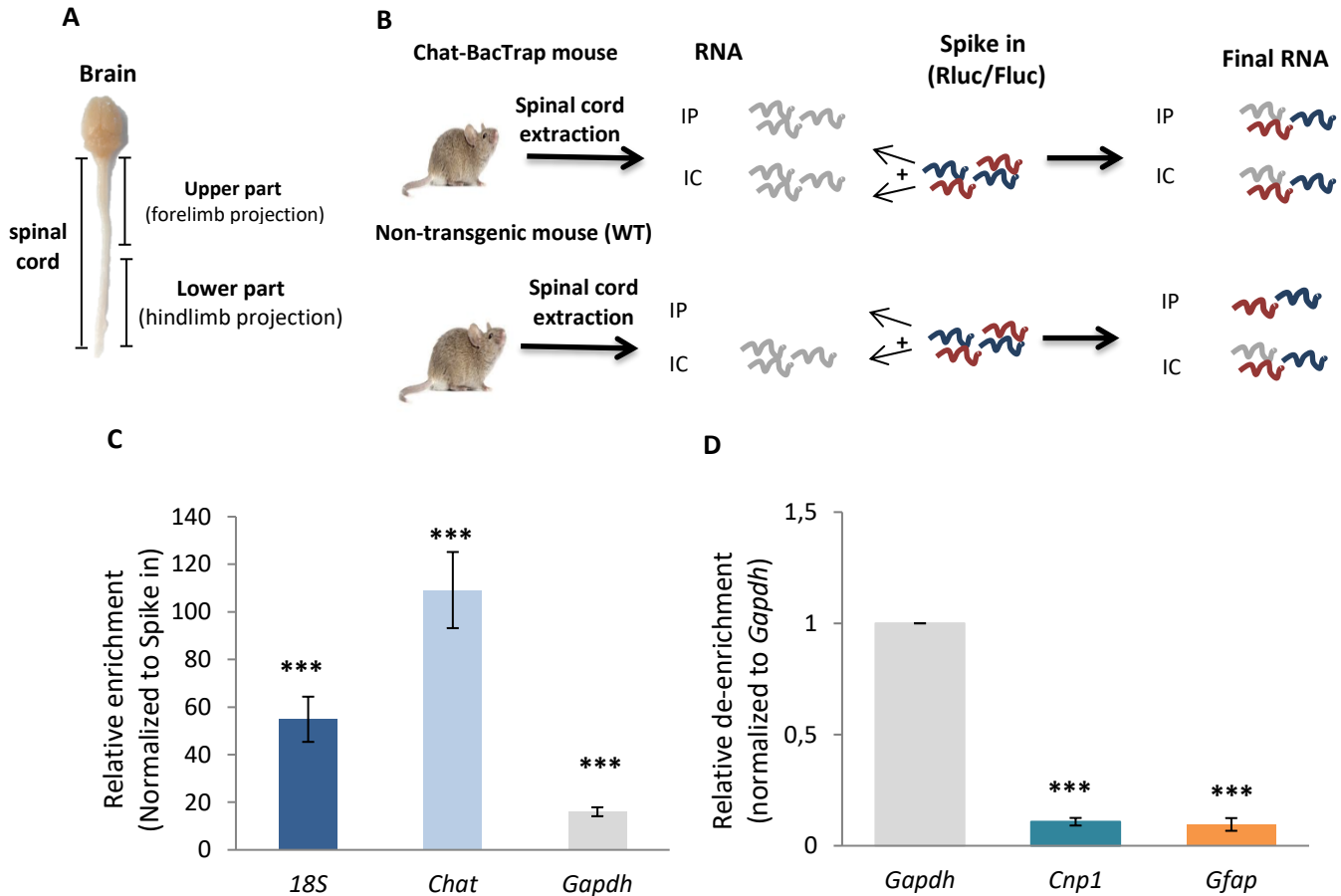
(A) Based on behavioral and denervation analyses, time points corresponding to 9 weeks and 14 weeks were selected as pre-symptomatic and early symptomatic phases of the disease, respectively for the females. (B) Schematic of the TRAP experiment with high-throughput RNA sequencing as the final read out.

#### 3.4.1. One spinal cord can be used with TRAP

The standard TRAP protocol for spinal cords in use in the Friese and Duncan labs consisted in the pooling of three upper parts of spinal cords per genotype (Figure 20 A). Since I would need to use a considerable number of animals for TRAP experiments, due to the number of replicates necessary for deep sequencing (5x), I decided to check whether the protocol could be optimized for one spinal cord per genotype and thus dramatically reduce the number of necessary animals. For optimization of the protocol, quantitative real time-polymerase chain reaction (qRT-PCR) was used. Spike ins (Fluc and Rluc) were used in this experiment (Figure 20 B), since the idea is to check how much enrichment I have over non-transgenic animals (pure WT). To check whether one spinal cord would be sufficient to get a good RNA yield and to test if the TRAP methodology is working, the relative enrichment of genes such as *18S*

### 3. Results

rRNA, *Chat* and *Gapdh* (Figure 20 C) and de-enrichment of genes such as *Gfap* and *Cnp1* (Figure 20 D) were calculated. *Chat* mRNA is used as a marker for MNs, *18S* rRNA for ribosomes, *Gfap* mRNA as a marker for astrocytes and *Cnp1* mRNA for oligodendrocytes. The relative enrichment of *Chat* and *18S* mRNAs and de-enrichment of *Gfap* and *Cnp1* mRNAs demonstrates that TRAP is efficiently immunoprecipitating RNA specifically from motor neuronal cells.



**Figure 20. TRAP from one single spinal cord gives good enrichment.**

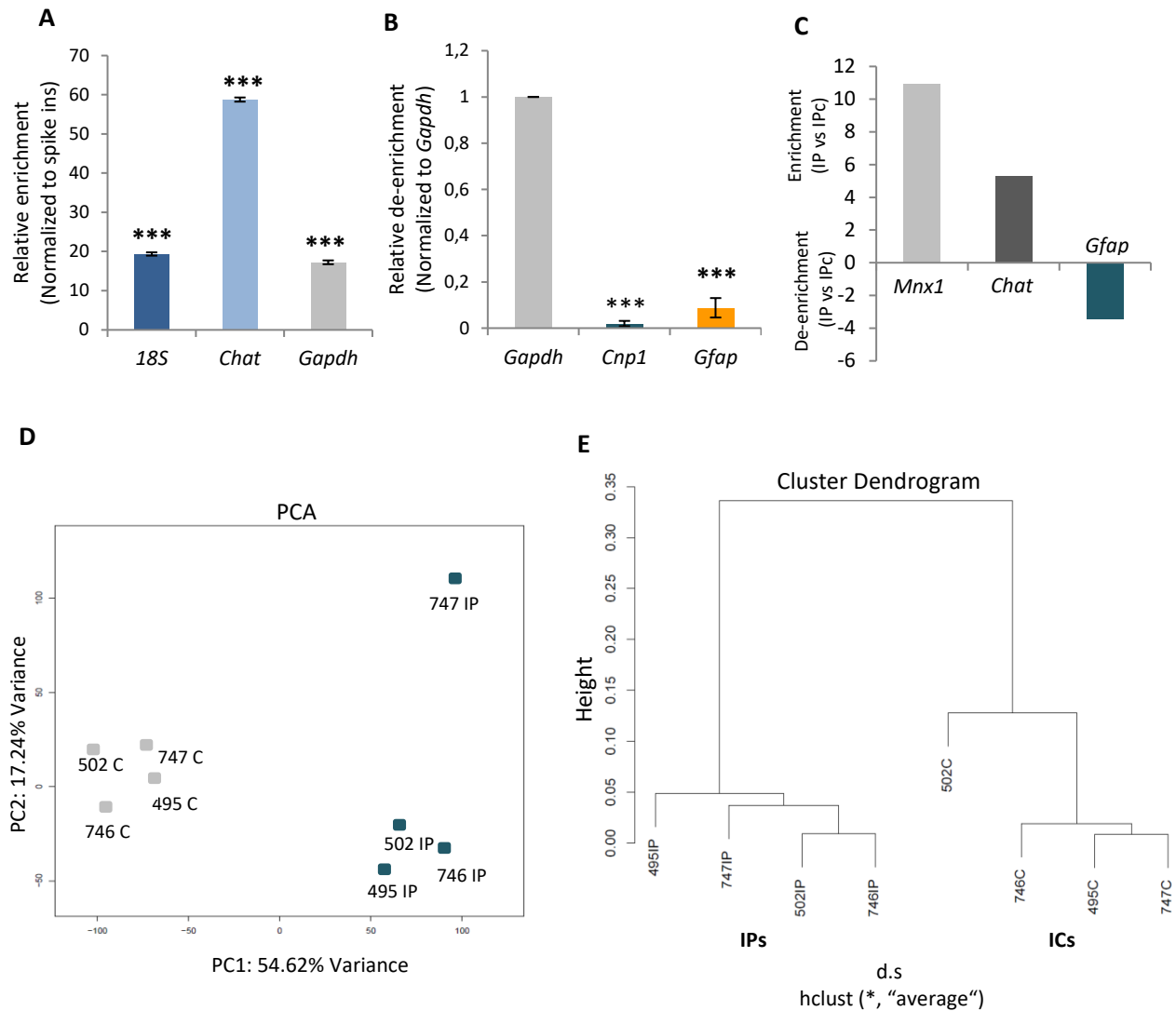
The TRAP protocol was optimized to reduce the number of animals used. (A) Image of an extracted mouse spinal cord divided into upper and lower part. (B) Schematic of the experiment. A single spinal cord was used per IP. A mixture of spike ins (Rluc and Fluc) was added to allow normalization and calculation of signal enrichment relative to WT control animals. (C) and (D) qRT-PCR was used as the readout method. (C) Relative enrichment of *18S*, *Gapdh* and *Chat* mRNAs was calculated over WT animals and used as positive control of the experiment. (D) *Gfap* and *Cnp1* mRNAs de-enrichment was calculated relative to *Gapdh* (used as housekeeping gene) which should be expressed in all cells. n=3 per genotype, error bars:  $\pm$ SEM; \*\*\*p<0.001.

### 3.4.2. Optimized TRAP protocol is compatible with high-throughput sequencing

After verifying by qRT-PCR that TRAP is indeed immunoprecipitating RNA from MNs, it was however necessary to test if the same protocol would give sufficient RNA yield for high-throughput sequencing. I performed a pilot experiment as proof of concept to verify if all the conditions for good genome-wide would be met. In the pilot experiment, a total number of four replicates were used (Figure 21). Before sequencing the samples, I tested by qRT-PCR the levels of expression of the genes *18S*, *Chat*, *Gapdh*, *Cnp1* and *Gfap* (Figure 21 A and B). TRAP was successful in immunoprecipitating RNA from MNs, since *Chat* is enriched and *Gfap* and *Cnp1* are de-enriched. Thus, by multiple criteria the revised TRAP protocol produced samples suitable for high-throughput sequencing.

To check if the samples were indeed compatible with high-throughput sequencing, certain parameters after the sequencing were checked, namely to verify again whether the IPs were specific from MN transcriptome. Enrichment for *Mnx1* and *Chat* genes, which are both MN markers, and de-enrichment of *Gfap* gene, were calculated (Figure 21 C). Two standard methods to assess the overall quality of a high-throughput sequencing dataset are principal component analysis (PCA) and hierarchical clustering (dendrogram). The PCA shows how samples cluster together (Figure 21 D), while the dendrogram reveals how similar the samples are (Figure 21 E). The PCA analysis shows that IPs and ICs cluster separately, indicating the presence of 2 groups. Regarding the dendrogram, the height of the bars indicates how similar two samples are. Here, the smaller the height is, the more similar two samples are. e.g. sample 502IP is more similar to 746IP than to 747IP.

### 3. Results

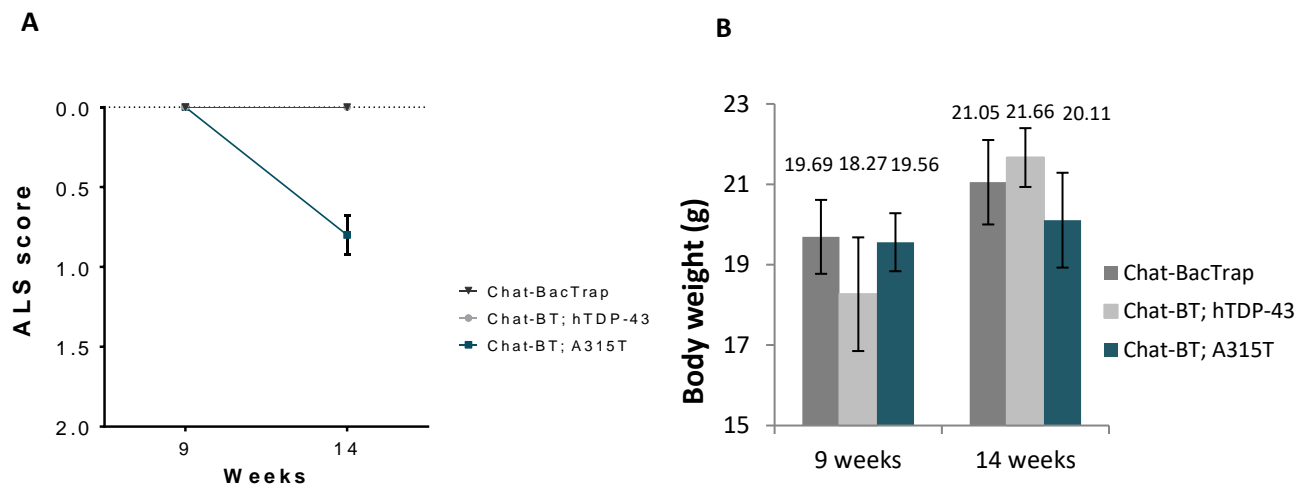


**Figure 21. Optimized TRAP protocol gives reliable high-throughput sequencing data in a pilot experiment.**

Prior to sequencing, samples were first tested by qRT-PCR to verify enrichment (A) and de-enrichment (B) patterns. (C-E) After sequencing and bioinformatics processing of the genome-wide data, several additional parameters were checked to verify performance. (C) Expected enrichment of MN-specific genes, such as *Mnx1* and *Chat* and de-enrichment of genes expressed in other spinal cord cell types, e.g. *Gfap*, were both verified. (D) Principal component analysis (PCA) plot showing how IP and IC samples cluster against each other. (E) Dendrogram displaying samples according to how strongly correlated they are. n=4; animals were labeled with the following numbers: 495, 502, 764, 747; error bars:  $\pm$ SEM; IC: input control; PCA: principal component analysis; PC: principal component. \*Sequencing and mining of these unpublished data was performed by Dr. Thomas Lingner in collaboration with Dr. Gabriela Salinas-Riester from the Transcriptome and Genome Analysis laboratory (TAL) sequencing core facility, University Medical Center Göttingen (UMG), Göttingen, Germany.

### 3.4.3. All A315T female animals were carefully checked for symptoms prior TRAP

Before performing TRAP from animals at pre- and early symptomatic phases, the ALS score (Figure 22 A) and the body weight of the animals was determined (Figure 22 B). The reason is to guarantee that all the animals carrying the A315T mutation used in the experiment are symptomatic at 14 weeks of age. All Chat-BT; A315T animals included in the TRAP experiment scored at least 1, according to the neurological score test, for one of their hindlimbs at 14 weeks of age. Similar to what was observed before, there are no differences in mutant female weight when comparing with the control animals (Chat-BacTrap and the Chat-BacTrap; hTDP-43 cohorts).



**Figure 22. The Chat-BT; A315T animals used in TRAP were early-symptomatic at 14 weeks of age.**

(A) Neurological score of all the animals used in TRAP. The capacity of full leg extension was evaluated at 9 weeks and 14 weeks. (B) Average of the measurements of the body weight of the animals used in TRAP experiments at 9 weeks and 14 weeks. The value of the average of weight of each group is written on top of each bar. BT: BacTrap; n=5-6; error bars:  $\pm$ SEM.

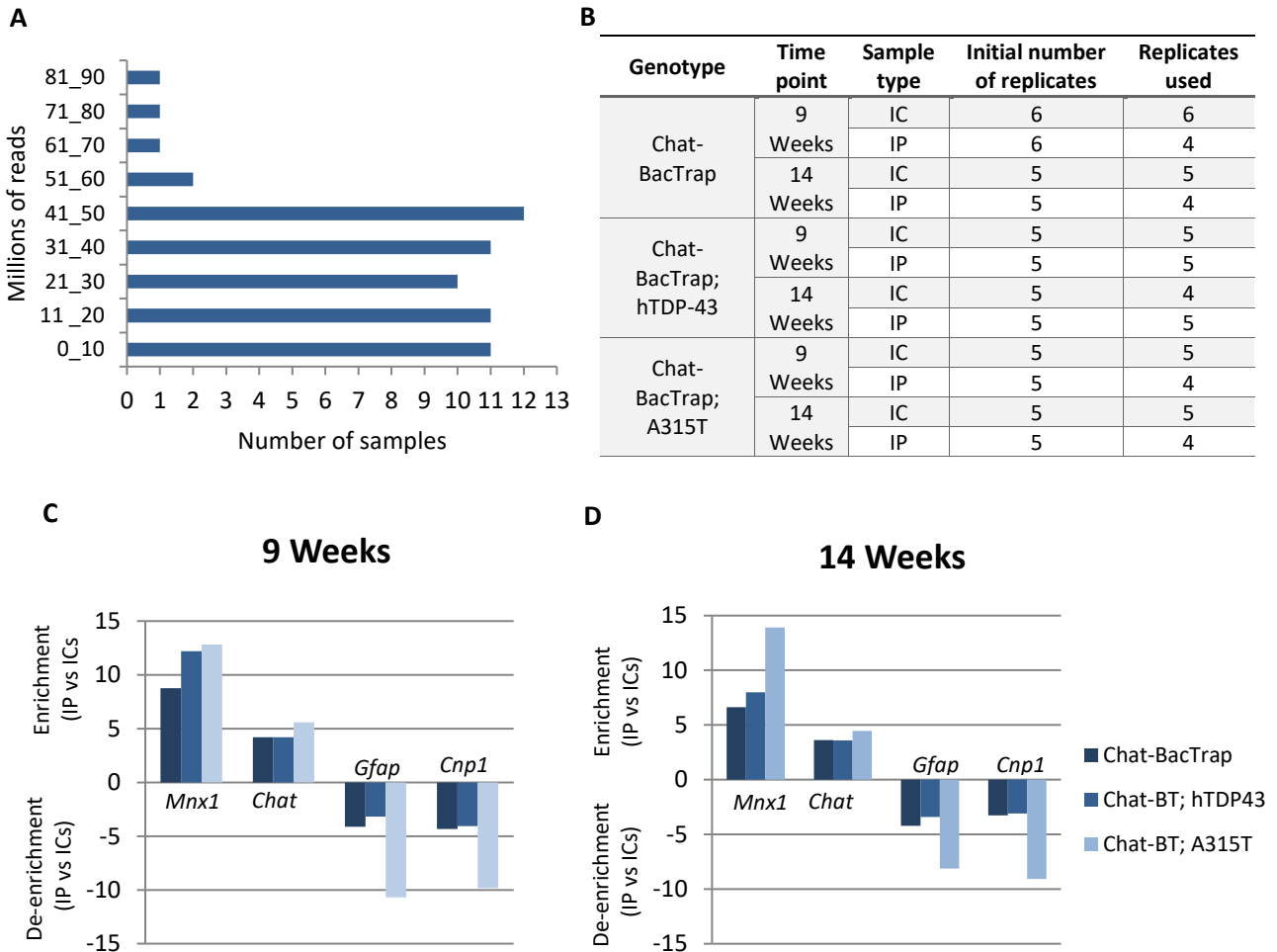
After the animals were carefully evaluated for symptoms, I isolated and purified RNA via TRAP from individual spinal cords and sent it to be high-throughput sequenced, at the TAL facility, Göttingen.

### 3.5. Genotype is the major driver of changes in female MN transcriptome

After deep sequencing the data was mined to check for data quality. Most of the sequenced samples got between 10 to 50 million assigned reads of RNA sequences (Figure 23 A). Six samples with zero assigned reads were excluded from the remaining analysis (Figure 23 B). To check for IP efficiency, the enrichment of *Mnx1* and *Chat* and the de-enrichment of *Gfap* and *Cnp1* genes was determined. At both 9 weeks (Figure 23 C) and 14 weeks (Figure 23 D) it is observed an enrichment of *Mnx1* and *Chat* and a de-enrichment of *Gfap* and *Cnp1*, for all the genotypes tested: Chat-BacTrap, Chat-BT; hTDP-43 and Chat-BT;

### 3. Results

A315T. These data show that the TRAP methodology was efficient in capturing ribosome associated mRNAs and that these mRNAs are strongly enriched for mRNAs from female spinal cord MNs.



**Figure 23. TRAP methodology efficiently purifies MN mRNAs from spinal cord of female ALS model and controls.**

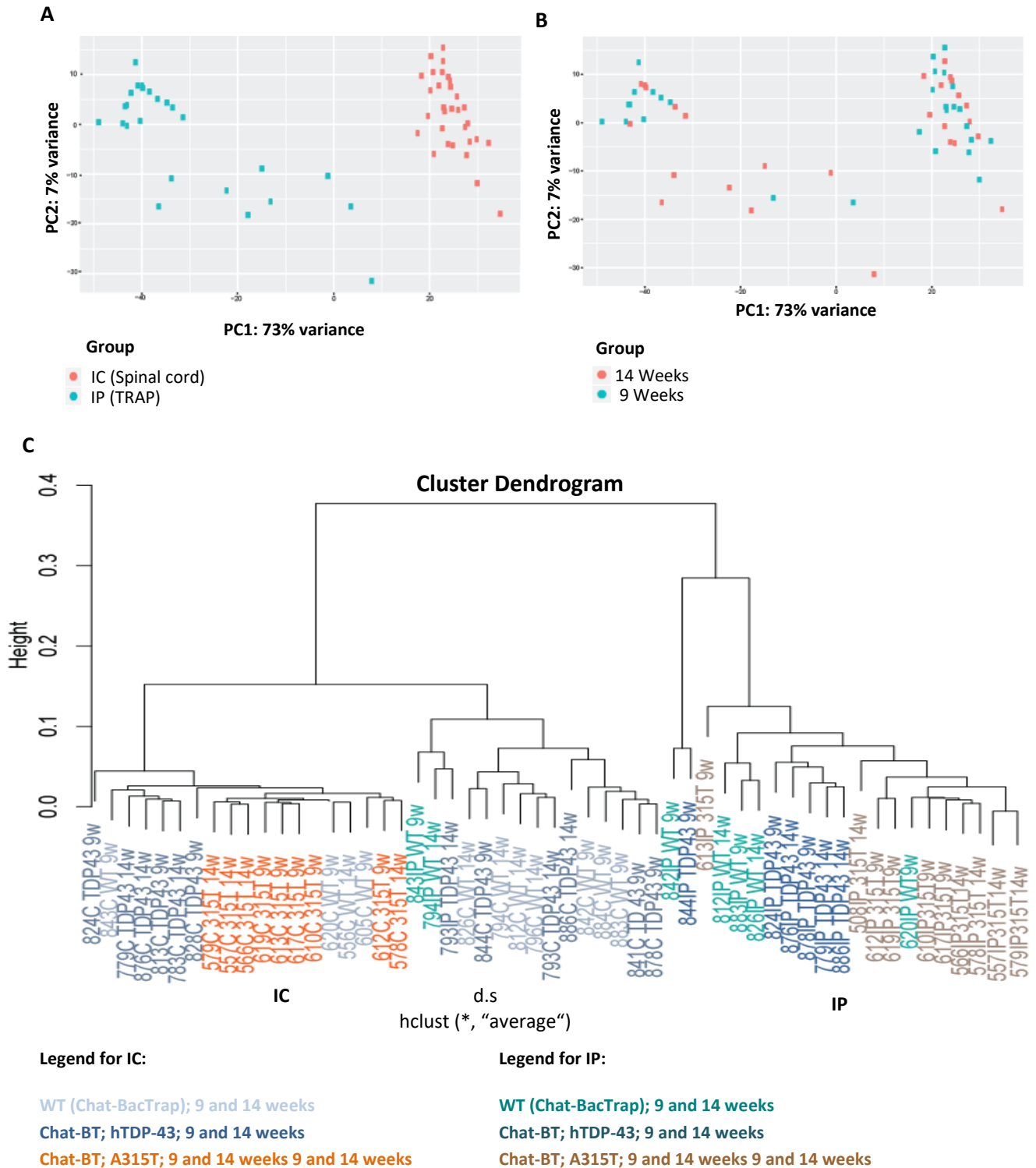
(A) Number of samples within each range of reads. (B) A total of six samples were excluded from downstream analysis. Efficiency of IPs versus ICs at 9 weeks (C) and 14 weeks (D) represented by relative enrichment and de-enrichment of specific genes. Average values from DESeq2 are shown. \*Mining of these unpublished data was performed by Dr Jan Broder Engler in collaboration with Prof. Dr. Manuel A. Friese's lab, Institute of Neuroimmunology and Multiple Sclerosis (INIMS), Center for Molecular Neurobiology Hamburg (ZMNH), Hamburg, Germany. BT: BacTrap.

PCA analysis is represented in Figure 24 A and B. In (A) is depicted how the ICs and IPs cluster and it is visible that both groups cluster separately, with the IPs showing bigger variance among samples. In (B) is calculated how the samples cluster based on time points (9 weeks vs 14 weeks). In terms of time points, the samples do not cluster in two individual groups as observed in (A) which indicates that there aren't many differences from one time point to the other.

In order to check how the samples cluster in terms of genotype, a dendrogram was generated (Figure 24 C). With this data configuration, it is possible to differentiate samples based on their genotype and time point. Both 9 weeks and 14 weeks seem to have similar properties for any given genotype, which confirms what the PCA plot showed in (B). However, when analyzing the distribution of samples based on genotypes, it is visible that samples from the same genotype cluster together. Thus, these data suggest that the major difference between samples is mainly driven by genotype and not by time points. In other words, most differences in expression detected in the Chat-BacTrap; A315T mutant animals were already present at 9 weeks, when the animals were pre-symptomatic. Conversely, the lists of GO terms for common pathways of the full pairwise DE sets of the Chat-BacTrap; A315T at 14 weeks and for 9 weeks and 14 weeks together can be found in appendix 9.1. The lists were generated by Dr. Thomas Lingner from the TAL sequencing core facility, UMG, Göttingen, Germany.

Only two exclusive pathways for the 14 weeks Chat-BacTrap; A315T mice are significant when corrected by Bonferoni's statistical test. These pathways are muscle contraction and skeletal muscle contraction. On the other hand, when analyzing both 9 weeks and 14 weeks together, the list indicates more common pathways that are significant after corrected by Bonferoni's test. Some of these pathways are cell adhesion, myelination, transport, response to hypoxia, sensory perception of sound, hear development and angiogenesis.

### 3. Results



**Figure 24. Major differences between samples are driven by genotype.**

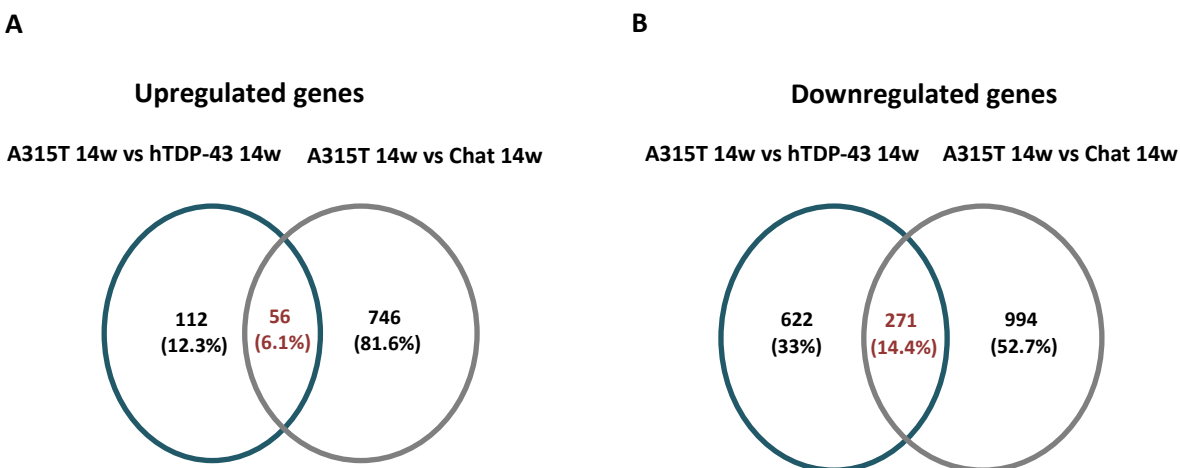
PCA analysis of ICs vs IPs (A) and 9 weeks vs 14 weeks (B). (C) Dendrogram. Overview of the similarity between samples by genotype and time point. BT: BacTrap. \*Mining of these unpublished data was performed by Dr. Dr Jan Broder Engler in collaboration with Prof. Dr. Manuel A. Friese's lab, INIMS, ZMNH, Hamburg, Germany.



### 3.6. Deregulated mRNAs were identified in diseased MNs

In order to identify deregulated mRNAs, the first strategy concentrated on identifying mRNAs whose levels are different between the Chat-BacTrap; A315T mutant 14-week group vs the Chat-BacTrap; A315T mutant 9-week group. This comparison revealed 4 candidates: *Efcab6*, *Prom2*, *Egf* and *Gm49339* (appendix 9.2). However, when comparing the relative levels of enrichment of these mRNAs in the control groups (Chat-BacTrap; A315T vs Chat-BacTrap and Chat-BacTrap; hTDP-43), it is observed that there are no differences of expression, leading to believe that these molecules do not show a clear correlation with disease onset in the mutant alone, which is the type of molecule I am most interested in finding.

Therefore, a different approach was then followed, where first the dataset from the Chat-BacTrap; A315T was compared with the dataset from the Chat-BacTrap at 14 weeks, and a list of up- and downregulated genes that were exclusively altered in the Chat-BacTrap; A315T was generated. Second, the same dataset from 14 weeks from the Chat-BacTrap; A315T was also compared to the dataset from 14 weeks Chat-BacTrap; hTDP-43 and a second list of up- and downregulated genes was also generated. Third, candidates there were present in both lists that were exclusively up- and downregulated in the Chat-BacTrap; A315T were selected. A total of 56 genes were exclusively upregulated and a total of 271 genes were exclusively downregulated in the Chat-BacTrap; A315T mice (Figure 25 A and B). The total list of exclusive genes can be found in appendix 9.3. The mining of the data was done by Dr. Jan Broder Engler, from INIMS, ZMNH, Hamburg.



**Figure 25. Strategy applied to identify candidates for mRNAs exclusively deregulated in Chat-BT; A315T mice.**

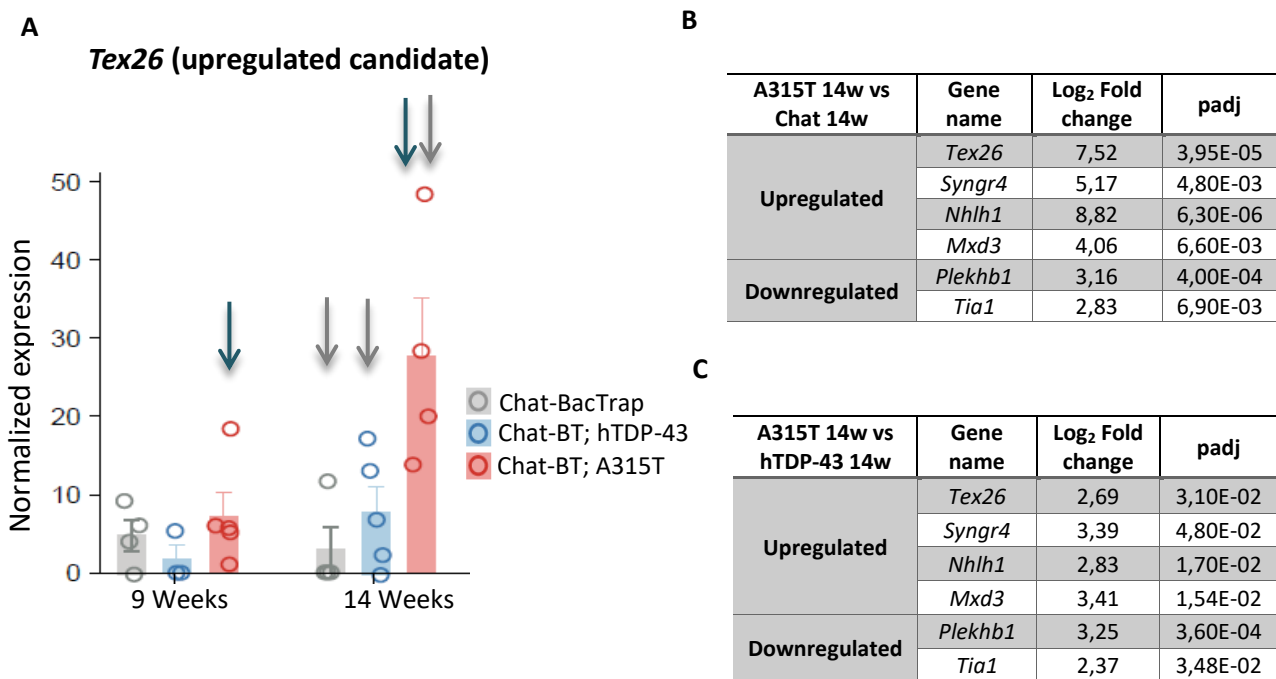
Venn diagrams for up- and downregulated candidates. 56 upregulated genes (A) and 271 downregulated genes (B) were identified to be exclusively deregulated in the Chat-BacTrap; A315T mice at 14 weeks. Legend: 14w: 14 weeks; A315T: Chat-BacTrap; A315T; hTDP-43: Chat-BacTrap; hTDP-43; chat: Chat-BacTrap. \*Mining of these unpublished data was obtained by Dr. Jan Broder Engler in collaboration with Prof. Dr. Manuel A. Friese's lab, INIMS, ZMNH, Hamburg, Germany.

### 3. Results

To facilitate the identification and prioritization of candidates with the potential to be disease drivers for follow-up assays, additional criteria were applied to the lists of up- and downregulated genes (Figure 26):

- To have a minimum 2.5x fold change in expression level of the Chat-BT; A315T vs. control groups at 14 weeks (early symptomatic phase of the disease)
- A trend to stronger phenotype at 14 weeks vs 9 weeks in Chat-BT; A315T group

Upregulated candidates had to fulfill both criteria while downregulated candidates at to fulfill at least one of the above criteria. A total of four upregulated and two downregulated candidates were selected. Results from high-throughput sequencing data from the final list of candidates from TRAP (IP) and spinal cord (IC) can be found in appendix 9.4 and 9.5, respectively.



**Figure 26. Identification of deregulated mRNAs in diseased MNs.**

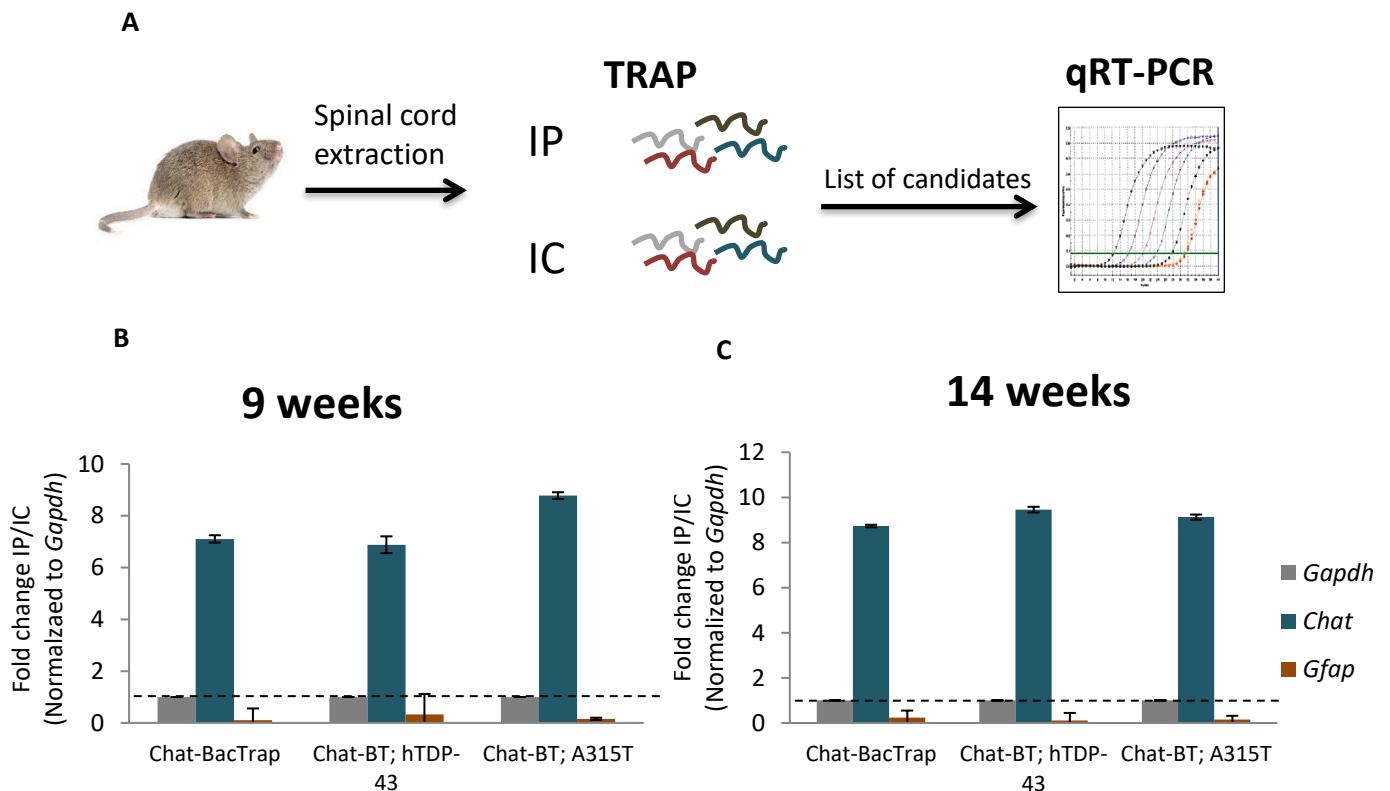
(A) Example of a candidate that meets the criteria. A minimum 2.5x fold change in expression level of the Chat-BT; A315T group vs both the Chat-BacTrap and Chat-BT; hTDP-43 groups is represented by the grey arrows (↓). A trend between the 9 weeks and 14 weeks for the Chat-BT; A315T group is represented by the blue arrows (↓). (B) and (C) Final lists of up- and downregulated genes emerged from the comparison 14 weeks between the Chat-BT; A315T vs Chat-BacTrap and Chat-BacTrap; A315T vs Chat-BacTrap; hTDP-43, respectively. Legend: 14w: 14 weeks; A315T: Chat-BacTrap; A315T; hTDP-43: Chat-BacTrap; hTDP-43; chat: Chat-BacTrap; BT: BacTrap; padj: pvalue adjusted; *Tex26*: Testis expressed 26; *Syngn4*: Synaptogyrin 4; *Nhlh1*: helix-loop-helix 1; *Mxd3*: MAX Dimerization Protein 3; *Plekhh1*: Pleckstrin Homology Domain Containing B1.

### 3.7. Potential disease drivers were validated in an independent cohort of animals

Validation of the candidates was done in independent cohorts of animals, by two different methods: 1) qRT-PCR was used to validate at the RNA level and 2) immunohistochemistry (IHC) to validate at the protein level.

#### 3.7.1. Validation at the RNA level

To validate the candidates at the RNA level, TRAP was performed on a new cohort of 9- and 14-week old mice of the same genotypes used for the original genome-wide experiment. qRT-PCR was used as the readout to look for the fold change of the Chat-BacTrap; A315T group vs the control groups (Figure 27 A). To verify whether TRAP efficiently immunoprecipitated RNA from MNs in this specific experiment, enrichment of *Chat* mRNA (Figure 27 B), and de-enrichment of *Gfap* mRNA was calculated (Figure 27 C). For both time points there was significant enrichment of *Chat* and de-enrichment of *Gfap* mRNA, which demonstrated that- within this specific experiment- TRAP was efficient in purifying ribosomes and associated mRNA from MNs.



**Figure 27. Samples for validation by qRT-PCR were efficiently immunoprecipitated via TRAP.**

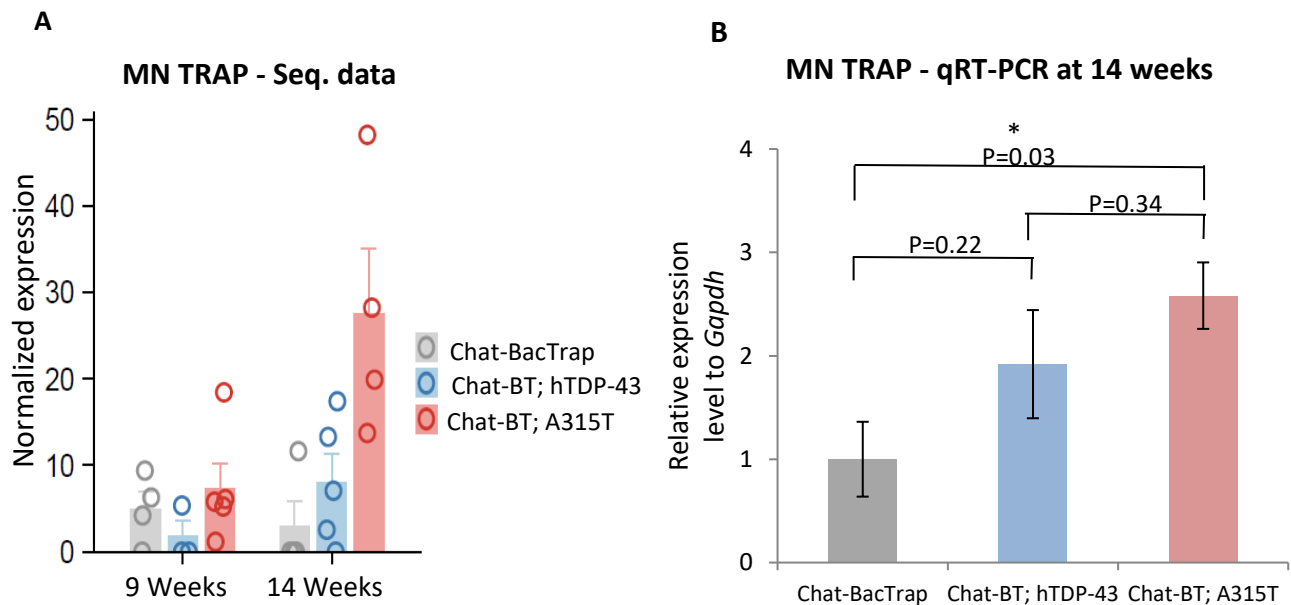
(A) Schematic of the TRAP validation experiment. TRAP was performed on mouse spinal cord from 9- and 14-week old mice with Chat-BacTrap, Chat-BacTrap; hTDP-43 and Chat-BacTrap; A315T genotypes. Levels of specific candidates were measured by qRT-PCR. TRAP efficiently immunoprecipitated ribosome-associated mRNA from MNs for both 9- (B) and 14- (C) week old mice. Data are normalized to *Gapdh*. BT: BacTrap. n=2 for 9 weeks; n=3 for 14 weeks; error bars:  $\pm$ SD and  $\pm$ SEM for 9 weeks and 14 weeks, respectively; 2 tail t-test; \*\*\*p<0.001.

### 3. Results

All six candidates in Figure 26 (B) and (C) were tested by qRT-PCR, but only four gave data that made it possible to infer about their regulation. The remaining candidates were not invalidated, but rather not possible to test via qRT-PCR since the initial RNA levels are too low and not detectable by the assay. This problem was bypassed in the deep-sequencing via additional steps to first enrich for mRNAs, followed by significant RNA amplification prior to sequencing.

#### 3.7.1.1. *Tex26* validated as an upregulated candidate at the RNA level

In my sequencing dataset, *Tex26* was identified as an upregulated candidate. In the Chat-BacTrap; A315T mutants, *Tex26* has a 3x fold change in expression levels when comparing with the control groups at 14 weeks and shows a trend between 9 weeks and 14 weeks (Figure 28 A). This trend is indicative of a transition between pre-symptomatic to early symptomatic phases of the disease. When tested by qRT-PCR at 14 weeks (Figure 28 B) it is visible a significant increase when comparing with the Chat-BacTrap group and a tendency regarding the Chat-BacTrap; hTDP-43.



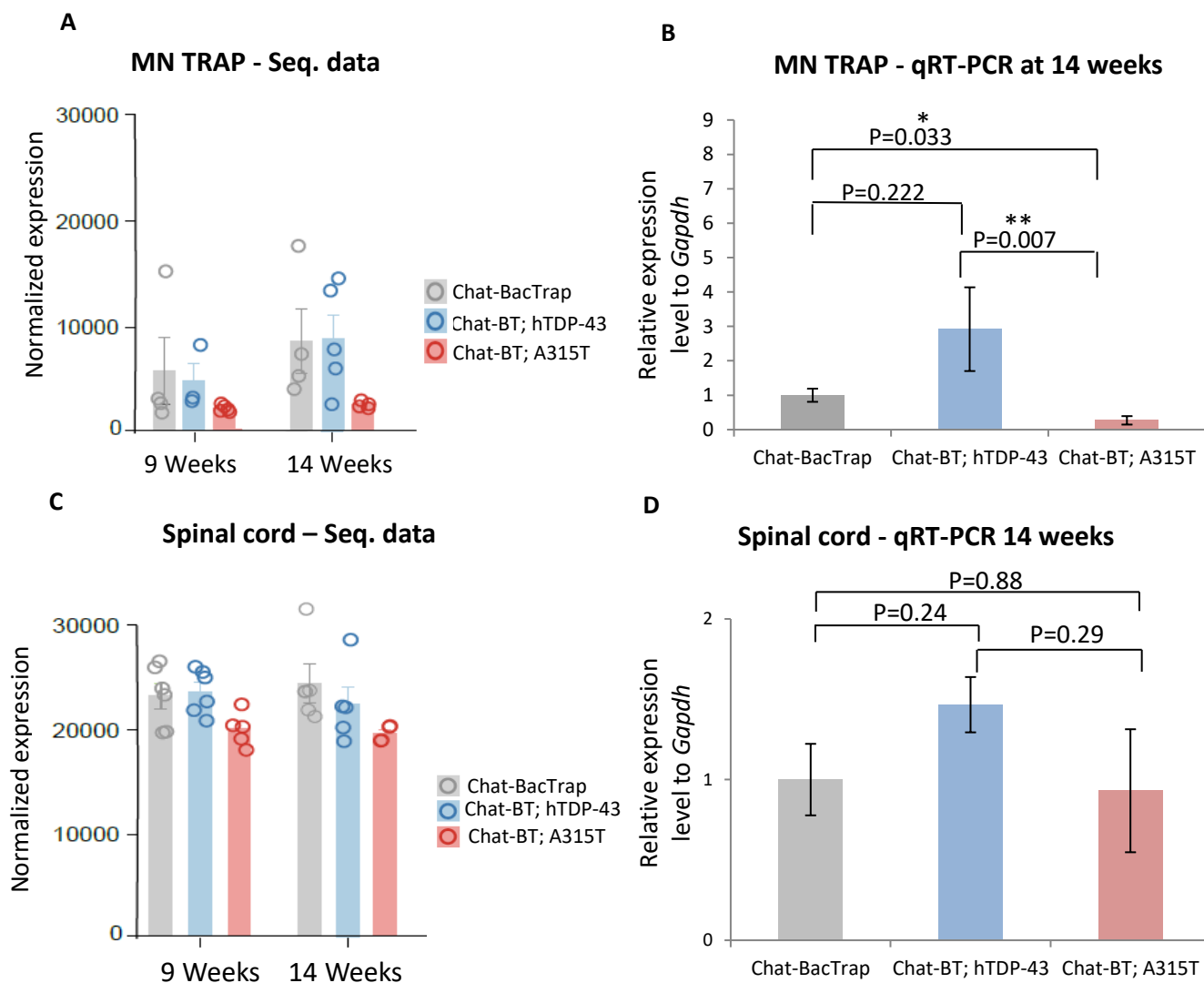
**Figure 28. *Tex26* is upregulated at the RNA level during early symptomatic phase of the disease.**

MN TRAP sequencing data from *Tex26* at 14 weeks. (B) qRT-PCR data from *Tex26* MN TRAP at 14 weeks. BT: BacTrap. n=3 for 14 weeks; error bars:  $\pm$ SEM; 2 tail t-test; \*p<0.05.

#### 3.7.1.2. *Plekhhb1* validated as a downregulated candidate at the RNA level

The second candidate that validated at the RNA level is *Plekhhb1*. This mRNA was identified as a downregulated candidate. Sequencing data showed that *Plekhhb1* has a significant reduction in RNA levels in the Chat-BacTrap; A315T mice in comparison to both controls at 14 weeks (Figure 29 A). These data are consistent with MN TRAP using qRT-PCR as readout (Figure 29 B).

Downregulated candidates that show high-level expression in spinal cord can emerge as false positives due to problems in IP efficiency leading to variable de-enrichment of material from neighbouring cells. Alternatively, it could have been that *PLEKHB1* was actually downregulated in the whole spinal cord. To guarantee that the down-regulation of *Plekhhb1* specifically in MNs is real, I checked in the sequencing data from IC or spinal cord and by qRT-PCR from the independent cohort for how *Plekhhb1* mRNA behaves (Figure 29 C and D). In both cases, no differences are found between genotypes at 14 weeks for spinal cord material which supports the idea that *Plekhhb1* mRNA is specifically downregulated in diseased MNs at 14 weeks of age.



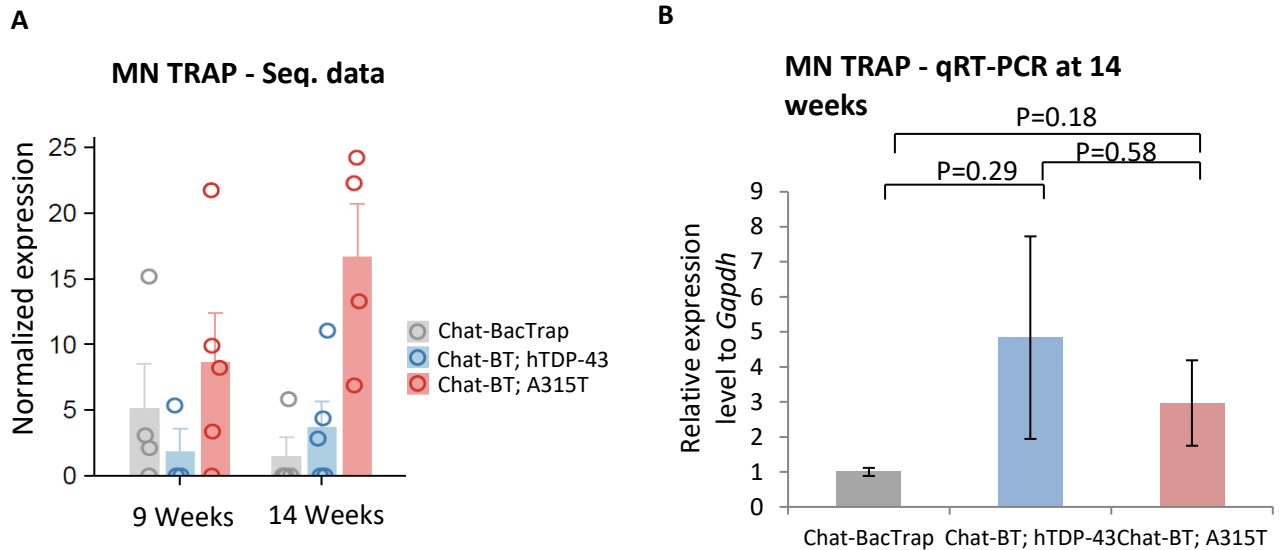
**Figure 29. *Plekhhb1* is downregulated at the RNA level during early symptomatic phase of the disease.**

(A) MN TRAP sequencing data from *Plekhhb1* at 14 weeks. (B) qRT-PCR data from *Plekhhb1* MN TRAP at 14 weeks. (C) Sequencing data from IC or spinal cord from *Plekhhb1* at 14 weeks. (D) qRT-PCR data from *Plekhhb1* IC or spinal at 14 weeks. BT: BacTrap; n=3 for 14 weeks; error bars:  $\pm$ SEM; 2 tail t-test; \*p<0.05; \*\*p<0.01.

### 3. Results

#### 3.7.1.3. *Syngn4* shows a trend as an upregulated candidate at the RNA level

*Syngn4* is another candidate whose RNA levels were possible to measure by qRT-PCR. According to the sequencing data, *Syngn4* emerged as an upregulated candidate at 14 weeks of age (Figure 30 A). However, when analyzing the data obtained from the MN TRAP - qRT-PCR, *Syngn4* showed a strong trend (average increase of 3X), but was not validated as an upregulated candidate at the RNA level using a standard T-test (Figure 30 B). The overall distribution of samples per group is simply too variable. Perhaps a higher number of replicates or improved assay might validate this candidate at the RNA level.

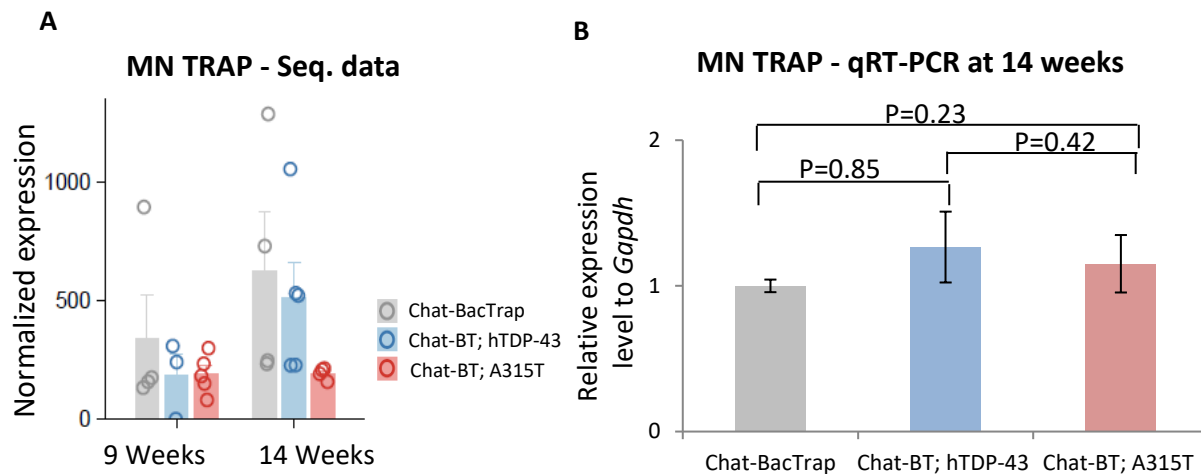


**Figure 30. *Syngn4* shows a strong tendency as an upregulated candidate at the RNA level.**

(A) *Syngn4* emerged as an upregulated candidate at 14 weeks in the sequencing dataset. (B) Data from the MN TRAP - qRT-PCR shows a strong trend of the Chat-BacTrap; A315T when comparing with the Chat-BacTrap group. BT: BacTrap; n=3 for 14 weeks; error bars:  $\pm$ SEM; 2 tail t-test.

#### 3.7.1.4. *Tia1* shows a trend towards different isoform regulation at the RNA level

*Tia1* was detected as a downregulated candidate in the sequencing data (Figure 31 A). However, when tested by qRT-PCR as the readout, there were no significant differences in *Tia1* mRNA levels between genotypes at 14 weeks of age (Figure 31 B), suggesting it may be a false positive.

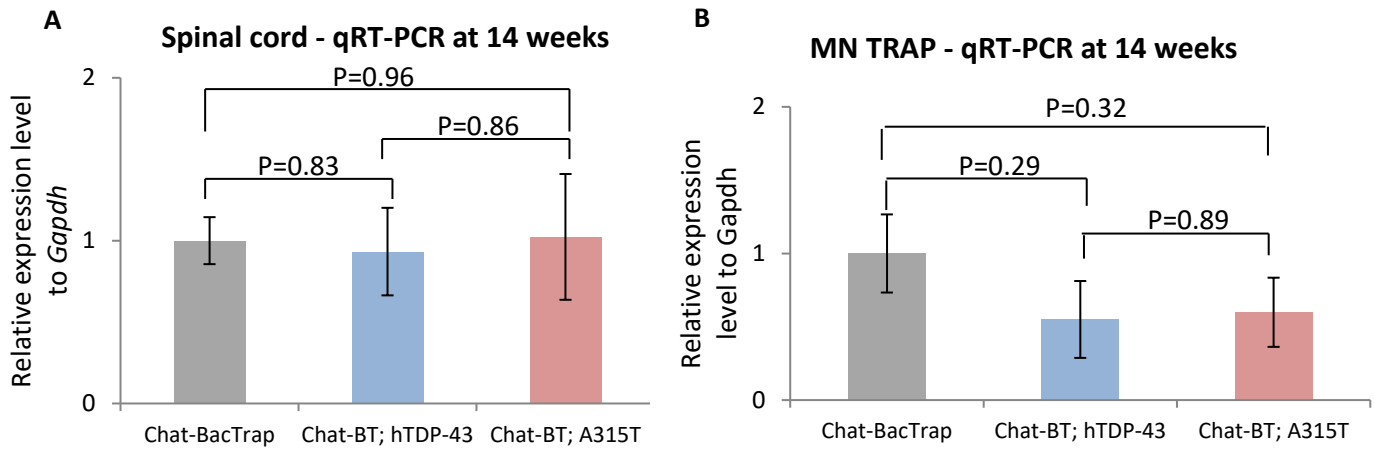


**Figure 31. *Tia1* shows no significant differences between genotypes at the coding sequencing part of the gene.**

(A) Sequencing data picked up *Tia1* as a downregulated candidate. (B) MN TRAP - qRT-PCR data shows that *Tia1* is a false positive candidate, since there are no significant differences between genotypes. BT: BacTrap; n=3 for 14 weeks; error bars:  $\pm$ SEM; 2 tail t-test.

However, mutations in this gene were recently shown to cause ALS/FTD and to affect SG formation and dynamics [171]. Thus, I decided to continue to investigate *TIA1*. Specifically, I hypothesized that one of the annotated 3'UTR mRNA isoforms of *Tia1* could have been selectively downregulated in the A315T animals due to alternative 3'end processing. The idea is that this would lead to *Tia1* emerging from the sequencing data as a downregulated candidate, even though there would actually be no difference in the levels of the coding sequence portion of the mRNA. In the mouse *Tia1* gene there are four annotated mRNA isoforms in the Ensembl database that can produce a protein. Out of these four, one has a much longer 3'UTR than the others. This is how it might be that *Tia1* could emerge as significantly downregulated in the sequencing data, without actually having reduced levels of the coding sequence. If the long 3'UTR isoform is significantly downregulated, far fewer reads would map to this locus and it would be identified as downregulated.

However, primers to the coding sequence would detect no difference in qRT-PCR, as observed. With specific primers designed against the 3'UTR of the longer isoform of *Tia1* RNA (202), it is possible to determine whether there is a reduction in *Tia1* levels for the long isoform. In Figure 32 (A), it is represented the levels of *Tia1-202* in the spinal cord at 14 weeks and as depicted there are no significant differences. When observing what happens in the MNs, Figure 32 (B), it is visible a trend in case of the Chat-BT; hTDP-43 and the Chat-BT; A315T, towards showing a reduction in the *Tia1-202* RNA levels. The lack of a possible trend between the Chat-BT; hTDP-43 and the Chat-BT; A315T *TIA1-202* levels, leads to believe that down-regulation of *Tia1-202* RNA might not be sufficient to cause disease.



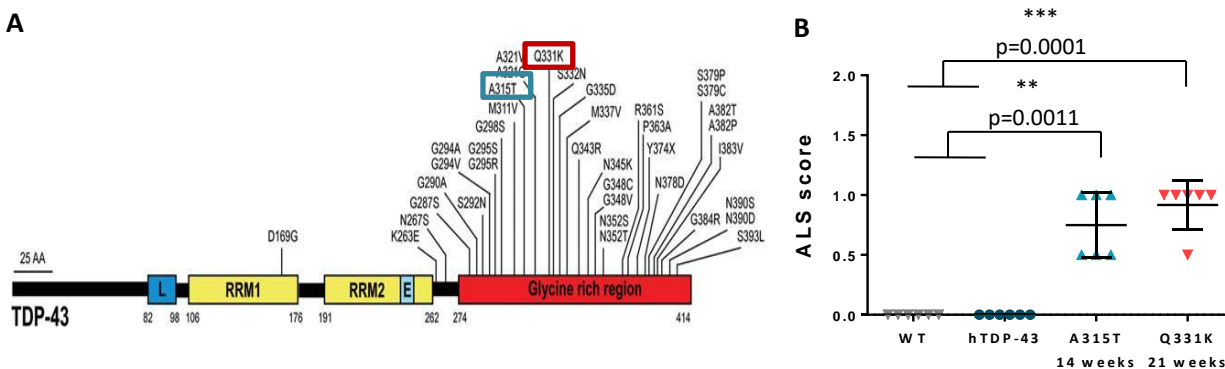
**Figure 32. *Tia1-202* RNA isoform shows a trend towards being downregulated.**

(A) *Tia1* RNA levels in spinal cord or IC at 14 weeks of age (B) *Tia1* RNA levels in MNs at 14 weeks. BT: BacTrap; n=3 for 14 weeks; error bars:  $\pm$ SEM; 2 tail t-test.

### 3.7.2. Validation at the protein level

Candidates were examined in protein validation assays in two independent ALS mouse lines. One expresses the patient mutations A315T, and is the line used for both the genome-wide and independent validation TRAP experiments. A second transgenic line expresses human *TARDBP* bearing the Q331K patient mutation (Figure 33 A). Validation in independent mouse model caused by a different patient mutant allele of TDP-43 is important to determine if these changes are A315T specific or if they are also observed in other ALS-TDP-43 mutant variants. The *hTARDBP-43<sup>Q331K</sup>* (Q331K) mouse line was characterized in the literature [56] and the symptomatic phase was described to start around three months of age. The line was also reported not to show any progression of the symptoms until ten months of age. Based on the literature, I tested the animals for symptoms at  $\sim$  six months of age (21 weeks). I used the neurological score test to determine if the animals were already symptomatic or not. The same test was also applied to the A315T mutant mouse line (Figure 33 B). All mutant animals considered for IHC show difficulties in extension of the hindlimbs.

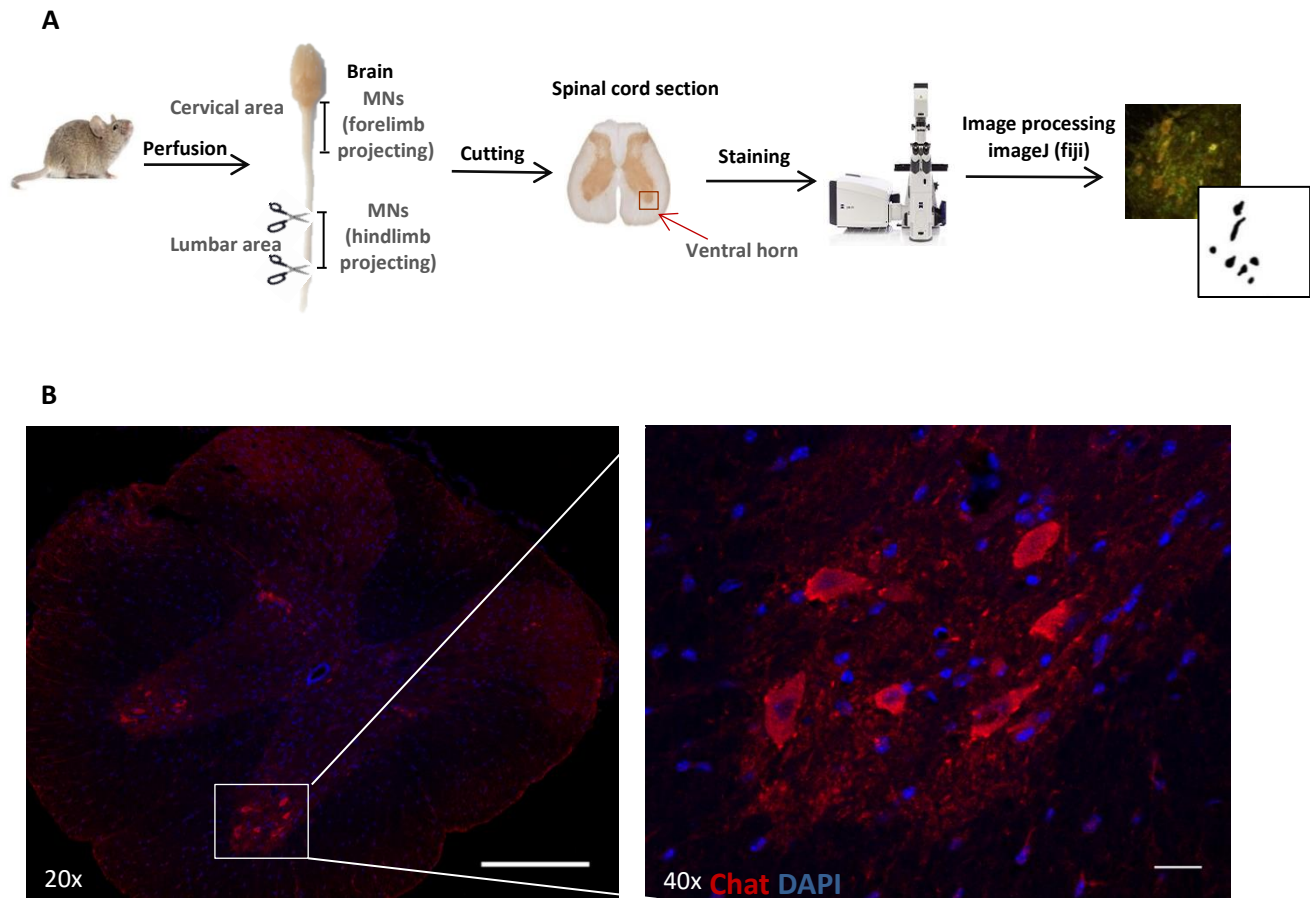




**Figure 33. Q331K mutant mice show ALS-like symptoms at 21 weeks of age according to the neurological score.**

(A) TDP-43 protein domain structure and localization of mutations [64]. In blue is represented the location of the A315T mutation and in red of the Q331K mutation. (B) ALS score for the A315T mouse line at 14 weeks and for the Q331K mouse line at 21 weeks of age.  $n=5$  for A315T and  $n=6$  for Q331K; error bars:  $\pm$ SEM, 2 tail t-test; \*\* $p<0.01$ , \*\*\* $p<0.001$ .

I isolated and cut the spinal cord from mice at both 9 weeks and 14 weeks for the A315T mutant line, hTDP-43 line and WT control littermates and at 21 weeks of age for the Q331K mutant line and WT control littermates. To minimize artifacts and variables, each set of experiments was done in parallel. This means that the spinal cords of a grouped batch of WT, hTDP-43 and A315T animals were perfused, cut and immunostained in parallel (Figure 34 A).

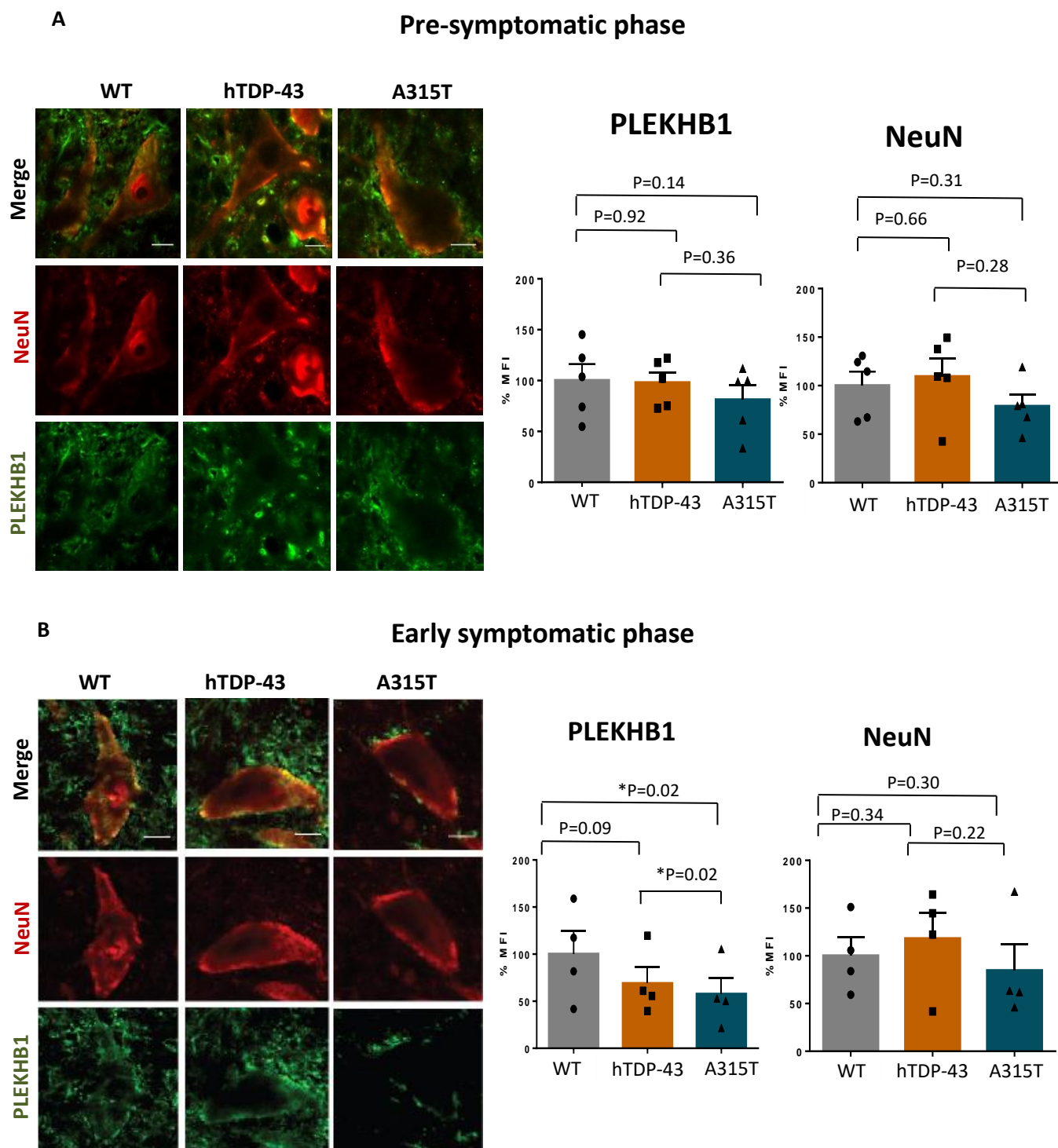


**Figure 34. IHC from spinal cord MNs.**

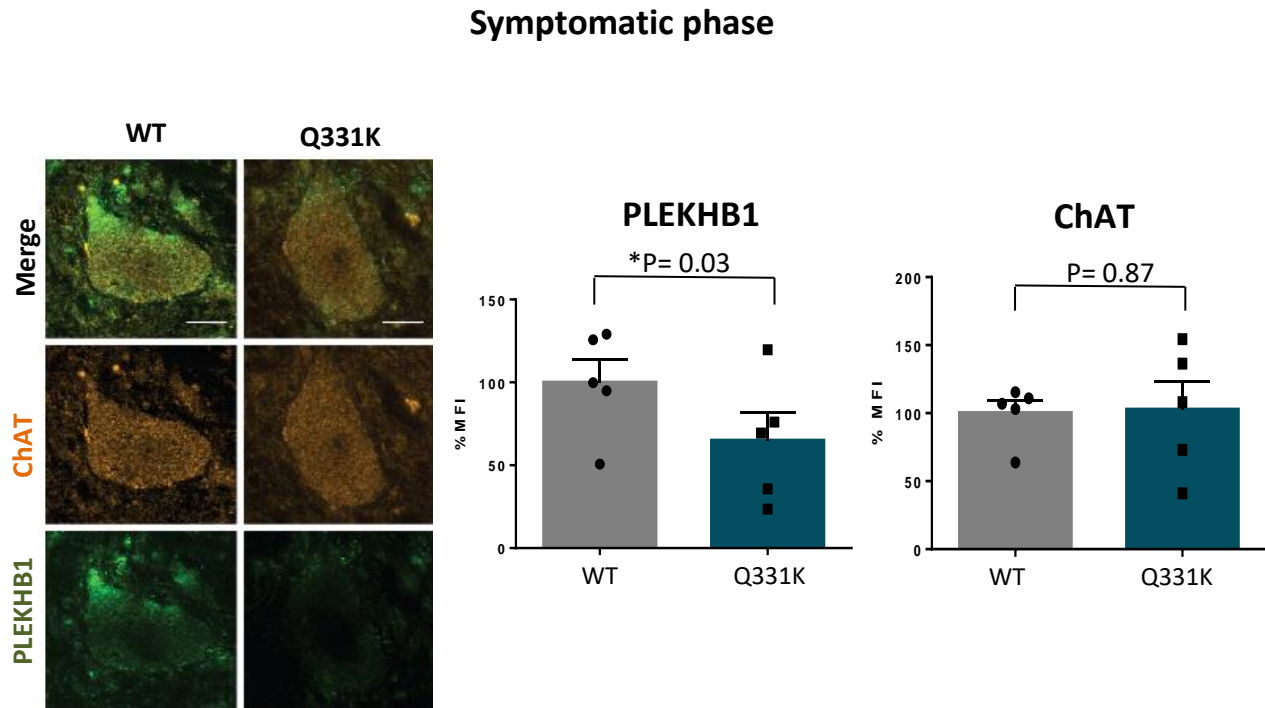
(A) Schematic overview of validation by IHC. Each „n“ of experiments is processed in parallel on the same day, so that different genotypes could be directly compared, minimizing this way the introduction of external variables to the assay. (B) IHC from a section of the spinal cord. MNs are labeled in red (ChAT protein staining) and the nuclei in blue (DAPI dye staining). Objectives used: 20x and 40x. scale bar: 10µm. Images were acquired by microscopy and processed with ImageJ software.

### 3.7.2.1. PLEKHB1 protein levels are decreased in spinal MNs of TDP-43 mutants

Spinal cord MNs were stained for PLEKHB1, ChAT, NeuN and with the dye DAPI to stain nuclei. ChAT and NeuN are both neuronal markers, with the difference that ChAT is specific for MNs (Figure 35). In the case of the A315T mouse line, at the pre-symptomatic phase (9 weeks) there are no significant differences between the A315T group and the controls (Figure 35 A). On the other hand, at early-symptomatic phase (14 weeks) the A315T mutant group shows a significant decreased in comparison to both of the controls (Figure 35 B). PLEKHB1 is therefore validated as a downregulated candidate during early symptomatic phase, in the A315T mouse line at the protein level.



PLEKHB1 protein levels in MNs were also significantly decreased in symptomatic Q331K mutants relative to respective control (Figure 36). Thus, PLEKHB1 is validated as a downregulated candidate not only in the A315T mutant line, but also in a completely independent model of ALS caused by mutant TDP-43.

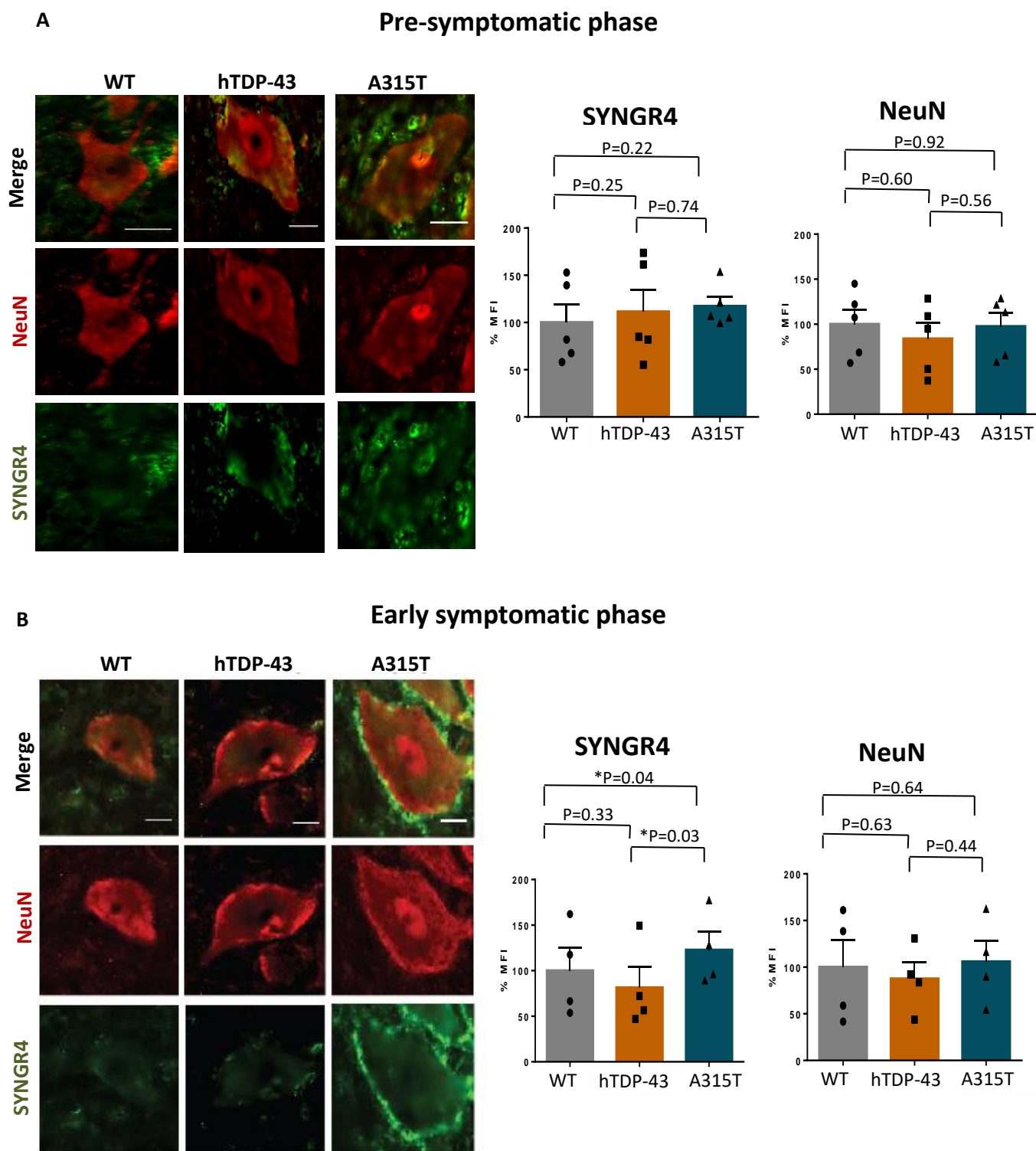


**Figure 36. PLEKHB1 protein is downregulated in diseased spinal cord MNs of mice expressing hTDP-43<sup>Q331K</sup>.**

IHC of spinal cord MNs at symptomatic phase (21 weeks). MNs were stained against PLEKHB1, ChAT, NeuN (data not showed) and DAPI. ChAT was used as a control of the experiment, since its intensity does not change over time in MNs. MFI: mean fluorescence intensity, n=5; scale bars: 10 $\mu$ m; error bars:  $\pm$ SEM; paired t-test; \*p<0.05. Images were acquired by microscopy and processed with ImageJ software.

### 3.7.2.2. SYNGR4 protein levels are increased in MNs of TDP-43 mutants

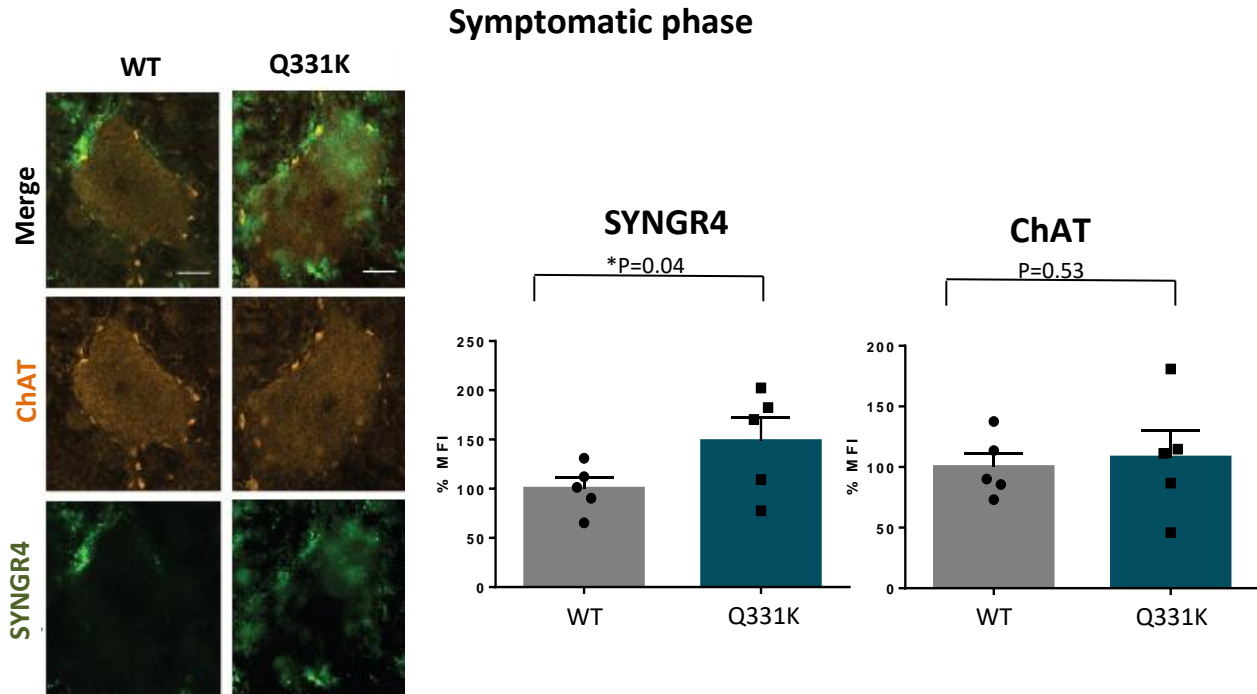
SYNGR4 protein levels were also determined by IHC (Figure 37). SYNGR4 protein levels were determined in spinal MNs for the A315T line and compared to the respective controls. During the pre-symptomatic phase there are no significant differences between the A315T group and the controls (Figure 37 A). In contrast, during the early-symptomatic phase, the A315T mutant group shows a significant increase of protein levels relative to both of the controls (Figure 37 B). Although the magnitude of the increase is not large, these data validate up-regulation of SYNGR4 within spinal MNs in the A315T mutant mouse line.





### 3. Results

SYNGR4 protein is also significantly upregulated in the symptomatic Q331K mutant mice vs. non-transgenic littermate controls. All together, these data demonstrate that SYNGR4 is upregulated in both the A315T and the Q331K mutant animals. Thus, upregulation of SYNGR4 within spinal MNs is observed in early disease in two independent models of ALS caused by mutant TDP-43 expression.



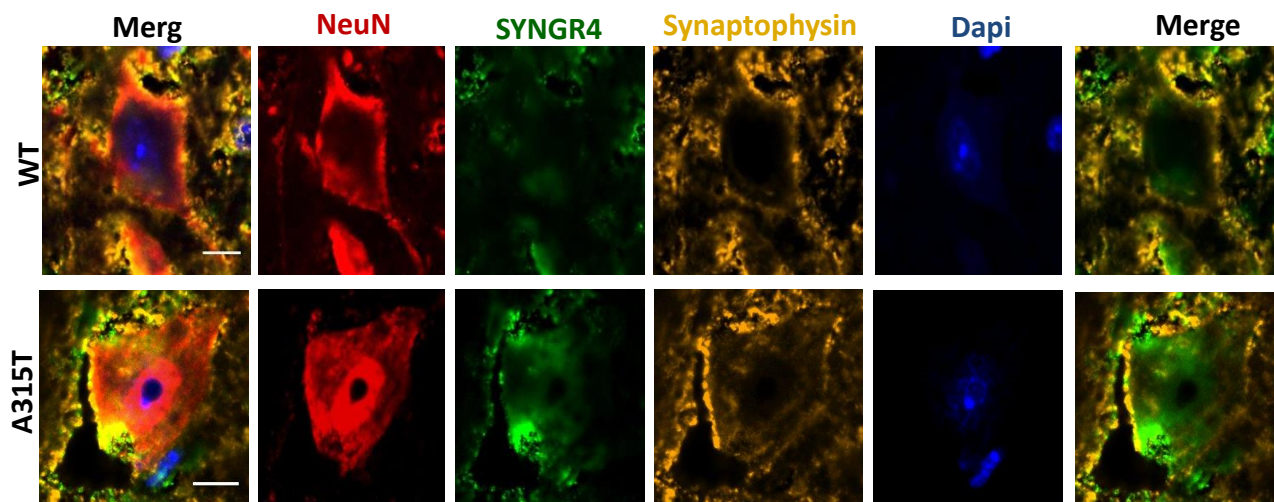
**Figure 38. SYNGR4 protein is also upregulated in diseased spinal cord MNs of mice expressing hTDP-43<sup>Q331K</sup>.**

IHC of spinal cord MNs at symptomatic phase (21 weeks). MNs were stained against PLEKHB1, ChAT, NeuN (data not showed) and DAPI (data not showed). ChAT was used as a control of the experiment, since its intensity is does not change over time in MNs. MFI: mean fluorescence intensity, n=5; scale bars: 10 $\mu$ m; error bars:  $\pm$ SEM; paired t-test; \*p<0.05. Images were acquired by microscopy and processed with ImageJ software.

#### 3.7.3. SYNGR4 protein does not colocalize with SVs

For some candidates with the potential to be disease drivers, no biological function has been described or it is challenging to connect them to ALS. However, SYNGR4 is part of a family of proteins implicated in neurotransmitter release and neurodegeneration [172]. Whether SYNGR4 is associated with synaptic vesicles is not known. I therefore checked whether this protein colocalizes with SVs by double staining for SYNGR4 and Synaptophysin, a classical marker for SVs.

I found that SYNGR4 and Synaptophysin do not colocalize in spinal cord MNs, indicating that SYNGR4 might not be involved in neurotransmitter release (Figure 39).



**Figure 39. SYNGR4 protein does not colocalize with SVs.**

Spinal cord MNs were stained against SYNGR4, Synaptophysin, NeuN and DAPI. Staining shows no colocalization in both the WT control group or in the A315T group during early symptomatic phase of the disease. Representative images of n=3 experiments. Scale bars: 10 $\mu$ m. Images were acquired by microscopy and processed with ImageJ software.

### 3.8. Comparison of neurodegenerative mechanisms in SOD1 and TDP-43 mouse models of ALS

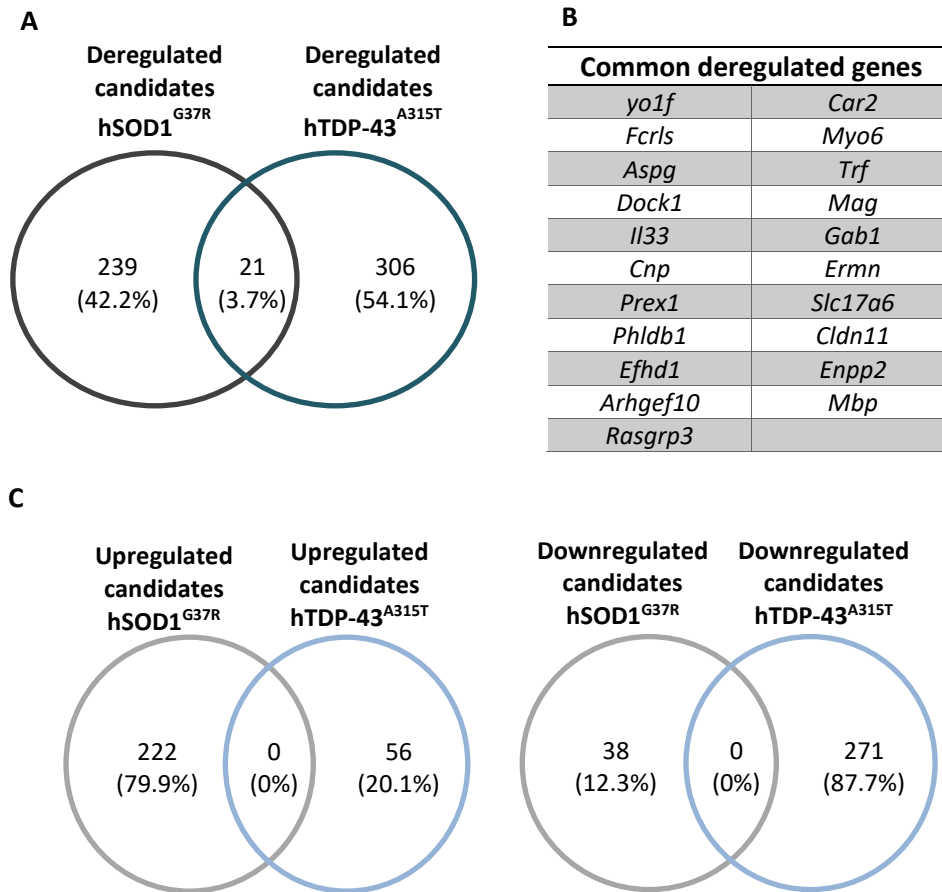
Seminal findings reveal altered localization and aggregation of TDP-43 in affected MNs in most forms of fALS and sALS, with the striking exception of SOD1-related disease. These and other studies have led to a paradigm shift, since they suggest that ALS-SOD may represent a fundamentally different form of disease with a distinct disease-driving pathway from ALS-TDP, and that specific therapies may be needed for both diseases. One promising avenue to identify disease-driving pathways would be a systematic comparison of neurodegenerative mechanisms in SOD1 and TDP-43 related mouse models of ALS. To date, no such comparison has been described.

A previous study performed MN TRAP with an ALS mouse model expressing hSOD1<sup>G37R</sup> (Sun S. et al.; 2015). In this study they focused on the symptomatic phase of the disease. To determine whether common genes might be affected in MNs of ALS caused by mutant SOD1 and mutant TDP-43, I compared my initial list of deregulated genes (appendix 9.3), with their list in order to look for common molecules (Figure 40). Three outcomes are possible: 1) no common candidates; 2) common candidates with the same pattern of deregulation; 3) common candidates with a different pattern of deregulation.

When I first compared the overall lists I found 21 genes, whose regulation is altered in MNs of both the hSOD1<sup>G37R</sup> and hTDP-43<sup>A315T</sup> mouse models (Figure 40 A and B). Interestingly, for these common genes the direction of deregulation was not preserved in the two models: genes that were upregulated in

### 3. Results

hTDP-43<sup>A315T</sup> MNs were downregulated in hSOD1<sup>G37R</sup> MNs and vice versa (Figure 40 C). This leads to the hypothesis that deregulated expression of these genes in either direction might play a role in disease.



**Figure 40. Comparison of deregulated genes in MNs of ALS models expressing hSOD1<sup>G37R</sup> versus hTDP-43<sup>A315T</sup>.**

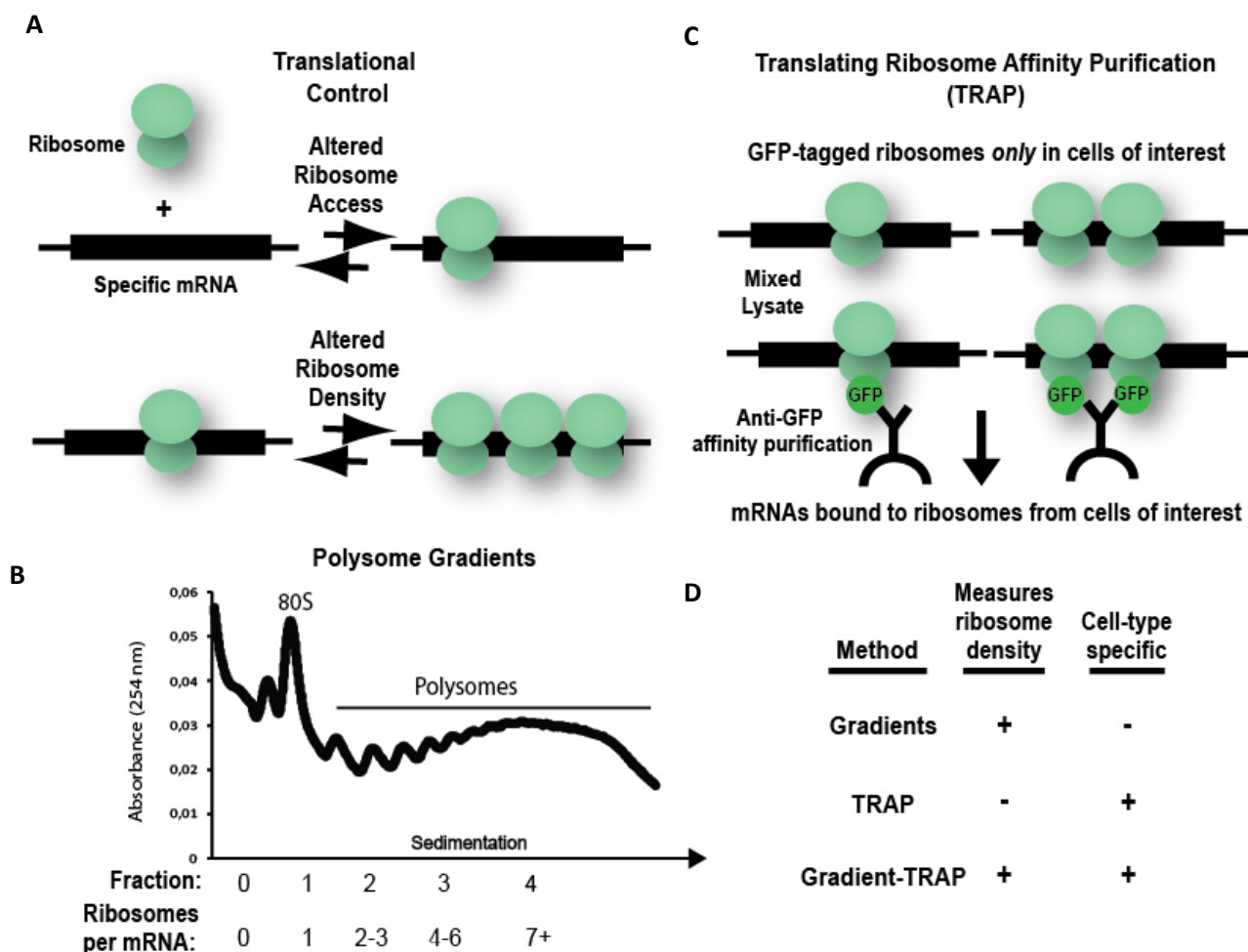
(A) Overall comparison of deregulated molecules from the hSOD1<sup>G37R</sup> list versus hTDP-43<sup>A315T</sup> list. (B) List of common candidates between the two datasets. (C) Comparison of identified up- and downregulated genes in both datasets. The list of deregulated candidates from the hSOD1<sup>G37R</sup> mutant animals is available from Sun S. et al., 2015 [173].

#### 3.9. Preliminary experiments to establish a new method to monitor translation: Gradient-TRAP

Numerous studies analyzing patient samples, as well as animal and cell-based disease models, strongly support altered RNA regulation by TDP-43 within MNs as a major cause of disease. One of the most important steps of RNA regulation is translation. To date no method available allows to monitor changes in ribosomal density in specific cell types *in vivo*. Thus, Gradient-TRAP aims to overcome the current limitations of the available methods by combining the power of sucrose gradients with TRAP (Figure 41). A premise for the rationale of Gradient-TRAP is the hypothesis that TRAP cannot detect changes in ribosome density, therefore missing potential differentially translated mRNAs. This method is especially



important in the case of mRNAs whose levels in the cell do not change but their protein levels do. As a proof of concept, an experiment was designed *in vitro* to test the robustness and reproducibility of the Gradient-TRAP. Later the method was optimized for an *in vivo* approach.



**Figure 41. Gradient-TRAP as a new method to measure translational control from specific cell types.**

(A) Translational control involves changes in ribosome access to or density on specific mRNAs. (B) Sucrose density gradient polysome profiling can measure both but requires significant starting material and lacks cell type-specific resolution. (C) Conversely, tagged-ribosome immunoprecipitation approaches, such as TRAP, enable access to mRNA bounded ribosomes from specific cells in a complex mixture. However, TRAP presumably cannot monitor ribosome density, since an mRNA should be immunoprecipitated whether it is bound by one ribosome, three, or ten. (D) Gradient-TRAP combines sucrose density gradient separation of mRNAs according to the number of bound ribosomes, with immunoprecipitation of tagged ribosomes and associated mRNAs from specific gradient fractions. Figure provided by Dr. Kent Duncan.

### 3.9.1. Establishment of conditions for Gradient-TRAP *in vitro*

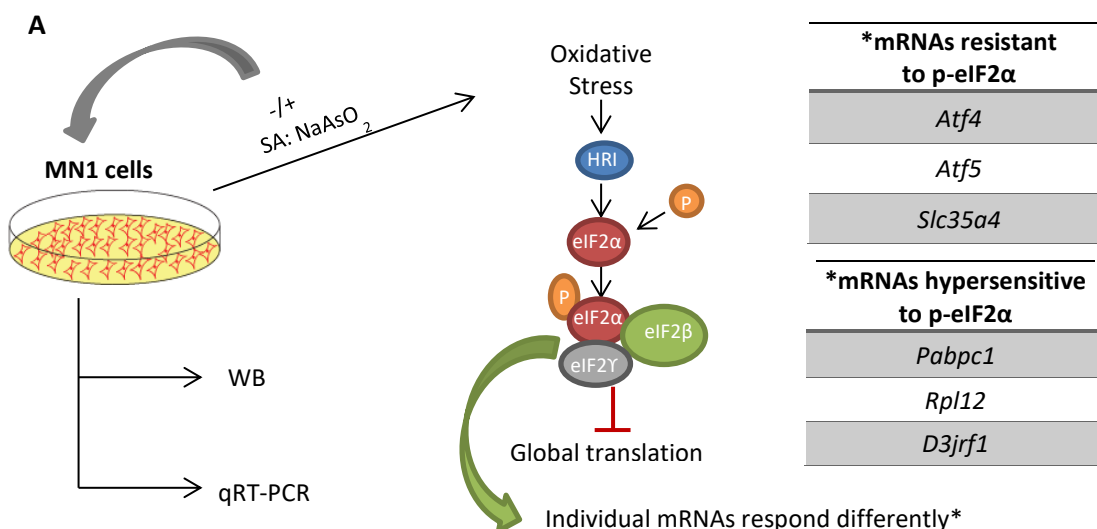
The idea was to find a well described system that is involved in alteration of translational status of mRNAs that can be applied as a proof of concept for the development of Gradient-TRAP. The MN-like cell

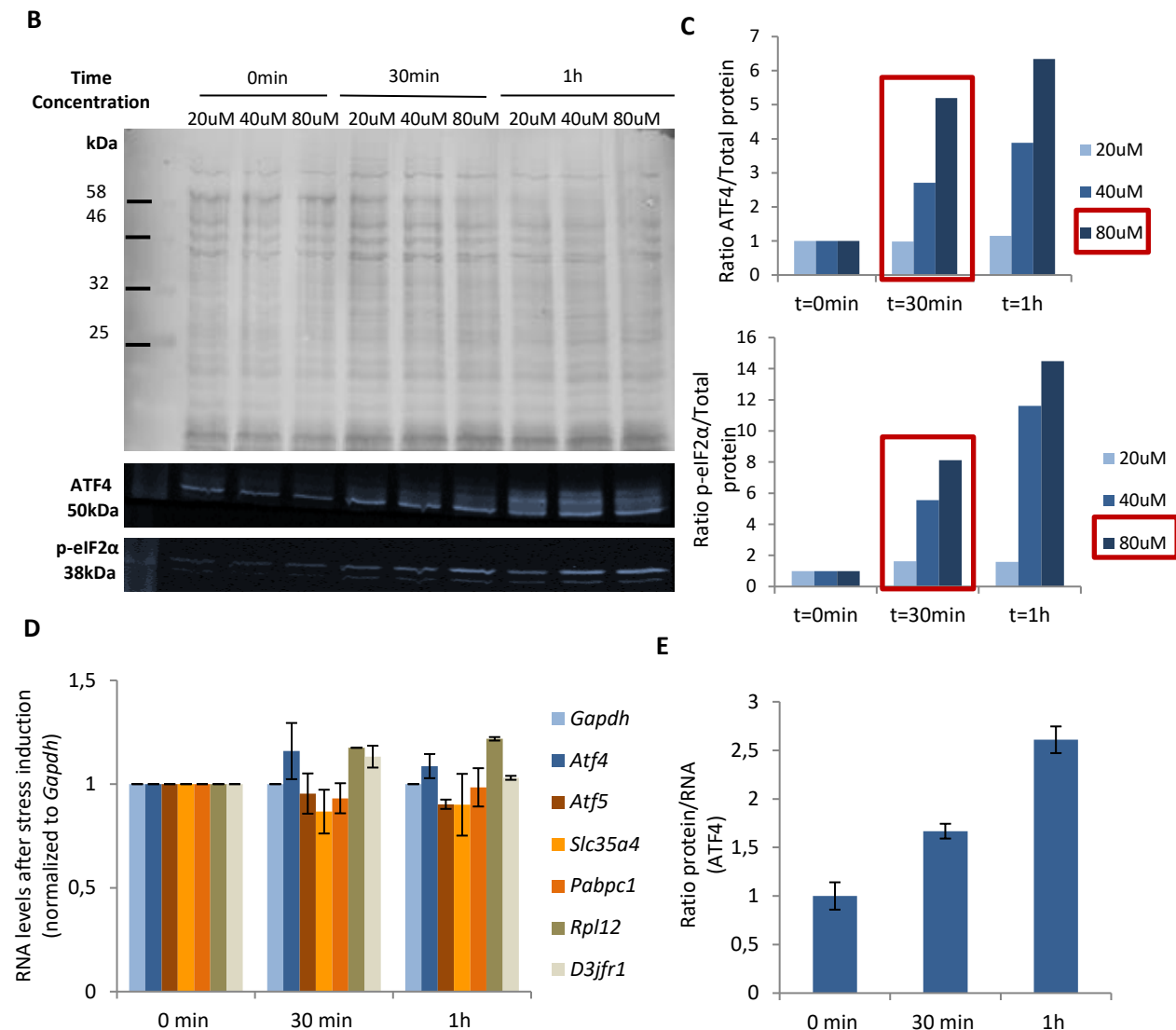
### 3. Results

line, MN1, was used to test the applicability of the method. Alteration in translational control was achieved by the presence of oxidative stress. Based on the literature it was reported that in the presence of oxidative stress, cells shut down global translation and only certain genes are translated [174]. In order for this process to take place, eIF2 $\alpha$  protein needs to be phosphorylated. This phosphorylation step is responsible for signaling inhibition of global translation. mRNAs, whose number of ribosomes increase upon stress induction, are called resistant mRNAs e.g. *Atf4*, *Atf5* and *Slc35a4*. On the other hand, mRNAs whose number of ribosomes decrease more strongly than what is observed for most mRNAs, upon stress induction are designated hypersensitive mRNAs, e.g. *Pabpc1*, *Rpl12* and *D3jfr1*. Importantly, the total levels of these mRNAs do not change under global translational arrest. The aim is to monitor the changes in ribosome density of these well described mRNAs upon stress induction by Gradient-TRAP.

The first step was to identify for MN1 cells the best concentration and time of exposure to the oxidative stress agent, sodium arsenite (SA): NaAsO<sub>2</sub>. In order to find such conditions, I checked via WB if the protein levels of ATF4 and p-eIF2 $\alpha$  are changed and by qRT-PCR if the RNA levels of specific RNAs were altered (Figure 42 A). After 30mins of exposure to 40 $\mu$ M and 80 $\mu$ M of NaAsO<sub>2</sub>, it is already visible an increase at the protein level of ATF4 and p-eIF2 $\alpha$ , which is stronger after 1h of exposure (Figure 42 B and C). 80 $\mu$ M of NaAsO<sub>2</sub> of exposure were defined as the optimal concentration to inhibit global translation, since it shows a stronger effect than 40 $\mu$ M.

Next, I evaluated in MN1 cells, the potential effects of 80 $\mu$ M of NaAsO<sub>2</sub> exposure for 30min or 1h on the levels of several mRNAs, including those whose translation was shown to be resistant or hypersensitive to this treatment in HEK293T cell [174]. No differences in mRNA levels relative to mock-treated control cells were detected for *Gapdh*, *Atf4*, *Atf5*, *SLC35a4*, *Pabpc1*, *Rpl12* or *D3jfr1* (Figure 42 D). For ATF4 the ratio of protein per RNA was calculated (Figure 40 E). Despite no changes at the RNA level of *Atf4* there is an increase at the protein level which is visible in the ratio. These results validate NaAsO<sub>2</sub>-treated MN1 cells as a system to study translational status of certain mRNAs, since as shown for ATF4, there are no changes at the RNA level upon stress induction, while there is in fact more protein being made.





**Figure 42. Model to establish Gradient-TRAP: NaAsO<sub>2</sub> induced oxidative stress in MN1 cells.**

(A) Schematic of the oxidative stress-induced pathway triggered by NaAsO<sub>2</sub> treatment and its impact on translation. A list of mRNAs whose translation should be resistant or hypersensitive to p-eIF2α was chosen based on the literature [174]. (B) Optimization of stress induction response: definition of best concentration and time of exposure to NaAsO<sub>2</sub> based on (C) p-eIF2α and ATF4 protein levels by WB. Representative of three independent experiments. (D) qRT-PCR as a readout to control for potential RNA level changes in mRNAs of interest upon stress induction. RNA levels were normalized to *Gapdh* levels (E) Ratio between protein and mRNA levels for ATF4. n=3, error bars: ±SEM.

### 3.9.2. NaAsO<sub>2</sub> massively down regulates translation and alters ribosome density on most mRNAs

After identifying conditions using NaAsO<sub>2</sub>-treated MN1 cells that would lead to translational changes without secondary effects on mRNA levels, I next examined the extent to which changes in ribosome density on specific mRNAs could be observed. By applying the polysome profiling method, it is possible to determine how the distribution of ribosomes on certain mRNAs is affected upon stress induction.

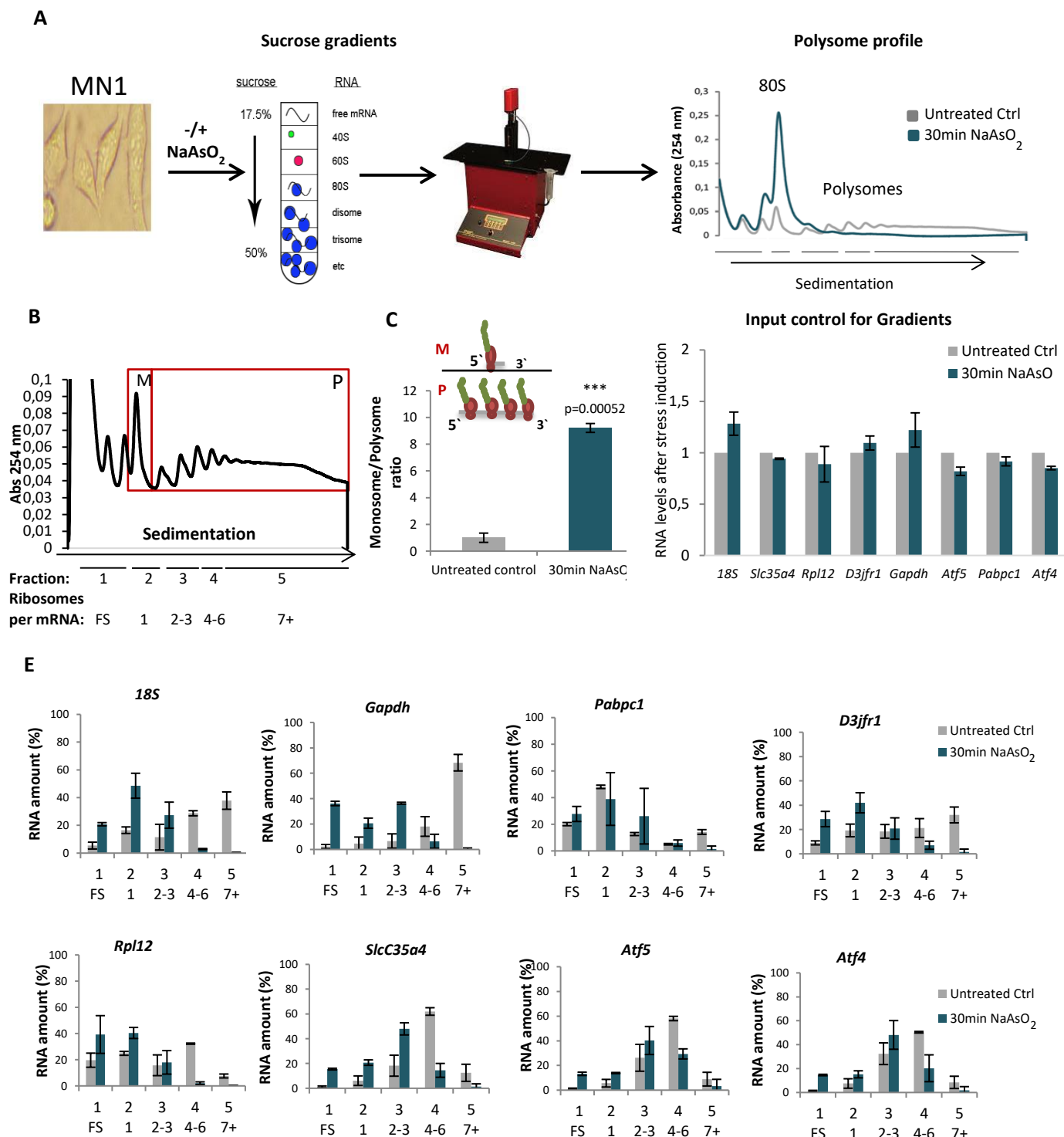
### 3. Results

---

Polysome profiling involves the generation of sucrose density gradients, ranging from 17.5-50% sucrose. The lysate of interest is loaded onto the gradients which are fractionated from the top to the bottom. The top contains the free ribosomal subunits, 40S, 60S, and free mRNA, and the subsequent layers are composed of mRNAs with increasing number of ribosomes bound to them. The gradient passes through an ultraviolet (UV) monitor which measures the concentration of nucleic acids. Based on the absorbance it is possible to discriminate between the number of ribosomes on the mRNA. Separate fractions based on ribosomal density are thereafter generated with the possibility of being collected for downstream applications.

MN1 cells were treated with 80 $\mu$ M of NaAsO<sub>2</sub> for 30min, after which, the cells were lysed and the RNAs were separated in a sucrose gradient according to the number of ribosomes bound to them (Figure 43 A). As expected, stress induction under these conditions led to an almost complete collapse of polysomes, with a corresponding increase in 80S monosomes (depicted by the blue line), as compared to the untreated control cells (depicted by the grey line). This shift is indicative of global translation arrest. An analytical measurement that can be calculated from the gradients is the monosome/polysome ratio. This coefficient aims to quantify the alterations in ribosome density on mRNAs on a global level. The ratio between the area of the monosome (80S) and the polysomes was calculated: a value above 1 is indicative of decreased ribosome density and typically indicates translation reduction, while a value below 1 is indicative of an increase in ribosome density per mRNA, which is observed when there is more translation or major ribosome stalling (Figure 43 B and C). After running the gradients, fractions containing the RNA separated according to their ribosomal density were collected and pooled together according to the scheme in Figure 43 (B). The free subunits (FS), the monosome, the 2-3 ribosomes, 4-6 ribosomes and 7 or more ribosomes per mRNA were collected separately, and RNA from these pools was purified. The addition of Spike ins and qRT-PCR allowed to determine the percentage of RNA amount per pooled fractions. The IC was used to calculate the overall levels of each mRNA. As observed before (Figure 42 D), there are no changes at the RNA level of these mRNAs upon stress induction (Figure 43 D). In striking contrast, the distribution of these mRNAs across the gradient fractions is profoundly altered by stress induction, reflecting changes in ribosome number per mRNA (Figure 43 E).

The hypersensitive RNAs, *Pabpc1*, *Rpl12* or *D3jfr1*, upon stress induction show, as expected, a shift in ribosomal density, where most of the mRNAs are either ribosome-bound free or bound to 1 ribosome (Figure 43 E). *Gapdh* was chosen as an additional RNA because this mRNA is known to be heavily translated and its translation not essential during global translation arrest [175], suggesting that upon stress induction one should expect a reduction in ribosome density on *Gapdh* mRNA. The distribution of ribosomes on *Gapdh* mRNAs is also decreased upon stress induction, showing that this RNA behaves similar to the “hypersensitive” ones in this assay. Importantly, its RNA levels did not change in the presence of NaAsO<sub>2</sub> (Figure 43 D). As expected, 18S rRNA under stress shifts out of the fractions with the most ribosomes bound, and thus serves as another positive control of global translation arrest. On the other hand, the previously identified “resistant” mRNAs like *Atf4*, *Atf5* and *Slc35a4* showed, when applying the polysome gradient method, still showed a pre-disposition towards fewer ribosomes translating their mRNA. Nevertheless, these mRNAs do show resistance to treatment, since the majority of these RNAs have between 2-6 ribosomes bound when comparing to the hypersensitive mRNAs or *Gapdh*.



**Figure 43. NaAsO<sub>2</sub> has a dramatic impact on translation and ribosome density in MN1 cells.**

Schematic of the *in vitro* experiment to test the effect of NaAsO<sub>2</sub> on translation. MN1 cells were treated with NaAsO<sub>2</sub>, followed by cell lysis. Ribosomes were separated on a sucrose gradient according to their density on mRNAs. (B) Fractions were pooled together as displayed. Fraction 1 contains only free subunits (FS); fraction 2 contains RNA with 1 ribosome bound, fraction 3 contains RNA with 2-3 ribosomes bound; fraction 4 contains RNA with 4-6 ribosomes bound and fraction 5 contains RNA with equal or more than 7 ribosomes bound. (C) Monosome to polysome ratio for untreated and treated cells with NaAsO<sub>2</sub>. n=3, error bars: ±SEM, t-test. (D) Input for the

### 3. Results

gradients: measurement of RNA levels after stress induction by qRT-PCR.  $n=2$ , error bars:  $\pm$  AD. (E) Percentage of RNA distribution across the gradients for untreated and treated cells.  $n=2$ , error bars:  $\pm$ AD. Spike ins were added for data normalization.

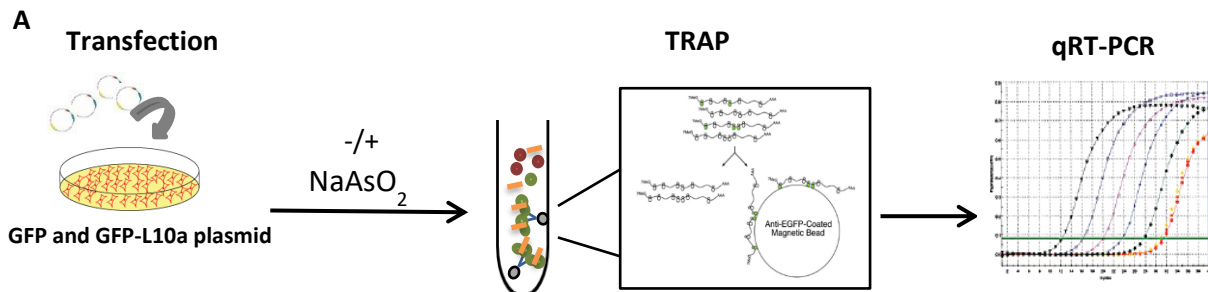
#### 3.9.3. Altered ribosome density is silent in TRAP

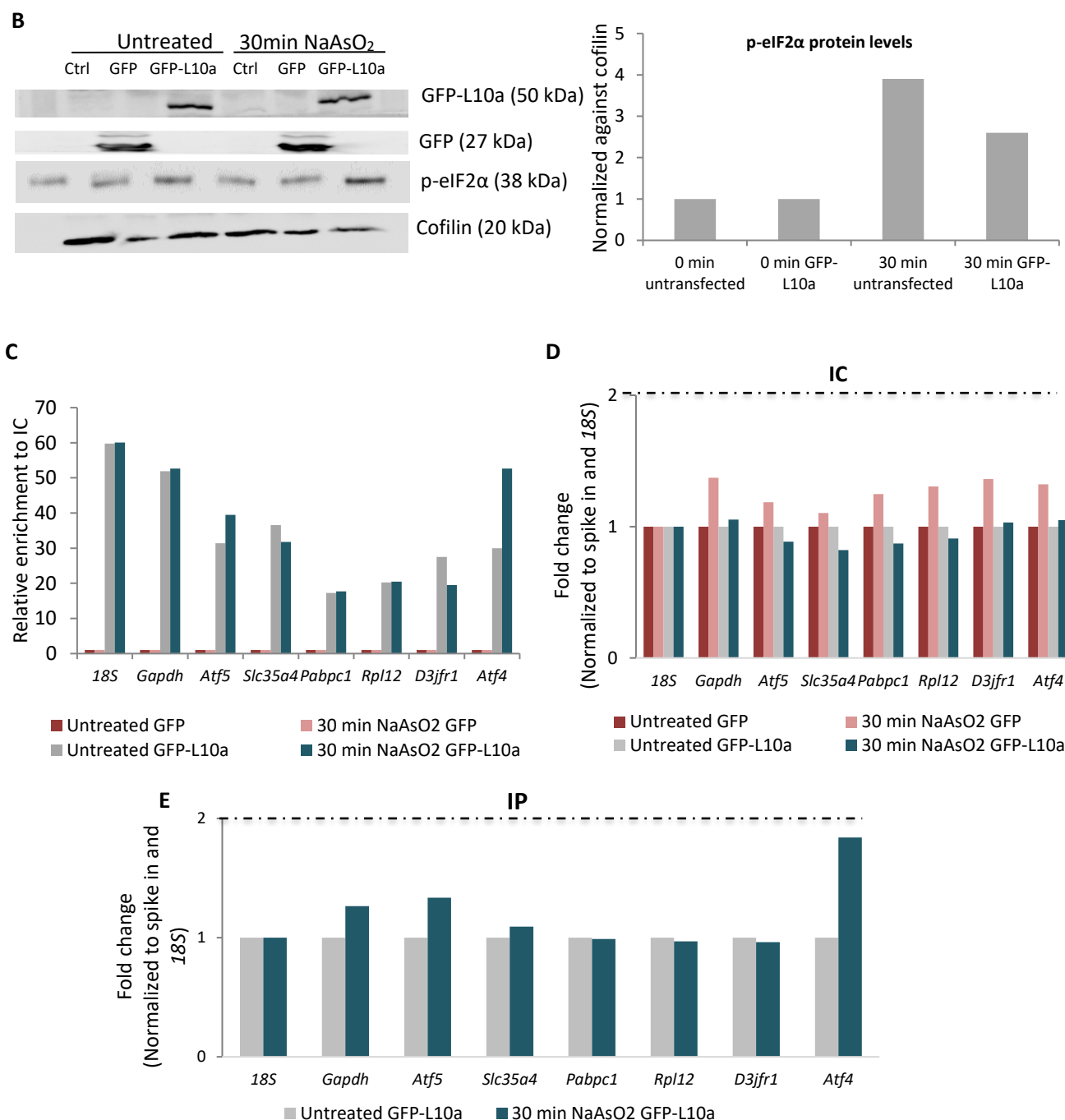
One reason to develop Gradient-TRAP is the assumption that TRAP alone cannot measure changes in ribosome density and thus fails to provide important information about an mRNA's translational status (Figure 41). While this is intuitive, it has not been explicitly tested. In order to determine whether this was indeed the case, MN1 cells were transfected with GFP and GFP-L10a plasmids followed by exposure to 30min of 80 $\mu$ M of NaAsO<sub>2</sub>. GFP plasmid was used as a control for GFP-L10a plasmid transfection. Untransfected MN1 cells were used as an additional control. After transfection, TRAP was performed and RNA levels determined by qRT-PCR (Figure 44 A).

I first verified transfection and the effectiveness of the stress treatment within this specific experiment using WB (Figure 44). MN1 cells were transfected efficiently with both plasmids and oxidative stress was also successfully induced, since the levels of p-eIF2 $\alpha$  protein were at least 3x higher than the respective controls (0min exposure to NaAsO<sub>2</sub>).

TRAP was performed with the GFP and GFP-L10a transfected samples. Here it is expected, that only the cells transfected with GFP-L10a plasmid will have RNA isolated via immunoprecipitation. To check for efficiency of TRAP in immunoprecipitating RNAs, the relative enrichment of the RNAs of interest was calculated. It is visible that in the presence of the GFP-L10a plasmid, there is enrichment of all the RNAs when comparing to the respective ICs. On the other hand, it is visible that for the samples containing the GFP plasmid there is no enrichment of the RNAs (Figure 44 C). When looking into the ICs from TRAP, there are no differences at the RNA levels as expected between untreated or 30min treated with NaAsO<sub>2</sub> at the RNA level (Figure 44 D). The TRAP IP (Figure 44 E) shows that TRAP alone cannot measure changes in ribosome density, failing to provide important information about an mRNA's translational status. This can be seen by the less than 2-fold change between RNA levels of untreated and treated samples.

To verify reproducibility of my results from this single experiment, Florian Stelzner, a Master's student in AG Duncan, performed this experiment three more times, following my protocol. Florian's results also clearly show that TRAP fails to detect major alterations in ribosome density, corroborating my preliminary observation reported here. These data were included in his Master's thesis for the Biology Department at the University of Hamburg.





**Figure 44. Evidence that TRAP fails to detect major changes in the number of ribosomes per mRNA.**

(A) Schematic of the experiment to test whether TRAP can detect changes in translation in the model. MN1 cells were transfected with GFP and GFP-L10a plasmids prior stress induction, followed by immunoprecipitated by TRAP. Spike ins were added for data normalization. (B) Confirmation of transfection of GFP and GFP-L10a plasmids and stress induction in MN1 cells by WB. p-eIF2α protein levels in untreated and treated samples n=1. (C) TRAP efficiency in immunoprecipitating RNAs. Relative enrichment in GFP-L10a vs. GFP control cells is shown. (D) Calculated fold change for both ICs and IPs. n=1.

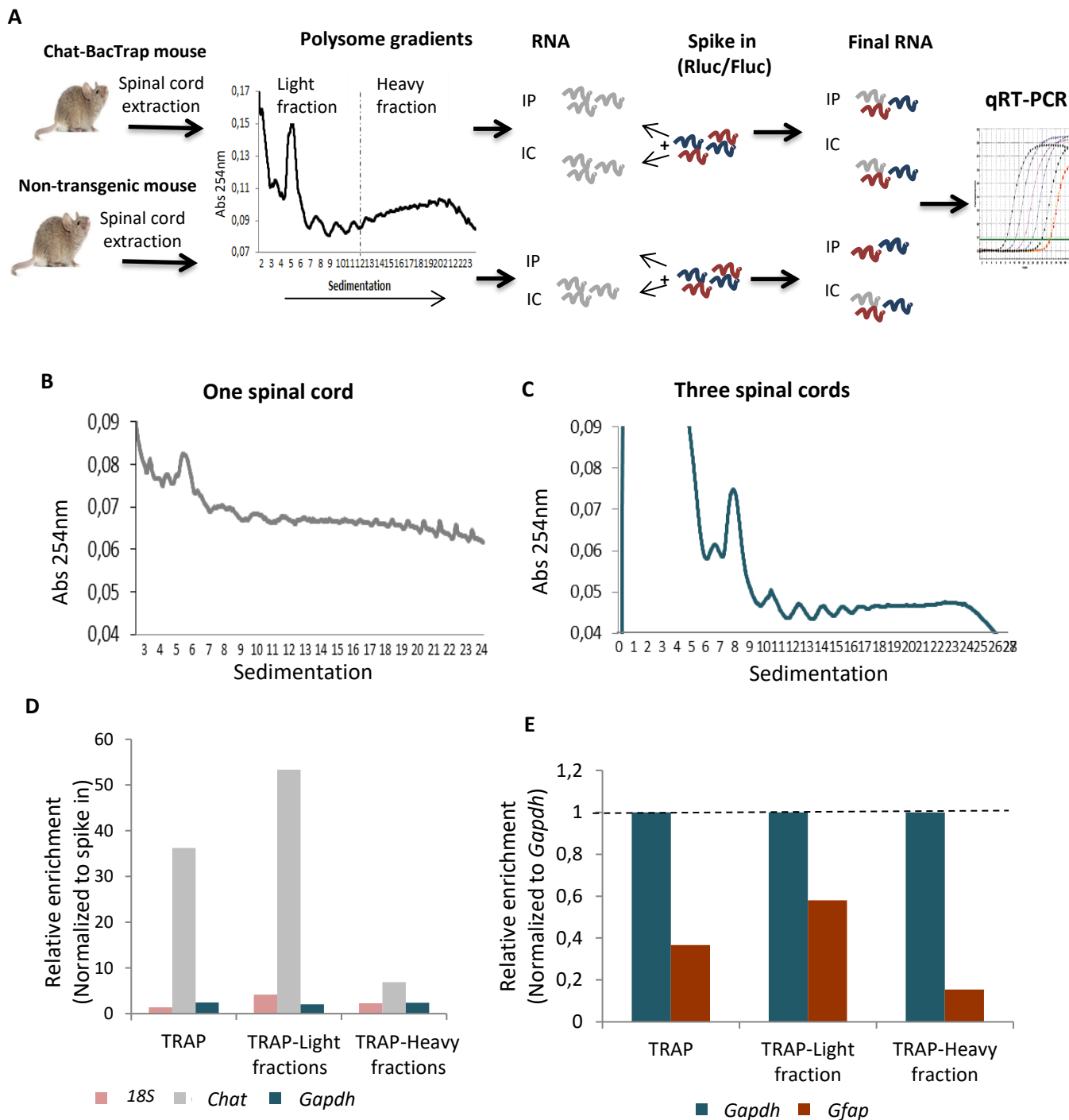
#### 3.9.4. Gradient-TRAP *in vivo* from mouse spinal cord

One of the aims of developing Gradient-TRAP is to be able to use this method in an *in vivo* context. For example to apply it to an ALS disease model in order to identify molecules whose RNA levels do not change, but whose translational status does, which might be relevant to disease. It is important to keep in mind that such mRNAs cannot be picked up by TRAP, thus information about potential disease drivers can be missing.

First, I set out to establish the conditions for spinal cord polysome gradients, combining our standard protocol with information from TRAP protocol. Spinal cords from mice were isolated and fractionated according to their ribosomal density. qRT-PCR was used to check if Gradient-TRAP is immunoprecipitating RNAs from MNs. Spike ins were used to calculate the enrichment over the WT animals (Figure 45 A). With the same rationale in mind as for TRAP, of using as few animals as possible, I started to try to obtain good polysome gradients with one single spinal cord (Figure 45 B). One spinal cord cannot produce good polysome gradients under our conditions, which has a direct impact on the pooling of the samples. Also, problems due to low RNA yield would make it difficult to use these types of samples for genome-wide applications, thus the developed protocol had to be optimized. Pooling of three spinal cords proved to give good polysome gradient profiles (Figure 45 C). From these gradients, samples were pooled according to the number of ribosomes sitting on the mRNA. Therefore, until four ribosomes bound on the mRNA, the samples were pooled and called “light fraction” and samples with equal or more than five ribosomes bound to the mRNA were pooled and denominated “heavy fraction”. RNA was isolated and purified via TRAP. Enrichment of MN-like genes and de-enrichment of non-MN-like genes were assessed to check whether the method worked (Figure 45 D and E). *Chat* mRNA is highly enriched in the light and heavy fractions and as well as in the designated TRAP samples, which is TRAP from non-fractionated samples. Enrichment of *Chat* mRNA is indicative of the presence of mRNAs from MNs. Furthermore, de-enrichment of *Gfap* mRNA confirms specificity for MNs mRNAs, since it is a marker for astrocytes.

These data provide a preliminary demonstration that it is possible to use Gradient-TRAP followed by qRT-PCR to purify MN ribosomes and associated mRNAs from specific regions of sucrose density gradients. For his Master’s Thesis, Florian Stelzner performed additional experiments with my guidance and using my protocol to determine whether Gradient-TRAP could be used from mouse tissue in a genome-wide configuration. He first performed with my help a pilot experiment for Gradient-TRAP to check if the method was reliable for deep sequencing. This indicated that RNA isolated via Gradient-TRAP can indeed be used for deep sequencing.





**Figure 45. Adapting Gradient-TRAP to *in vivo* material.**

(A) Spinal cords from non-transgenic mice and from Chat-BacTrap mice were extracted and loaded on sucrose gradients. Fractions containing the RNA were collected as displayed and the RNA was isolated via TRAP and analyzed via qRT-PCR. (B) Gradients from both non-transgenic mice and from Chat-BacTrap mice had to be optimized. Pooling of three spinal cords is necessary to give reliable polysomes, (B) and (C). (D) and (E) Controls of TRAP efficiency in immunoprecipitating RNAs. (D) Visible enrichment of *Chat*, *Gapdh* and *18S* and (E) de-enrichment of non-MN mRNA, *Gfap*. n=1.



## **4. Discussion and future perspectives**



## 4. Discussion and future perspectives

ALS is a devastating neurological disease that leads to progressive loss of MN function. It is almost always fatal and there is currently no curative treatment [22, 176, 177]. One reason for the lack of good therapeutic options is that the underlying disease-causing cellular and molecular mechanisms are not well understood.

In this present study I have identified proteins whose expression is altered in MNs as disease develops. Using mouse models of ALS caused by patient mutations in TDP-43, I applied a cell-selective genome-wide sequencing-based approach, TRAP, to identify a list of mRNAs with altered ribosome association in MNs as disease begins. Subsequently, I have validated changes in protein levels for some. Because the deregulation of these candidates correlates with disease onset, I reasoned that proteins with these properties are excellent candidates to function as “disease drivers”.

Further, I started the development of a method, Gradient-TRAP, that allows measuring changes in ribosomal density on mRNAs from specific cell types, *in vivo*. The method sought to enable the identification of mRNAs whose levels do not change, although their translational status does. I have established conditions to study in cell culture, whether Gradient-TRAP can detect ribosomal density changes. Moreover, I obtained evidence suggesting that TRAP alone fails to give insight into ribosomal density changes. Finally, I showed in a pilot experiment with qRT-PCR as readout, that Gradient-TRAP appears to function when performed from adult mouse spinal cord using an MN Chat-BacTrap line.

There are different interesting questions and directions to follow up on this study which I will address in this section.

### 4.1. Correct establishment of disease onset is necessary to identify potential disease drivers

Disease drivers are molecules whose deregulation leads to the development of a disease. Good candidates for disease drivers are proteins whose levels are specifically altered around the time when disease starts, since this correlation suggests a possible causal relationship. In order to identify this class of proteins, it was important to establish correctly the time of disease onset, so that the transition between pre-symptomatic and early symptomatic phases could be clearly defined.

The mouse lines used in this project were already well characterized in the literature [118, 160, 163]. However, to have the best chance to identify potential disease drivers, I decided it would be crucial to accurately determine disease onset by myself. This decision was influenced by:

- 1) The fact that it was reported that the A315T male mice develop symptoms earlier than the A315T female mice
- 2) The hTDP-43 mouse line was reported to not develop ALS like symptoms

3) hTDP-43 and A315T lines were crossed with the Chat-BacTrap mouse line and it was necessary to investigate whether the *Chat::L10a-GFP* transgene would also develop phenotypes on its own

4) The way the animals were housed and handled in the animal facility could also play a role in the development of the disease

For behavioral analysis, four independent tests - neurological score, peak body weight, rotarod and grip strength - were conducted to help identifying disease onset. All these tests were described previously in the literature as being the indicated ones to recognize ALS phenotypes in mice [166, 169, 178]. All the applied tests focus on different parameters that when analyzed all together allowed to establish a time line of when the animals started developing symptoms and which body parts were affected first. Based on these results it is possible to infer that motor deficits due to lack of coordination, strength and balance in the hindlimbs are the first phenotypes to be observed (rotarod data). On the other hand, lack of strength in the forelimbs seemed to be the last phenotype to be visible (grip strength data).

Further, it was reported that the A315T male and female mice develop ALS-like symptoms at different stages, with males showing motor coordination deficits around 71 days (~2.5 months) and females around 141 days (~ 4.5 months) of age [179]. Likewise, I decided to investigate whether the same phenomenon would still be observed under my behavioral conditions. From the very first day of tests, it was clear that there was a difference in performance between male and female mice. When summarizing all the tests together it is possible to conclude that the males develop ALS phenotypes earlier than the females. More specifically, according to the behavioral data the male mice show already motor deficits at 8 weeks of age, while the female mice started to manifest the same phenotypes only with 12 weeks of age.

One possible explanation for this difference in sexes could be the hTDP-43<sup>A315T</sup> protein expression levels. When I checked by WB the hTDP-43<sup>A315T</sup> protein levels from spinal cord lysates, I observed that the mutant male mice at 17 weeks seem to have higher expression levels when compared with the mutant female mice. However, at 9 weeks, when male mice are already symptomatic and female pre-symptomatic, there are no significant differences in mutant protein levels. This result seems to show that differences in transgene expression alone are not the reason why males develop disease phenotypes earlier than females.

Interestingly, the common ALS model expressing transgenic hSOD1<sup>G93A</sup> protein, also shows sex differences, with male mice developing the disease earlier. One study reported a role for estrogen in protecting females, suggesting that gonadal hormones can modify the course of disease [180]. A good starting point to determine what is causing the discrepancy in the A315T ALS mouse model would be to also look for a protective effect of estrogen. Similarly, in humans, men seem to have higher incidence of ALS than women at an early age [9]. Little is known about estrogen's protective effect on ALS. However, one study revealed a positive association between a longer reproductive time-span and susceptibility to ALS and survival rate, suggesting that longer exposure to female hormones could exert a neuroprotective effect on MNs [181]. Several other factors have been proposed to be at the origin of sex differences: different environmental toxins, different biological responses to exogenous toxins, possibly underlying

differences between the male and female nervous systems, differences in the role of gonadal hormones (estrogen, progesterone and testosterone) and different abilities to repair damage. However, more studies are necessary to shed light on the specific pathways and mechanisms by which these factors might be acting [9].

When establishing disease onset, it became clear that only in the A315T female cohort it is possible to define a clear transition between pre-symptomatic and early symptomatic phases of the disease for the time points that I tested, since the A315T male cohort already shows symptoms at 8 weeks of age. To sum up, two time points were defined based on the behavioral data from the mutant female mice. The first time point corresponds to pre-symptomatic phase (9 weeks) and the second time point to the early symptomatic phase (14 weeks) of the disease. These two time points were chosen to try to identify mRNAs and encoded proteins whose deregulation would correlate with disease onset, following the logic outlined previously, that molecules that behave in this way are good candidates to be disease drivers.

One important concern was whether the presence of the *Chat::L10a-GFP* transgene would cause phenotypes on its own or modify the phenotypes of the other lines. This concern arises mainly from the fact that the transgene integrates randomly into the mouse genome, which can disrupt a normal gene sequence. Such insertions can lead to unexpected phenotypes even in heterozygous mice because of haploinsufficiency [182]. Moreover, when crossing the Chat-BacTrap line with the both the hTDP-43 and A315T mouse lines, there is a possibility that the combination of these transgenes could generate new phenotypes, as e.g. faster progression of the disease, or perhaps mask some of the symptoms. Based on my behavioral and biochemical results, it is possible to conclude that the *Chat::L10a-GFP* transgene has no phenotypes on its own and no detectable influence on the development of the disease.

In my experiments, both female and male A315T mice show ALS phenotypes significantly earlier than what was reported in the literature [179]. This provides a clear demonstration of why a thorough behavioral analysis with our colony was important to define timepoints for the genome-wide TRAP experiments. These differences could be due to genetic background of the mice and/or to the different housing and handling conditions. As mentioned before, a previous behavioral study with this A315T line where the mutant animals had approximately 80% C57Bl/6J background found motor deficits beginning at around 2.5 months of age and this background appears to be more suitable for colony maintenance when comparing with animals with a congenic C57Bl6/J background [179]. Our lines were acquired from the Jackson Laboratory where this line was bred to be congenic on the C57Bl6/J background (i.e. >99%). In addition, our animals were crossed always with animals with a C57Bl6/J background. This could explain the earlier onset of the disease (detected the earliest in this project by behavioral testing at 2 months of age). Additionally, the housing and handling of the animals should be taken into consideration. Here, I can only speculate that this factor can play a role since I didn't perform a side by side comparison of behavior in animals under my conditions and the conditions from the study from Esmaili M. A. et al.; 2012 [179].

In the same study, the A315T line was also reported to develop gastric problems and thus the animals die of presumptive reduction in motility originating in the ileocaecal area of the gastrointestinal tract before full development of ALS-like symptoms [179]. Later it was published that when the A315T line is

fed with gel food it delays the development of gastric problems in both male and female mice, and consequently the premature death of these animals before full development of ALS-like symptoms [164]. Since I focused, on my thesis, on the pre-symptomatic and early symptomatic phases of the disease, the development of the gastric problems at this stage is inexistent or minimal, making it possible to use these animals as ALS mouse models to identify possible disease drivers without being necessary to feed the line with gel food.

To support the presence of phenotypes detected by the behavioral data, the NMJ of a mixed cohort of female and male mice was stained and the percentage of pathological endplates determined. Here the results showed that at 14 weeks of age, time point corresponding to early symptomatic phase, there is already visible de-ervation of the NMJ. This data supports the behavioral one, suggesting that the A315T mouse line develops ALS-like symptoms well in advance of any gastric problems and can be used to study early stages of ALS caused by mutant TDP-43.

To investigate whether the animals get sick due to an increase in protein levels, mutation or combination of both, I checked the total TDP-43 protein levels in the different lines. In order to conclude what is causing the sickness, a direct comparison of the TDP-43 levels in both the hTDP-43 and the A315T animals is necessary. In an ideal situation, both hTDP-43 and the A315T animals would have similar expression levels, allowing to conclude that the presence of the mutation would be causing the disease. However, my spinal cord quantification of total TDP-43 protein revealed that hTDP-43 and the A315T animals have different total levels of TDP-43 protein thus, making it impossible to infer whether it is simply TDP-43 overexpression or the presence of the mutation that is causing disease in these animals.

My data demonstrated that a careful behavioral analysis was important to establish disease onset and focus on the transition between pre-symptomatic and early symptomatic phases of the disease. Relying solely on previous studies does not confer an accurate establishment of the phases of the disease. Moreover, since only the female A315T mice showed clear pre-symptomatic and early symptomatic phases of the disease, this sex was chosen to be used in the downstream steps to identify potential disease drivers.

#### 4.2. Both up and downregulated mRNAs and proteins were identified in diseased MNs

##### 4.2.1. Purification of the motor neuronal translome from ALS models via TRAP

After successfully establishing disease onset and defining clear time points corresponding to pre- and early symptomatic phases of the disease in the female cohorts, the TRAP methodology was used in order to have access to the translome of MNs. One question was whether it would be possible to optimize the available TRAP protocol in the Duncan lab, in order to use fewer animals. The old protocol required the pooling of three upper parts of independent spinal cords, which mandates a large number of animals. I optimized the TRAP protocol, so that one spinal cord from one animal could be used instead



of three upper parts of three animals, reducing this way the number of mice used. The optimization of TRAP was first assessed with qRT-PCR as the readout method to verify whether mRNAs bound to GFP-tagged ribosomes were being immunoprecipitated and if these RNAs were from MNs. In order to verify these parameters, side by side TRAP from transgenic animals (Chat-BacTrap) versus non-transgenic animals (WT) was done and the relative enrichment of specific genes calculated relative to a spike-in control.

The presence of spike ins made it possible to compare the relative enrichment of RNAs from MNs of Chat-BacTrap animals versus WT, since it allows normalization to the WT sample where in a perfect experiment no RNA isolation via TRAP would be expected due to the lack of GFP-tagged ribosomes. It was checked by qRT-PCR that there is enrichment of a MN mRNA (*Chat*) and de-enrichment of non-MN mRNAs (*CNP1* and *GFAP*) and thus TRAP under these modified conditions was efficiently and specifically isolating RNA from MNs.

Next , I checked in a pilot experiment if this modified TRAP protocol was compatible with genome-wide high-throughput sequencing. This was important for several reasons. In particular, both TRAP and high-throughput sequencing are time-consuming and expensive methods. Moreover, I did not want to breed large cohorts of mice for these experiments without being confident that I could achieve the goal of analyzing the MN transcriptome with my TRAP protocol.

In the pilot experiment, the isolated RNA was first checked by qRT-PCR prior to high-throughput sequencing for enrichment of MN-like genes (*Chat* and *Mnx1*) and de-enrichment of non-MN-like genes (*Cnp1* and *Gfap*) to ensure the TRAP protocol worked in conferring cell specificity. Enrichment was also assessed after deep-sequencing and confirmed to be comparable to what was determined by qRT-PCR for these specific mRNAs. Additional MN-specific mRNAs were also enriched in the TRAP IP samples and many other non-MN mRNAs were significantly de-enriched, further supporting purification of MN ribosomes and associated mRNAs via the modified TRAP protocol. Additional standard metrics for quality of genome-wide dataset analyses were also performed. PCA and a hierarchical clustering dendrogram show whether similar samples would cluster together or apart. As expected 2 separate clusters, one for IP samples and another for IC samples were identified, showing a clear difference between MNs (IPs) and spinal cord material (ICs). These data confirm that the MN transcriptome can be successfully purified and characterized when the modified TRAP protocol that I developed is combined with deep sequencing.

To summarize, the refinement of TRAP was an important part of this project because it enabled me to reduce the number of animals used to one third of those required in the original protocol. In addition, it was important to check if those changes were compatible with a genome-wide approach before doing the real experiment to save animal lives and to reduce the time and cost of experiments.

### 4.2.2. Genotype rather than age is the major driver of mutant TDP-43's effect on the MN transcriptome

TRAP from Chat-BacTrap, Chat-BacTrap; hTDP-43 and Chat-BacTrap; A315T female animals at 9 weeks and 14 weeks was also successful, since enrichment of MN-like genes (*Chat* and *Mnx1*) and de-

enrichment of non-MN-like genes (*Cnp1* and *Gfap*) was observed. Moreover, PCA analysis revealed a clear separation of IP samples vs IC samples. However, no clear separation of samples based on time points was observed, indicating that age is not the major driver of the putative effects of hTDP-43<sup>A315T</sup> protein. Nevertheless, when analyzing the samples based on genotypes (dendrogram data), it is seen that often that samples with the same same genotype cluster together regardless of the time point, which leads to believe that genotype is driving most of the changes in the female MN transcriptome.

Since I am interested in the transition between pre-symptomatic and early symptomatic phases of the disease and these two phases are very close one another, one would not expect to see several differences in the dataset driven by these two time points. Whereas, in a later stage of the disease one would expected to find more differences driven by disease progression. By focusing on the early events of the disease, I am aiming to reduce the number of possible mRNAs that are deregulated but aren't disease drivers. As seen in my data, genotype is playing a role in sample clustering. This result is interesting because it shows that something is already different in these animals prior the development of phenotypes. One could speculate that such differences are already present upon birth. Nevertheless, a similar side by side study would have to be performed with new born animals to check if these differences are present or not. I speculate that a compensatory mechanism allows the "normal" function of the system until a certain point where a designated threshold is met, after which phenotypes start to develop.

##### 4.2.3. A short list of deregulated genes was generated

To identify potential disease drivers, the first strategy adopted was to compare the Chat-BacTrap; A315T at 9 weeks with the Chat-BacTrap; A315T at 14 weeks. However, from this comparison the four candidates that emerged did not seem to be correlating with disease, because even though there was a significant difference between 9 weeks to 14 weeks in the A315T mutant samples, these samples did not show significantly different RNA expression levels relative to both controls. A different strategy was then adopted. This new approach consisted in focusing first on the time point 14 weeks and within this time point to compare the Chat-BT; A315T group with the Chat-BacTrap group and determine which candidates are exclusively up or down for the Chat-BT; A315T group. The same principal was also applied to the comparison between Chat-BT; A315T group and the Chat-BT; hTDP-43 group. A final list was made after both lists were crossed to identify common candidates that where simultaneously up- or downregulated in both lists (appendix 9.3). The final generated lists of up- and downregulated candidates were narrowed down to select candidates that best would fit in the definition of disease drivers. For this task, the sequencing profile for each candidate identified was carefully examined to see how its profile for the time point 9 weeks appeared in all the genotypes and how this compared to 14 weeks. In other words, the pre-symptomatic time point was considered as a point of reference to look for mRNAs that show a tendency to show either up- or down-regulation specifically in the Chat-BT; A315T group during the transition from 9 weeks to 14 weeks. By applying these criteria, I believe to have increased the chances of finding regulatory changes that have a good chance to be disease drivers. The final list was compiled of four upregulated candidates and two downregulated candidates.

### 4.3. Validation of altered regulation of mRNAs and/or proteins

Genome-wide studies routinely generate false positives. Therefore, it is necessary to validate the data through different methods, ideally using independent cohorts of animals. In the case of this project I decided to validate the identified candidates by applying two different methods: qRT-PCR and IHC. Spinal cords from independent cohorts of animals were collected at time points corresponding to pre-symptomatic and early symptomatic phases of the disease for both validation methods.

#### 4.3.1. Validation of altered mRNA levels in an independent TRAP cohort

To measure the RNA levels, TRAP followed by qRT-PCR was used as the readout method. This method examines whether if the altered signal in TRAP-IPs from disease MNs observed by high-throughput sequencing are indeed deregulated. For the time point corresponding to the early symptomatic phase, *Tex26* and *Plekhhb1* could be validated as up- and downregulated candidates, respectively. Out of the six candidates, I obtained data for four. The lack of data for all the candidates arises from the low RNA yield from TRAP, which seems not to be sufficient for reliable detection of many mRNAs in qRT-PCR. This problem was bypassed with genome-wide sequencing due to an extra amplification step of the generated library (complementary DNA (cDNA)), making it possible to detect more candidates. A possible solution to verify the validity of all the candidates would be to do also an extra step of amplification prior to qRT-PCR. However, the amplification kits that might enable this are also very expensive. Ultimately, determining whether the observed altered mRNA regulation affects protein levels in MNs is of greater interest, and I decided to focus on protein level analysis, rather than pursue further validation at the RNA level. A detailed discussion about the validation at the RNA level of the four candidates for which data could be obtained appears below. Data referent to pre-symptomatic phase can be found in appendix 9.6.

##### 4.3.1.1. *Tex26* mRNA is upregulated in MNs at disease onset in an independent TRAP cohort

For the time point corresponding to the early symptomatic phase, *Tex26* and *Plekhhb1* could be validated as up- and downregulated candidates, respectively. *Tex26* shows a significantly higher RNA expression levels in Chat-BT; A315T mutant mice relative to the Chat-BacTrap mice in the TRAP IP samples. However, between the Chat-BT; A315T mice and the Chat-BT; hTDP-43 mice there is only a trend of *Tex26* RNA in the Chat-BT; A315T, to be upregulated. For this validation method only three replicates were used, while for the deep-sequencing five to six replicates were used. An increase in the number of replicates might potentially give more biological meaningful data.

##### 4.3.1.2. *Plekhhb1* mRNA is downregulated in MNs at disease onset in an independent TRAP cohort

*Plekhhb1* emerged as a downregulated candidate in the dataset and the same pattern was detected in the TRAP validation experiment. Unlike *Tex26*, which is not abundant in the CNS, the abundance of *Plekhhb1*

in the CNS facilitates its detection by qRT-PCR. In line with this, the RNA levels of *Plekhhb1* in the IPs (MNs) and ICs (spinal cord) were measured to avoid false positives. This type of result can be a problem with downregulated candidates with higher expression levels in spinal cord, which is the case for *Plekhhb1*. In this case, the IP can fail to immunoprecipitate exclusively GFP-tagged ribosomes bound to RNA from MNs, bringing with it RNAs from other cell types. In both the original sequencing data and the qRT-PCR data from the TRAP experiment with an independent cohort, *Plekhhb1* spinal cord RNA levels do not change significantly between genotypes, supporting the result that *Plekhhb1* is specifically downregulated in spinal cord MNs.

##### 4.3.1.3. *Syngn4* mRNA might be upregulated in MNs at disease onset in an independent TRAP cohort

*Syngn4*, identified as an upregulated candidate, could also be tested by qRT-PCR. This candidate shows a strong trend towards up-regulation between its RNA levels in the Chat-BT; A315T mice and Chat-BacTrap mice. Unfortunately, due to the wide spread of the data of the RNA levels of the Chat-BT; hTDP-43 mice it is not possible to compare it with the RNA data levels from the Chat-BT; A315T mice. More meaningful data could be achieved by increasing the number of replicates used.

##### 4.3.1.4 *Tia1* mRNA 3' end processing might be altered in MNs by hTDP-43<sup>A315T</sup> expression

*Tia1* was identified as a downregulated candidate. When tested by qRT-PCR, there were no differences among genotypes at 14 weeks of age when primers against the coding sequence of the gene were used. This suggested that *Tia1* mRNA might simply be a false positive. However, since mutations in the *TIA1* gene have been directly linked to ALS, I considered an alternative explanation for apparent downregulation in the sequencing data that would not be observed when using coding sequence primers in qRT-PCR. When looking into the products of the *Tia1* gene, it was observed that this gene can code for multiple mRNA isoforms (Information about *Tia1* gene products was consulted on ensembl website (<https://www.ensembl.org/index.html>), appendix 9.7). One mRNA isoform has a much longer 3'UTR than the others, accounting for ~2/3 of the mRNA sequence. Thus one hypothesis that could explain the significantly reduced *Tia1* signal in the sequencing data, but no difference by qRT-PCR with coding sequence primers would be a significant reduction in the levels of the long isoform, due to alternative use of the proximal poly(A) site when mutant TDP-43 protein is present. The underlying premise based on the fact that the genome-wide sequencing method maps short sequencing reads derived from the mRNAs to the entire sequence of the *Tia1* gene. Thus, if there were a significant reduction in the presence of the long 3'UTR isoform, but not change in the coding sequence primer reads, this could lead to this being identified as "downregulated" in differential expression analysis. However, since the qRT-PCR assay uses primers targeting the coding sequence of *Tia1*, it would show no difference, since it can only measure effects on the coding sequence amplicon examined and it cannot provide information about altered 3' end processing.

In a preliminary test of this hypothesis, qRT-PCR was repeated with primers specifically recognizing the long 3'UTR isoform. This revealed a trend towards reduction of this RNA in spinal cord MNs of the Chat-BT; A315T mutant mice relative to the Chat-BacTrap control at 14 weeks. However, a similar trend was

also observed for Chat-BT; hTDP-43 mice. This comparison is important because lack of a trend or significance indicates that the change is not correlated with disease onset and therefore its deregulation at this stage is unlikely to be sufficient for disease. The quality of these data is, regrettably, not the best. These experiments need to be repeated with an increased number of replicates and should be examined by independent methods (e.g. quantitative FISH with isoform-specific probes). Nevertheless, I decided to include these preliminary data in this thesis, since they establish an interesting hypothesis that could be tested carefully through future experiments.

Assuming it is occurring, what might be the potential biological significance of altered *Tia1* 3'end processing? The different mRNA isoforms actually encode TIA1 protein isoforms that differ at the C-terminus, suggesting the potential for regulation of TIA1 protein function via alternative polyadenylation. TIA1 is an RNA-binding protein and a major component of stress granules, which have been suggested to be important in ALS etiology. Indeed, *TIA1* mutations in patients affect SG dynamics. In live cells, TIA1 mutations delayed SG disassembly and promoted the accumulation of non-dynamic SGs that harbored TDP-43. Furthermore, TDP-43 in SGs became less mobile and insoluble. The identification of TIA1 mutations in ALS/FTD reinforces the importance of RNA metabolism and SG dynamics in ALS/FTD pathogenesis [171]. Importantly, the alternative mRNA and protein isoforms of mouse *Tia1* appear to be conserved in humans. Thus, if this hypothesis proves to be true, the same phenomenon could conceivably be happening with human *TIA1* mRNA in MNs of ALS patients when TDP-43 is overexpressed and/or TDP-43 mutations are present.

An important point that could also make difficult the overall achievement of significance in the validation by qRT-PCR is the method used to normalize the data. In the deep-sequencing the normalized expression values were calculated over the total number of gene counts. By qRT-PCR the normalization was done against the expression level of a house keeping gene, *Gapdh*. This difference in normalization could also explain why TIA1 and other mRNAs didn't validate.

Overall, the validation data by qRT-PCR didn't reveal clear results for all the candidates. Nevertheless, it was possible to get a feeling for what needs to be improved if this technique is to be used in this context again: 1) a higher number of replicates and 2) an extra amplification step prior to qRT-PCR, analogous to the procedure used for high-throughput sequencing.

### 4.3.2. Validation of altered protein levels in MNs at disease onset

The second method used to validate the potential disease drivers was IHC. With IHC I aimed to quantify the corresponding protein levels in MNs. The underlying hypothesis is that the changes in ribosome association of specific mRNAs within MNs observed in TRAP will lead to corresponding changes in protein levels in MNs. Ideally, they would also correlate with disease onset, consistent with the TRAP results and original goal of the TRAP experiments.

I examined the proteins encoded by two mRNAs that were tested in the independent TRAP experiment described above: PLEKHB1 and SYNGR4. These two proteins were chosen in order to directly compare the analysis of protein levels to the TRAP-qRT-PCR results and because commercially antibodies were

available for them. Two different ALS mouse models caused by mutant TDP-43 were used for these experiments. First, I examined levels of these proteins by IHC in spinal MNs for both the A315T line and respective controls. I also tested whether protein levels would change in a completely independent model of ALS caused by expressing hTDP-43 with a different patient mutation (hTDP-43<sup>Q331K</sup>). The goal in this case was to determine whether any effects on protein levels in MNs would be specific to ALS caused by the A315T mutation or reflect a more general deregulation in ALS caused by TDP-43. The identification of common effects caused by different mutations in TDP-43 allows hypothesizing about common affected downstream pathways which would make it easier to find a possible target for therapeutics.












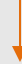
Spinal cord sections of the lumbar area were co-stained with antibodies recognizing either neuronal markers, (ChAT or NeuN), as well as antibodies to the candidates of interest. Since I was interested in checking the protein levels in MNs, it is necessary to distinguish these cells from the other cell types. Both ChAT and NeuN stain the cell body which allowed me to quantify the protein levels only in the cell body. Since none of my candidates considered for validation has been described in the literature to be present in cell processes, I decided to investigate first whether the presence of these proteins is altered in the cell body. An interesting follow up experiment would indeed be, to check how these protein levels change in other parts of MNs, namely in processes such as axons and dendrites.

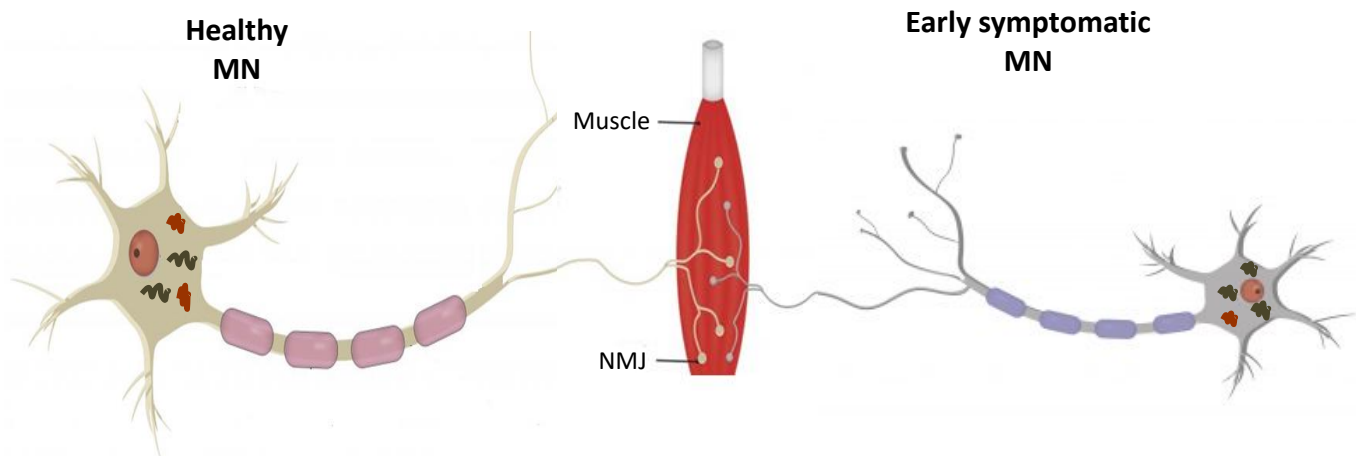
Through this method, I validated TDP-43-induced changes for two candidates at the protein level, PLEKHB1 and SYNGR4, which were down- and upregulated, respectively. Both candidates were deregulated in both the hTDP-43<sup>A315T</sup> and in the hTDP-43<sup>Q331K</sup> mutant lines in the early symptomatic phase which allows to conclude that the effects of hTDP-43 expression are not mutant specific. However, based on the protein levels, these candidates both have the potential to be disease drivers since in the hTDP-43<sup>A315T</sup> and in the hTDP-43<sup>Q331K</sup> mutant animals there is a significant alteration of the levels of both PLEKHB1 and SYNGR4 to both of the controls (WT and hTDP-43 animals).

TRAP followed by qRT-PCR is, as mentioned before, a time and money consuming method and as seen by the data presented are not very reliable. One alternative to this method would be to do dual in situ hybridization-IHC (ISH-IHC). This technique has been recently developed and aims to measure both the RNA levels of molecules of interest and the corresponding protein levels at the same time [183]. This technique would in this case, replace both the need to perform TRAP followed by qRT-PCR and IHC as the readout, since motor neuronal protein markers would be used to select MNs and respective mRNAs. Moreover, the number of animals used would also be reduced.



To sum up, I have applied the TRAP methodology to MNs of the mouse spinal cord at time points of pre-symptomatic and early symptomatic phases of the disease. Within the scope of this study, I have identified several mRNAs whose ribosome-associated levels are altered in MNs when the hTDP-43<sup>A315T</sup> protein is expressed. Moreover, I have validated two at the protein level, PLEKHB1 and SYNGR4 (Table 4; Figure 46).

Table 4. Overview of the validation stage of the candidates by qRT-PCR and IHC.

RNA deep-sequencing		qRT-PCR	IHC	
Candidate	Type of candidate	A315T Symptomatic	A315T Symptomatic	Q331K Symptomatic
PLEKHB1 	Downregulated			
SYNGR4 	Upregulated	Tendency 		
TEX26 	Upregulated		?	?
TIA1 	Downregulated	Tendency 	?	?



**Figure 46. Identified changes in MNs when hTDP-43<sup>A315T</sup> and hTDP-43<sup>Q331K</sup> proteins are present.**

This study has identified two candidates to be “disease drivers” in ALS caused by mutant TDP-43: PLEKHB1 and SYNGR4. Ribosome association of the mRNAs encoding these proteins, as well as levels of the proteins themselves are altered in MN by expression of the hTDP-43<sup>A315T</sup> mutant protein. Importantly, these changes were not observed in mice expressing WT hTDP-43 at levels insufficient to cause disease. Moreover, they correlate with disease onset and were also not observed in pre-symptomatic MNs of the mutant animals. Altered protein levels in MNs during early disease were also observed in another mouse model of ALS caused by a different patient allele of TDP-43, supporting a general role in ALS. Moreover, this study also demonstrated at during early symptomatic phase of the disease it is already visible a mild denervation of the NMJ. Figure Adapted from: <https://www.neura.edu.au/>. Legend: PLEKHB1 protein: ; SYNGR4 protein: .

### 4.4. No common potential disease drivers were identified in SOD1 and TDP-43 dataset

Recent human genetic studies have highlighted the concept that ALS pathogenesis may involve several different molecular triggers that ultimately lead to an apparently similar disease phenotype [22]. This raises the question of whether these pathways converge at some point to cause disease or are distinct at the molecular level. Answering this question has major implications for treatment, since common downstream disease-causing molecules would be ideal therapeutic targets. Conversely, if specific forms of ALS are fundamentally different, tailored therapies for the specific disease categories will need to be developed and the relevant specific targets will need to be delineated.

Although TDP-43 aggregates are detected in most sALS cases, they are typically not detected in SOD1-related disease [33], suggesting that, results from the SOD1 model might only be translatable for patients with *SOD1* mutations. While SOD1-mediated disease is thought to result primarily from increased oxidative stress, mitochondrial dysfunction, excitotoxicity, and neuroinflammation [184], it remains unclear the extent to which these factors contribute to TDP-43-related disease. In sum, the current view of many researchers is that SOD1 may actually represent a special form of ALS with a distinct pathological course, an idea consistent with clinical heterogeneity in the disease course [22]. Determining what differentiates or unites these diseases on the molecular level requires analyzing how the pattern of expressed proteins changes specifically in MNs as disease progresses in each model. Therefore, as a starting point, I have compared the generated list from my dataset with a generated list from Sun S. et al.; 2015. Sun S. et al.; 2015 generated via the same methodology -TRAP- at the time point corresponding to symptomatic phase, a list of MN deregulated candidates that emerged from the comparison of animals with the SOD1<sup>G37R</sup> mutation versus non-transgenic control animals.

When comparing both lists, without specifically looking into up and downregulated candidates, I found 21 common genes whose deregulation is present in both ALS causing mutations. However, when I examined whether those genes would have the same pattern of deregulation, I observed that all the 21 candidates actually have opposite patterns of deregulation. For example, *Car2* is downregulated in my hTDP-43<sup>A315T</sup> MN-TRAP dataset, while in the hSOD1<sup>G37R</sup> dataset it appears to be upregulated.

The first conclusion from this result is the fact that either with an up- or downregulated mechanism these molecules, if validated, seem to be involved in ALS pathology, since in both datasets they are exclusively deregulated in the mutant animals. Whether these alterations are causing ALS or are a consequence of upstream altered pathways remains to be determined. However, interestingly, none of these molecules are part of my short list of candidates that I believe have the best chance to be disease drivers. In line with this, I hypothesize that these molecules could be altered due to upstream events in their pathways, rather than being disease drivers themselves. Another idea supporting this claim is the fact that in the Sun S. et al.; 2015 study, only disease onset animals were used. In my study I used pre-symptomatic and early symptomatic animals, with the intention that it would enable me to find potential disease drivers that show deregulation specifically during the transition from the pre-symptomatic to early symptomatic phase.

Interesting as these observations may be, this analysis has a number of caveats that make it challenging to interpret with confidence, for example:



- 1) The experiments took place in different laboratories and were executed by different people
- 2) The animals were housed and handled by different people and in different environments
- 3) The protocols for TRAP, cDNA library preparation, and sequencing were not exactly the same
- 4) The sequencing data analysis and mining pipeline though potentially similar, is not exactly the same
- 5) Possible different genetic backgrounds of the animals used (in this study animals were in a C57Bl6/J genetic background and in Sun S. et al.; 2015 in an unspecified C57BL/6 genetic background)

In order to have a more extensive and accurate knowledge of whether there are common molecular pathways caused by different ALS mutations, a side by side TRAP experiments from MNs of both hSOD1<sup>G37R</sup> and hTDP-43<sup>A315T</sup> mouse models of ALS at time points corresponding to pre-symptomatic and to early symptomatic phase should be performed.

Another key aspect of the study of Sun S. et al.; 2015 is the fact that not only the transcriptome from MNs were analyzed, but also the one from astrocytes and oligodendrocytes. One important conclusion was that initial damage occurs in MNs at disease onset. Deep-sequencing data from MNs revealed alterations in ER stress, synapses and metabolic abnormalities. While very few RNA changes were detected in astrocytes at early stages. These changes are involved in inflammation and metabolism, while oligodendrocytes dysregulation occurs only after disease initiation and involves alterations in myelination and lipid signaling pathways [173]. Thus, the data of Sun et al. show that in an SOD1 mutant mouse model of ALS, the disease is initially MN specific, supporting the MN focus study of this thesis.

### 4.5. Potential role of validated targets in ALS pathology

Six possible candidates were isolated due to their RNA expression level profiles. Within the scope of this thesis, four candidates were studied deeper to understand whether they could possibly be disease drivers. Despite some have validated as having a potential role in causing disease, it is important to understand how these molecules are connected to ALS by identifying the underlying mechanisms or pathways leading to it. In order to create a putative model of how these deregulated molecules could possibly disrupt cell homeostasis, it is necessary to first know which type of molecules they are and which role they play in the cell.

#### 4.5.1. PLEKHB1 is involved in the recruitment of membrane proteins

PLEKHB1, also known as PKL1, eectin-1 or PHR1, was first described in the literature in 1999 as being preferentially expressed in human and mouse retina and brain. In retina, it was found in the outer segment of both cones and rods, where it is an integral membrane protein [185]. This anchoring property is due to its C-terminus, which contains a transmembrane domain. Its N-terminus contains a pleckstrin homology domain (PHD). These domains have been best described for their ability to bind phosphoinositides with high affinity and specificity, although recently it was demonstrated that less than

10% of all PH domains share this property [186]. In addition to photoreceptors, specific PLEKHB1 splicing isoforms are also found in olfactory receptor neurons, vestibular and cochlear hair cells and in cells with a possible sensory function, including peripheral retinal ganglion cells, cochlear interdental cells, and neurons of the circumventricular organ. Despite its presence in sensory cells, mice lacking PLEKHB1 do not have sensory deficits [187]. PLEKHB1 interacts directly with myosin 1c and VIIa tails, which are suggested to play a role in anchoring the actin cytoskeleton to the plasma membrane of the vestibular and cochlear sensory cells [188]. Another study also revealed through ISH that PLEKHB1 expression was prominent in photoreceptors, oligodendrocytes, and Schwann cells, suggesting that PLEKHB1 is a mediator of post-Golgi protein trafficking in cells that produce large amounts of membrane. PLEKHB1 also seems to be involved in ciliogenesis. Its gene expression increased when rat tracheal epithelial cells were stimulated. Also, RNA blotting showed high expression levels in the brain and lower levels in the liver, spleen, trachea, and lung [189]. The PHD of this protein was also found to interact with CVB3 VP1, a major structural protein of coxsackievirus B3 (CVB3), known to cause CNS diseases including aseptic meningitis and encephalitis [190].

Despite being found in cells of the nervous system, nothing is known about the role of this protein in MNs or its connection to ALS. However, since PLEKHB1 was showed to interact directly with myosins and to play a role in post-Golgi protein trafficking mediation, I can hypothesize about a putative role of PLEKHB1 in altered protein trafficking which leads to ALS pathology.

The trans-Golgi network (TGN) is the major sorting station for newly synthesized proteins and lipids in the biosynthetic pathway. From there a number of different constitutive and regulated routes emerge, that deliver proteins either to the cell surface or to a number of compartments of the endosomal system [191]. These transport events are facilitated by cytoskeletal elements, particularly microtubules and their associated motor proteins (myosins, kinesins and dyneins) [192]. Based on link between motor proteins and post-Golgi protein trafficking, I speculate that PLEKHB1's role in post-Golgi protein trafficking requires its interection with myosin proteins. Myosins are motor proteins that bind to actin and hydrolyse ATP to generate force and movement along actin filaments [193], playing significant roles in cargo transport within neurons and other cell types [194, 195], muscle contraction, cytokinesis, membrane trafficking, and signal transduction [196]. I postulate that in the presence of mutant hTDP-43<sup>A315T</sup> protein, reduced levels of PLEKHB1 might impair myosin functions in the cell. One function that could easily be affected by defects in the interaction between myosins and PLEKHB1 is axonal transport. In fact, impairment of cargo transport in axons has been observed in ALS pathology. Here, SOD1<sup>G93A</sup> transgenic mice showed defects in both anterograde and retrograde axonal transport [197] and impairment of axonal retrograde transport is one of the earliest axonal pathologies in SOD1<sup>G93A</sup> transgenic mice, suggesting that deficits in axonal transport are a key pathogenic event in ALS [198]. To prove this hypothesis, new experiments targeting myosin in MNs would need to be done. Specifically, to first check if a direct interaction between myosins and PLEKHB1 exists in MNs through *in vitro* co-immunoprecipitation of proteins [199], using MN like cells, e.g. MN1, or *in vivo* from isolated MNs [200].

Taken together, the data presented in this thesis for PLEKHB1 suggest that a lack of increase in its levels could be a factor that drives disease onset. Nevertheless, additional experiments need to be done to

verify if this candidate is indeed driving the disease and second to study how this protein can be targeted for therapeutic purposes. Since PLEKHB1 levels are decreased when mutant TDP-43 protein is present, one experiment that could be done to check if PLEKHB1 is driving the disease would be to reduce the levels of PLEKHB1 in WT animals and to check whether with time they would develop at least a subset of disease symptoms. To achieve reduction of PLEKHB1, one could generate a *Plekhhb1* KO mouse and study it in the homozygous and/or heterozygous state. In fact, a *Plekhhb1* KO mouse of this protein was already generated but it was studied in the context of the sensory system. The KO animals were viable and with no abnormalities detected in growth and behavior [187]. According to these data, reduction of PLEKHB1 protein levels alone does not appear to be sufficient to cause ALS-like symptoms in mice (the mice in this study were analyzed at 6 months and 1 year). This finding is consistent with no mutations in *PLEKHB1* having been identified in ALS genetic studies to date. It is also perhaps not surprising, given that ALS, like cancer and most neurodegenerative diseases is believed to require “multiple hits” before disease is manifest. Assuming lowered levels of PLEKHB1 actually do drive disease, presumably effects of mutant TDP-43 on at least one other mRNA are important for this effect.

Arguably the more interesting experiment would be to check whether reduced PLEKHB1 is necessary for disease. In this case the goal would be to increase the levels of PLEKHB1 in the hTDP-43<sup>A315T</sup> mutant mice and determine whether this can delay disease onset and/or slow symptom progression. Ideally, the manipulation would restore WT protein levels in MNs of mutant mice. Both behavioral assays and pathological readouts (e.g. NMJ denervation) would be used to monitor disease. Several approaches could be used to increase expression of PLEKHB1 by genetic manipulation. Classical transgenic lines could be generated, although expression can be variable. Alternatively, a knockin (KI) by inserting an additional copy of the *PLEKHB1* gene in the *Rosa 26* locus, could be pursued [201]. This could be combined with loxP sites that would render expression sensitive to Cre in order to give additional control over expression (e.g. via Chat-Cre for MN-specific expression in spinal cord). Finally, delivery of rAAVs containing PLEKHB1 in spinal cord could be performed. This would enable analysis of whether restoring PLEKHB1 protein levels after symptom onset can have any therapeutic benefit. Obviously, answering this question would be important if PLEKHB1 is to have translational potential in a clinical setting for sALS, since these patients, by definition, cannot be detected in the pre-symptomatic phase.

#### 4.5.2. SYNGR4 might be involved in protein transport

SYNGR4 is a member of the synaptogyrin family. This family is characterized by four isoforms that contain four transmembrane regions with a tyrosine-phosphorylated tail: two neuronal (SYNGR1 and 3), one ubiquitous (SYNGR2/cellugyrin) and one with unknown functions/properties (SYNGR4). SYNGR1 and 3 are abundant in SVs and are believed to be involved in various aspects of the SV cycle, including vesicle biogenesis, exocytosis, endocytosis, recycling, and neurotransmission [202-204]. These isoforms are encoded by multigene classes in mammals and evolutionarily conserved [205]. SYNGR2, on the other hand, is found in all tissues, apart from the brain. It has been proposed to be a component of synaptic-like microvesicles (SLMVs), where its presence is critical for SLMV formation [202, 206-208].

SYNGR2 also been reported to be an enhancer in viral infection. The study of bunyavirus infection in mammalian cells demonstrated that SYNGR2 interacts with viral nonstructural proteins. Together, they are transported into inclusion bodies during infection. Silencing of SYNGR2 expression is important to viral replication since it reduced inclusion body formation and decreased virus titers [204]. Moreover, SYNGR2 is suggested to be a component of ubiquitous intracellular transport vesicles that mediate protein transport between sorting endosomes and the endocytic recycling compartment and/or TGN. Further, Chapel A., et al.; 2013, suggested that this cellular protein is a lysosomal transporter protein [209], supporting that SYNGR2 may exist in cytoplasmic vesicles.

Very little is known about SYNGR4. The preliminary data generated in this thesis, aiming to investigate if this protein would have similar functions to SYNGR1 and 3, revealed that this protein is most likely not associated to SVs, since it failed to colocalize with Synaptophysin, a classical marker for SVs on the pre-synaptic side. Thus, based on these data it is here hypothesized that this protein could have similar functions to SYNGR2. Indeed, SYNGR4 has been described by the “Human Protein Atlas” (<https://www.proteinatlas.org/ENSG00000105467-SYNGR4/cell>) to localize at the Golgi apparatus. However, information about its function and its link to ALS remain elusive.

In the dataset generated in this thesis, SYNGR4 was identified as an upregulated candidate. If SYNGR4 is presumably upregulated, one possible way to study whether this protein is driving the disease would be to reduce partially or completely its levels in MNs of diseased animals and observe if ALS-like phenotypes would develop. Up to date, no animals with partially or full abolishment of SYNGR4 were made or characterized. This lack of information makes it difficult to know if this protein is essential to survival and development of the animals. A proposed experiment to reduce the levels of SYNGR4 is to take advantage of the CRISPR/CAS9-mediated gene editing methodology. The generated animals would then be crossed with TDP-43 ALS mouse lines (hTDP-43 over expressing and A315T line) and a comprehensive behavioral study would need to take place. Ideally, the same behavioral tests described in this thesis would be applied. Pathological readouts in MNs and NMJs could also be examined.

Likewise, experiments to determine its function would also shed light about which pathways could be targeted for therapeutics. A good starting point would be to check whether this protein has similar functions to SYNGR2 and to check whether it is present at the Golgi apparatus. Co-localization experiments by IHC could be a good starting point to check for common functions. Moreover, based on my data from IHC, there seems to be a concentration of this protein more in the membrane area of the MNs rather than the cytoplasm suggesting a possible role in the membrane.

##### 4.5.3. TEX26's function is unknown

TEX26 was identified as an upregulated candidate. Unfortunately, there are no studies made on this protein yet and no related protein domains that can be identified, which makes it hard to extrapolate about the potential role of this protein in ALS. Nevertheless, the lack of information on this candidate does not make it uninteresting: this candidate is special because of the profile obtained from deep-sequencing data. Here, it is visible a clear and strong transition in the ribosome-associated mRNA levels of this candidate between pre-symptomatic and early symptomatic phases of the disease. The idea of

doing a genome-wide approach was exactly to be able to identify new molecules that could be potentially involved in ALS pathology. Based on the “Human Protein Atlas” (<https://www.proteinatlas.org/ENSG00000175664-TEX26/tissue>) this protein seems to be expressed in male tissues, especially testis, which is surprising, given that I detect the mRNA associated with ribosomes in female motor neurons. A custom-made antibody against TEX26 was generated. At the moment of the writing of this thesis, the validation of the antibody is being made, by WB and IHC in MN1 cells transfected with a plasmid expressing TEX26 protein (data not shown) in the presence and absence of small interfering (siRNA). The validation of the antibody is important to guarantee that the right protein is being studied. If the custom antibody proves specific, it would be a useful tool for determining potential effects on TEX26 levels in MNs and for beginning to understand what this protein might do in any cell.

#### 4.5.4. TIA1 down regulation caused by TDP-43 could altered SG dynamics and ultimately lead to ALS

TIA1 is an RBP that plays a crucial role in promoting SG assembly and is implicated in RNA processing and translational regulation [107, 210-212]. TIA1 protein was also shown to regulate genes involved in multiple processes like apoptosis, cell proliferation and cell inflammation [212-215]. TIA1 is composed of three RRM and a C-terminal Gly-rich LCD, which undergoes phase separation [107, 171]. This protein is normally found in the nucleus, where it selectively regulates alternative mRNA splicing, but can also shuttle between nucleus and cytoplasm [211, 213, 216]. Shuttling happens in the presence of stress conditions where TIA1 exits the nucleus, aggregates, and bind transcripts to form SGs. Proteomic studies of SGs showed to be enriched for proteins encoding predicted prion-like or LCDs, including many ALS-linked RBPs [88, 217].

Depending on the type of cellular stress (e.g. heat shock, hypoxia, osmotic and oxidative stress), a variety of signaling pathways can be activated leading to the modulation of gene expression patterns, affecting either transcription or post-transcriptional events [218]. RBPs play a major role in post-transcriptional regulation during stress, yielding global repression of protein translation. This is achieved by the formation of SGs which house translationally arrested mRNAs [219]. SGs are known to be involved in sorting mRNA for storage, decay or re-initiation during stressful conditions [220, 221].

Recently, in 2017, several mutations were identified within the C terminal portion of the LCD of TIA1 in fALS and sALS cases, and since then several other mutations in *TIA1* have also been found [171, 222, 223]. Brain and spinal cord autopsy tissue samples from patients with *TIA1* mutations revealed cytoplasmic TDP-43 pathology and inclusions of hyaline Lewy body-like, but no TIA1 pathology [171, 224]. Functional studies have revealed that mutations in the LCD part of the TIA1 protein increased phase separation which delays SG disassembly and promoted accumulation of TDP-43. However, like in the case of TDP-43, whether TIA1 mutations cause ALS due to a gain of function, loss of function or combination of both is still unknown.

Unlike the other candidates, a link between TIA1 and ALS pathology has already been established. Furthermore, another important link between TIA1 and TDP-43 has also been found. This connection is

especially important for the results of this thesis, due to the identification of TIA1 as a downregulated candidate. TDP-43 down-regulation has been shown to influence the stoichiometry of TIA1. In SA stressed patient lymphoblastoid cells lines, expressing the patient mutant protein TDP-43<sup>R361S</sup> impacts SG formation, as well as TIA1 protein and RNA levels [85]. Moreover, it was also demonstrated that TDP-43 participates in the regulation of SGs, since depletion of TDP-43 delays SG nucleation and secondary aggregation via the deregulation of key nucleating factors TIA-1 and G3BP, at the mRNA level. Here, SG formation and resolution were assessed in HeLa cells transfected with control or TDP-43 siRNA prior treatment with SA. Furthermore, the number and size of TIA-1- and G3BP-positive SGs are reduced in cells depleted of TDP-43 and subsequently treated with oxidative stress [85]. TDP-43 therefore contributes positively to SG assembly and their maintenance, as well as cellular survival following acute oxidative stress. Thus, the contribution of TDP-43 to the assembly and disassembly of SGs offers an important mechanism by which TDP-43 may regulate gene expression in response to stress as well as during cellular recovery/survival [85].

The genome-wide sequencing data described in this thesis indicated that levels of ribosome-associated *Tia1* mRNA are downregulated in the presence of hTDP-43<sup>A315T</sup> protein. Nevertheless, tests by qRT-PCR on the coding sequence revealed no significant differences between the mutant and control groups. However, I obtained preliminary evidence that there may be less of the *Tia1-202* isoform being made in the presence of the hTDP-43<sup>A315T</sup> protein, since this mRNA showed a clear trend to be downregulated. At this stage, better results are needed to prove that *Tia1-202* mRNA levels selectively decrease upon expression of mutant TDP-43. For that, one could try to apply dual ISH-IHC on mouse spinal cord MNs. This would be a good technique to determine if there are isoform differences and to check for the protein levels at the same time. For this experiment, specific fluorescence ISH probes designed against the 3' UTR of the *Tia1-202* isoform would have to be designed.

Regardless of the mRNA isoform levels, other experiments focusing on protein levels could also be done to check for the overall levels of this protein in MNs. A possible follow up experiment would be to do IHC. More specifically, to stain mouse spinal cord MNs with TIA1 and TDP-43 to see if there is colocalization between these proteins and at the same time to see what happens to SGs' morphology (size, fluorescence intensity and number). Since direct access to two different ALS-causing mutation mouse lines on TDP-43 are available (A315T and Q331K), this study could be performed in both, which would allowed to investigate if TIA1 is commonly altered in the presence of both mutations.

In the study from McDonald K. K. et al.; 2010, it was demonstrated that depletion of TDP-43 increases the levels of *Tia1* mRNA and protein, whereas in cultured cells with the TDP-43<sup>D169G</sup> and TDP-43<sup>R361S</sup> disease causing mutations an increase of the protein levels of TIA1 was only observed in the presence of mutant TDP-43<sup>R361S</sup> [85]. Interestingly, the TDP-43<sup>D169G</sup> mutation is found in the RRM1 domain and the TDP-43<sup>R361S</sup> mutation in the C-terminal of the TDP-43 protein. The fact that the TDP-43<sup>D169G</sup> mutation did not disturb SG formation, led the authors to suggested that independent mechanisms caused by different mutations on the same gene may lead to ALS pathology.

From the follow up experiments that could be done to shed light on the role of TIA1 in ALS in the presence of hTDP-43<sup>A315T</sup> protein, several outcomes are possible:

- 1) No alterations indicative of TIA1 deregulation at the RNA and protein levels
- 2) Reduction of *Tia1-202* isoform mRNA levels with increased/reduced protein levels
- 3) No alteration in TIA1 protein levels, but visible deregulation of SGs
- 4) Alterations in TIA1 are only present in the hTDP-43<sup>A315T</sup> mutant animals or present in both the hTDP-43<sup>A315T</sup> and the hTDP-43<sup>Q331K</sup> mutant animals.

Regardless of the outcome, any new information about the involvement of TIA1 in ALS will help to unravel how this protein could be used as a potential target to treat disease.

Currently, IHC experiments aiming to determine TIA1 protein levels in MNs, as well as morphological changes in SGs are being performed and should shed light on altered regulation of TIA1 and SGs in MNs of ALS models *in vivo*.

### 4.6. Novelty of this study

Although this thesis features many novel elements, a paper describing TRAP applied to MNs of A315T mice appeared while this study was in progress. MacNair L., et al.; 2015, [225] used TRAP to examine the transcriptome of MNs at time points corresponding to pre-symptomatic and symptomatic phases of the disease caused by a different TDP-43<sup>A315T</sup> mutant mouse line. One difference between the study of MacNair L., et al.; 2015 and this thesis is that their model is on the genetic background C3H C57BL/6, and therefore develops symptoms much later than the lines used in this thesis. Perhaps more importantly, the genome-wide approach used was also very different. MacNair L., et al.; 2015 used microarrays to identify the candidates, whereas in this thesis, high-throughput sequencing was used. From their study only 24 candidates emerged and none of those coincide with any of the 327 identified in this study (appendix 9.8). The lack of common candidates could derive from the two different methods used to identify which RNAs are deregulated. Overall, RNA high-throughput sequencing is considered a more robust approach since:

- High-throughput sequencing does not require species or transcript specific probes like microarrays
- Microarrays have a limited measurement of gene expression due to background at the low end and signal saturation at the high end. On the other hand, high-throughput sequencing produces discrete, digital sequencing read counts, and can quantify expression across a larger dynamic range ( $>10^5$  for RNA-Seq vs.  $10^3$  for microarrays)
- High-throughput sequencing can detect a higher percentage of differentially expressed genes, especially genes with low expression
- High-throughput sequencing coverage depth can easily be increased to detect rare transcripts, single transcripts per cell, or weakly expressed genes

Moreover, in this thesis, I focused on the early symptomatic phase of the disease, and this group on the symptomatic phase. Further, I did an additional control comparison: Chat-BacTrap; A315T vs Chat-BacTrap; hTDP-43 to help with the identification of mRNAs that are deregulated in disease rather than simply by hTDP-43 overexpression. This important control was not included in the other study. To sum up, due to all the differences pointed out above, this could be the reason that no common candidates were found. Moreover, I think my study is more comprehensive and has a better chance to identify disease-driving proteins by virtue of its design.

#### 4.7. Gradient-TRAP enables the measurement of ribosome density in specific cell types *in vivo*

RNA-Seq-based methods for studying mRNA levels are highly sensitive, providing major insights into transcriptional regulation in specific cell types within complex tissues. In contrast, methods to study translational regulation within specific cell types in a mixed population remain limited. Translational control involves changes in ribosome access to or density on specific mRNAs. Sucrose-density gradient polysome profiling can measure both, but requires significant starting material, and thus lacks cell type-specific resolution. Conversely, TRAP enables access to the “translatome” from specific cells in a complex mixture. However, TRAP presumably cannot monitor ribosome density, since an mRNA should be immunoprecipitated whether it is bound by one, three, or ten ribosomes. To overcome these limitations, I performed experiments to help establish a new method: Gradient-TRAP. This method combines sucrose density gradient separation of mRNAs according to the number of bound ribosomes, with immunoprecipitation of tagged ribosomes and associated mRNAs from specific gradient fractions.

##### 4.7.1. NaAsO<sub>2</sub> massively down regulates translation and alters ribosome density

I optimized in a cell culture model the best conditions of stress induction. Here, 80μM during 30min of exposure to NaAsO<sub>2</sub> was sufficient to induce stress in MN1 cells which was assessed by an increase in the phosphorylation levels of p-eIF2α protein and increased levels of ATF4 protein by WB. An increase in the phosphorylation level of p-eIF2α is the classic pathway for inhibition of global translation, thus controlling for this step is a good way to verify if oxidative stress induction is working. ATF4 is an activating transcription factor that belongs to the ATF subfamily of the basic leucine zipper (bZIP) transcription factor superfamily. ATF4 is a master regulator that plays a crucial role in the adaptation to stresses by regulating the transcription of many genes [226]. Upon stress induction, the mRNA levels of this gene do not change but their ribosomal density does, making this gene a perfect candidate to study translational changes. mRNAs with a described similar pattern are *Atf5* and *Slc35a4*. Moreover, mRNAs whose ribosomal density changes drastically, hypersensitive mRNAs, are also interesting candidates to be studied in the context of Gradient-TRAP: *Pabpc1*, *Rpl12* and *D3jfr1*. The mRNA levels of these genes were determined after stress induction by qRT-PCR, and as expected no differences were found. According to the literature, mRNAs like *Atf4*, *Atf5* and *Slc35a4* are called resistant because when the cells are under stress the translation levels of these mRNAs are increased (more ribosomes translating the



mRNA). On the other hand, mRNAs like *Pabpc1*, *Rpl12* and *D3jfr1* are called hypersensitive which means that their translation status is reduced (fewer ribosomes translating the mRNA). Through polysome profiling it is possible to directly detect such changes.

Polysome profiling in this context enables two things: 1) to control for stress induction and 2) to check for changes in ribosomal access to these RNAs. Stress induction can be directly detectable by the crash in polysomes when comparing to the untreated control and changes in ribosomal access can be determined by qRT-PCR on individual fractions. The so called hypersensitive RNAs – *Pabpc1*, *Rpl12* and *D3jfr1* - show indeed a ribosomal profile concomitant with a hypersensitive behavior. Under normal conditions most of these mRNAs have a relatively similar percentage of ribosomal distribution on them in most of the fractions (between 10% to 30%). However, upon stress induction the percentage of RNAs per ribosomal density shifts to RNAs completely depleted of ribosomes or RNAs with 1 ribosome bound to them. Approximately 70-80% of these RNAs have either no ribosomes or only 1 ribosome bound upon stress induction. GAPDH was included in this study because it is known to be an abundant protein in cells and to have a high ribosomal density on its RNA under cellular normal conditions [175]. In my results it was observed that under normal conditions, 75% of *Gapdh* mRNA has seven or more ribosomes bound per mRNA. However, upon stress induction it was observed that this mRNA behaves as a hypersensitive one. There is a clear shift from the deepest fraction (seven or more ribosomes per mRNA) to lighter fractions (95% of the mRNA are either ribosome-free or have a maximum of 3 ribosomes). *18S* is an rRNA and it was used as a positive control of the experiment. Its levels in deep fractions are supposed to be reduced upon global translation arrest and this is exactly what I observed.

On the other hand, the resistant mRNAs –*Slc35a4*, *Atf4* and *Atf5*-, as described in the literature, show indeed resistance features, but behave somewhat differently from what was described in the study from Andreev D. E. et al.; 2015. Upon stress induction, most of these RNAs still have between 2-6 ribosomes bound to them, but this still reflects fewer ribosomes on these mRNAs than the control situation. As described in some studies, the protein levels of ATF4 increase with stress induction [227, 228]. The study from Andreev D. E. et al.; 2015, which helped conceiving this proof of concept experiment, showed an increase of ribosome density on *Atf4* mRNA, which is accompanied by an increase in corresponding protein levels. Nevertheless, an interesting result from the polysome profiling is the fact that the number of ribosomes on *Atf4* mRNAs is decreased upon stress induction but the protein levels seem to be increasing. One possible explanation for the reduction seen by polysome profiling could be that by applying this method, ribosomal density is being measured in the entire mRNA sequence of *Atf4*, while in the study made by Andreev D. E. et al.; 2015 only ribosomal density in the coding sequence was measured [174], which means that the two uORFs from *Atf4* mRNA that can also accommodate ribosomes were not considered for their study. I hypothesize that upon stress there is a reduction in the overall number of ribosomes on the mRNA, but the relative number of ribosomes on the *Atf4* coding sequence actually increases. A reliable method to actually visualize if this is the case, would be ribosome profiling. Indeed, this was the method used by Andreev D. E. et al.; 2015, but as mentioned before, only the coding sequenced was studied. Ribosome profiling allows to determine which portions of the genome are actually being translated into protein, relying on the fact that a translating ribosome encloses a ~30 nucleotide portion of this mRNA template and protects it from nuclease digestion. These

protected sequences can then be genome-wide-sequenced, giving direct information of the location where the ribosome was bound [229].

Nevertheless, I am interested in developing a method to measure alterations in ribosome density in specific cell types *in vivo*, which brings me to a key point of these results: based on these data, I have verified that under these conditions it is possible to detect ribosomal density changes. Even though the system in play didn't reveal exactly what was expected from the literature, the main aim of this step was achieved. It is possible to conclude that NaAsO<sub>2</sub> massively down regulates translation and alters ribosome density on mRNAs whose levels do not change.

##### 4.7.2. Altered ribosome density is silent in TRAP

A key point in the development of Gradient-TRAP is to first determine directly whether large changes in ribosome density on specific mRNAs cannot be reliably detected by TRAP alone. Clearly, if TRAP alone can already detect such changes then combining TRAP with gradients would not be necessary. This seems unlikely on theoretical grounds, but needed to be verified experimentally.

In this step, MN1 cells were transfected with GFP and GFP-L10a plasmids separately in order to immunoprecipitate the ribosomes attached to the mRNAs. Transfection efficiency and stress induction were assessed by WB. The presence of both plasmids was visualized and the protein levels of p-EIF2 $\alpha$  calculated. After checking for the basic conditions of the experiment, TRAP was performed from GFP and GFP-L10a transfected cells. The GFP-transfected cells were used as the negative control of the experiment since no ribosomes attached to mRNA are expected to be immunoprecipitated via TRAP from these cells; any signal seen here is background. To check if TRAP was able to efficiently immunoprecipitate RNAs from GFP-L10a transfected cells, it is necessary to determine the relative enrichment to the input material (IC). Here, it is expected to obtain high levels of RNA for all the genes in the cells transfected with GFP-L10a relative to the respective IC. In the case of the cells transfected with the GFP plasmid no enrichment was observed, as expected. A control for the mechanism of stress induction is to check for the RNA levels of these genes in the IC. As shown, there are no differences in the RNA levels upon stress induction, demonstrating what was previously observed, that these genes have no alterations in the RNA levels and regulation occurs instead at the translational level, mainly by effects on ribosome density on these mRNAs.

Once all the controls were checked, the fold change between the sample exposed to NaAsO<sub>2</sub> and the untreated control sample was determined. The fold change is a measure of the RNA levels. To be able to say that TRAP cannot measure ribosome density it is necessary to have a fold change for each gene less than two, since this is a standard cutoff used for differential expression analysis in genome-wide assays. This threshold can indeed be lowered, but the robustness of the data will also decrease. For all the genes tested it is possible to verify that there is no increase or decrease detectable in the mRNA levels. Even though this experiment was done only once, it is already indicative that TRAP alone cannot measure ribosomal density changes. Three more replicates of this experiment were done by Florian Stelzner, in

consultation with me and using my protocol. He confirmed that altered ribosome density is silent in TRAP and included these data in his Master's thesis.

### 4.7.3. *In vivo* Gradient-TRAP can be used to monitor translation from specific cell types

Gradient-TRAP is intended to be a method that could be used with *in vivo* material. For this purpose, I optimized the technique to be used with mouse spinal cord tissue to purify MN ribosomes and associated mRNAs. Here, I used Chat-BacTrap and littermate wt control animals. In this optimization part, one spinal cord was replaced with the pooling of three full spinal cords. This alteration was necessary because the yield of RNA was too low, which could be easily seen at the generated profiles, since there was very low resolution on the polysome part. This made it difficult to identify individual fractions. When three spinal cords were pooled together this resolution problem was overcome.

For an easy and direct assessment of the method, I did TRAP from pooled fractions. Here fractions that contained from FS to four ribosomes sitting on the mRNA were pooled together to one fraction and called the light fraction. The fractions containing five or more ribosomes on the mRNA were also pooled in one fraction and denominated the heavy fraction. The reason to divide the fractions in this scheme, was to first evaluate if TRAP could actually be done from samples containing high concentrations of sucrose. This division aimed to minimize the TRAP costs while assessing its performance in this configuration.

In line with what was done to check previously if TRAP is effectively immunoprecipitating RNAs from spinal cord MNs, I check for *Chat* mRNA enrichment and *Gfap* de-enrichment. As observed there is an enrichment of *Chat* RNA in both the light and heavy pooled fractions. Also, the positive control of the experiment, TRAP from non fractionated samples, is showing *Chat* enrichment. Changes in enrichment and de-enrichment between pooled fractions can be due to the preference of certain mRNAs to be translated in a more light or heavy fashion way. For example, *Chat* mRNA seems to be preferentially translated with less ribosomal density. De-enrichment of *Gfap* is also visible. However, since the values obtained are considered background it is hard to infer whether there is the same effect as for *Chat* or not.

This initial data from Gradient-TRAP suggested that the technique can indeed be applied to *in vivo* material and that sucrose solutions do not interfere with TRAP efficiency. Working closely with me, Florian Stelzner, a Master's student in the Duncan group went on to use the optimized protocol to determine if it can be used in a genome-wide configuration. The results from a pilot experiment with deep-sequenced RNA provided preliminary evidence that Gradient-TRAP can be used together successfully with deep-sequencing. Subsequently, with my assistance, Florian went on to generate data proving that this method can yield robust data in a genome-wide configuration. Moreover, he showed that this method can reveal apparent differences between the translational status of specific mRNAs in MNs of male vs. female mice that could not be observed otherwise. These results are included in part in his thesis.



## **5. Conclusions**



## 5. Conclusions

The aim of this thesis was to identify proteins that could be possible disease drivers in mouse models of ALS caused by expressing patient mutant alleles of TDP-43. By applying TRAP to mouse spinal cord tissue, it was possible to isolate RNAs bound to ribosomes (translatome) specifically from MNs. Several steps of optimization and verification were necessary to ensure the efficiency of the TRAP method. Based on extensive behavioral tests, TRAP was applied to defined time points corresponding to pre-symptomatic and early symptomatic phases of ALS, in order to increase the chances of identifying potential disease-driver proteins. Importantly, I confirmed that the *Chat::L10a-GFP* transgene did not develop phenotypes on its own or modify the disease phenotypes of the other lines. In support of the behavioral data, collaborators could show a mild denervation of the NMJ at the timepoint selected to be early symptomatic, providing cellular evidence that this time point indeed reflects the early symptomatic phase of the disease.

From the sequencing data, six candidates were selected as potential disease drivers (PLEKHB1, TIA1, TEX26, SYNGR4, MXD3 and NHLH1). The veracity of these candidates as potential disease drivers was further pursued first by TRAP with an independent cohort followed by qRT-PCR and second by spinal cord IHC, to check if both RNA and protein levels were altered, respectively. Validation by TRAP followed by qRT-PCR was unfortunately not entirely successful, since the RNA levels of most of the candidates were low, as was the number of replicates used, leading to variable results in many cases. IHC, on the other hand, gave clear data for the two candidates tested (PLEKHB1 and SYNGR4). Importantly, not only were these candidates tested in the A315T mutant mouse line, but also in the Q331K mutant mouse line, showing that deregulation of these candidates is not mutation specific, and therefore may reflect a more general aspect of ALS pathology. For PLEKHB1, SYNGR4 and TEX26, there are no studies showing a link between these genes or the encoded proteins and ALS pathology. The lack of this link makes it impossible to relate these proteins to ALS without further experimentation. At the same time, it also makes these findings interesting, since the point of doing a genome-wide approach is presumably to identify new molecules that could be important in ALS.

The connection between PLEKHB1 and myosins and their putative role in ALS pathology seems to be an interesting idea to investigate further. Moreover, the fact that TIA1 is involved in ALS pathology and that it emerged as a potential gene candidate to be a disease driver, makes a follow up on this candidate worthwhile at both the RNA and protein levels, with emphasis on SG morphology.

I used TRAP to identify the mRNAs and proteins described above. During these studies, we realized that TRAP might provide an insufficient view of cellular translation, but that combining TRAP with sucrose density gradients might give significantly more insight. In this context, groundwork was performed to establish a new method "Gradient-TRAP". This method aims to measure ribosome density changes on mRNAs from specific cells types *in vivo*, overcoming this way the limitations of TRAP and polysome profiling. I first developed an *in vitro* proof of concept system to verify if Gradient-TRAP would detect changes in the number of ribosomes. MN1 cells were stressed with NaAsO<sub>2</sub> and the distribution of ribosomes on specific RNAs was determined. As expected there were massive changes at the ribosome

density level, but no alterations at the mRNA level. As hypothesized, TRAP alone was unable to reveal even massive ribosome density changes on specific mRNAs. Furthermore, I could show that Gradient-TRAP can be done from mouse *in vivo* spinal cord material with qRT-PCR as a readout method. These experiments were fundamental to understand whether the basic concept of Gradient-TRAP was solid and possible to perform. This technique was developed with the primary goal of exploring possible effects on translation in ALS that would fail to be detected by TRAP. Nevertheless, this method can be used in a wide variety of other contexts to study ribosomal density changes in specific cell types within a mixed population.

To sum up, using TRAP from MNs, I have revealed new molecules whose deregulation could conceivably drive development of ALS symptoms when mutant TDP-43 is present. Moreover, I provided crucial groundwork for the development of Gradient-TRAP, a new method to more accurately measure the translational status of specific mRNAs within specific cell types.



## **6. Materials**



## 6. Materials used in the experimental procedures of the thesis

### 6.1. Buffers and media

#### 6.1.1. Genotyping

**Table 5. Lysis buffer for tail biopsies.**

Reagents	Final concentration
TRIS base (pH=8)(Roth, #4855.2)	50 mM
KCl (Ambion, #AM9640G)	50 mM
EDTA (Roth, #8043.2)	2.5 mM
NP-40 (Thermo fisher, #28324)	0.45 %
Tween 20 (Fluca, #93773)	0.45 %
Proteinase K (Thermo fisher, #NC9463757)	0.3 mg/ml

#### 6.1.2. WB

**Table 6. RIPA buffer.**

Reagents	Final concentration
TRIS base (pH=8)	10 mM
NaCl	150 mM
EDTA	10 mM
NP40	1 %
Sodium dodecyl sulfate (SDS) (Serva, #20765)	0.1 %
Protease- Inhibitor complete EDTA-free (Roche, #11836170001)	1 Table

**Table 7. Running buffer.**

Reagents	Final concentration
TRIS base (pH=8.3)	125 mM
Glycine (Roth, #3908.3)	960 mM
SDS	0.5 %

**Table 8. Transfer buffer.**

Reagents	Final concentration
TRIS base	5 mM
Glycine	400 mM
SDS	0.004 %
Methanol (Roth, #4627.5)	20 %

**Table 9. TBST-Tween buffer.**

Reagents	Final concentration
TRIS (PH=7.4)	100 mM
Glycine	1500 mM
Tween-20	0.05 %

## 6.1.3. TRAP Buffers

**Table 10. 0.15M KCl washing buffer.**

Reagents	Final concentration
HEPES (Affymetrix, #16924) (pH=7.4)	20 mM
MgCl <sub>2</sub> (Ambion, #AM9530G)	5 mM
KCl	150 mM
NP-40	1%
Dithiothreitol (DTT) (Sigma, #D9779)	0.5 mM
Cycloheximide (CHX)(100mg/ml) (Sigma, #C7698)	100 µg/mL

**Table 11. Dissection buffer.**

Reagents	Final concentration
(10X) HBSS (Life technology, #14065-49)	1x
HEPES (pH=7.4)	2.5 mM
Glucose (Sigma, #G7528)	35 mM
Sodium carbonate (Sigma, #S6297)	4 mM
CHX	100 µg/mL

**Table 12. Lysis buffer.**

Reagents	Final concentration
HEPES (pH=7.4)	20 mM
KCl	150 mM
MgCl <sub>2</sub>	5 mM
DTT	0.5 mM
Protease- Inhibitor complete EDTA-free	1 Tablet
CHX	100 µg/mL
Rnasin (Promega, #N2615)	40 U/mL
Superasin (Ambion, #AM2696)	20 U/mL

**Table 13. 0.35M KCl washing buffer.**

Reagents	Final concentration
HEPES (pH=7.4)	20 mM
MgCl <sub>2</sub>	5 mM
KCl	350 mM
NP-40	1%
DTT	0.5 mM
CHX	100 µg/mL

## 6.1.4. MN1 cell line

**Table 14. MN1 cell line medium composition.**

Reagents	Final concentration
Dulbecco's modified Eagle's medium high-glucose GlutaMAX culture medium (Gibco, #10566016)	500ml
Fetal Bovine Serum (FBS) (Gibco, #10270-106)	10 %
Penicillin/Streptomycin (Gibco, #15140122)	1 %
HEPES (Gibco, #15630-056)	2.4 %

## 6.1.5. Polysome profiling

**Table 15. Lysis/Gradient buffer.**

Reagents	Final concentration
TRIS-HCl (pH=7.4)	20 mM
NaCl	150 mM
MgCl <sub>2</sub>	5 mM
DTT	1 mM
CHX	100 µg/mL
Rnasin	40 U/mL
Supersasin	20 U/mL

## 6.2. Primers

**Table 16. Primer sequences used in genotyping PCR reactions.**

Primer name	Sequence forward	Sequence reverse
Chat	CCT ACG GCG TGC AGT GCT TCA GC	CGG CGA GCT GCA CGC TGC CGT CCT C
hTDP-43	TGG AGA AGT TCT TAT GGT GCA GGT C	GCC ACC TGG ATT ACC ACC AA
hTDP-43 Flag	GGA CGA CGA CGA TAA GTCT GA	GCC ACC TGG ATT ACC ACC AA
Actin	AGA GGG AAA TCG TGC GTG AC	CAA TAG TGA TGA CCT GGC CGT

**Table 17. Mouse primer sequences (Invitrogen) used for qRT-PCR.**

Gene name	Forward primer (5'-3')	Reverse primer (5'-3')
<i>Chat</i>	CCA TTG TGA AGC GGT TTG GG	GCC AGG CGG TTG TTT AGA TAC A
<i>Gapdh</i>	TTG ATG GCA ACA ATC TCC AC	CGT CCC GTA GAC AAA ATG GT
<i>Cnp1</i>	TGC TTG ATG ATA CCA ACC ACG	GCT GGG CAC AGT CTA GTC G
<i>Gfap</i>	GTA AAG ACT GTG GAG ATG CGG GAT GGT TGA G	GTG CTG GTG TGG GTG GGA ACT GAG
<i>L10a</i>	CAT GAG CAG CAA AGT C	TAT TGG AGC ATC CTA ATA CA
<i>18S</i>	CTT AGA GGG ACA AGT GGC G	ACG CTG AGC CAG TCA GTG TA
<i>D3jf1</i>	TCC TTT CGA ACT TGT GCT GA	TGT GGA AGA AGG TTT GGA TCA
<i>Slc35a4</i>	GGT GAA GTC CAA CAG TGG CG	ACT GCT GAT GCC CTC AGT TT
<i>Atf4</i>	TTG TCC GTT ACA GCA ACA CTG	GCA GCA GCA CCA GGC TCT
<i>Atf5</i>	TAT GAG GTC CTT GGG GTG	ACC CGC TCA GTC ATC CAA T
<i>Pabpc1</i>	CAG GAA GCA GCT GAA AGA GC	TCC AAG CTC TGC TTC CTC GTT
<i>16S</i>	GCA GGC CTA ACA CAT GCA A	CAC TCG TCA GCG AAG CAG
<i>28S</i>	CAG TAC GAA TAC AGA CCG	GGC AAC AAC ACA TCA TCA G
<i>Rpl12</i>	AAG ATC GGT CCT CTG GGT CT	ATC TGG GCC TGT CTG TTC TG
<i>Rluc</i>	TGG TAA CGC GGC CTC TTC T	GCC TGA TTT GCC CAT TAC CAA
<i>Fluc</i>	ACC GAA TTC GAG ATG GAA GAC GCC AAA AAC	GTC TAC GTG TAT AGC TCC ACT TG
<i>Egfp</i>	ACG TAA ACG GCC ACA AGT TC	AAG TCG TGC TGC TTC ATG TG
<i>Tex26</i>	ACA AGA TGG CCC GGT ATA GGA	TGT CAC CTG ACT GGA GCT T
<i>Plekhhb1</i>	AGA GTC AAG CCC CAC TTC TG	GAC TTT CCA GGA TGG AGT CG
<i>Syng4</i>	CCT GGC AGA CAA TGA GAC TG	GAG GAC AAG ATG ACC AGG GA
<i>Tia1</i>	TGG ATA CAG CAG GAA ATG ACC	CAT TAT CTT CCG CCC ATT CA
<i>TIA1 (202: long isoform)</i>	TAG ATT GTC CTT CTC TTG CTT TTC C	AAT GAA AGG GAC CTC TAG CAC AAA
<i>Mxd3</i>	TGC CCC GAT GAG ATG AAG TC	CAA GAC CCT TTT TGC CAG CTA

## 6.3. Antibodies

**Table 18. List of primary antibodies used in WB and IHC.**

Antigen	Dilution WB	Dilution IHC	Species	Code	Company
GAPDH	1:1000		Rabbit	G8795	Sigma-Aldrich
Flag M2	1:1000		Mouse	F1804	Sigma-Aldrich
ATF4	1:200		Rabbit	10835-1-AP	Proteintech
ATF5	1:500		Rabbit	PA5-46842	Thermo Fisher Scientific
GFP	1/5000		Rabbit	ab13970	Abcam
TDP-43	1:1000		Rabbit	3448	CST
p-EIF2 $\alpha$	1:1000		Rabbit	3597	Cell Signaling
EIF2 $\alpha$	1:1000		Mouse	2103	Cell Signaling
Cofilin	1:1000		Rabbit	ab42824	Abcam
NeuN		1:400	Rabbit	ABN91	Millipore
ChAT		1:100	Rabbit	AB144P	Millipore
PLEKHB1		1:100	Rabbit	orb326560	Biorbyt
SYNGR4		1:200	Rabbit	OAPB01027	Aviva Systems Biology
2H3		1:50	Mouse	AB 2314897	DSHB
SV2		1:50	Mouse	AB 2315387	DSHB

**Table 19. List of secondary antibodies used in WB and IHC.**

Antigen	Conjugate	Host	Dilution WB	Dilution IHC	Code	Company
Rabbit-IgG	HRP	Goat	1:10000		1858415	Thermo Fisher Scientific
Mouse-IgG	HRP	Goat	1:10000		1858413	Thermo Fisher Scientific
Rabbit-IgG	IRDye 680LT	Goat	1:15000		925-68021	Li-Cor
Mouse-IgG	IRDye 680LT	Goat	1:15000		925-68020	Li-Cor
Rabbit-IgG	IRDye 800CW	Goat	1:15000		926-68171	Li-Cor
Mouse-IgG	IRDye 800CW	Goat	1:15000		925-32210	Li-Cor
Goat-IgG	Alexa 647	Donkey		1:400	705-605-147	Jackson Immuno Research
Rabbit-IgG	Alexa 555	Donkey		1:400	ab150062	Abcam
Chicken-IgG	Alexa 488	Donkey		1:400	703-545-155	Jackson Immuno Research
Mouse-IgG	Alexa 488	Donkey		1:250	A-21202	Thermo Fisher Scientific

## 6.4. Technical equipment

**Table 20. Equipment used in the ZMNH.**

Type of device	Company	Origin
2720 Thermal cycler	Applied Biosystems	
UV-transilluminator chamber	Bio-Rad	USA
Fujifilm LAS-4000 luminescent image analyzer	Fukifilm	Germany
Li-Cor Odyssey CLx	Li-Cor	USA
Balance	Kern	Germany
Grip strength monitor	TSE Systems	Germany
Rotarod	TSE Systems	Germany
Magnet	Invitrogen	Germany
Rotator	Labnet	Germany
NanoDrop 2000 Spectrophotometer	Thermo Fisher Scientific	Germany
Qubit fluorometer	Invitrogen	USA
7900HT Fast Real-time PCR machine	Life Technologies	USA
Cryostat (microm HM 560)	Thermo Fisher Scientific	Germany
Microm HM 450/KS 34 freezing microtome	Thermo Fisher Scientific	Germany
Zeiss LSM 700 microscope	Carl Zeiss	Germany
Gradient former (model 108)	BioComp	USA
Piston Gradient Fractionator (model 152)	BioComp	USA
UV monitor (model EM-1 Econo)	Bio-Rad	Germany
Bright filed microscope, Axiovert 40CFL	Carl Zeiss	Germany
UV-Visible spectrophotometer, ultraspec 3000	Scintek Instruments	USA
Heraeus HERA cell incubator	Thermo Fisher Scientific	Germany

### 6.5. Software

Image processing and analysis: ImageJ 1.51h (Fiji-NIH, USA), Image Studio Lite Ver. 5.2. (Li-COR Biosciences, Germany), Adobe Photoshop CS6 (64bits) (Adobe, USA), Adobe Illustrator CS6 (64bits) (Adobe, USA).

Real-time PCR analysis: Sequence detection systems (SDS) 2.4 software (Applied Biosystems, USA) and Excel Microsoft office 2010 (Microsoft, USA).

Data analysis, figure generation and statistics: Excel Microsoft office 2010 (Microsoft, USA), with GraphPad Prism 6, version 6.07, USA), Adobe Photoshop CS6 (64 bits) (Adobe, USA), Adobe Illustrator CS6 (64 bits) (Adobe, USA) and gradient profile program, version 6.10 (BioComp, USA).

Management of the mouse colonies: Database software TBase (4Dv14.3, Germany) was used.

Analysis of gene product isoforms: online ensembl database (EMBL-EBI), was used (<https://www.ensembl.org/index.html>).

Mining of the sequencing data: online software for Venn diagrams, Venny 2.1. (CSIC, Spain), (<http://bioinfoqp.cnb.csic.es/tools/venny/>), sequencing quality was checked with the *FastQC* software ([www.bioinformatics.babraham.ac.uk/projects/fastqc/](http://www.bioinformatics.babraham.ac.uk/projects/fastqc/)), read count files were pre-processed and analyzed in the R/Bioconductor environment using the DESeq2 package (PMID: 25516281, version 1.8.2), Samples were de-multiplexed with *bcl2fastq2* (Illumina, version 2.17), detection and removal of putative PCR duplicates was performed using the *rmdup* command of the *Samtools* software (PMID: 19505943, version 0.1.19), gene annotation was performed using *Mus musculus* entries from Ensembl (PMID: 27899575) via the biomaRt package (PMID: 19617889, version 2.24.1), GO biological processes and KEGG pathways was determined using the DAVID web server for gene functional annotation (PMID: 19131956, version 6.8).

Data and text generation: Word and Excel Microsoft Office 2010 (Microsoft, USA) and references with EndNote X8 (Thomson Reuters, USA).



## **7. Methods**



## 7. Methods

### 7.1. Experimental animals

All the animal procedures including caring, handling and experiments in the context of this thesis were performed in accordance with the German legislation, § 8 des Tierschutzgesetzes vom 18. Mai 2006 (BGBl. I S. 1207, 1313), and approved by the local authorities of the city of Hamburg with the license name “Analyse von Änderungen des Motorneuronalen Translatoms im Mausmodell der Amyotrophen Lateralsklerose”. In this thesis five lines of mice were acquired from the Jackson laboratory, USA (Table 21).

**Table 21. Mouse lines used in the experimental procedure for the development of this thesis.**

Name	Jackson's original strain name	Reference (origin of the line)
<b>C57BL/6J</b>	C57BL/6J	-
<b>Chat-BacTrap</b>	Chat-EGFP/Rpl10a bacTRAP C57BL/6J	[160]
<b>hTDP-43</b>	JAX 016608-C57BL/6-Tg ( <i>prnp-TARDBP</i> )3Cptrc/J	[163]
<b>hTDP-43<sup>A315T</sup></b>	JAX 010700- B6.Cg-Tg ( <i>prnp-TARDBP</i> *A315T)95Balo/J	[118]
<b>hTDP-43<sup>Q331K</sup></b>	B6N.Cg-Tg( <i>Prnp-TARDBP</i> *Q331K)103Dwc/J	[56]
<b>hTDP-43<sup>WT</sup></b>	B6N.Cg-Tg( <i>Prnp-TARDBP</i> )96Dwc/J	[56]

The C57BL/6J strain was acquired by the ZMNH mouse facility from the Jackson laboratory. All the ALS related lines were backcrossed with these mice to:

- Have all in the same genetic background
- Expand the lines
- Obtain all the necessary genotypes to perform the desired experiments

A minimum of 10 crosses to C57BL/6J mice was performed in order to consider a line in the same background. For each experiment, the animals were housed in the same environment and handled the same way to minimize the introduction of external variables as much as possible.

### 7.2. Genotyping

Genotyping of the animals took place twice for animals involved in experiments and once for all the animals used for expanding the colonies and breeding at the animal facility. The first tail biopsies were collected before weaning (until 3 weeks after birth) and the re-genotyping was done after the animals

## 7. Methods

---

were euthanized for experiments. Genotyping was done by technical assistant students, under the supervision of either Katrin Küchler, TA in the laboratory, or me.

A portion of the tail was removed with sterile scissors and put in 250µl of freshly prepared lysis buffer (Table 5) followed by an overnight incubation at 55°C while shaking.

### 7.2.1. PCR

A PCR reaction was used to amplify DNA and was prepared according to Table 22, as follows:

**Table 22. PCR reaction mix per each sample.**

Reagent	Volume (µl)
Forward primer (10µM)	0.45
Reverse primer (10µM)	0.45
dNTP's (10mM each)	1.5
5x Buffer GoTaq	3
Genomic DNA	1
Polymerase (Go Taq, Promega, # M791A)	0.1
H <sub>2</sub> O	Up to 15

The primers sequence can be seen in Table 16. Each PCR reaction was set up according to the protocol in Table 23 and the reaction took place in a 2720 Thermal cycler.

**Table 23. PCR protocol.**

Step	Thermoprofile	Time (min)	Temperature (°C)	n. of cycles
1	Initial denaturation	2	95	1x
2	Denaturation	1	95	35 x
3	Primer annealing	1	60	
4	Amplification	1	72	
5	Final extension	7	72	1x
6	Resting temperature	-	4	1x

The PCR products were separated by electrophoresis in a 2% agarose gel in 1x TBE buffer at 10V/cm. An UV-transilluminator chamber was used to visualize the results.

### 7.3. WB

WB was done from both mice spinal cord material and from the cell line MN1.

For spinal cords extraction the animals were anesthetized with a mixture of 80% of CO<sub>2</sub> and 20% O<sub>2</sub> prior being euthanized with 100% of CO<sub>2</sub>, at 9 and 17 weeks of age and the tissue was thereafter lysed in RIPA buffer (Table 6) in a dounce homogenizer and left for 45 min on ice. The samples were then centrifuged twice at 20000g for 15min each, at 4°C, and the supernatant was collected.

For MN1 cells, the cells were first washed with ice cold 1X phosphate buffered saline (PBS) and lysed in 500µl of lysis buffer (RIPA buffer). The cells were scraped from the plates and incubated on ice for 10min. With a 27G needle (BIBraun, #4657705) the lysate was triturated and later centrifuged at 20000g for 10min at 4°C. The supernatant was collected into new tubes.

Protein concentration was determined by Bio-Rad Protein assay (#500-0006, USA), following manufacturer's instructions. Equal amounts of protein (usually, 25ug total protein) were separated in a 10-12% SDS-PAGE gel in 1x running buffer (Table 7) and transferred to a nitrocellulose or PVDF membranes. Immunoblotting to nitrocellulose or PVDF was performed either with wet transfer under standard conditions (using transfer buffer (Table 8) at 1h30min at 100V) or using an iBlot rapid transfer device (Life Technologies) according to the manufacturer's guidelines. The membranes were blocked with 5% milk in TBS-Tween solution (Table 9) for 1h at RT and probed overnight at 4°C with primary antibodies diluted as indicated in Table 18. On the next day, the membranes were washed 3x for 10min each with TBS-Tween. Membranes were then incubated for 2h at RT with secondary antibodies (see Table 19). Finally, the membranes were washed 3x for 10min each with TBS-Tween.

Signals from bands were either visualized using HRP-conjugated secondary antibodies and Super Signal West Pico or Femto reagent (Thermo Fisher Scientific, #34080, #34096, respectively) and imaged on a LAS-4000 luminescent image analyzer or by using fluorescent secondary antibodies and imaged on a Li-Cor Odyssey CLx. Total protein staining was performed using Revert Total Protein Stain Kit (Li-Cor, #926-11010) according to the manufacturers' instructions. Analysis of the density of the bands was done either with ImageJ or with Image Studio Lite. A t-test was used to calculate the significance among samples. Data is presented as mean ± SEM and \*, \*\* and \*\*\* indicates a p-value of p<0.05, p<0.01 and p<0.001, respectively.

#### 7.4. Behavioral experiments

During weaning (three weeks of age), the animals were put into cages according to gender and genotype. Two weeks prior to the start of the behavioral experiments, the animals were transported to a new room where they stayed during the timeframe of the behavioral experiments. During the two weeks prior the beginning of the experiments, I started handling the animals one by one, daily, so that they would get used to me. This type of interaction reduces anxiety in the animals and helps establishing trust, which is important to avoid bias while performing the tests. The handling refers to the habituation of an animal to being grabbed and moved from its environment of comfort to a new environment (from its cage to a new cage with new bedding material for 5 minutes). In the interest of the animal welfare, the animals were monitored daily from the start of the handling to the final day of tests.

For behavioral experiments, each tested group was initially composed of 12 animals of the same genotype and gender (female and male mice) as depicted in Table 24. Behavioral tests were conducted under the guidelines from “working with ALS mice: Guidelines for preclinical testing & colony management”, provided by the Jackson laboratory [166].

**Table 24. Genotypes tested in behavioral analyses.**

Genotypes	Genders tested
WT strain	Females and males
Chat-BacTrap	Females and males
hTDP-43	Females and males
Chat-BacTrap; hTDP-43	Females and males
A315T	Females and males
Chat-BacTrap; A315T	Females and males

Four tests were conducted on each group of animals: neurological score, peak body weight, grip strength and rotarod. Animals were tested at 8, 12 and 16 weeks of age for the following test: neurological score, grip strength and rotarod. The animals were tested for the neurological score and peak body weight on the same day of the week (Tuesdays). On the following day, the animals were tested with the rotarod (Wednesdays) and on the last day (Thursdays) for grip strength. The experiments were conducted in a dark room, under a red light, when the animals were in their active phase of the day (awake stage).

7.4.1. Neurological score

The neurological score ranges from 0 (no ALS symptomology) to 4 (end stage) and aims to assess the capacity of extension of both hindlimbs of an animal. Criteria used to evaluate each score can be seen in Table 25. [167]. Both hindlimbs of each animal were assessed and the corresponding average was calculated per time point tested. Here the animals were grabbed gently by the tail, while the forelimbs were still grabbing the lid of the cage. Each animal was tail-lifted for 5 seconds and the experiment was conducted 3 times to assure the presence or absence of any symptoms.

**Table 25. ALS neurological score. Adapted from Jackson laboratory guidelines [167].**

Score	Criteria
0	<b>No ALS symptomology:</b> Full extension of the hindlimbs away from the lateral midline when mouse is suspended by its tail, and can hold this for 2 seconds, suspended 2-3 times
1	<b>Initial pre-ALS symptomology:</b> Collapse or partial collapse of the leg extension towards lateral midline (weakness) or trembling of the hindlimbs during tail suspension
2	<b>Definitive neurological disease:</b> Toes curl under at least twice during walking 30.5 cm, or any part of the foot is dragging along the cage bottom
3	<b>Advanced disease:</b> Rigid paralysis or minimal joint movement, foot not being used for forward motion
4	<b>End stage:</b> Mouse cannot right itself within 30 seconds from either side

#### 7.4.2. Peak body weight

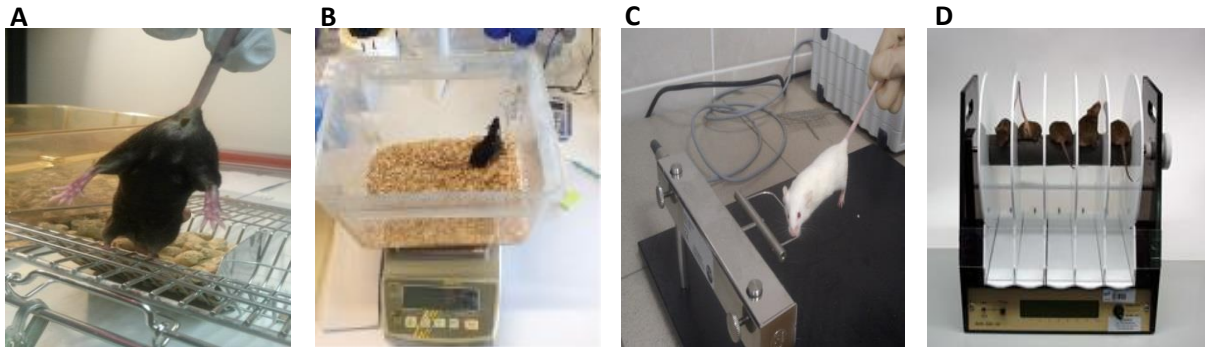
This test comprehends the measurement of the weight of the animals. Since the animals were quite juvenile and therefore changes in body weight happen often, the animals were weighed at 7, 9, 12 and 16 weeks of age. Each animal was put on a calibrated empty cage on top of a balance.

#### 7.4.3. Grip strength

The grip strength test provides a measurement of the strength the mice have in their forelimbs. Each animal was tested per time point three times. The final result per time point is calculated as the average of the three measurements.

#### 7.4.4. Rotarod

The rotarod aims to assess muscle weakness and coordination by measuring the latency to fall of the mice. The mice are put on the rolling part of the device which was adjusted to a starting velocity of 7 rpm. The velocity increases with time to a final value of 34 rpm. The mice are left to run for a maximum of 300s. During the first time, the animals were given a habituation period of 2 trials to get used to the device followed by the real testing. Each mouse was tested three times per time point and an average of the three experiments per time point was done.



**Figure 47. Representative images of the tests applied to the mice to evaluate disease onset and progression.**

(A) Neurological score evaluation. (B) Peak body weight assessment. Muscle weakness/coordination was evaluated by (C) Grip strength and (D) rotarod measurements.

For peak body weight, grip strength and rotarod data processing was done with Excel and statistical analysis in GraphPad Prism 6 software. Each group tested was composed of 8-12 animals. A two-way repeated measurement ANOVA (2-way RM ANOVA) test was used to calculate the significance among genotypes within the same time point and among genotypes at different time points. The Bonferroni's post hoc test was used if a significant difference was found from the analysis of variance. Data is

## 7. Methods

---

presented as mean  $\pm$  SEM and \*, \*\* and \*\*\* indicates a p-value of  $p < 0.05$ ,  $p < 0.01$  and  $p < 0.001$ , respectively.

### 7.5. Muscle dissection and NMJ IHC

The mice were anesthetized with a mixture of Ketamine (*Ketanes<sup>®</sup>*) (12 mg/ml) and Xylazine (*Rompun<sup>®</sup>*) (1.6 mg/ml) and after deep sleep induction, they were perfused with 4% paraformaldehyde (PFA) (Roth, #0335.1) in PBS. The hindlimbs were extracted by cutting at the top of the hip of the animal. The skin was then carefully removed. Post-fixation of the hindlimbs was done in 4% PFA solution for 1h at RT. The samples were washed with PBS and all residual connective tissue was then removed. Muscles suitable for whole-mount (lumbrical muscles) were immediately prepared according to the immunohistochemistry protocol below. The larger muscles that required sectioning (medial gastrocnemius, soleus, and tibialis anterior) were first cryoprotected by immersion in 30% sucrose overnight. After rinsing in 1xPBS, 100 $\mu$ m sections were cut on a freezing microtome.

NMJs were then labeled using a modified laboratory protocol for visualizing pre-synaptic proteins 2H3 or SV2 (medium weight neurofilament/synaptic vesicle protein) and post-synaptic AChRs. Muscles were placed in tetramethylrhodamine- $\alpha$  bungarotoxin (TRIC- $\alpha$ BTX) (1:500) (Biotium) for 30 minutes, followed by incubation with 4% Triton X in PBS for 1h30 and later blocked with blocking solution of 2% Triton X and 4% bovine serum albumin (BSA) in 1x PBS for 30 minutes. The primary antibodies, 2H3 and SV2 (Table 18) (made up in block solution) were incubated for 3 days at 4°C followed by 4 washes of 20 minutes with 1xPBS. The samples were incubated with the secondary antibody, Alexa 488 (Table 19) (made up in 1xPBS) overnight at 4°C. On the following day, the samples were washed 4x for 20 minutes with 1xPBS. Muscles were mounted in Mowiol on glass slides and stored at -20°C prior to imaging.

Quantification was performed on a standard fluorescence microscope. NMJ occupancy was judged as full, partial or vacant (on visual inspection), along with a manual count of the number of axonal inputs per NMJ. 40 NMJs were assessed per muscle. Mean counts for each group were compared by Mann-Whitney test (GraphPad, San Diego, CA). The staining and analysis of the data was done by Dr. Ross A. Jones in collaboration with Prof. Dr. Thomas H. Gillingwater's lab, from the University of Edinburgh, Edinburgh, UK.

### 7.6. RNA isolation via TRAP

The TRAP methodology was adapted from the original protocol from "Cell-Type-Specific mRNA Purification by Translating Ribosome Affinity Purification (TRAP)", [230]. Prior to each experimental procedure of TRAP all the benches and tools used, were cleaned with 70% ethanol (EtOH) and RNase ZAP solution (Ambion, #AM9780) to avoid contamination of samples with foreign RNA.



### 7.6.1. Affinity matrix preparation

300µl per IP of Streptavidin MyOne T1 Dynabeads (Invitrogen, #65602) were transferred to tubes in a magnet on ice. The tubes were left on the magnet for 1min, after which the supernatant was removed and the beads washed with 900µl PBS (Roth, #9150.1). The beads were then incubated with 120µl of Biotinylated Protein L (Fisher, #PI-29997) for 35min at room temperature (RT) on a rotator. The tubes were put on the magnet and the supernatant was removed. The coated beads were washed 5x with 3% IgG and protease-free bovine serum albumin (BSA) solution in PBS.

The beads were re-suspended in 1ml 0.15M KCl buffer (Table 10) and 50ug of 19C8 and 19F7 antibodies (Memorial Sloan Kettering Cancer Center, New York, USA) were added. The mixture was incubated at RT for 1h on a rotator. The supernatant was removed with the help of the magnet and the beads were washed with 0.15M KCl buffer 3x, after which were re-suspended in 200µl of 0.15M KCl buffer. The IPs were stored on ice until the spinal cords were extracted and lysed.

### 7.6.2. Tissue lysate preparation

For this experiment, 5-6 animals per gender and genotype were collected for both time points, pre-symptomatic (9 weeks) and symptomatic (14 weeks) (Table 26).

**Table 26. Number of animals used in the TRAP experiment.**

Time point	Genotype	Females	Males
9 weeks	Chat-BacTrap	6	5
	Chat-BacTrap; hTDP-43	6	5
	Chat-BacTrap; A315T	5	5
14 weeks	Chat-BacTrap	5	5
	Chat-BacTrap; hTDP-43	5	5
	Chat-BacTrap; A315T	5	5

Animals were anesthetized with a mixture of 80% of CO<sub>2</sub> and 20% O<sub>2</sub> prior being euthanized with 100% of CO<sub>2</sub>. Spinal cords were removed and washed with dissection buffer (Table 11). The tissue was then transferred to a glass homogenizer on ice with 1ml of lysis buffer (Table 12). Several strokes were applied (~12) until the tissue was completely homogenized, after which it was transferred to a tube on ice. The homogenate was centrifuge at 4°C for 10min at 2000g. The supernatant was collected to a new tube on ice and 10% NP-40 and 300mM dihexanoylphosphatidylcholine (DHPC) (Avanti, #850306P) were added to a final concentration of 1% and 30mM, respectively.

The mixture was left on ice for 5 min and centrifuged at 4°C for 10min at 20000g. The supernatant was transferred to a new tube on ice. 50µl of each spinal cord lysate was collected as IC and the remaining volume was incubated overnight at 4°C on a rotator with the 200µl of the previously prepared beads. On the second day the beads were washed 4x with 0.35M KCl buffer (Table 13). After the final wash the supernatant was discarded from the beads and 800µl of trizol (Life Technologies, #15596026) was added to both IPs and ICs.

## 7. Methods

---

### 7.6.3. RNA clean up and purification protocol

RNA clean up and purification was executed under the hood. The samples containing the same amount of Trizol were incubated on ice for 5min. When necessary, spike ins (Rluc and Fluc) were added 1ng per sample. 200µl of chloroform per tube was added and the tubes were hand-shaken vigorously for 15sec. The solution was then incubated at RT for 3min followed by 15min centrifugation at 4°C, 12000g.

The upper phase was transferred to a fresh tube and an equal amount of 100% EtOH was added. The mixture was transferred to sterile columns (PureLink RNA kit, Ambion, #121830025, Germany) to purify the RNA. The columns containing the solution were processed according to the protocol provided by the company. The final RNA was then eluted in 60µl of RNA free water (H<sub>2</sub>O) (Ambion, #AM9922).

The purified RNA was treated with DNase I (Roche) to digest DNA, for 15min at 37°C. The RNA was concentrated by an overnight sodium acetate precipitation (68.4µl of 5M sodium acetate (Sigma, #S2889), 347µl of 100% EtOH (Roth, #9065.4), 2µl of GlycoBlue (Ambion, #AM9515)) at -80°C.

On the third day the samples were directly from the -80°C freezer, centrifuged at 13000g for 15min at 4°C. The samples were washed twice with 70% EtOH with a spinning in between at 13000g for 15min at 4°C. The pellets were left to dry at RT for 15min and after re-suspended in 14µl of RNA free water.

### 7.7. RNA concentration determination

The RNA concentration was obtained by measuring the samples on a Nanodrop or by using the Qubit according to the manufacturer's instructions. To correctly nanodrop the samples, it was necessary to run a blank sample (solvent used to dilute the RNA: RNase free water) before running the samples of interest.

When using the Qubit kit, the Qubit working solution was diluted 1:200 in the Qubit buffer (the volume was adjusted to the total number of samples). Samples were diluted 1:200 in the newly prepared working solution, whereas the standard points were diluted 10:200. The prepared solutions were vortexed for 10sec and incubated for 2min at RT followed by measurements on the fluorometer.

### 7.8. cDNA synthesis

The RNA was reverse transcribed to cDNA using Superscript II (Invitrogen, #18064014). The RNA was mixed with 50ng of random primers, 4µl of 2.5mM dNTPs (and H<sub>2</sub>O when necessary) and heated to 65°C for 5min, followed by a cooled down step on ice. Next, 4µl of first strand buffer, 1µl of 0.1M DTT and 2µl of RNasin were added to each sample. The samples were then incubated at 25°C for 2min after which, 1µl of Superscript II was added and the samples were again incubated at 42°C for 50min. The enzyme was heat inactivated when the samples were heated to 70°C for 15min. The enzyme was heat

inactivated by incubating the samples at 70°C for 15min. The RNA strands were digested with 1µl of RNase H, (NEB, #M0297S) for 20min at 37°C and the enzyme was later inactivated by incubation for 10min at 70°C.

### 7.9. Real-time PCR

Real-time PCR primers were selected from pre-design primers from the mouse primer depot website ([www.mouseprimerdepot.nci.nih.gov](http://www.mouseprimerdepot.nci.nih.gov)) (Table 17). The primers were diluted to 100 pmol/µl and kept as stock. 24µl of forward and 24µl of reverse primers were added to 1952µl of RNA free H<sub>2</sub>O in order to have a stock with both primers (primer mix) for each gene of interest. The cDNA was diluted 1:5 in H<sub>2</sub>O. 5µl of diluted cDNA was pipetted to each well of the plate together with 5µl of the primer mix and with 10µl of FastStart Universal SYBR Green Master ROX (Roche, #04913914001) to a final volume of 20µl. Each sample had between 2-3 biological replicates. The plate was sealed and spun down. The real-time PCR was performed on the 7900HT Fast Real-time PCR machine. The real-time PCR protocol consisted in:

**Table 27. Real-time PCR protocol.**

Step	Thermoprofile	Time (min:sec)	Temperature (°C)	n. of cycles
1	Initial denaturation	2	50	1x
2	Denaturation	10	95	1x
3	Denaturation	0:15	95	40x
	Annealing	1	60	
4	Final extension	0:15	95	1x
		0:15	60	
		0:15	95	

Biological replicates with more than 0.5 CT different from the mean of the biological replicates was excluded from analysis. A minimum of 3 replicates was considered for statistical analysis. Excel was used to calculate the significance by applying T-test. Data is presented as mean ± SEM and \*, \*\* and \*\*\* indicates a p-value of p<0.05, p<0.01 and p<0.001, respectively.

### 7. 10. Sequencing

The sequencing of the TRAP samples was done in collaboration with Dr. Gabriela Salinas and Dr. Thomas Lingner from the TAL facility, UMG, Göttingen, Germany. Here, the RNA samples were prepared with the "TruSeq RNA Sample Prep Kit v2" according to the manufacturer's protocol (Illumina). 50bp single-end sequencing was conducted using a HiSeq 4000 (Illumina).

### 7.11. Bioinformatics

The data mining of the sequencing was done by Dr. Jan Broder Engler from INIMS, ZMNH, Hamburg, Germany.

Samples were de-multiplexed with *bcl2fastq2* (Illumina, version 2.17) and sequencing quality was checked with the *FastQC* software ([www.bioinformatics.babraham.ac.uk/projects/fastqc/](http://www.bioinformatics.babraham.ac.uk/projects/fastqc/)).

Sequencing reads were aligned to the genome reference sequence of *Mus musculus* (assembly version GRCm38, downloaded from [www.ensembl.org](http://www.ensembl.org)) using the *STAR* software package (PMID: 23104886, version 2.5), allowing up to 2 mismatches in 51bp. Quantification of gene expression was performed with the *featureCounts* program (PMID: 24227677, version 1.4.5) in standard configuration.

The resulting read count files were pre-processed and analyzed in the R/Bioconductor environment using the *DESeq2* package (PMID: 25516281, version 1.8.2). Specifically, the data were normalized and tested for differentially expressed genes based on a generalized linear model likelihood ratio test assuming negative binomial data distribution. Adjusted p-values in *DESeq2* are calculated in terms of false discovery rate values (FDR). Candidates for differential gene expression were identified using a log<sub>2</sub>-fold-change cutoff of -1/+1 and an adjusted p-value cutoff (FDR) of 0.05. Here, we evaluated the comparison of genotypes (e.g. (1) Chat-bacTrap vs. Chat-bacTrap; A315T and (2) Chat-bacTrap; hTDP-43 vs. Chat-bacTrap; A315T) and time points ((3) 9 weeks vs. 14 weeks for the Chat-bacTrap; A315T). The candidate sets of (1) and (2) were overlapped to identify genes which are exclusively up-/downregulated in the mutant (Chat-bacTRAP; A315T) at 14 weeks. Overlap venn diagrams were created using the Venny tool (<http://bioinfoq.cnb.csic.es/tools/venny/index.html>). Gene annotation was performed using *Mus musculus* entries from Ensembl (PMID: 27899575) via the biomaRt package (PMID: 19617889, version 2.24.1).

Functional enrichment of the exclusive candidates in terms of GO biological processes and KEGG pathways was determined using the DAVID web server for gene functional annotation (PMID: 19131956, version 6.8). Furthermore, reactome pathway analysis (PMID: 26656494) four *Mus musculus* pathways was carried out on these lists.

### 7.12. IHC

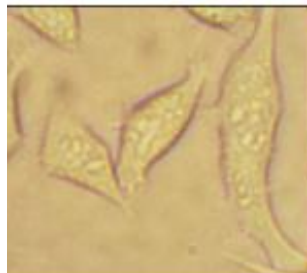
The mice were anesthetized with a mixture of Ketamine (*Ketanest*<sup>®</sup>) (12 mg/ml) and Xylazine (*Rompun*<sup>®</sup>) (1.6 mg/ml) and after deep sleep induction, they were perfused with 4% PFA in PBS. Post-fixation of the spinal cord was done in 4% PFA solution for 2h at RT, after which the tissue was incubated in 20% sucrose solution until it sank completely. The tissue was then cut in 3 parts, corresponding to the cervical, thoracic and lumbar regions of the spinal cord and embedded in Tissue-Tek (Sakura, #4583) prior to storage at -80°C.

Sections of the lumbar part of the spinal cord were further cut on a cryostat with a width of 12 $\mu$ m. The tissue was blocked with 10% normal donkey serum (Jackson Immuno Research, #017-000-121) in 0.1% triton X100 in PBS at RT for 45min. The antibodies against NeuN, PLEKHB1, SYNGR4 and ChAT (see Table 18) were diluted in 0.1% triton X100 in PBS solution and left overnight at 4°C. On the next day, the slices were washed 3x with PBS and incubated with secondary antibodies (Alexa 647, Alexa 555 and Alexa 488, Table 19), in 1x PBS for 3h at RT. After the incubation period, the slices were washed 3x with PBS. The slides were incubated with DAPI (1:1000) (Thermo fisher, #62248) in PBS for 10min and embedded in Roti mounting medium before sealing of the slide. The slices were stored at -20°C. Images were acquired with a Zeiss LSM 700 microscope and processed using ImageJ Fiji. A total of 5-6 images per experiment were taken and a total of 4-5 age matched animals per genotype were used.

Statistical analysis was done using GraphPad Prism 6 software. Significance was calculated by applying a paired-test. Data is presented as mean  $\pm$  SEM and \*, \*\* and \*\*\* indicates a p-value of  $p < 0.05$ ,  $p < 0.01$  and  $p < 0.001$ , respectively.

### 7.13. MN1 cell culture

MN1 cells result from the fusion of a neuroblastoma cell line with a cell line of murine MNs (Figure 48). This fusion originated an immortalized cell line with characteristics of MN-like cells. Within these characteristics lies the appearance of extended neurites and the production of choline acetyltransferase (ChAT), a protein used to identify MNs [231]. This cell line was selected due to the fact that TDP-43 is altered in MNs of ALS patients. The usage of this cell line aims to overcome possible deficits of starting material needed for the proof of concept of the development of the method Gradient-TRAP.



**Figure 48. MN1 cells in culture medium.**

#### 7.13.1. Maintenance of the MN1 cell culture

MN1 cells were grown in T-175 flasks (Sarstedt, #83.3912.002) supplement with D-MEM high glucose GlutaMAX (Gibco, #61965-026) culture medium (Table 14) and incubated at 37°C with 5% CO<sub>2</sub>, in an incubator. The cells were passaged to a new flask every 2-3 days when a confluence of 80-90% was reached. Before each passage, the old medium was removed and the cells on the T-flask were washed with 1x warmed sterile PBS. Next, the cells were removed from the flask with 0.05% Trypsin-EDTA

(Gibco, #25300-054) after 3min incubation at 37°C, by tapping on the sides of the T-flask. Trypsin-EDTA solution was inactivated by adding an excess of fresh medium to the cells. 10-20% of the volume was moved to a new flask containing pre-warmed medium. The flask was swirled to allow an even distribution of the cells and returned to the incubator.

### 7.13.2. Preservation and usage of the MN1 cell line

Cells were collected from a confluent flask, counted using a , spun down and re-suspended in freezing medium (final concentration:  $1 \times 10^6$  cells/ml). The freezing medium consists of 60% growth medium, 30% FBS and 10% dimethyl sulfoxide (DMSO) (Thermo fisher, #85190). The cells were aliquoted in CryoPure tubes (Sarstedt, #72.379.007) and placed in a Cryo 1°C freezer container (Nalgene, #5100-0001). For long-term storage, the vials containing the cells were put in liquid nitrogen cryo tanks.

Frozen cells were thawed by quick transfer of the vial from the cryo tank to a 37°C water bath, where it was swirled until complete thawed of the liquid. Pre-warm growth medium was added to the thawed cells and the new mixture was transferred to a 15ml falcon tube containing growth medium to a total volume of 10ml and centrifuged at 1500rcf for 5min at RT. This step allows removing DMSO which is a toxic agent to the cells. The medium was removed and the pellet re-suspended in 1ml of growth medium and transferred to 25 T-flask. Once the flask was confluent, the cells were transferred to a T-175 flask.

### 7.13.3. Transfection of MN1 cells

In the context of developing the method Gradient-TRAP, the cells were transferred with pEGFP-C2 plasmid (Clontech) or pEGFP-C2 plasmid containing the L10a sequence (kindly provided by Nathaniel Heintz and Myriam Heiman). To obtain transiently transfected cells,  $2 \times 10^6$  cells were plated in 10cm dishes in growth medium on the day prior to the transfection (equivalent to 30% confluency) in order to obtain 60-70% confluence of cells for transfection. Effectene transfection reagent (Qiagen, #301427) was used according to the manufacturer's instructions. Briefly, 2ug of plasmid DNA was diluted in buffer EC up to a total volume of 300ul. 16ul of enhancer was added to the mixture which was vortexed for 10sec followed by incubation at RT for 5min. 60μl of Effectene transfection reagent was added to the DNA-enhancer mixture which was again vortexed for 10sec and incubated at RT for 10min. During this incubation period the growth medium of the dishes containing the cells was removed and cells were washed once with pre-warmed PBS, followed by addition of 7ml of fresh, pre-warmed growth medium. After the incubation period, 3ml of growth medium was added to the DNA-enhancer mixture. The final mixture was added dropwise to the dishes which were then swirled and returned to the incubator. 24h after the transfection the cells were ready to be used.

#### 7.14. Oxidative stress induction in MN1 cells

24h after transfection the plated cells were treated with SA (Sigma, #57400) at different times of exposure and with different concentrations of SA (0min, 15min, 30min, 1h, 2h, 3h, 4h and 0 $\mu$ m, 20 $\mu$ m, 40 $\mu$ m and 80 $\mu$ m, respectively) in order to identify the best conditions. The readout method was western blot for protein level detection (described in 7.3.) and real-time PCR for RNA level detection (described in 7.9.).

#### 7.15. Polysome profiling from MN1 cells

of lysis buffer (Table 15). The cells were scraped from the plates and incubated on ice for 10min. Lysates were triturated with a 27G needle and then centrifuged at 20,000g for 10min at 4°C. The supernatant was collected to a new tube.

OD260 units were measured either by using the Nanodrop or the Qubit as described in section 7.7. The RNA concentration was normalized to the sample containing the lowest value to ensure as little bias as possible.

Once the lysates was prepared, the sucrose gradients were formed and cooled at 4°C. First, fresh sucrose solutions of 17.5% and 50% were made in gradient buffer (Table 15). Using a cannula, the open-top polyclear centrifuge tube (Seton, #7031) was filled with the low-density sucrose solution, 17.5% up to the half. Using a second cannula, the high-density sucrose solution was layered slowly below the low-density solution up to the half of the tube. Tubes were capped and formed into a gradient using the SHORT Sucr 17-50% wv setting on the gradient former (Figure 49).



**Figure 49. Gradient former from BioComp.**

After forming the gradients, these were carefully weighed on a balance to ensure that they all have the same weight. The same amount of the normalized lysates was afterwards loaded onto the tubes containing the gradients. The loaded gradients were ultracentrifuged in a SW40Ti rotor at 35000rpm for 2h15min at 4°C. After centrifugation the tubes were kept at 4°C until their fractionation.

The gradients were fractionated using a Piston Gradient Fractionator (Figure 50). The samples were fractionated from the top to the bottom of the tube. The piston was set to move at 0.3mm/sec per sample, resulting in the gradient being collected in 27 tubes each containing approximately 500 $\mu$ l of

volume. As samples were being fractionated, they passed through a UV monitor which is set to absorb at 254nm in order to measure RNA absorbance. The final absorbance readouts were transmitter to and processed into a graph form by using the gradient profile program.

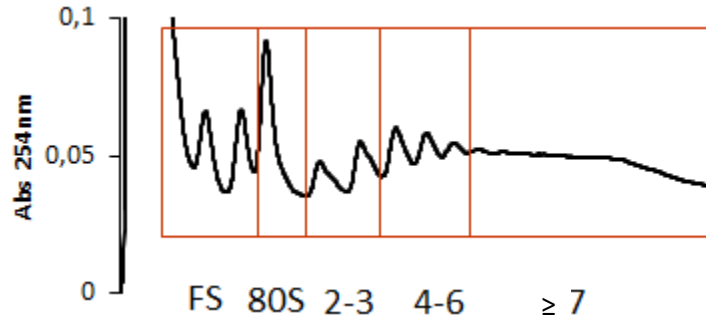


**Figure 50. Piston Gradient Fractionator.**

The fractionator allows to fractionate gradients by letting the sample pass through a UV monitor (not shown) to determine the RNA levels of each fraction. Adapted from [232].

7.15.1. Strategy to pool the fractions

After fractionation, fractions were pooled according to the scheme presented in Figure 51. RNA was purified as detailed in 7.6.3 and genes of interest were analyzed via real-time PCR as described in 7.8 and 7.9.



**Figure 51. Scheme of the pooled RNA fractions.**

The RNA from each fraction was pooled according to the number of ribosomes on the mRNA. Legend: FS: free subunits, 80S: monosome, 2-3: disome to trisome, 4-6: between 4 to 6 ribosomes on the mRNA and  $\geq 7$ : 7 or more ribosomes on the mRNA.



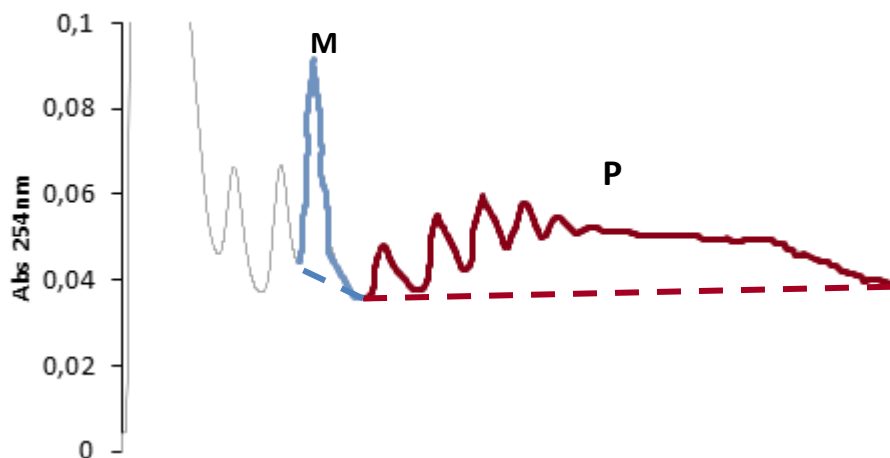
### 7.16. Polysome profiling from spinal cord

Polysome profiling was also done from mouse spinal cord. One single spinal cord vs three pooled spinal cords were tested in order to establish the best conditions to have a clear profile and RNA to be extracted from the fractions in amounts that can be downstream analyzed. The spinal cord lysates were obtained by following the protocol in 7.6.2. RNA concentration determination, loading of the sample onto the gradients, ultracentrifugation and fractionation was done as described above in section 7.15.

### 7.17. Monosome to polysome calculation

The monosome to polysome (M/P) ratio provides information about translation regulation by indicating if there is an increase or a decrease in ribosome density when comparing to the control group. An increase in the M/P ratio is indicative of a decrease in ribosome density on the mRNAs and consequently a reduction in overall translation. On the other hand, a decrease in the M/P ratio indicates that there are more ribosomes bound to mRNAs, typically reflecting an increase in overall translation levels or slower elongation and/or enhanced ribosome stalling.

M/P ratios were calculated by drawing a line below the monosome peak across the polysome profile. A vertical line was drawn at the lowest point between the monosome and disome peaks allowing to calculate the exact area beneath the monosome and the remaining polysomes (Figure 52). These areas are calculated using ImageJ to count the pixels. Once the areas were calculated, the ratio can be calculated and subsequently compared among all the samples.



**Figure 52. A representative profile where the monosome (M) and polysome (P) areas are highlighted.**

The M/P ratio was calculated by measuring the area of the M, represented in blue color and the area of the P, represented in red color. The areas were measured by ImageJ software.

Statistical analysis was performed for multiple (minimum 3) repetitions of the same type of experiment. GraphPad Prism 6 software was used to calculate the significance by applying the two tailed T-test. Data are presented as mean  $\pm$  SEM and \*, \*\* and \*\*\* indicates a p-value of  $p < 0.05$ ,  $p < 0.01$  and  $p < 0.001$ , respectively.

### 7.18. Gradient-TRAP

Gradient-TRAP combines both polysome profiling and TRAP. This method was developed with both MN1 cells, as proof of concept, and mouse spinal cord tissue.

#### 7.18.1. Gradient-TRAP from MN1 cells

MN1 cell lysates were prepared according to the previous described protocol in section 7.13.3 and 7.14 and the polysome profiles were obtained also as described in section 7.15. The fractions were pooled as in section 7.15.1. Once the fractions were pooled, the samples were stored at  $-80^{\circ}\text{C}$ , until the affinity matrix for TRAP was prepared.

The protocol for TRAP was followed as described in section 7.6, with some adjustments. Due to the high volume from the pooled fractions the immunoprecipitation was done in 15ml falcon tubes instead of the 1.5ml eppendorf tubes. From this step on all the volumes of the reagents and buffers were adjusted to the new volume of sample. The RNA was extracted, purified and analyzed as in sections 7.7, 7.8 and 7.9.

#### 7.18.2. Gradient-TRAP from spinal cord

After testing one spinal cord vs three pooled spinal cords, it was observed that to obtain optimized data from polysome profile it is necessary to work with the pooled version of the method. Hence, for Gradient-TRAP, three spinal cords were always pooled and the polysome profile were obtained as described in section 7.1.5. Like done for MN1 cells, after the pooling of the fractions (section 7.14.1), the lysed tissue was stored at  $-80^{\circ}\text{C}$ , until the affinity matrix for TRAP was ready.

In the same line, the protocol for TRAP was followed as described in section 7.5, with the same adjustments as for MN1 cells. The RNA was extracted, purified and analyzed as in sections 7.7, 7.8 and 7.9.

## **8. Bibliography**



## 8. Bibliography

1. Rowland, L.P. and N.A. Shneider, *Amyotrophic lateral sclerosis*. N Engl J Med, 2001. **344**(22): p. 1688-700.
2. Tandan, R. and W.G. Bradley, *Amyotrophic lateral sclerosis: Part 1. Clinical features, pathology, and ethical issues in management*. Ann Neurol, 1985. **18**(3): p. 271-80.
3. Stifani, N., *Motor neurons and the generation of spinal motor neuron diversity*. Front Cell Neurosci, 2014. **8**: p. 293.
4. Brown, R.H. and A. Al-Chalabi, *Amyotrophic Lateral Sclerosis*. N Engl J Med, 2017. **377**(2): p. 162-172.
5. Mulder, D.W., *Clinical limits of amyotrophic lateral sclerosis*. Adv Neurol, 1982. **36**: p. 15-22.
6. Taylor, J.P., R.H. Brown, Jr., and D.W. Cleveland, *Decoding ALS: from genes to mechanism*. Nature, 2016. **539**(7628): p. 197-206.
7. Cote, M.P., L.M. Murray, and M. Knikou, *Spinal Control of Locomotion: Individual Neurons, Their Circuits and Functions*. Front Physiol, 2018. **9**: p. 784.
8. Pasinelli, P. and R.H. Brown, *Molecular biology of amyotrophic lateral sclerosis: insights from genetics*. Nat Rev Neurosci, 2006. **7**(9): p. 710-23.
9. McCombe, P.A. and R.D. Henderson, *Effects of gender in amyotrophic lateral sclerosis*. Gend Med, 2010. **7**(6): p. 557-70.
10. Wijesekera, L.C. and P.N. Leigh, *Amyotrophic lateral sclerosis*. Orphanet J Rare Dis, 2009. **4**: p. 3.
11. Fang, F., et al., *Amyotrophic lateral sclerosis in Sweden, 1991-2005*. Arch Neurol, 2009. **66**(4): p. 515-9.
12. Bonaparte, J.P., et al., *ALS incidence in Nova Scotia over a 20-year-period: a prospective study*. Can J Neurol Sci, 2007. **34**(1): p. 69-73.
13. Tobin, K., et al., *Age-period-cohort analysis of trends in amyotrophic lateral sclerosis incidence*. J Neurol, 2016. **263**(10): p. 1919-26.
14. Miller, R.G., J.D. Mitchell, and D.H. Moore, *Riluzole for amyotrophic lateral sclerosis (ALS)/motor neuron disease (MND)*. Cochrane Database Syst Rev, 2012(3): p. CD001447.
15. Dharmadasa, T. and M.C. Kiernan, *Riluzole, disease stage and survival in ALS*. Lancet Neurol, 2018. **17**(5): p. 385-386.
16. Cruz, M.P., *Edaravone (Radicava): A Novel Neuroprotective Agent for the Treatment of Amyotrophic Lateral Sclerosis*. P T, 2018. **43**(1): p. 25-28.
17. Rothstein, J.D., *Edaravone: A new drug approved for ALS*. Cell, 2017. **171**(4): p. 725.
18. Ikeda, K. and Y. Iwasaki, *Edaravone, a Free Radical Scavenger, Delayed Symptomatic and Pathological Progression of Motor Neuron Disease in the Wobbler Mouse*. PLoS One, 2015. **10**(10): p. e0140316.
19. Nagase, M., et al., *Increased oxidative stress in patients with amyotrophic lateral sclerosis and the effect of edaravone administration*. Redox Rep, 2016. **21**(3): p. 104-12.
20. Cleveland, D.W. and J.D. Rothstein, *From Charcot to Lou Gehrig: deciphering selective motor neuron death in ALS*. Nat Rev Neurosci, 2001. **2**(11): p. 806-19.
21. *Amyotrophic lateral sclerosis and other motor neuron diseases*. Adv Neurol, 1991. **56**: p. 1-546.
22. Turner, M.R., et al., *Controversies and priorities in amyotrophic lateral sclerosis*. Lancet Neurol, 2013. **12**(3): p. 310-22.
23. Chen, S., et al., *Genetics of amyotrophic lateral sclerosis: an update*. Mol Neurodegener, 2013. **8**: p. 28.
24. Al-Chalabi, A. and P.M. Visscher, *Motor neuron disease: Common genetic variants and the heritability of ALS*. Nat Rev Neurol, 2014. **10**(10): p. 549-50.

## 8. Bibliography

---

25. Therrien, M., P.A. Dion, and G.A. Rouleau, *ALS: Recent Developments from Genetics Studies*. Curr Neurol Neurosci Rep, 2016. **16**(6): p. 59.
26. Rosen, D.R., et al., *Mutations in Cu/Zn superoxide dismutase gene are associated with familial amyotrophic lateral sclerosis*. Nature, 1993. **362**(6415): p. 59-62.
27. Pardo, C.A., et al., *Superoxide dismutase is an abundant component in cell bodies, dendrites, and axons of motor neurons and in a subset of other neurons*. Proc Natl Acad Sci U S A, 1995. **92**(4): p. 954-8.
28. Radunovic, A., et al., *Copper and zinc levels in familial amyotrophic lateral sclerosis patients with CuZnSOD gene mutations*. Ann Neurol, 1997. **42**(1): p. 130-1.
29. Rotunno, M.S. and D.A. Bosco, *An emerging role for misfolded wild-type SOD1 in sporadic ALS pathogenesis*. Front Cell Neurosci, 2013. **7**: p. 253.
30. Shibata, N., et al., *Cu/Zn superoxide dismutase-like immunoreactivity in Lewy body-like inclusions of sporadic amyotrophic lateral sclerosis*. Neurosci Lett, 1994. **179**(1-2): p. 149-52.
31. Shibata, N., et al., *Immunohistochemical study on superoxide dismutases in spinal cords from autopsied patients with amyotrophic lateral sclerosis*. Dev Neurosci, 1996. **18**(5-6): p. 492-8.
32. McAlary, L., J.A. Aquilina, and J.J. Yerbury, *Susceptibility of Mutant SOD1 to Form a Destabilized Monomer Predicts Cellular Aggregation and Toxicity but Not In vitro Aggregation Propensity*. Front Neurosci, 2016. **10**: p. 499.
33. Mackenzie, I.R., et al., *Pathological TDP-43 distinguishes sporadic amyotrophic lateral sclerosis from amyotrophic lateral sclerosis with SOD1 mutations*. Ann Neurol, 2007. **61**(5): p. 427-34.
34. Peters, O.M., M. Ghasemi, and R.H. Brown, Jr., *Emerging mechanisms of molecular pathology in ALS*. J Clin Invest, 2015. **125**(6): p. 2548.
35. Neumann, M., et al., *Ubiquitinated TDP-43 in frontotemporal lobar degeneration and amyotrophic lateral sclerosis*. Science, 2006. **314**(5796): p. 130-3.
36. Arai, T., et al., *TDP-43 is a component of ubiquitin-positive tau-negative inclusions in frontotemporal lobar degeneration and amyotrophic lateral sclerosis*. Biochem Biophys Res Commun, 2006. **351**(3): p. 602-11.
37. Kabashi, E., et al., *TARDBP mutations in individuals with sporadic and familial amyotrophic lateral sclerosis*. Nat Genet, 2008. **40**(5): p. 572-4.
38. Sreedharan, J., et al., *TDP-43 mutations in familial and sporadic amyotrophic lateral sclerosis*. Science, 2008. **319**(5870): p. 1668-72.
39. Deng, H.X., et al., *FUS-immunoreactive inclusions are a common feature in sporadic and non-SOD1 familial amyotrophic lateral sclerosis*. Ann Neurol, 2010. **67**(6): p. 739-48.
40. Deng, H.X., et al., *Mutations in UBQLN2 cause dominant X-linked juvenile and adult-onset ALS and ALS/dementia*. Nature, 2011. **477**(7363): p. 211-5.
41. Schipper, L.J., et al., *Prevalence of brain and spinal cord inclusions, including dipeptide repeat proteins, in patients with the C9ORF72 hexanucleotide repeat expansion: a systematic neuropathological review*. Neuropathol Appl Neurobiol, 2016. **42**(6): p. 547-60.
42. Ramesh, N. and U.B. Pandey, *Autophagy Dysregulation in ALS: When Protein Aggregates Get Out of Hand*. Front Mol Neurosci, 2017. **10**: p. 263.
43. Williams, K.L., et al., *UBQLN2/ubiquilin 2 mutation and pathology in familial amyotrophic lateral sclerosis*. Neurobiol Aging, 2012. **33**(10): p. 2527 e3-10.
44. Nishimura, A.L., et al., *A mutation in the vesicle-trafficking protein VAPB causes late-onset spinal muscular atrophy and amyotrophic lateral sclerosis*. Am J Hum Genet, 2004. **75**(5): p. 822-31.
45. Chen, H.J., et al., *Characterization of the properties of a novel mutation in VAPB in familial amyotrophic lateral sclerosis*. J Biol Chem, 2010. **285**(51): p. 40266-81.
46. Tsuji, S., *The neurogenomics view of neurological diseases*. JAMA Neurol, 2013. **70**(6): p. 689-94.

47. Turner, M.R., et al., *Genetic screening in sporadic ALS and FTD*. J Neurol Neurosurg Psychiatry, 2017. **88**(12): p. 1042-1044.
48. Laferriere, F. and M. Polymenidou, *Advances and challenges in understanding the multifaceted pathogenesis of amyotrophic lateral sclerosis*. Swiss Med Wkly, 2015. **145**: p. w14054.
49. Su, X.W., et al., *Genetic heterogeneity of amyotrophic lateral sclerosis: implications for clinical practice and research*. Muscle Nerve, 2014. **49**(6): p. 786-803.
50. Riancho, J., et al., *The increasing importance of environmental conditions in amyotrophic lateral sclerosis*. Int J Biometeorol, 2018.
51. Van Damme, P., W. Robberecht, and L. Van Den Bosch, *Modelling amyotrophic lateral sclerosis: progress and possibilities*. Dis Model Mech, 2017. **10**(5): p. 537-549.
52. Turner, M.R., et al., *Mechanisms, models and biomarkers in amyotrophic lateral sclerosis*. Amyotroph Lateral Scler Frontotemporal Degener, 2013. **14 Suppl 1**: p. 19-32.
53. Sabatelli, M., A. Conte, and M. Zollino, *Clinical and genetic heterogeneity of amyotrophic lateral sclerosis*. Clin Genet, 2013. **83**(5): p. 408-16.
54. Huang, C., et al., *Mutant TDP-43 in motor neurons promotes the onset and progression of ALS in rats*. J Clin Invest, 2012. **122**(1): p. 107-18.
55. Voigt, A., et al., *TDP-43-mediated neuron loss in vivo requires RNA-binding activity*. PLoS One, 2010. **5**(8): p. e12247.
56. Arnold, E.S., et al., *ALS-linked TDP-43 mutations produce aberrant RNA splicing and adult-onset motor neuron disease without aggregation or loss of nuclear TDP-43*. Proc Natl Acad Sci U S A, 2013. **110**(8): p. E736-45.
57. Ilieva, H., M. Polymenidou, and D.W. Cleveland, *Non-cell autonomous toxicity in neurodegenerative disorders: ALS and beyond*. J Cell Biol, 2009. **187**(6): p. 761-72.
58. Polymenidou, M., et al., *Misregulated RNA processing in amyotrophic lateral sclerosis*. Brain Res, 2012. **1462**: p. 3-15.
59. Corcia, P., et al., *Phenotype and genotype analysis in amyotrophic lateral sclerosis with TARDBP gene mutations*. Neurology, 2012. **78**(19): p. 1519-26.
60. Ayala, Y.M., et al., *Structural determinants of the cellular localization and shuttling of TDP-43*. J Cell Sci, 2008. **121**(Pt 22): p. 3778-85.
61. la Cour, T., et al., *Analysis and prediction of leucine-rich nuclear export signals*. Protein Eng Des Sel, 2004. **17**(6): p. 527-36.
62. Sun, Y. and A. Chakrabartty, *Phase to Phase with TDP-43*. Biochemistry, 2017. **56**(6): p. 809-823.
63. King, O.D., A.D. Gitler, and J. Shorter, *The tip of the iceberg: RNA-binding proteins with prion-like domains in neurodegenerative disease*. Brain Res, 2012. **1462**: p. 61-80.
64. Lagier-Tourenne, C., M. Polymenidou, and D.W. Cleveland, *TDP-43 and FUS/TLS: emerging roles in RNA processing and neurodegeneration*. Hum Mol Genet, 2010. **19**(R1): p. R46-64.
65. March, Z.M., O.D. King, and J. Shorter, *Prion-like domains as epigenetic regulators, scaffolds for subcellular organization, and drivers of neurodegenerative disease*. Brain Res, 2016. **1647**: p. 9-18.
66. Kawahara, Y. and A. Mieda-Sato, *TDP-43 promotes microRNA biogenesis as a component of the Drosha and Dicer complexes*. Proc Natl Acad Sci U S A, 2012. **109**(9): p. 3347-52.
67. Buratti, E., et al., *TDP-43 binds heterogeneous nuclear ribonucleoprotein A/B through its C-terminal tail: an important region for the inhibition of cystic fibrosis transmembrane conductance regulator exon 9 splicing*. J Biol Chem, 2005. **280**(45): p. 37572-84.
68. D'Ambrogio, A., et al., *Functional mapping of the interaction between TDP-43 and hnRNP A2 in vivo*. Nucleic Acids Res, 2009. **37**(12): p. 4116-26.
69. Sun, Y., et al., *Binding of TDP-43 to the 3'UTR of its cognate mRNA enhances its solubility*. Biochemistry, 2014. **53**(37): p. 5885-94.

70. Wang, I.F., et al., *The self-interaction of native TDP-43 C terminus inhibits its degradation and contributes to early proteinopathies*. Nat Commun, 2012. **3**: p. 766.
71. Zhang, Y.J., et al., *The dual functions of the extreme N-terminus of TDP-43 in regulating its biological activity and inclusion formation*. Hum Mol Genet, 2013. **22**(15): p. 3112-22.
72. Chang, C.K., et al., *The N-terminus of TDP-43 promotes its oligomerization and enhances DNA binding affinity*. Biochem Biophys Res Commun, 2012. **425**(2): p. 219-24.
73. Harrison, A.F. and J. Shorter, *RNA-binding proteins with prion-like domains in health and disease*. Biochem J, 2017. **474**(8): p. 1417-1438.
74. Ou, S.H., et al., *Cloning and characterization of a novel cellular protein, TDP-43, that binds to human immunodeficiency virus type 1 TAR DNA sequence motifs*. J Virol, 1995. **69**(6): p. 3584-96.
75. Cohen, T.J., V.M. Lee, and J.Q. Trojanowski, *TDP-43 functions and pathogenic mechanisms implicated in TDP-43 proteinopathies*. Trends Mol Med, 2011. **17**(11): p. 659-67.
76. Ling, S.C., M. Polymenidou, and D.W. Cleveland, *Converging mechanisms in ALS and FTD: disrupted RNA and protein homeostasis*. Neuron, 2013. **79**(3): p. 416-38.
77. Bhardwaj, A., et al., *Characterizing TDP-43 interaction with its RNA targets*. Nucleic Acids Res, 2013. **41**(9): p. 5062-74.
78. Polymenidou, M., et al., *Long pre-mRNA depletion and RNA missplicing contribute to neuronal vulnerability from loss of TDP-43*. Nat Neurosci, 2011. **14**(4): p. 459-68.
79. Tollervey, J.R., et al., *Characterizing the RNA targets and position-dependent splicing regulation by TDP-43*. Nat Neurosci, 2011. **14**(4): p. 452-8.
80. Buratti, E. and F.E. Baralle, *Characterization and functional implications of the RNA binding properties of nuclear factor TDP-43, a novel splicing regulator of CFTR exon 9*. J Biol Chem, 2001. **276**(39): p. 36337-43.
81. Ayala, Y.M., et al., *TDP-43 regulates its mRNA levels through a negative feedback loop*. EMBO J, 2011. **30**(2): p. 277-88.
82. Budini, M. and E. Buratti, *TDP-43 autoregulation: implications for disease*. J Mol Neurosci, 2011. **45**(3): p. 473-9.
83. Pesiridis, G.S., et al., *A "two-hit" hypothesis for inclusion formation by carboxyl-terminal fragments of TDP-43 protein linked to RNA depletion and impaired microtubule-dependent transport*. J Biol Chem, 2011. **286**(21): p. 18845-55.
84. Udan-Johns, M., et al., *Prion-like nuclear aggregation of TDP-43 during heat shock is regulated by HSP40/70 chaperones*. Hum Mol Genet, 2014. **23**(1): p. 157-70.
85. McDonald, K.K., et al., *TAR DNA-binding protein 43 (TDP-43) regulates stress granule dynamics via differential regulation of G3BP and TIA-1*. Hum Mol Genet, 2011. **20**(7): p. 1400-10.
86. Parker, S.J., et al., *Endogenous TDP-43 localized to stress granules can subsequently form protein aggregates*. Neurochem Int, 2012. **60**(4): p. 415-24.
87. Anderson, P. and N. Kedersha, *RNA granules: post-transcriptional and epigenetic modulators of gene expression*. Nat Rev Mol Cell Biol, 2009. **10**(6): p. 430-6.
88. Jain, S., et al., *ATPase-Modulated Stress Granules Contain a Diverse Proteome and Substructure*. Cell, 2016. **164**(3): p. 487-98.
89. Wolozin, B., *Regulated protein aggregation: stress granules and neurodegeneration*. Mol Neurodegener, 2012. **7**: p. 56.
90. Li, Y.R., et al., *Stress granules as crucibles of ALS pathogenesis*. J Cell Biol, 2013. **201**(3): p. 361-72.
91. Bentmann, E., C. Haass, and D. Dormann, *Stress granules in neurodegeneration--lessons learnt from TAR DNA binding protein of 43 kDa and fused in sarcoma*. FEBS J, 2013. **280**(18): p. 4348-70.
92. Wu, L.S., et al., *TDP-43, a neuro-pathosignature factor, is essential for early mouse embryogenesis*. Genesis, 2010. **48**(1): p. 56-62.



93. Sephton, C.F., et al., *TDP-43 is a developmentally regulated protein essential for early embryonic development*. J Biol Chem, 2010. **285**(9): p. 6826-34.
94. Dammer, E.B., et al., *Coaggregation of RNA-binding proteins in a model of TDP-43 proteinopathy with selective RGG motif methylation and a role for RRM1 ubiquitination*. PLoS One, 2012. **7**(6): p. e38658.
95. Giordana, M.T., et al., *TDP-43 redistribution is an early event in sporadic amyotrophic lateral sclerosis*. Brain Pathol, 2010. **20**(2): p. 351-60.
96. Dormann, D. and C. Haass, *TDP-43 and FUS: a nuclear affair*. Trends Neurosci, 2011. **34**(7): p. 339-48.
97. Johnson, B.S., et al., *TDP-43 is intrinsically aggregation-prone, and amyotrophic lateral sclerosis-linked mutations accelerate aggregation and increase toxicity*. J Biol Chem, 2009. **284**(30): p. 20329-39.
98. Barmada, S.J., et al., *Cytoplasmic mislocalization of TDP-43 is toxic to neurons and enhanced by a mutation associated with familial amyotrophic lateral sclerosis*. J Neurosci, 2010. **30**(2): p. 639-49.
99. Halliday, G., et al., *Mechanisms of disease in frontotemporal lobar degeneration: gain of function versus loss of function effects*. Acta Neuropathol, 2012. **124**(3): p. 373-82.
100. Xu, Z. and C. Yang, *TDP-43-The key to understanding amyotrophic lateral sclerosis*. Rare Dis, 2014. **2**(1): p. e944443.
101. Wang, W., et al., *The inhibition of TDP-43 mitochondrial localization blocks its neuronal toxicity*. Nat Med, 2016. **22**(8): p. 869-78.
102. Wang, I.F., et al., *TDP-43, the signature protein of FTLD-U, is a neuronal activity-responsive factor*. J Neurochem, 2008. **105**(3): p. 797-806.
103. Liu-Yesucevitz, L., et al., *ALS-linked mutations enlarge TDP-43-enriched neuronal RNA granules in the dendritic arbor*. J Neurosci, 2014. **34**(12): p. 4167-74.
104. Alami, N.H., et al., *Axonal transport of TDP-43 mRNA granules is impaired by ALS-causing mutations*. Neuron, 2014. **81**(3): p. 536-543.
105. Spriggs, K.A., M. Bushell, and A.E. Willis, *Translational regulation of gene expression during conditions of cell stress*. Mol Cell, 2010. **40**(2): p. 228-37.
106. Aulas, A., S. Stabile, and C. Vande Velde, *Endogenous TDP-43, but not FUS, contributes to stress granule assembly via G3BP*. Mol Neurodegener, 2012. **7**: p. 54.
107. Gilks, N., et al., *Stress granule assembly is mediated by prion-like aggregation of TIA-1*. Mol Biol Cell, 2004. **15**(12): p. 5383-98.
108. Khalfallah, Y., et al., *TDP-43 regulation of stress granule dynamics in neurodegenerative disease-relevant cell types*. Sci Rep, 2018. **8**(1): p. 7551.
109. Lee, K.H., et al., *C9orf72 Dipeptide Repeats Impair the Assembly, Dynamics, and Function of Membrane-Less Organelles*. Cell, 2016. **167**(3): p. 774-788 e17.
110. Kim, H.J., et al., *Therapeutic modulation of eIF2alpha phosphorylation rescues TDP-43 toxicity in amyotrophic lateral sclerosis disease models*. Nat Genet, 2014. **46**(2): p. 152-60.
111. Couthouis, J., et al., *A yeast functional screen predicts new candidate ALS disease genes*. Proc Natl Acad Sci U S A, 2011. **108**(52): p. 20881-90.
112. Aulas, A., et al., *G3BP1 promotes stress-induced RNA granule interactions to preserve polyadenylated mRNA*. J Cell Biol, 2015. **209**(1): p. 73-84.
113. Capitini, C., et al., *TDP-43 inclusion bodies formed in bacteria are structurally amorphous, non-amyloid and inherently toxic to neuroblastoma cells*. PLoS One, 2014. **9**(1): p. e86720.
114. Igaz, L.M., et al., *Expression of TDP-43 C-terminal Fragments in Vitro Recapitulates Pathological Features of TDP-43 Proteinopathies*. J Biol Chem, 2009. **284**(13): p. 8516-24.

## 8. Bibliography

---

115. Langellotti, S., et al., *A novel Drosophila model of TDP-43 proteinopathies: N-terminal sequences combined with the Q/N domain induce protein functional loss and locomotion defects*. *Dis Model Mech*, 2016. **9**(6): p. 659-69.
116. Nonaka, T., et al., *Prion-like properties of pathological TDP-43 aggregates from diseased brains*. *Cell Rep*, 2013. **4**(1): p. 124-34.
117. Estes, P.S., et al., *Wild-type and A315T mutant TDP-43 exert differential neurotoxicity in a Drosophila model of ALS*. *Hum Mol Genet*, 2011. **20**(12): p. 2308-21.
118. Wegorzewska, I., et al., *TDP-43 mutant transgenic mice develop features of ALS and frontotemporal lobar degeneration*. *Proc Natl Acad Sci U S A*, 2009. **106**(44): p. 18809-14.
119. Zhou, H., et al., *Transgenic rat model of neurodegeneration caused by mutation in the TDP gene*. *PLoS Genet*, 2010. **6**(3): p. e1000887.
120. Xiao, S., et al., *RNA targets of TDP-43 identified by UV-CLIP are deregulated in ALS*. *Mol Cell Neurosci*, 2011. **47**(3): p. 167-80.
121. Sephton, C.F., et al., *Identification of neuronal RNA targets of TDP-43-containing ribonucleoprotein complexes*. *J Biol Chem*, 2011. **286**(2): p. 1204-15.
122. Ling, J.P., et al., *TDP-43 repression of nonconserved cryptic exons is compromised in ALS-FTD*. *Science*, 2015. **349**(6248): p. 650-5.
123. Zhang, Z., et al., *Downregulation of microRNA-9 in iPSC-derived neurons of FTD/ALS patients with TDP-43 mutations*. *PLoS One*, 2013. **8**(10): p. e76055.
124. Colombrita, C., et al., *TDP-43 and FUS RNA-binding proteins bind distinct sets of cytoplasmic messenger RNAs and differently regulate their post-transcriptional fate in motoneuron-like cells*. *J Biol Chem*, 2012. **287**(19): p. 15635-47.
125. Freibaum, B.D., et al., *Global analysis of TDP-43 interacting proteins reveals strong association with RNA splicing and translation machinery*. *J Proteome Res*, 2010. **9**(2): p. 1104-20.
126. Bramham, C.R. and D.G. Wells, *Dendritic mRNA: transport, translation and function*. *Nat Rev Neurosci*, 2007. **8**(10): p. 776-89.
127. Liu-Yesucevitz, L., et al., *Local RNA translation at the synapse and in disease*. *J Neurosci*, 2011. **31**(45): p. 16086-93.
128. Higashi, S., et al., *TDP-43 associates with stalled ribosomes and contributes to cell survival during cellular stress*. *J Neurochem*, 2013. **126**(2): p. 288-300.
129. Ayala, Y.M., T. Misteli, and F.E. Baralle, *TDP-43 regulates retinoblastoma protein phosphorylation through the repression of cyclin-dependent kinase 6 expression*. *Proc Natl Acad Sci U S A*, 2008. **105**(10): p. 3785-9.
130. Liu, E.Y., C.P. Cali, and E.B. Lee, *RNA metabolism in neurodegenerative disease*. *Dis Model Mech*, 2017. **10**(5): p. 509-518.
131. Fontana, F., K. Siva, and M.A. Denti, *A network of RNA and protein interactions in Fronto Temporal Dementia*. *Front Mol Neurosci*, 2015. **8**: p. 9.
132. Deng, H., P. Wang, and J. Jankovic, *The genetics of Parkinson disease*. *Ageing Res Rev*, 2018. **42**: p. 72-85.
133. Gendron, T.F., R. Rademakers, and L. Petrucelli, *TARDBP mutation analysis in TDP-43 proteinopathies and deciphering the toxicity of mutant TDP-43*. *J Alzheimers Dis*, 2013. **33** Suppl 1: p. S35-45.
134. Scotter, E.L., H.J. Chen, and C.E. Shaw, *TDP-43 Proteinopathy and ALS: Insights into Disease Mechanisms and Therapeutic Targets*. *Neurotherapeutics*, 2015. **12**(2): p. 352-63.
135. Cestra, G., et al., *Control of mRNA Translation in ALS Proteinopathy*. *Front Mol Neurosci*, 2017. **10**: p. 85.
136. Crick, F.H., *On protein synthesis*. *Symp Soc Exp Biol*, 1958. **12**: p. 138-63.

137. Genuth, N.R. and M. Barna, *Heterogeneity and specialized functions of translation machinery: from genes to organisms*. Nat Rev Genet, 2018.
138. Krishnamurthy, S. and M. Hampsey, *Eukaryotic transcription initiation*. Curr Biol, 2009. **19**(4): p. R153-6.
139. Washburn, R.S. and M.E. Gottesman, *Regulation of transcription elongation and termination*. Biomolecules, 2015. **5**(2): p. 1063-78.
140. Schaefer, B., et al., *The evolution of posttranscriptional regulation*. Wiley Interdiscip Rev RNA, 2018: p. e1485.
141. Nicchitta, C.V., et al., *Pathways for compartmentalizing protein synthesis in eukaryotic cells: the template-partitioning model*. Biochem Cell Biol, 2005. **83**(6): p. 687-95.
142. Willett, M., et al., *Localization of ribosomes and translation initiation factors to talin/beta3-integrin-enriched adhesion complexes in spreading and migrating mammalian cells*. Biol Cell, 2010. **102**(5): p. 265-76.
143. Hinnebusch, A.G., *The scanning mechanism of eukaryotic translation initiation*. Annu Rev Biochem, 2014. **83**: p. 779-812.
144. Richter, J.D. and J. Collier, *Pausing on Polyribosomes: Make Way for Elongation in Translational Control*. Cell, 2015. **163**(2): p. 292-300.
145. Aitken, C.E. and J.R. Lorsch, *A mechanistic overview of translation initiation in eukaryotes*. Nat Struct Mol Biol, 2012. **19**(6): p. 568-76.
146. Jackson, R.J., C.U. Hellen, and T.V. Pestova, *The mechanism of eukaryotic translation initiation and principles of its regulation*. Nat Rev Mol Cell Biol, 2010. **11**(2): p. 113-27.
147. Keeling, P.J. and Y. Inagaki, *A class of eukaryotic GTPase with a punctate distribution suggesting multiple functional replacements of translation elongation factor 1alpha*. Proc Natl Acad Sci U S A, 2004. **101**(43): p. 15380-5.
148. Taylor, D.J., et al., *Structures of modified eEF2 80S ribosome complexes reveal the role of GTP hydrolysis in translocation*. EMBO J, 2007. **26**(9): p. 2421-31.
149. Jackson, R.J., C.U. Hellen, and T.V. Pestova, *Termination and post-termination events in eukaryotic translation*. Adv Protein Chem Struct Biol, 2012. **86**: p. 45-93.
150. Pisarev, A.V., et al., *The role of ABCE1 in eukaryotic posttermination ribosomal recycling*. Mol Cell, 2010. **37**(2): p. 196-210.
151. Goldstein, J.L., A.L. Beaudet, and C.T. Caskey, *Peptide chain termination with mammalian release factor*. Proc Natl Acad Sci U S A, 1970. **67**(1): p. 99-106.
152. Drummond, D.A. and C.O. Wilke, *The evolutionary consequences of erroneous protein synthesis*. Nat Rev Genet, 2009. **10**(10): p. 715-24.
153. Kapur, M. and S.L. Ackerman, *mRNA Translation Gone Awry: Translation Fidelity and Neurological Disease*. Trends Genet, 2018. **34**(3): p. 218-231.
154. Anderson, L. and J. Seilhamer, *A comparison of selected mRNA and protein abundances in human liver*. Electrophoresis, 1997. **18**(3-4): p. 533-7.
155. Gygi, S.P., et al., *Correlation between protein and mRNA abundance in yeast*. Mol Cell Biol, 1999. **19**(3): p. 1720-30.
156. Kapeli, K. and G.W. Yeo, *Genome-wide approaches to dissect the roles of RNA binding proteins in translational control: implications for neurological diseases*. Front Neurosci, 2012. **6**: p. 144.
157. Zong, Q., et al., *Messenger RNA translation state: the second dimension of high-throughput expression screening*. Proc Natl Acad Sci U S A, 1999. **96**(19): p. 10632-6.
158. Ingolia, N.T., et al., *Genome-wide analysis in vivo of translation with nucleotide resolution using ribosome profiling*. Science, 2009. **324**(5924): p. 218-23.
159. Ingolia, N.T., L.F. Lareau, and J.S. Weissman, *Ribosome profiling of mouse embryonic stem cells reveals the complexity and dynamics of mammalian proteomes*. Cell, 2011. **147**(4): p. 789-802.

160. Heiman, M., et al., *A translational profiling approach for the molecular characterization of CNS cell types*. Cell, 2008. **135**(4): p. 738-48.
161. Sanz, E., et al., *Cell-type-specific isolation of ribosome-associated mRNA from complex tissues*. Proc Natl Acad Sci U S A, 2009. **106**(33): p. 13939-44.
162. Kim, T., C.S. Lim, and B.K. Kaang, *Cell type-specific gene expression profiling in brain tissue: comparison between TRAP, LCM and RNA-seq*. BMB Rep, 2015. **48**(7): p. 388-94.
163. Xu, Y.F., et al., *Wild-type human TDP-43 expression causes TDP-43 phosphorylation, mitochondrial aggregation, motor deficits, and early mortality in transgenic mice*. J Neurosci, 2010. **30**(32): p. 10851-9.
164. Herdewyn, S., et al., *Prevention of intestinal obstruction reveals progressive neurodegeneration in mutant TDP-43 (A315T) mice*. Mol Neurodegener, 2014. **9**: p. 24.
165. Veldink, J.H., et al., *Sexual differences in onset of disease and response to exercise in a transgenic model of ALS*. Neuromuscul Disord, 2003. **13**(9): p. 737-43.
166. Melanie Leitner Ph.D., S.M.P.D., and Cathleen Lutz Ph.D., *Working with ALS Mice: Guidelines for preclinical testing & colony management*. p. 28.
167. Lou, W.P., et al., *In vivo interrogation of central nervous system transcriptome by polyribosome fractionation*. J Vis Exp, 2014(86).
168. Dunham, N.W. and T.S. Miya, *A note on a simple apparatus for detecting neurological deficit in rats and mice*. J Am Pharm Assoc Am Pharm Assoc, 1957. **46**(3): p. 208-9.
169. Philips, T. and J.D. Rothstein, *Rodent Models of Amyotrophic Lateral Sclerosis*. Curr Protoc Pharmacol, 2015. **69**: p. 5 67 1-21.
170. Cappello, V. and M. Francolini, *Neuromuscular Junction Dismantling in Amyotrophic Lateral Sclerosis*. Int J Mol Sci, 2017. **18**(10).
171. Mackenzie, I.R., et al., *TIA1 Mutations in Amyotrophic Lateral Sclerosis and Frontotemporal Dementia Promote Phase Separation and Alter Stress Granule Dynamics*. Neuron, 2017. **95**(4): p. 808-816 e9.
172. McInnes, J., et al., *Synaptogyrin-3 Mediates Presynaptic Dysfunction Induced by Tau*. Neuron, 2018. **97**(4): p. 823-835 e8.
173. Sun, S., et al., *Translational profiling identifies a cascade of damage initiated in motor neurons and spreading to glia in mutant SOD1-mediated ALS*. Proc Natl Acad Sci U S A, 2015. **112**(50): p. E6993-7002.
174. Andreev, D.E., et al., *Translation of 5' leaders is pervasive in genes resistant to eIF2 repression*. Elife, 2015. **4**: p. e03971.
175. Panda, A.C., J.L. Martindale, and M. Gorospe, *Polysome Fractionation to Analyze mRNA Distribution Profiles*. Bio Protoc, 2017. **7**(3).
176. Joyce, P.I., et al., *SOD1 and TDP-43 animal models of amyotrophic lateral sclerosis: recent advances in understanding disease toward the development of clinical treatments*. Mamm Genome, 2011. **22**(7-8): p. 420-48.
177. Rothstein, J.D., *Current hypotheses for the underlying biology of amyotrophic lateral sclerosis*. Ann Neurol, 2009. **65 Suppl 1**: p. S3-9.
178. Knippenberg, S., et al., *Significance of behavioural tests in a transgenic mouse model of amyotrophic lateral sclerosis (ALS)*. Behav Brain Res, 2010. **213**(1): p. 82-7.
179. Esmaeili, M.A., et al., *Premature death of TDP-43 (A315T) transgenic mice due to gastrointestinal complications prior to development of full neurological symptoms of amyotrophic lateral sclerosis*. Int J Exp Pathol, 2013. **94**(1): p. 56-64.
180. Choi, C.I., et al., *Effects of estrogen on lifespan and motor functions in female hSOD1 G93A transgenic mice*. J Neurol Sci, 2008. **268**(1-2): p. 40-7.

181. de Jong, S., et al., *Endogenous female reproductive hormones and the risk of amyotrophic lateral sclerosis*. J Neurol, 2013. **260**(2): p. 507-12.
182. Haruyama, N., A. Cho, and A.B. Kulkarni, *Overview: engineering transgenic constructs and mice*. Curr Protoc Cell Biol, 2009. **Chapter 19**: p. Unit 19 10.
183. Wang, F., et al., *RNAscope: a novel in situ RNA analysis platform for formalin-fixed, paraffin-embedded tissues*. J Mol Diagn, 2012. **14**(1): p. 22-9.
184. Ferraiuolo, L., et al., *Molecular pathways of motor neuron injury in amyotrophic lateral sclerosis*. Nat Rev Neurol, 2011. **7**(11): p. 616-30.
185. Xu, S., et al., *PHR1 encodes an abundant, pleckstrin homology domain-containing integral membrane protein in the photoreceptor outer segments*. J Biol Chem, 1999. **274**(50): p. 35676-85.
186. Lemmon, M.A., *Pleckstrin homology (PH) domains and phosphoinositides*. Biochem Soc Symp, 2007(74): p. 81-93.
187. Xu, S., et al., *PHR1, a PH domain-containing protein expressed in primary sensory neurons*. Mol Cell Biol, 2004. **24**(20): p. 9137-51.
188. Etournay, R., et al., *PHR1, an integral membrane protein of the inner ear sensory cells, directly interacts with myosin 1c and myosin VIIa*. J Cell Sci, 2005. **118**(Pt 13): p. 2891-9.
189. Andrews, K.L., et al., *KPL1, which encodes a novel PH domain-containing protein, is induced during ciliated cell differentiation of rat tracheal epithelial cells*. Exp Lung Res, 2000. **26**(4): p. 257-71.
190. Zhou, Y., et al., *In vitro interaction between coxsackievirus B3 VP1 protein and human pleckstrin homology domain retinal protein (PHR1)*. Virus Genes, 2015. **51**(2): p. 182-9.
191. Lippincott-Schwartz, J., et al., *Kinesin is the motor for microtubule-mediated Golgi-to-ER membrane traffic*. J Cell Biol, 1995. **128**(3): p. 293-306.
192. Keller, P. and K. Simons, *Post-Golgi biosynthetic trafficking*. J Cell Sci, 1997. **110 ( Pt 24)**: p. 3001-9.
193. Foth, B.J., M.C. Goedecke, and D. Soldati, *New insights into myosin evolution and classification*. Proc Natl Acad Sci U S A, 2006. **103**(10): p. 3681-6.
194. Hirokawa, N., S. Niwa, and Y. Tanaka, *Molecular motors in neurons: transport mechanisms and roles in brain function, development, and disease*. Neuron, 2010. **68**(4): p. 610-38.
195. Vale, R.D., *The molecular motor toolbox for intracellular transport*. Cell, 2003. **112**(4): p. 467-80.
196. Soo, K.Y., M. Farg, and J.D. Atkin, *Molecular motor proteins and amyotrophic lateral sclerosis*. Int J Mol Sci, 2011. **12**(12): p. 9057-82.
197. Morfini, G.A., et al., *Axonal transport defects in neurodegenerative diseases*. J Neurosci, 2009. **29**(41): p. 12776-86.
198. Bilsland, L.G., et al., *Deficits in axonal transport precede ALS symptoms in vivo*. Proc Natl Acad Sci U S A, 2010. **107**(47): p. 20523-8.
199. Yaciuk, P., *Co-immunoprecipitation of protein complexes*. Methods Mol Med, 2007. **131**: p. 103-11.
200. Beaudet, M.J., et al., *High yield extraction of pure spinal motor neurons, astrocytes and microglia from single embryo and adult mouse spinal cord*. Sci Rep, 2015. **5**: p. 16763.
201. Friedrich, G. and P. Soriano, *Promoter traps in embryonic stem cells: a genetic screen to identify and mutate developmental genes in mice*. Genes Dev, 1991. **5**(9): p. 1513-23.
202. Belfort, G.M. and K.V. Kandror, *Cellugyrin and synaptogyrin facilitate targeting of synaptophysin to a ubiquitous synaptic vesicle-sized compartment in PC12 cells*. J Biol Chem, 2003. **278**(48): p. 47971-8.
203. Valtorta, F., et al., *Synaptophysin and synapsin I as tools for the study of the exo-endocytotic cycle*. Cell Biol Int Rep, 1989. **13**(12): p. 1023-38.

204. Sun, Q., et al., *Synaptogyrin-2 Promotes Replication of a Novel Tick-borne Bunyavirus through Interacting with Viral Nonstructural Protein NSs*. J Biol Chem, 2016. **291**(31): p. 16138-49.
205. Kedra, D., et al., *Characterization of the human synaptogyrin gene family*. Hum Genet, 1998. **103**(2): p. 131-41.
206. Janz, R. and T.C. Sudhof, *Cellugyrin, a novel ubiquitous form of synaptogyrin that is phosphorylated by pp60c-src*. J Biol Chem, 1998. **273**(5): p. 2851-7.
207. Kupriyanova, T.A. and K.V. Kandror, *Cellugyrin is a marker for a distinct population of intracellular Glut4-containing vesicles*. J Biol Chem, 2000. **275**(46): p. 36263-8.
208. Kioumourtzoglou, D., et al., *Alternative routes to the cell surface underpin insulin-regulated membrane trafficking of GLUT4*. J Cell Sci, 2015. **128**(14): p. 2423-9.
209. Chapel, A., et al., *An extended proteome map of the lysosomal membrane reveals novel potential transporters*. Mol Cell Proteomics, 2013. **12**(6): p. 1572-88.
210. Kedersha, N.L., et al., *RNA-binding proteins TIA-1 and TIAR link the phosphorylation of eIF-2 alpha to the assembly of mammalian stress granules*. J Cell Biol, 1999. **147**(7): p. 1431-42.
211. Del Gatto-Konczak, F., et al., *The RNA-binding protein TIA-1 is a novel mammalian splicing regulator acting through intron sequences adjacent to a 5' splice site*. Mol Cell Biol, 2000. **20**(17): p. 6287-99.
212. Dixon, D.A., et al., *Regulation of cyclooxygenase-2 expression by the translational silencer TIA-1*. J Exp Med, 2003. **198**(3): p. 475-81.
213. Forch, P., et al., *The apoptosis-promoting factor TIA-1 is a regulator of alternative pre-mRNA splicing*. Mol Cell, 2000. **6**(5): p. 1089-98.
214. Heck, M.V., et al., *Dysregulated expression of lipid storage and membrane dynamics factors in Tia1 knockout mouse nervous tissue*. Neurogenetics, 2014. **15**(2): p. 135-44.
215. Sanchez-Jimenez, C. and J.M. Izquierdo, *T-cell intracellular antigen (TIA)-proteins deficiency in murine embryonic fibroblasts alters cell cycle progression and induces autophagy*. PLoS One, 2013. **8**(9): p. e75127.
216. Le Guiner, C., et al., *TIA-1 and TIAR activate splicing of alternative exons with weak 5' splice sites followed by a U-rich stretch on their own pre-mRNAs*. J Biol Chem, 2001. **276**(44): p. 40638-46.
217. Monahan, Z., F. Shewmaker, and U.B. Pandey, *Stress granules at the intersection of autophagy and ALS*. Brain Res, 2016. **1649**(Pt B): p. 189-200.
218. Kedersha, N. and P. Anderson, *Stress granules: sites of mRNA triage that regulate mRNA stability and translatability*. Biochem Soc Trans, 2002. **30**(Pt 6): p. 963-9.
219. Guil, S., J.C. Long, and J.F. Caceres, *hnRNP A1 relocalization to the stress granules reflects a role in the stress response*. Mol Cell Biol, 2006. **26**(15): p. 5744-58.
220. Henao-Mejia, J. and J.J. He, *Sam68 relocalization into stress granules in response to oxidative stress through complexing with TIA-1*. Exp Cell Res, 2009. **315**(19): p. 3381-95.
221. Anderson, P. and N. Kedersha, *Stress granules: the Tao of RNA triage*. Trends Biochem Sci, 2008. **33**(3): p. 141-50.
222. Caulfield, J.J., et al., *GM-CSF increases the ability of cultured macrophages to support autologous CD4+ T-cell proliferation in response to Dermatophagoides pteronyssinus and PPD antigen*. Immunology, 1997. **92**(1): p. 123-30.
223. Zhang, K., et al., *Genetic analysis of TIA1 gene in Chinese patients with amyotrophic lateral sclerosis*. Neurobiol Aging, 2018. **67**: p. 201 e9-201 e10.
224. Hirsch-Reinshagen, V., et al., *Clinical and neuropathological features of ALS/FTD with TIA1 mutations*. Acta Neuropathol Commun, 2017. **5**(1): p. 96.
225. MacNair, L., et al., *MTHFS and DDX58 are novel RNA-binding proteins abnormally regulated in amyotrophic lateral sclerosis*. Brain, 2016. **139**(Pt 1): p. 86-100.

226. B'Chir, W., et al., *The eIF2alpha/ATF4 pathway is essential for stress-induced autophagy gene expression*. Nucleic Acids Res, 2013. **41**(16): p. 7683-99.
227. Vattam, K.M. and R.C. Wek, *Reinitiation involving upstream ORFs regulates ATF4 mRNA translation in mammalian cells*. Proc Natl Acad Sci U S A, 2004. **101**(31): p. 11269-74.
228. Harding, H.P., et al., *Regulated translation initiation controls stress-induced gene expression in mammalian cells*. Mol Cell, 2000. **6**(5): p. 1099-108.
229. Ingolia, N.T., et al., *The ribosome profiling strategy for monitoring translation in vivo by deep sequencing of ribosome-protected mRNA fragments*. Nat Protoc, 2012. **7**(8): p. 1534-50.
230. Heiman, M., et al., *Cell type-specific mRNA purification by translating ribosome affinity purification (TRAP)*. Nat Protoc, 2014. **9**(6): p. 1282-91.
231. Salazar-Grueso, E.F., S. Kim, and H. Kim, *Embryonic mouse spinal cord motor neuron hybrid cells*. Neuroreport, 1991. **2**(9): p. 505-8.
232. Y.C. Bor , J.S., Y. Li , J. Coyle , D. Rekosh & Marie-Louise Hammarskjold, *Northern Blot analysis of mRNA from mammalian polyribosomes*. PROTOCOL EXCHANGE 2006.





## **9. Appendix**



## 9. Appendix

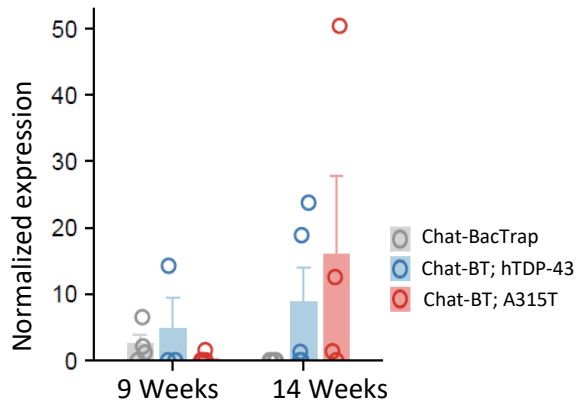
### 9.1. GO biological processes (David tool)

Exclusive pathways for 14 weeks Chat-BacTrap; A315T group	Counts	p-Value	Benjamin
Muscle contraction	13	2,80E-06	9,13E-03
Skeletal muscle contraction	9	1,80E-05	2,90E-02
Regulation of muscle contraction	7	5,70E-04	4,60E-01
Response to testosterone	8	6,40E-04	4,00E-01
Positive regulation of transcription from RNA polymerase II promoter	71	6,50E-04	3,40E-01
Regulation of release of sequestered calcium ion into cytosol by sarcoplasmic reticulum	6	9,20E-04	3,90E-01
Cardiac muscle contraction	9	1,80E-03	5,60E-01
Positive regulation of angiogenesis	15	1,80E-03	5,20E-01
Positive regulation of cytosolic calcium ion concentration	17	1,80E-03	4,80E-01
Single organismal cell-cell adhesion	14	1,80E-03	4,50E-01
Synaptic transmission, cholinergic	7	2,50E-03	5,20E-01
Sarcomere organization	7	3,00E-03	5,60E-01
Aging	18	3,70E-03	6,00E-01
Positive regulation of ERK1 and ERK2 cascade	19	3,80E-03	5,80E-01
Negative regulation of transcriptome from RNA polymerase II promoter	52	3,80E-03	5,60E-01
Transcription, DANN-template	115	4,00E-03	5,60E-01
cAMP-mediated signaling	7	4,20E-03	5,50E-01
Epithelial cell differentiation	10	4,30E-03	5,40E-01
Cellular response to exogenous dsRNA	5	4,60E-03	5,40E-01
Regulation of transcription, DNA-template	135	4,90E-03	5,50E-01

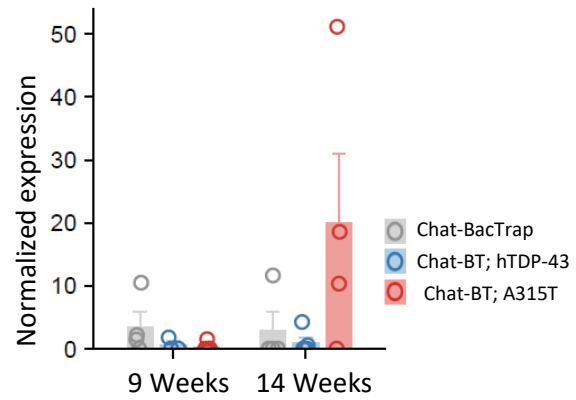
Exclusive pathways comun for 9 and14 weeks Chat-BacTrap; A315T group	Counts	p-Value	Benjamin
Cell adhesion	33	5,80E-09	1,30E-05
Myelination	11	3,40E-07	3,70E-04
Positive regulation of MAPK cascade	13	1,40E-06	1,00E-03
Negative regulation of neuron differentiation	11	3,20E-06	1,70E-03
Negative regulation of angiogenesis	10	1,50E-05	6,60E-03
Regulation of cell migration	10	2,60E-05	9,60E-03
Positive regulation of cytosolic calcium ion concentration involved in phospholipase C-activating	7	3,30E-05	1,00E-02
Heart development	17	9,80E-05	2,60E-02
Sensory perception of sound	12	1,30E-04	3,00E-02
Transport	61	1,30E-04	2,90E-02
ERK1 and ERK2 cascade	6	1,60E-04	3,10E-02
Response to hypoxia	14	1,60E-04	3,00E-02
Positive regulation of peptidyl-tyrosin phosphorylation	10	2,20E-04	3,70E-02
Regulation of keratinocyte proliferation	4	2,80E-04	4,20E-02
Angiogenesis	15	4,20E-04	5,90E-02
Ion transport	26	4,20E-04	5,60E-02
Cellular response to interferon-gamma	8	4,60E-04	2,80E-02
Lipid metabolic process	22	5,20E-04	6,10E-02
Oligodendrocyte differentiation	6	5,90E-04	6,50E-02
Cellular sodium ion homeostasis	5	6,40E-04	6,70E-02

9.2. List of up and downregulated genes: Chat-BacTrap; A315T 9 weeks vs Chat-BacTrap; A315T 14 weeks

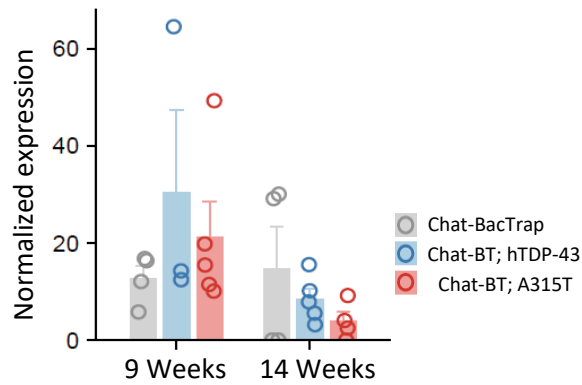
**Prom2 (upregulated candidate)**



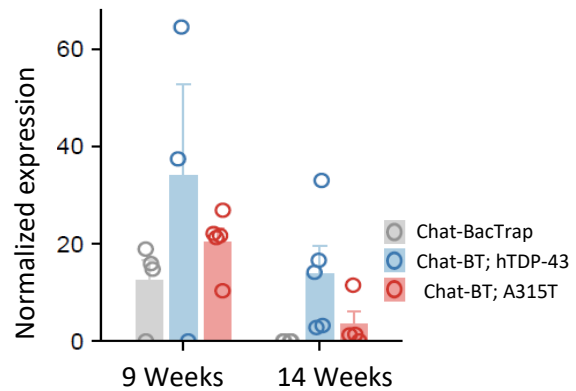
**Gm49339 (upregulated candidate)**



**Efcab6 (downregulated candidate)**



**Egf (downregulated candidate)**



## 9.3. List of up- and downregulated genes

Upregulated genes	Downregulated genes
<i>Cldn9</i>	<i>Ndp</i>
<i>Lilrb4a</i>	<i>Car2</i>
<i>Ppl</i>	<i>Epb4112</i>
<i>Arl11</i>	<i>Gng11</i>
<i>6430531B16Rik</i>	<i>Mal</i>
<i>Gm26873</i>	<i>Cflar</i>
<i>Gm14276</i>	<i>Trim59</i>
<i>Gm10548</i>	<i>Mboat1</i>
<i>Gm26805</i>	<i>Sox2</i>
<i>Xrra1</i>	<i>Fgfr2</i>
<i>Glt28d2</i>	<i>Il33</i>
<i>Rpsa-ps1</i>	<i>Plp1</i>
<i>Gm26706</i>	<i>Selenop</i>
<i>Xkr5</i>	<i>Ermn</i>
<i>Tfcp2l1</i>	<i>Suclg2</i>
<i>Ighg2b</i>	<i>Tgfbrap1</i>
<i>Lypd8</i>	<i>Stx2</i>
<i>Sftpb</i>	<i>Gpr37</i>
<i>Gm2693</i>	<i>Ednrb</i>
<i>Gm15645</i>	<i>Plxnb1</i>
<i>2700068H02Rik</i>	<i>Slain1</i>
<i>Mxd3</i>	<i>Gjc3</i>
<i>Fndc8</i>	<i>Prr5l</i>
<i>Nhlh1</i>	<i>Hoxb9</i>
<i>4930431P03Rik</i>	<i>Mlph</i>
<i>Atp6v0a4</i>	<i>Tmem125</i>
<i>B3gnt7</i>	<i>F3</i>
<i>Rad21l</i>	<i>Stxbp3</i>
<i>Zfp82</i>	<i>Plekhb1</i>
<i>Gm8174</i>	<i>Tmtc4</i>
<i>Col28a1</i>	<i>Dsg2</i>
<i>B130024G19Rik</i>	<i>Apln</i>
<i>2810408A11Rik</i>	<i>Arhgef10</i>
<i>Cnr2</i>	<i>Cldn11</i>
<i>Gm15559</i>	<i>Gatm</i>
<i>Pcdhga11</i>	<i>Efhd1</i>
<i>Tex26</i>	<i>Lbx1</i>

## 9. Appendix

---

<i>Dalir</i>	<i>Mpped2</i>
<i>Gm14114</i>	<i>Dbx2</i>
<i>Cldn23</i>	<i>Cyp2j12</i>
<i>Krt90</i>	<i>Cox8b</i>
<i>Cct8l1</i>	<i>Olig1</i>
<i>2010308F09Rik</i>	<i>Gpr17</i>
<i>Gm15760</i>	<i>Garem2</i>
<i>Gm4342</i>	<i>Ccdc62</i>
<i>4931415C17Rik</i>	<i>Olig2</i>
<i>Gm11190</i>	<i>Gpc5</i>
<i>Gm37460</i>	<i>Cmtm5</i>
<i>Nlrp6</i>	<i>Etv1</i>
<i>Zap70</i>	<i>A230009B12Rik</i>
<i>Gm10676</i>	<i>Phldb1</i>
<i>Gm11954</i>	<i>Myo6</i>
<i>Syng4</i>	<i>Gm37111</i>
<i>Tgm4</i>	<i>Serpind1</i>
<i>Gm37242</i>	<i>Gm19744</i>
	<i>Lrp2bp</i>
	<i>Bbox1</i>
	<i>Evi2a</i>
	<i>Fa2h</i>
	<i>Itgb8</i>
	<i>Mobp</i>
	<i>Enpp1</i>
	<i>Dnah3</i>
	<i>Gm22513</i>
	<i>Prkcq</i>
	<i>C730034F03Rik</i>
	<i>Nkx2-2</i>
	<i>Prex1</i>
	<i>Vamp8</i>
	<i>Cnp</i>
	<i>Gpld1</i>
	<i>mt-Rnr2</i>
	<i>Gm13546</i>
	<i>Tifab</i>
	<i>Gab1</i>
	<i>Gja6</i>
	<i>Ppef1</i>
	<i>mt-Tp</i>

---

	<i>Sowahb</i>
	<i>Nde1</i>
	<i>Slc1a3</i>
	<i>Enpp2</i>
	<i>Lyve1</i>
	<i>Siglech</i>
	<i>Dpt</i>
	<i>Mog</i>
	<i>mt-Rnr1</i>
	<i>Ppfibp2</i>
	<i>Gabpa</i>
	<i>Gm37768</i>
	<i>Snora7a</i>
	<i>Gm12326</i>
	<i>mt-Nd1</i>
	<i>Cdh19</i>
	<i>Ipcef1</i>
	<i>mt-Nd4</i>
	<i>Acy3</i>
	<i>Col9a3</i>
	<i>Apobec1</i>
	<i>Sulf1</i>
	<i>Trf</i>
	<i>mt-Nd2</i>
	<i>Txlnb</i>
	<i>Tnfaip6</i>
	<i>Prkd1</i>
	<i>Plppr5</i>
	<i>Litaf</i>
	<i>Nfe2l3</i>
	<i>Efemp1</i>
	<i>Gm38103</i>
	<i>ErbB3</i>
	<i>Kcnj10</i>
	<i>mt-Nd6</i>
	<i>Ptgds</i>
	<i>Clic6</i>
	<i>Lpar1</i>
	<i>Nupr1l</i>
	<i>Ecscr</i>
	<i>Gpm6b</i>

## 9. Appendix

---

	<i>Slc12a2</i>
	<i>Rgcc</i>
	<i>Aif1l</i>
	<i>Grm3</i>
	<i>Mbp</i>
	<i>Tnni1</i>
	<i>Rasgrp3</i>
	<i>Ttyh1</i>
	<i>Gstm7</i>
	<i>Gjb6</i>
	<i>Unc13c</i>
	<i>Atp1a2</i>
	<i>Aspg</i>
	<i>mt-Cytb</i>
	<i>Slc2a4</i>
	<i>Cdk5rap2</i>
	<i>Cd86</i>
	<i>Slc17a6</i>
	<i>Serinc5</i>
	<i>Efnb3</i>
	<i>Slc39a12</i>
	<i>Rnasel</i>
	<i>Agt</i>
	<i>Tmem88b</i>
	<i>Adgrv1</i>
	<i>Ftx</i>
	<i>Gpr34</i>
	<i>Otor</i>
	<i>Slc1a2</i>
	<i>Alox8</i>
	<i>Gpr37l1</i>
	<i>Dao</i>
	<i>0610043K17Rik</i>
	<i>lfitm1</i>
	<i>Fabp7</i>
	<i>Hapln1</i>
	<i>Ankub1</i>
	<i>Gjb1</i>
	<i>S1pr5</i>
	<i>Ybx3</i>
	<i>mt-Nd5</i>



---

	<i>Slc45a3</i>
	<i>Atp10b</i>
	<i>mt-Te</i>
	<i>Six5</i>
	<i>Pou3f1</i>
	<i>Bcas1</i>
	<i>H2-Q2</i>
	<i>Adgrf4</i>
	<i>Tril</i>
	<i>Gm21781</i>
	<i>Pycard</i>
	<i>Smtnl2</i>
	<i>E130201H02Rik</i>
	<i>Myo1f</i>
	<i>Prrg4</i>
	<i>Pls1</i>
	<i>Gsn</i>
	<i>Crhbp</i>
	<i>Itih3</i>
	<i>Fcrls</i>
	<i>mt-Co1</i>
	<i>Kirrel2</i>
	<i>Dock1</i>
	<i>Toporsos</i>
	<i>Etnppl</i>
	<i>Hepacam</i>
	<i>Emp2</i>
	<i>Ifit3</i>
	<i>Apod</i>
	<i>Tac2</i>
	<i>P2ry13</i>
	<i>Arnt</i>
	<i>mt-Tm</i>
	<i>Fam107a</i>
	<i>Mag</i>
	<i>Ldlrad3</i>
	<i>Tmem63a</i>
	<i>Lrrk1</i>
	<i>Gja1</i>
	<i>Lpar4</i>
	<i>Ccnyl1</i>

## 9. Appendix

---

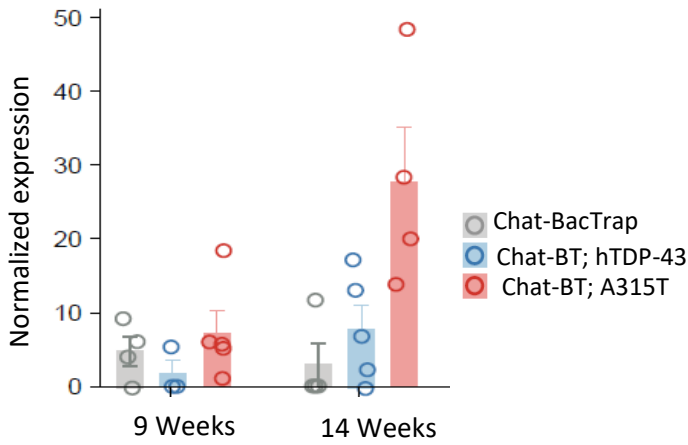
	<i>Rnf144a</i>
	<i>Folr1</i>
	<i>Tspan8</i>
	<i>Smyd1</i>
	<i>Timp4</i>
	<i>Gm10451</i>
	<i>Plin4</i>
	<i>S100a1</i>
	<i>Pi15</i>
	<i>Tmem252</i>
	<i>Sgk2</i>
	<i>Sparc</i>
	<i>Fbxw15</i>
	<i>Kctd14</i>
	<i>Chil1</i>
	<i>E130114P18Rik</i>
	<i>Klk10</i>
	<i>Zcchc24</i>
	<i>Gm12504</i>
	<i>Ppfibp1</i>
	<i>Mgp</i>
	<i>Lgi1</i>
	<i>Man2a1</i>
	<i>Col6a2</i>
	<i>Plip</i>
	<i>Atp8b1</i>
	<i>Dapp1</i>
	<i>Aspn</i>
	<i>Ntsr2</i>
	<i>Pdzph1</i>
	<i>Galr1</i>
	<i>Islr</i>
	<i>Calr4</i>
	<i>Htra3</i>
	<i>Shisa8</i>
	<i>Mir124a-1hg</i>
	<i>Cdr1</i>
	<i>Gm37144</i>
	<i>Slc6a11</i>
	<i>Samsn1</i>
	<i>Rn7sk</i>

---

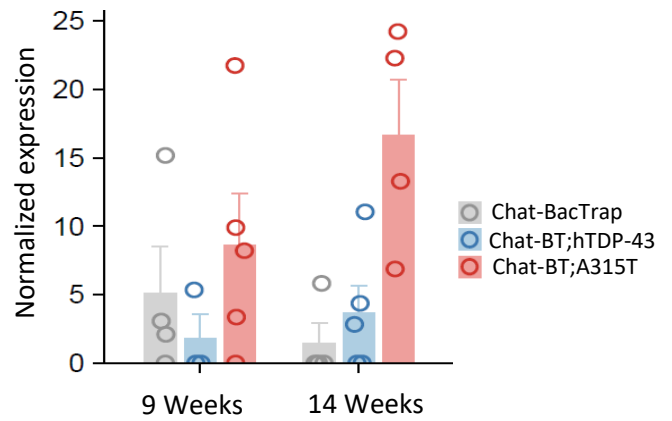
	<i>Fyco1</i>
	<i>Dnah5</i>
	<i>Tjp1</i>
	<i>Fam167b</i>
	<i>B230323A14Rik</i>
	<i>Tia1</i>
	<i>Galnt4</i>
	<i>Gucy2c</i>
	<i>Thbs1</i>
	<i>S1pr1</i>
	<i>Chd7</i>
	<i>Slc47a1</i>
	<i>Phldb2</i>
	<i>Npbwr1</i>
	<i>Mylpf</i>
	<i>Car3</i>
	<i>Gpx8</i>
	<i>Slc30a3</i>
	<i>Casq1</i>
	<i>Tmsb15b2</i>
	<i>Meg3</i>
	<i>Ttyh2</i>
	<i>Cyp2d22</i>
	<i>Gm38157</i>
	<i>Ccnd2</i>
	<i>Fbn2</i>
	<i>Atp1b2</i>
	<i>Calcr</i>
	<i>Cd101</i>

9.4. MN TRAP (IP) - High-throughput sequencing data

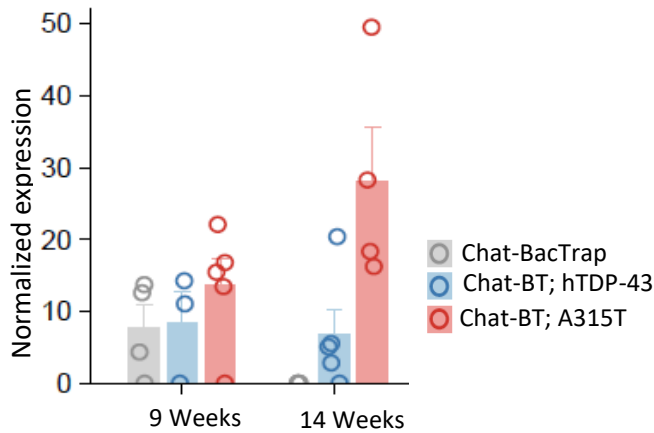
**Tex26 (upregulated candidate)**



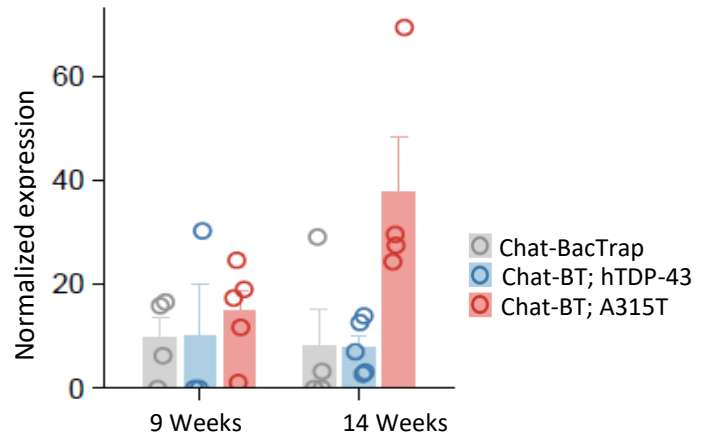
**Syngn4 (upregulated candidate)**



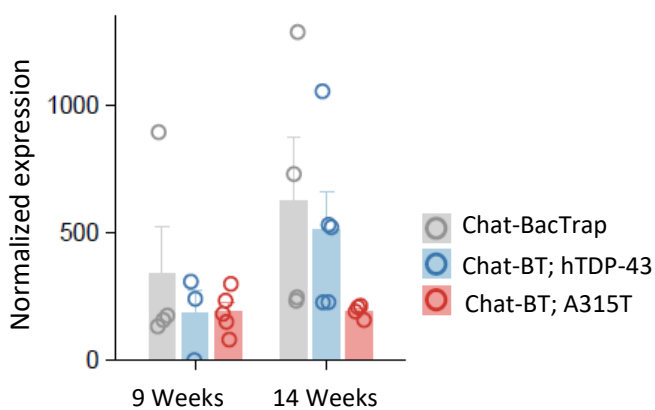
**Nhlh1 (upregulated candidate)**



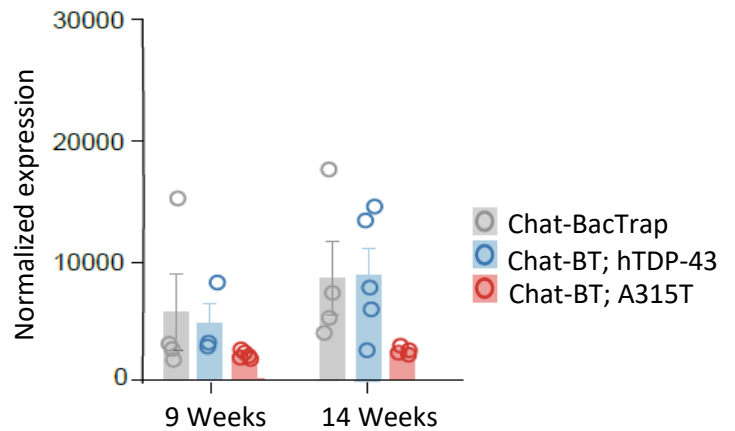
**Mxd3 (upregulated candidate)**



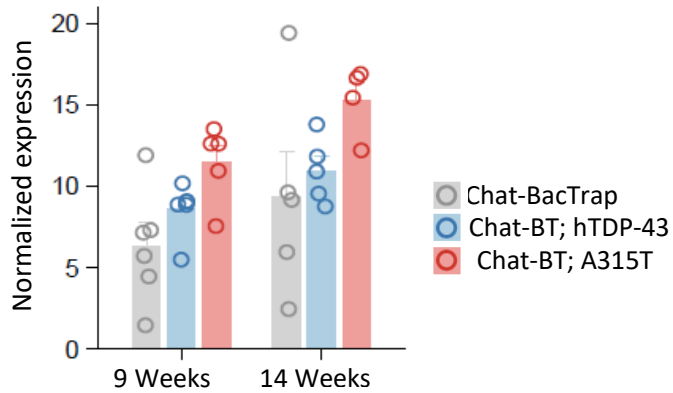
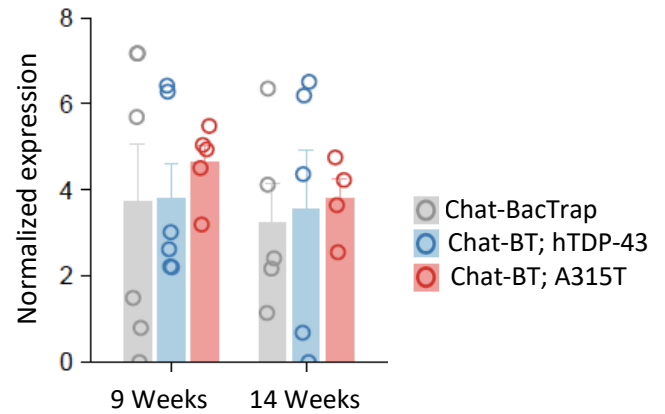
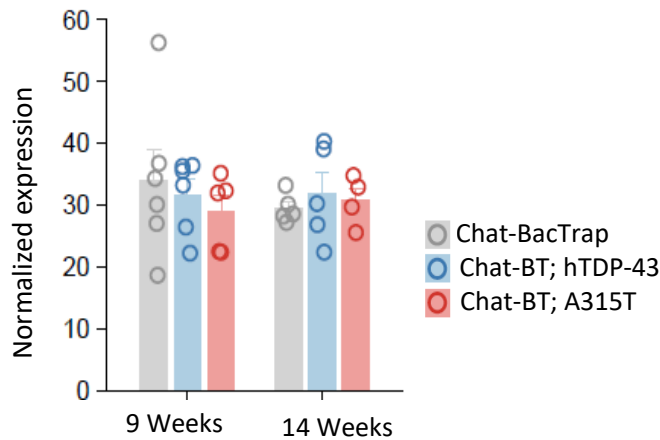
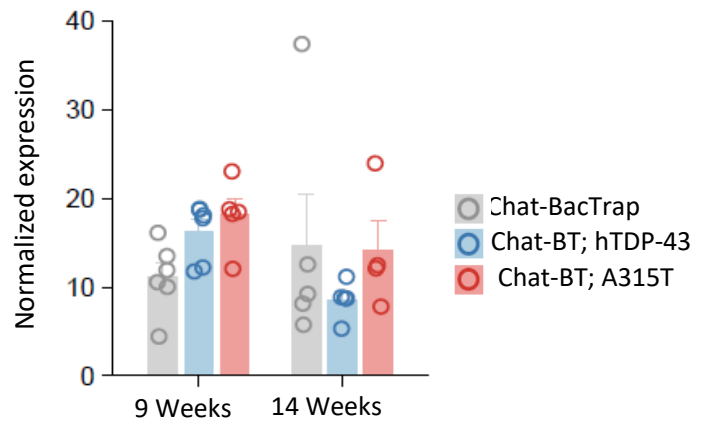
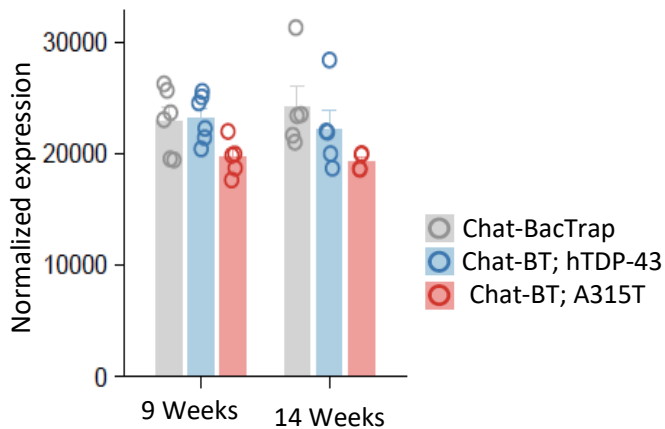
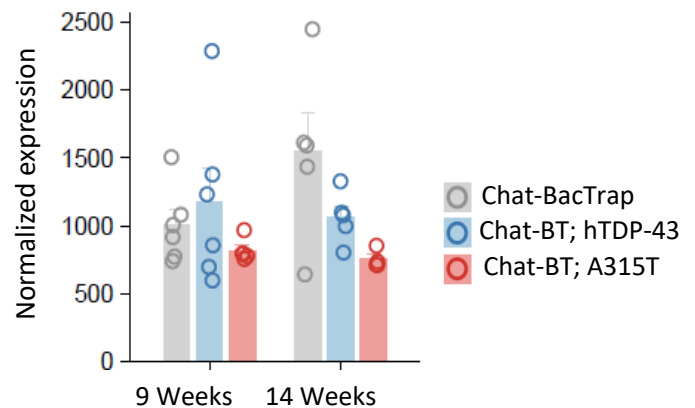
**Tia1 (downregulated candidate)**



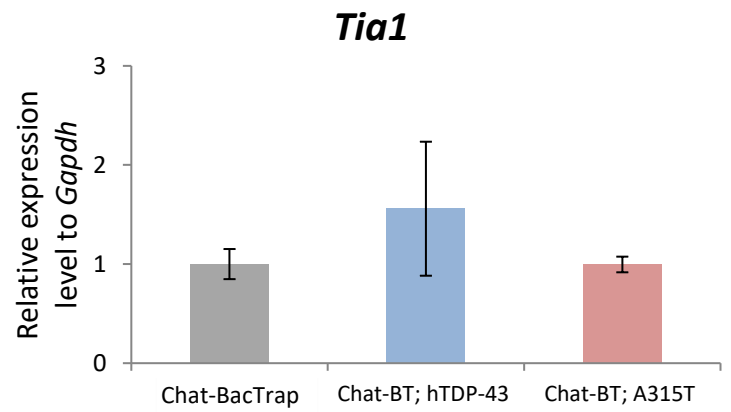
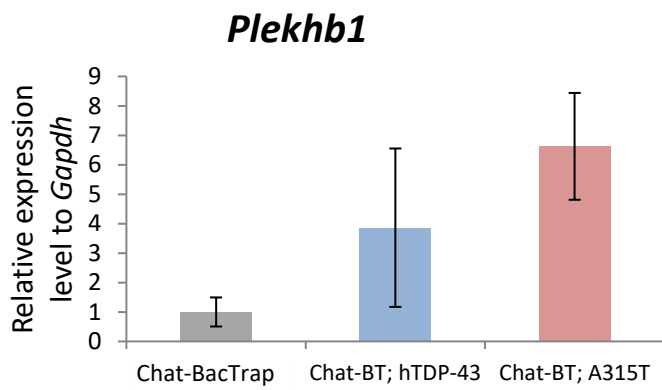
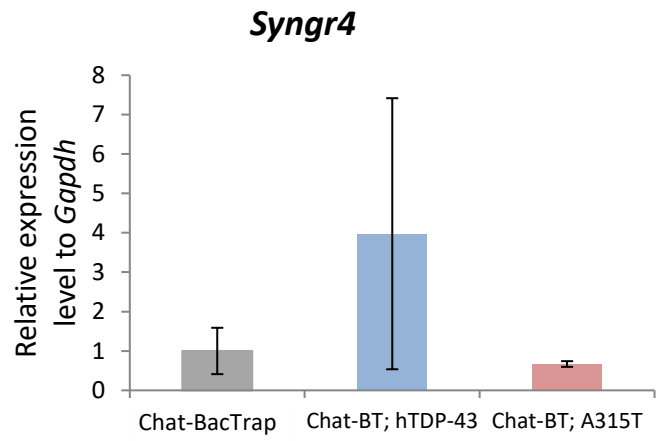
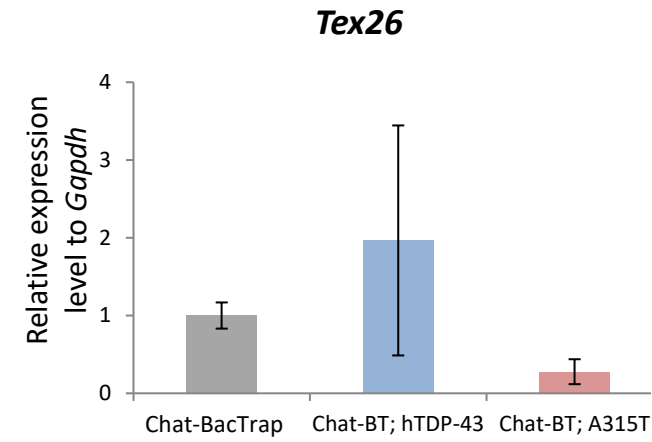
**Plekhh1 (downregulated candidate)**



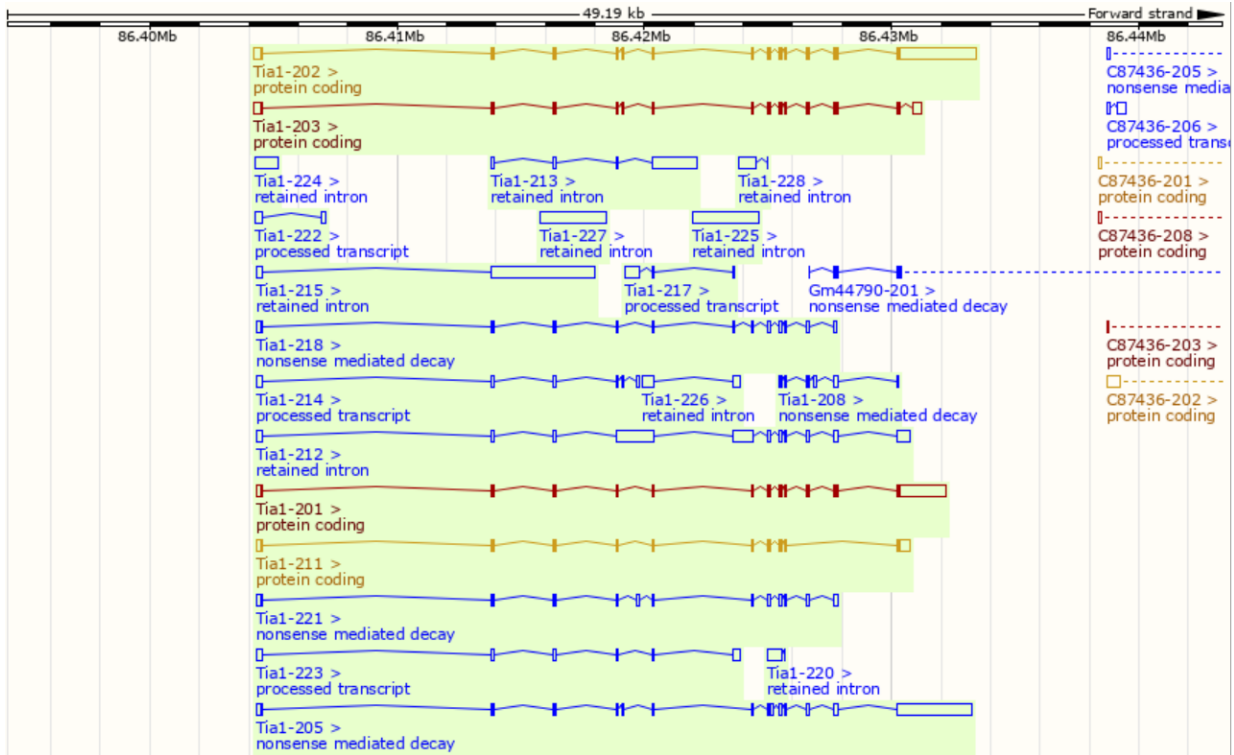
## 9.5. Spinal cord (IC) - High-throughput sequencing data

***Tex26* (upregulated candidate)*****Syngn4* (upregulated candidate)*****Nhlh1* (upregulated candidate)*****Mxd3* (upregulated candidate)*****Plekhh1* (downregulated candidate)*****Tia1* (downregulated candidate)**

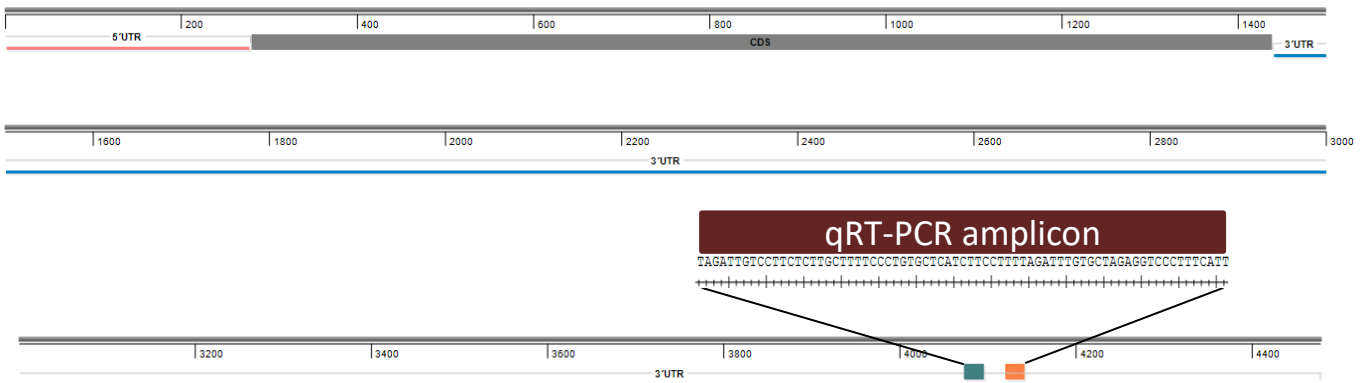
9.6. MN TRAP (IP) – qRT-PCR from 9 weeks



9.7. *Tia1* mouse gene product isoforms

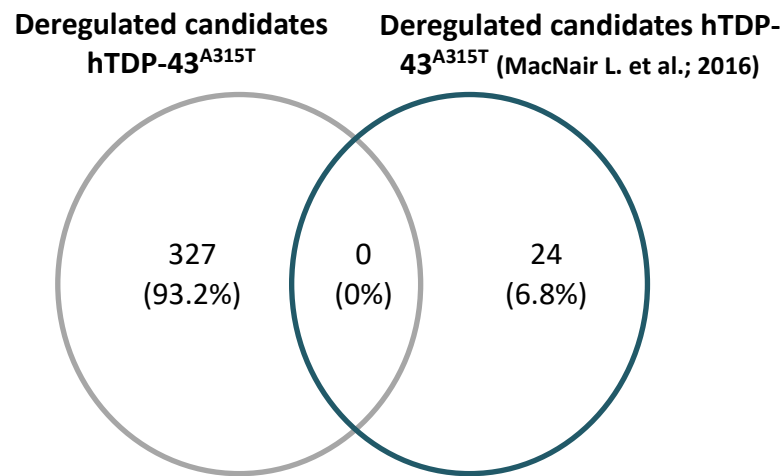


***Tia1-202***



- Legend:**
- Forward qRT-PCR primer
  - Reverse qRT-PCR primer

9.8. Venn diagram comparison of the candidates: this study vs the study from MacNair L. et al.; 2016





## **Eidesstattliche Versicherung**

Declaration on oath

**Hiermit erkläre ich an Eides statt, dass ich die vorliegende Dissertationsschrift selbst verfasst und keine anderen als die angegebenen Quellen und Hilfsmittel benutzt habe.**

I hereby declare, on oath, that I have written the present dissertation by my own and have not used other than the acknowledged resources and aids.

Hamburg, den

Unterschrift



Universitätsklinikum Hamburg-Eppendorf  
Zentrum für Molekulare Neurobiologie Hamburg  
Forschungsgruppe:  
Neuronale Translationskontrolle

Dr. Kent Duncan  
Forschungsgruppenleiter  
Martinistraße 52  
D-20246 Hamburg  
Gebäude S50, Raum 3.23  
Telefon: +49 (0) 40 7410-56274  
Fax: +49 (0) 40 7410-53436  
Kent.Duncan@zmnh.uni-hamburg.de  
www.uke.de/zmnh  
Hausanschrift:  
Falkenried 94 / Martinistr. 85  
D-20251 Hamburg

Universitätsklinikum Hamburg-Eppendorf | Martinistraße 52 | 20246 Hamburg  
Zentrum für Molekulare Neurobiologie | Forschungsgruppe Dr. Kent Duncan

## English Language Thesis Certification: Rita Francisco Marques

Hamburg, 25.10.2018

To whom it may concern:

**Rita Francisco Marques**, who was born on 17<sup>th</sup> of November 1989 and has matriculation number 67496986 is submitting her doctoral dissertation in English. The title of her thesis is: **'Identification of potential disease-driving proteins in mouse models of ALS caused by mutant TDP-43'**.

I hereby certify as a native speaker and molecular biologist that the English language used in this thesis is sufficiently correct for submission.

Yours truly,

**Kent Duncan, Ph.D.**

Universität Hamburg  
Universitätsklinikum Hamburg-Eppendorf  
Zentrum für Molekulare Neurobiologie  
AG Duncan  
Falkenried 94 · D-20251 Hamburg



Universitätsklinikum Hamburg-Eppendorf  
Körperschaft des öffentlichen Rechts  
Gerichtsstand: Hamburg  
USt-ID-Nr.: DE21 8618 948

Vorstandsmitglieder:  
Prof. Dr. Burkhard Göke (Vorsitzender)  
Prof. Dr. Dr. Uwe Koch-Gromus  
Joachim Prölß | Rainer Schoppik

Bankverbindung:  
HSH Nordbank  
IBAN-Nr.: DE97210500000104364000  
BIC: HSHNDE33